

Spatial Description-Based Approach Towards Integration of Biomedical Atlases

Nurzi Juana Binti Mohd Zaizi

Submitted for the degree of Doctor of Philosophy

Heriot-Watt University

School of Mathematical and Computer Sciences

June 2015

The copyright in this thesis is owned by the author. Any quotation from the thesis or use of any of the information contained in it must acknowledge this thesis as the source of the quotation or information.

Abstract

Biomedical imaging has become ubiquitous in both basic research and the clinical sciences. As technology advances the resulting multitude of imaging modalities has led to a sharp rise in the quantity and quality of such images. Whether for epidemiological studies, educational uses, clinical monitoring, or translational science purposes, the ability to integrate and compare such image-based data has become increasingly critical in the life sciences and eHealth domain. Ontology-based solutions often lack spatial precision. Image processing-based solutions may have difficulties when the underlying morphologies are too different. This thesis proposes a compromise solution which captures location in biomedical images via spatial descriptions. Three approaches of spatial descriptions have been explored. These include: (1) spatial descriptions based on spatial relationships between segmented regions; (2) spatial descriptions based on fiducial points and a set of spatial relations; and (3) spatial descriptions based on fiducial points and a set of spatial relations, integrated with spatial relations between segmented regions. Evaluation, particularly in the context of mouse gene expression data, a good representative of spatio-temporal biological data, suggests that the spatial description-based solution can provide good spatial precision. This dissertation discusses the need for biomedical image data integration, the shortcomings of existing solutions and proposes new algorithms based on spatial descriptions of anatomical details in the image. Evaluation studies, particularly in the context of gene expression data analysis, were carried out to study the performance of the new algorithms.

Acknowledgements

I would like to express sincere gratitude and appreciation to my supervisor Dr. Albert Burger and my co-supervisor Professor Richard Baldock for proposing and managing this thesis. Their guidance, constructive criticism and encouragement was valuable all those years. At many stages in the course of this research project I benefited from their generous advice, particularly when exploring ideas. Their assistance and guidance contributed enormously to the production of this thesis. Their supervisions, discussions, suggestions and close attention have truly helped the progression and smoothness of the research work and is much indeed appreciated.

I would like to thank all the staff in the School of Mathematical and Computer Sciences, Heriot Watt University for their most welcoming support and friendly environment. Furthermore, I also would like to thank every member at the Medical Research Council (MRC) for their kind assistance and support especially to Nick Burton who helped me learned Java Woolz smoothly. I would like to extend my sincerest thanks and appreciation to Dr. Chris Armit, a senior editor at the Medical Research Council (MRC) who provided me the biologist defined gold standard mappings.

Besides MRC group, there were numerous people in BISEL Heriot Watt University, who I like to thank for their enormous help that assist me making this journey successful. I would like to mention Dr. Kenneth McLeod for his enormous support in providing generous advice, valuable discussion and comments throughout this research. Also to Karen Sunderland and Gus Ferguson with whom I worked very closely in the beginning of my studies. The collaboration that I had with the team was the highlight of my time spends at this university, and I will cherish it the most.

ACADEMIC REGISTRY
Research Thesis Submission



Name:	Nurzi Juana Binti Mohd Zaizi		
School/PGI:	School of Mathematical & Computer Sciences		
Version: <i>(i.e. First, Resubmission, Final)</i>	Final	Degree Sought (Award and Subject area)	PhD Computer Science

Declaration

In accordance with the appropriate regulations I hereby submit my thesis and I declare that:

- 1) the thesis embodies the results of my own work and has been composed by myself
- 2) where appropriate, I have made acknowledgement of the work of others and have made reference to work carried out in collaboration with other persons
- 3) the thesis is the correct version of the thesis for submission and is the same version as any electronic versions submitted*.
- 4) my thesis for the award referred to, deposited in the Heriot-Watt University Library, should be made available for loan or photocopying and be available via the Institutional Repository, subject to such conditions as the Librarian may require
- 5) I understand that as a student of the University I am required to abide by the Regulations of the University and to conform to its discipline.

* *Please note that it is the responsibility of the candidate to ensure that the correct version of the thesis is submitted.*

Signature of Candidate:		Date:	26/06/2015
-------------------------	---	-------	------------

Submission

Submitted By <i>(name in capitals)</i> :	
Signature of Individual Submitting:	
Date Submitted:	

For Completion in the Student Service Centre (SSC)

Received in the SSC by <i>(name in capitals)</i> :			
Method of Submission <i>(Handed in to SSC; posted through internal/external mail):</i>			
E-thesis Submitted (mandatory for final theses)			
Signature:		Date:	

Please note this form should bound into the submitted thesis.

Updated February 2008, November 2008, February 2009, January 2011

Contents

Contents	iv
List of Figures	viii
List of Tables	xvii
1 Introduction	1
1.1 Motivation	3
1.2 Objectives	5
1.3 Contribution to Knowledge	5
1.4 Organisation of the Thesis	6
1.5 Publications	7
2 Literature Review	8
2.1 Introduction	8
2.2 Biomedical Atlases	8
2.2.1 The Edinburgh Mouse Atlas	9
2.2.2 The e-Mouse Atlas of Gene Expression	11
2.2.3 Allen Developing Mouse Brain Atlas	12
2.2.4 The GENSAT Brain Atlas	12
2.3 Mapping Primitives	15
2.3.1 Spatial Relations as Mapping Primitives	15
2.3.2 Fiducial Points as Mapping Primitives	18
2.4 Image Mapping Techniques	20
2.4.1 Ontology-based Mappings	20
2.4.2 Image Processing-based Mappings	25
2.5 Similarity Measures	26
2.5.1 Hausdorff Distance	27
2.5.2 Overlay Distance	27
2.6 Representation of Spatial Rules	28

Contents

2.6.1	Predicate Logic	28
2.6.2	Spatial Rules	29
2.7	Woolz Image Processing	29
2.7.1	Woolz Objects	29
2.7.2	Woolz Library	31
2.8	Image Mapping Problems Overview	32
2.8.1	Image Mapping Classification	32
2.8.1.1	Image Matching vs Region Mapping	33
2.8.1.2	Image Segmentation	33
2.8.1.3	Variation of Morphology	35
2.8.1.4	Criteria for Matching Images/Regions	36
2.8.2	Overview of Mapping Solutions	39
2.8.2.1	Image Processing-based Method	39
2.8.2.2	Ontology-based Method	42
2.9	Summary	44
3	Developing Spatial Description-Based Integration	46
3.1	Introduction	46
3.2	Spatial Descriptions Based on Spatial Relationships between Segmented Regions	47
3.2.1	Design Rationale	47
3.2.1.1	Representation of Topology	47
3.2.1.2	Representation of Arrangement	48
3.2.1.3	Representation of Direction	49
3.2.2	Mapping Method	49
3.2.3	Formalism	50
3.2.4	Algorithm	54
3.3	Spatial Descriptions Based on Fiducial Points and a Set of Spatial Relations	58
3.3.1	Design Rationale	58
3.3.2	Mapping Method	59
3.3.3	Formalism	61
3.3.4	Algorithm	63
3.3.5	Mapping Identical, Scale Changed, Rotated and Morphologically Different Images	64

3.4	Spatial Descriptions Based on Fiducial Points and a Set of Spatial Relations, Integrated with Spatial Relations between Segmented Regions	67
3.4.1	Mapping Method	68
3.4.2	Formalism	70
3.5	Selected Mapping Approach	70
3.6	Biologist Mapping Results	72
3.6.1	Selection of Fiducial Points	73
3.6.2	Image Region Mappings	75
3.7	Summary	78
4	The Calibration of Spatial Description-Based Integration	80
4.1	Introduction	80
4.2	Analysis of Spatial Descriptions Based on Fiducial Points and a Set of Spatial Relations	80
4.2.1	Impact of Number of Fiducial Points on Result Accuracy . . .	83
4.2.2	Impact of Number of Fiducial Lines on Result Accuracy . . .	84
4.2.3	Impact of Fiducial Point Positioning on Result Accuracy . . .	85
4.2.4	Impact on Result Accuracy of Fiducial Point Locations at the Boundary of the Embryo Part or a Location Inside the Embryo Part	87
4.2.5	Impact of Distribution of Area Sizes Made by Fiducial Points on Result Accuracy	91
4.2.6	Results and Analysis	92
4.2.7	Discussion	97
4.3	Overview of Well-defined Fiducial Points	97
4.3.1	Analysis of Mapping Using Well-defined Fiducial Points	99
4.3.2	Discussion	103
4.4	Summary	103
5	The Evaluation of Spatial Description-Based Integration	105
5.1	Introduction	105
5.2	Demonstration of Problems Associated with Image Region Mappings	106
5.3	Analysis of Image Region Mappings in Identical Images	111
5.3.1	Ontology-Based Method	112
5.3.2	Image Processing Algorithm	117
5.3.3	Spatial Description Fiducial Points-Based Method	122
5.3.4	Results and Analysis	124

Contents

5.4	Analysis of Image Region Mappings in Non-Identical Images	124
5.4.1	Mapping between Non-Identical Images that are Not Identical in Their Morphologies	125
5.4.2	Mapping between Similar Images Not Identical in Morphology	130
5.4.3	Mapping between Non-Identical Images with Same Morphology	133
5.4.4	Results and Analysis	138
5.5	Application of Techniques for Gene Expression Queries	139
5.6	Summary	144
6	Conclusions and Future Work	146
6.1	Introduction	146
6.2	Summary	147
6.3	Future Work	150
	Appendix A Table Results	152
	Appendix B Spatial Queries	158
	Appendix C Biologist Gold Standard	162
	References	172

List of Figures

2.1	Excerpt from the 3D Digital Atlas of the EMAP. The application allows users to navigate in the three-dimensional embryo space corresponding to viewing parameters, and to define arbitrary two-dimensional sections.	10
2.2	Excerpt from the EMAGE mouse atlas. The listings are the results of possibly detected genes corresponding to the painted location in the mouse embryo image.	11
2.3	Excerpt from the Allen Developing Mouse Brain Atlas. The application allows users to navigate in the anatomical structure nomenclature and annotated space of the image to search for gene expression annotations.	13
2.4	Excerpt from the GENSAT Brain Atlas. The listings are the results of gene expression annotations corresponding to the selected location in the mouse brain image.	14
2.5	Topological relations between two spatial regions according to Egenhofer and Herring [31].	16
2.6	Directional relations between entities a and b where c_a is the centroid of a and c_b is the centroid of b	17
2.7	Directional relations between entities a and b defined using minimum bounding boxes.	17
2.8	Example fiducial points probability maps of top femur head, carina, aortic arch, Th12 vertebra and top of kidney in sagittal view [41]. . .	19
2.9	Example fiducial points and segmented anatomical regions: heart(red), liver(brown), kidneys(orange), spleen(light blue), bladder(yellow) and prostate (pink) [42].	20
2.10	2D illustration of image processing-based mapping with 5 fiducial point correspondences between the two images for anatomical space mapping.	21

List of Figures

2.11	A 3D image structure in woolz [71].	30
2.12	An image in 2D. The image corresponds to a section view through a 3D image space. One of a number of possible woolz objects can be defined over an arbitrary region of a discrete 2D space. The arbitrary region can be defined and saved into a woolz object by using the MAPaint software. Each woolz object corresponds to a discrete region of 2D space and has a coordinate (k, l) , where k is the column coordinate while l is the line coordinate [71].	31
2.13	The mapping of (a) one query image (i.e. the midline image of an embryo) onto three potential target images: (b) the image slice at 0.100mm distance from midline, (c) the image slice at 0.200mm distance from midline, and (d) the image slice at 0.300mm distance from midline.	33
2.14	The mapping of region <i>liver</i> from (a) the midline image onto the following possible result regions: (b) the <i>liver</i> in an image with exactly the same morphology (i.e. identical images), (c) the <i>liver</i> in an image with a different morphology (i.e. the image slice near to the midline), and (d) the <i>liver</i> in another example of an image with a different morphology (i.e. the image of a different embryo at the same developmental stage).	34
2.15	The image consists of 49 segmented regions (painted domains) and is labelled according to the anatomical names.	35
2.16	Two non-identical mouse embryo images with the same structures: <i>liver</i> , <i>heart</i> , and <i>lung</i> . However, these structures are different in their morphologies.	36
2.17	Two non-identical mouse embryo images with morphologically the same set of structures in terms of scale, orientation and position. The visual content of both images is only similar at the higher scene level: both images are entirely different at the pixel-level.	37
3.1	The mapping method using spatial relationships between segmented regions maps (a) query region x to (b) a location somewhere inside the area highlighted in green (the result region y).	54
3.2	Flow diagram of the proposed <i>SpaRTAD</i> algorithm	56
3.3	Anatomical regions in Image 1 and Image 2 with (a)~(b) disjointness, (c)~(d) connectedness, (e)~(f) disjointness and connectedness	57
3.4	A fiducial point, a fiducial line and a query region.	59

List of Figures

3.5	Ontology-based mappings identify corresponding elements between two ontologies (mapping of structure <i>head</i> from Ontology 1 to structure <i>head</i> in Ontology 2) based on spatial relations between anatomical structures. The image processing-based mappings align images (mapping of a voxel from Image 1 to the corresponding voxel in Image 2) based on equivalent voxel/pixel intensities and image warping algorithms using fiducial points (landmarks). The proposed spatial description fiducial points-based method fits in between these two as it employs both fiducial points and spatial relations.	60
3.6	The spatial description fiducial points-based method maps (a) the query region x to (b) the result region y	64
3.7	Example of rotated images. Region x is <i>between</i> fiducial lines $L1$ and $L2$	65
3.8	In all three images, the centroid of the structure in the middle denotes a fiducial point. This particular fiducial point is then linked to the centroids of two other structures which remain in the same position. The white areas denote the acceptable location for query region x . . .	66
3.9	The blue circle in (a) is entirely below the line drawn between two fiducial points. However, part of the blue circle in (b) lies a little above the line.	67
3.10	An embryo with anatomical regions a, b, c, d, e, f and g , with four fiducial points $P1, P2, P3$ and $P4$. The spatial description fiducial points-based method maps (a) the query region X to (b) the result region Y . Then, the spatial description using spatial relationships between segmented regions make the result region Y narrower as in (c) the result region Z	69
3.11	A biologist was asked to identify the location of 14 fiducial points in a pair of images. This example shows the mapping of fiducial points between two midline images from two consecutive Theiler Stages of the same embryo. The material for the exercise in this section is provided in Appendix C.	74

List of Figures

3.12 The mapping of an identifiable region, for example, the *heart* between two midline images from two consecutive Theiler Stages of the same embryo. A biologist was given the left image with the blue area as the query region. He was then asked to draw the area in the right image that matches the query region. In the above example, the blue area in the right image was drawn by a biologist as the query result region corresponding to the query region in the left image. The material for the exercise in this section is provided in Appendix C. 76

3.13 The mapping of a random region denoted as query region x between two midline images from two consecutive Theiler Stages of the same embryo. A biologist was given the left image with the blue area as the query region. Then, he was asked to draw the area in the right image that matches the query region. In the above example, the blue area in the right image was drawn by a biologist as the query result region corresponding to the query region x in the left image. The material for the exercise in this section is provided in Appendix C. 77

4.1 Abstract representation for evaluation of mapping using fiducial points. 81

4.2 Tree structure corresponding to the nomenclature for the components in the abstract representation in Figure 4.1. This nomenclature mimics the *part-of* hierarchy of the actual anatomy. 82

4.3 Average percentage of accuracy produced by different numbers of fiducial points. The more fiducial points are included the higher the average percentage of accuracy. Moreover, the query region area versus the number of fiducial points affects mapping accuracy. 84

4.4 Average percentage of accuracy involving 4 and 24 fiducial lines served by query region size. The average percentage of accuracy is higher when more fiducial lines are used. 85

4.5 Positioning for 8 fiducial points in (a) Set A (b) Set B (c) Set C 86

4.6 Average percentage of accuracy in three different positioning sets of 8 fiducial points served by query region area. The same number of fiducial points placed at different positions produces different average percentages of accuracy. Mapping accuracy gets better when fiducial points are in even distribution. 87

4.7 Selection of 8 fiducial points (a) at both boundary of the embryo part and inside the embryo part (b) inside the embryo part (c) at the boundary of the embryo part. 88

List of Figures

4.8 Average percentage of accuracy by selecting 8 fiducial points at the boundary of the embryo part, inside the embryo part or a combination of both, produced by query region area. Mapping accuracy increases when more definable areas are created through the fiducial points. 89

4.9 Three images (assume that this image represents a whole mouse embryo part) with the same number of fiducial points creating a different number of segments. The number of segments generated is influenced by fiducial point location. Images 1 and 2 have the same number of segments, but different sizes. Fiducial points located inside the embryo part created more segments than where fiducial points were all placed at the boundary of the embryo part. Again, mapping is more accurate when more segments are created through the fiducial points. 90

4.10 The placement of 8 fiducial points creating 54 definable areas on an (a) even distribution of different areas (b) strongly uneven distribution of different areas. 91

4.11 Average percentage of accuracy in two images with the same number of defined areas but varying in size produced by query region size. Mapping is more accurate where there is less variation in area size. 92

4.12 The actual size of the (a) model parameter image (b) query region of 200x200 squared pixels. 95

4.13 The actual size of the (a) model parameter image (b) query region of 50x50 squared pixels. 96

4.14 Sagittal view of TS23 mouse embryo image with 14 well-defined fiducial points identified during literature review (Chapter 2) 98

4.15 The percentage of accuracy served by the combination of 7 fiducial points. None of these combinations yielded the highest accuracy for all anatomical locations. 102

4.16 The percentage of accuracy served by the combination of 9 fiducial points. None of these combinations yielded the highest accuracy for all anatomical locations. 102

4.17 The percentage of accuracy served by the combination of 11 fiducial points. None of these combinations yielded the highest accuracy for all anatomical locations. 103

4.18 The percentage of accuracy served by the number of fiducial points. The more fiducial points are included the higher the percentage of accuracy. 104

List of Figures

5.1	Image regions mapped between similar images but not identical in their morphologies. The ontology-based method has mapped the <i>liver</i> in (a) image <i>I1</i> to the (b) result region in image <i>I2</i> . In contrast, the image processing algorithm failed in this mapping.	107
5.2	Image regions mapped between non-identical images that are not identical in their morphologies. The ontology-based method has mapped the <i>liver</i> in (a) image <i>I1</i> to the (b) result region in image <i>I2</i> . In contrast, the image processing algorithm has failed in this mapping.	108
5.3	Mappings of image regions between non-identical images with the same morphology. The ontology-based method has mapped the <i>liver</i> in (a) image <i>I1</i> to the (b) result region in image <i>I2</i> . In contrast, the image processing algorithm failed in this mapping.	109
5.4	The mapping of image regions between two slices of an embryo. The ontology-based method has mapped the <i>pituitary</i> in (a) image <i>I1</i> to the (b) result region in image <i>I2</i> . Region <i>pituitary</i> is annotated in image <i>I1</i> but not in image <i>I2</i> . The two ontologies provide different definitions for the <i>pituitary</i> . Defining the similarities between these two definitions using an ontology matching approach based on the set intersection have resulted in a low mapping precision.	111
5.5	Anatomical location of liver (a) in its actual location, and (b) the corresponding match location resulting from the ontology-based method.	113
5.6	Anatomical location of midgut (a) in its actual location, and (b) the corresponding match location resulting from the ontology-based method.	114
5.7	Anatomical location of lung (a) in its actual location, and (b) the corresponding match location resulting from the ontology-based method.	114
5.8	Anatomical location of thalamus (a) in its actual location, and (b) the corresponding match location resulting from the ontology-based method.	115
5.9	Anatomical location of pancreas (a) in its actual location, and (b) the corresponding match location resulting from the ontology-based method.	115
5.10	Anatomical location of adrenal gland cortex (a) in its actual location, and (b) the corresponding match location resulting from the ontology-based method.	116

List of Figures

5.11 Anatomical location of metanephros (a) in its actual location, and (b) the corresponding match location resulting from the ontology-based method. 116

5.12 Anatomical location of femur (a) in its actual location, and (b) the corresponding match location resulting from the ontology-based method. 117

5.13 Mapping of anatomical location of liver resulting from the ASIFT image processing algorithm. 118

5.14 Mapping of anatomical location of midgut resulting from the ASIFT image processing algorithm. 118

5.15 Mapping of anatomical location of lung resulting from the ASIFT image processing algorithm. 119

5.16 Mapping of anatomical location of thalamus resulting from the ASIFT image processing algorithm. 119

5.17 Mapping of anatomical location of pancreas resulting from the ASIFT image processing algorithm. 120

5.18 Mapping of anatomical location of adrenal gland cortex resulting from the ASIFT image processing algorithm. 120

5.19 Mapping of anatomical location of metanephros resulting from the ASIFT image processing algorithm. 121

5.20 Mapping of anatomical location of femur resulting from the ASIFT image processing algorithm. 121

5.21 Percentage accuracy for the eight anatomical locations produced by the image processing algorithm, the ontology-based method, and the fiducial points-based method involving all 14 well-defined fiducial points. The results suggest that the spatial description fiducial points-based method can provide mapping accuracy as good as both the image processing algorithm and the ontology-based method. *IP* denotes the image processing algorithm, *Ontology* denotes the ontology-based method and *SD* denotes the spatial description fiducial points-based method. 123

5.22 Mapping of fiducial points between two midline images of different embryos at Theiler Stage 23 based on 14 fiducial points, as identified in the literature review, selected by a biologist. There are only eight relevant fiducial points between the two images. 127

List of Figures

5.23 Extended selection of fiducial points between two midline images of different embryos at Theiler Stage 23 selected by a biologist. There are four additional fiducial points selected. Thus, the images have 12 relevant fiducial points between them. 128

5.24 Extended selection of fiducial points between two midline images of different embryos at Theiler Stage 23 selected by a non-biologist. There are 13 additional fiducial points selected (labelled as p1 to p13). Thus, the images have 21 relevant fiducial points between them. 129

5.25 The percentage of accuracy for regions mapped between two midline images of different embryos at the same developmental stage served by six mapping approaches. 130

5.26 Mapping of fiducial points between two midline images from two consecutive Theiler Stages (TS23 to TS24) of the same embryo based on 14 fiducial points identified in the literature review, selected by a biologist. There are only four relevant fiducial points between the two images. 131

5.27 Extended selection of fiducial points between two midline images from two consecutive Theiler Stages (TS23 to TS24) of the same embryo, selected by a non-biologist. There are 13 additional fiducial points selected (labelled as p1 to p13). Thus, the images have 17 relevant fiducial points between them. 132

5.28 The percentage of accuracy for regions mapped between two midline images from two consecutive Theiler Stages of the same embryo served by five mapping approaches. 133

5.29 Mapping of fiducial points between two exact same images of different image modalities, selected by a biologist. There are 10 relevant fiducial points between the two images. 135

5.30 Extended selection of fiducial points between two exact same images of different image modalities, selected by a biologist. There are four additional fiducial points selected. Thus, the images have 14 relevant fiducial points between them. 136

5.31 Extended selection of fiducial points between two exact same images of different image modalities, selected by a non-biologist. There are 13 additional fiducial points selected (labelled as p1 to p13). Thus, the images have 23 relevant fiducial points between them. 137

5.32 The percentage of accuracy for regions mapped between two same images of different image modalities served by six mapping approaches. 138

List of Figures

5.33	Mapping of region <i>lung</i> from the Kaufman Digital Atlas to the Edinburgh Mouse Atlas and the number of detected genes retrieved for region <i>lung</i> from EMAGE.	141
5.34	The recall of genes expression query results for six anatomical locations resulting from using the spatial description fiducial points-based method based on the fiducial points as selected in Sets 1, 2 and 3 (See Figures 5.22 to 5.24 for these sets of fiducial points).	142
5.35	The precision of genes expression query results for six anatomical locations resulting from using the spatial description fiducial points-based method based on the fiducial points as selected in Sets 1, 2 and 3 (See Figures 5.22 to 5.24 for these sets of fiducial points).	143
5.36	The precision of genes expression query results for six anatomical locations resulting from using the spatial description fiducial points-based method based on the number of fiducial points selected by a biologist and a non-biologist.	144
B.1	Anatomical location of liver (a) in its actual location, and (b) the corresponding matched location resulting from image processing algorithm by [63].	158
B.2	Anatomical location of midgut (a) in its actual location, and (b) the corresponding matched location resulting from image processing algorithm by [63].	159
B.3	Anatomical location of lung (a) in its actual location, and (b) the corresponding matched location resulting from image processing algorithm by [63].	159
B.4	Anatomical location of thalamus (a) in its actual location, and (b) the corresponding matched location resulting from image processing algorithm by [63].	160
B.5	Anatomical location of pancreas (a) in its actual location, and (b) the corresponding matched location resulting from image processing algorithm by [63].	160
B.6	Anatomical location of femur (a) in its actual location, and (b) the corresponding matched location resulting from image processing algorithm by [63].	161
B.7	Anatomical location of metanephros (a) in its actual location, and (b) the corresponding matched location resulting from image processing algorithm by [63].	161

List of Tables

2.1	Image Mapping Cases	32
3.1	Description of Images	72
4.1	Standard deviations of 54 areas defined through 8 fiducial points as arranged in Figures 4.10(a) and 4.10(b)	94
5.1	The resulting accuracy and the detection time when mapping used the ontology-based method.	112
5.2	The resulting accuracy and the detection time when mapping used the image processing algorithm.	117
5.3	Accuracy and detection time results when mapping using the spatial description fiducial points-based method.	122
A.1	Results corresponding to fig. 4.3	152
A.2	Results corresponding to fig. 4.4	152
A.3	Results corresponding to fig. 4.6	152
A.4	Results corresponding to fig. 4.8	153
A.5	Results corresponding to fig. 4.11	153
A.6	Results corresponding to fig. 4.15	153
A.7	Results corresponding to fig. 4.16	154
A.8	Results corresponding to fig. 4.17	155
A.9	Results corresponding to fig. 4.18	155
A.10	Results corresponding to fig. 5.21	156
A.11	Results corresponding to fig. 5.25	156
A.12	Results corresponding to fig. 5.28	156
A.13	Results corresponding to fig. 5.32	157
A.14	Results corresponding to fig. 5.34	157
A.15	Results corresponding to fig. 5.35	157
A.16	Results corresponding to fig. 5.36	157

Chapter 1

Introduction

Biomedical imaging informatics has become a crucial part of modern healthcare, clinical research, and basic biomedical sciences. Rapid improvement of imaging technology and advances in imaging modalities in recent years have resulted in a significant increase in the quantity and quality of such images. Whether for epidemiological studies, educational uses, for monitoring the clinical progress of a patient or for translational science purposes, being able to integrate and compare such image-based data has developed into an increasingly critical component in the eHealth domain and in life sciences. The work presented in this thesis is rooted in the latter and uses examples from biomedical atlases.

A biomedical atlas consists of a graphical model, the ontology associated with the graphical model, and a mapping between those two. The ontology contains a collection of anatomical domains and relations among those domains. The graphical model is the canonical image for a mammal with those anatomical domains. Three of the main atlases in the current domain of interest are the e-Mouse Atlas of Gene Expression (EMAGE) [1], the Allen Developing Mouse Brain Atlas [2], and the GENSAT Brain Atlas [3]. These atlases are the data resources for gene expression information. Gene expression information describes whether or not a gene is expressed in a location of a particular anatomical structure related to a model organism [4]. The research in this thesis focuses on the mouse embryo as model organism.

The Allen Developing Mouse Brain Atlas is a data source storing gene expression data across seven developmental stages of the mouse brain [5]. EMAGE [6] is another example of a mouse atlas covering gene expression data for anatomical structures corresponding to the EMAP Anatomy Ontology [7]. Gene expression data for the mouse brain is also available from EMAGE. The GENSAT brain atlas is yet another type of mouse atlas providing gene expression data for the mouse brain. GENSAT

is a gene expression atlas of both the developing and adult mouse, and stores gene expression data for anatomical structures corresponding brain and spinal cord [3].

Although the EMAGE, the GENSAT brain atlas and the Allen Developing Mouse Brain Atlas are fundamental resources, they cannot be considered complete. There are a number of explanations for this, including differences in experimental design and various interpretations of results [8]. In addition, different update routines may cause data from these atlases to remain incomplete. As a consequence, these atlases may provide different results even for the same gene expression query. To illustrate this, consider the gene *Efna2* and the structure of midbrain at Theiler Stage 19. At the time this thesis was written, the EMAGE contained two experiments for this combination, suggesting that *Efna2* is expressed. The Allen Developing Mouse Brain Atlas also shows this structure at the same developmental stage and indicates that *Efna2* is also expressed. The GENSAT brain atlas also has this structure, however, indicating that there are currently no experimental results in their database for the gene *Efna2*. With available evidence from EMAGE and the Allen Developing Mouse Brain Atlas, the most likely conclusion is that the gene *Efna2* is expressed in midbrain at Theiler Stage 19; however, if the user depends on a single resource, in this case the GENSAT brain atlas, incorrect conclusions may be reached. Consequently, consideration of data from all resources is required to build as complete a picture of the domain [9].

In addition to incompleteness, these atlases often suffer from inconsistency [8]. Inconsistency is implied when one biomedical atlas publishes an annotation suggesting the gene is expressed in a particular structure, and a second annotation suggests that it is not [10]. Such variability is often associated with the complexity of the underlying experiments, including unrecognised differences in experiments, and human error on the part of the resource's curators [10]. All resources must be exploited to generate full and complete query results. Therefore, the integration of anatomical space in the context of same-species atlases can facilitate the sharing of biomedical data from many resources.

The mapping of anatomical space across different model organisms [11], such as the linking of human and mouse embryo model organisms, can be useful in facilitating comparison of biomedical atlas data across species. Integrating data from cross-species atlases is useful for the expression of homologous genes in the experimental field [12]. Corresponding organs and genes in different species can be homologous. Homologous genes are the same form of genes expressed in a particular body part of two different species. These sets of genes can be compared meaningfully to facilitate analysis, modelling and prediction in biomedicine [13; 14; 15]. For example, inte-

grating data between the mouse atlas and the chick atlas to facilitate the comparison of homologous genes between the two organisms assists biologists in understanding which genes are important in foetal development [16]. Consequently, integration of biomedical atlases is vital both within and across species boundaries.

Although there are many different methods to integrate data from these resources, it is the use of image-based data integration that is considered in this thesis. Image-based data integration typically involves anatomical space mapping. Given two images $C1$ and $C2$, mapping one image onto another implies, for each anatomical region in image $C1$, trying to find a corresponding region with the same hypothesised meaning, in image $C2$. These anatomical regions occupy unique anatomical spaces in the corresponding images. Of the existing solutions to this problem, ontology-based solutions tend to lack spatial precision. Image processing-based solutions have difficulties when the underlying morphologies are too different from one another.

This thesis presents the spatial description-based solution; a new technique to facilitate image-based data integration and overcome many limitations of established techniques using spatial descriptions of anatomical details within images.

1.1 Motivation

We propose to achieve integration of biomedical atlases by mapping the images of different biomedical atlases. However, the implementation of this approach involves a number of problems. First, different biomedical atlases may have a different number of segmented regions in their images, causing one structure to correspond to parts of several structures, and vice versa. The mapping of images to achieve biomedical atlas integration may require the alignment of representations of anatomy differing in structure and domain coverage. Second, these images may have the exact same anatomical structures, but the morphology may vary with scale, orientation, and position. Besides morphological differences, it is normal for many anatomical structures to change in shape and spatial arrangement. For example, bent fingers and or a beating heart may cause a wide variety of segmented images in the animal. Moreover, there are a wide variety of postures in which animals are imaged [17]. Third, different biomedical atlases may have the same segmented images using different anatomical names, causing interoperability issues in finding corresponding anatomical regions between these images.

Finding anatomical region correspondences between images can be carried out via image processing. Since the image processing technique takes into account a given image's voxels/pixels, the most significant advantage of this technique is that

it provides high spatial precision. However, this technique may have difficulties when the underlying morphologies between the two compared images are too different. Morphologies concern the different formation of an anatomical structure in terms of shape, size, colour and so on. Since images with different morphologies are subject to different voxel/pixel distributions, a large variation in voxel/pixel distributions can cause the images to become very different. As a result, this technique may not work when mappings involve two images which are too different. Therefore, the primary motivation of the research described in this thesis is to investigate the feasibility of developing a new mapping technique which provides an alternative to the image processing-based solution that may fail when the images have different underlying morphologies.

An ontology-based solution may work when an image processing-based solution does not. An ontology-based solution makes use of a rule-based system. A rule-based system allows semantic content or knowledge about an image to be explicitly captured in rules. Therefore, this technique can facilitate mapping between images with differing formation of shape, size, and structures. However, an ontology-based solution often lacks spatial precision. Any ontology is commonly subject to limitation of its descriptive power, i.e. an ontology cannot be thoroughly described within itself. All categories in an ontology can be equated with sets. All categories of an ontology are proper subsets of T , except T itself. Therefore, ontology-based integration can provide mappings with better spatial precision only if the ontology has the means to describe everything that exists in an image. Nevertheless, when an ontology describes itself, T should be a proper subset of T , which is impossible. The conclusion is that the ontology-based solution is relatively low in spatial precision. Therefore, the second motivation of the research described in this thesis is to investigate the feasibility of developing an alternative mapping technique, which overcomes the issue of low spatial precision of ontology-based solution. In addition, ontology-based solutions require the two ontologies to be relatively similar in terms of vocabulary and domain coverage. This is often not the case. Similar ontologies with different vocabularies can be aligned [18]; however, none of the existing tools are perfect, and multiple alignment tools produce varying similarity measures for a certain alignment [19]. Therefore, the final motivation behind this research is to investigate the feasibility of developing an alternative technique which solves the interoperability problem caused by different anatomical names and vocabularies used between ontologies.

1.2 Objectives

The overall objective of this thesis is to create a set of spatial rules in order to determine corresponding regions across images of biomedical atlases, providing an efficient representation structure to conceptualise anatomical space to guide the process of mapping an image, which will further demonstrate that the spatial description-based solution can enable the integration of biomedical atlases. We avoid the extra complexity of image segmentation by considering easily-segmented anatomical regions.

Besides, the scope of this thesis lies within 2D image space. This simplification allows us to concentrate on the primary problem: anatomical space mapping. This thesis describes anatomical conceptualisation of anatomical space from ontology to image processing via spatial description, within the context of mouse atlas applications. More specifically, this work has been conducted within the context of the Edinburgh Mouse Atlas Project [6; 7; 20] and the e-Mouse Atlas of Gene Expression [1; 20], digital atlases of mouse embryo development, projects of MRC HGU in Edinburgh.

1.3 Contribution to Knowledge

This thesis provides five main contributions to knowledge:

1. The key contribution of this research over previous work is the ability to perform biologically meaningful image region mappings.
2. The spatial description-based solution: this is a new technique for integrating image-based data towards the integration of biomedical atlases. This technique provides an alternative to the image processing-based solution that may fail when the images have different underlying morphologies. This technique solves the mapping of identical images acquired in different modalities (i.e. the visual content may be similar only at the higher scene level, but entirely different at the pixel-level), as that image processing is not capable with these. This technique also overcomes the limitations of an ontology-based solution that may not be available for images without painted domains, or when there are no matching ontologies.
3. Exploitation of the combination of fiducial points and directional relations in order to perform mapping and getting rid of region segmentation. The latter is often the most difficult problem to solve in image analysis, but is required for the ontologies to work.

4. There are no other existing approaches that have combined directional reasoning with anatomical space, or that have even incorporated fiducial points with directional relations to describe anatomical space. However, directional reasoning using landmark points or point features has been conducted in non-biomedical fields such as the geospatial domain.
5. Results in gene expression evaluation, relating to how spatial description can be used in the context of biomedical atlas application.

1.4 Organisation of the Thesis

The remainder of this thesis is organised as follows:

Chapter 2 begins with an introduction to biomedical atlases. There is a particular focus on the example of biomedical atlases within the context of mouse atlas applications. Three biomedical atlases are briefly described. These are the e-Mouse Atlas of Gene Expression (EMAGE), the Allen Developing Mouse Brain Atlas and the GENSAT Brain Atlas. The chapter then provides an overview of two mapping primitives: spatial relations and fiducial points. These two types of mapping primitives are able to determine corresponding anatomical regions across images. Then, existing techniques in image mapping are presented: the ontology-based and image processing-based techniques. A brief explanation on similarity measuring is then given. The chapter then provides a basic introduction to the formal logic for representation of spatial rules used within the thesis, followed by a basic introduction on the woolz image processing system. Finally, the chapter provides an overview of image mapping problems and discusses the categorisation of the issues associated with image mapping.

Chapter 3 describes the methodology and development of the proposed spatial description-based solution. Research was conducted in five phases. The first phase involves the investigation and scoping of a new mapping technique, designed by identifying the categories of spatial relations necessary to describe the locations of anatomical regions in an image. The second phase involves the investigation and scoping of a new mapping technique using fiducial points to describe the locations of anatomical regions in an image prior to establish mappings. The third phase involves identifying the advantages of a combined mapping technique, inspired by the approaches designed under phases two and three. The fourth phase identifies the

final approach proposed, which is to be compared against the existing approaches discussed in the literature review. The fifth phase involves an experienced biologist producing mapping samples. The purpose of acquiring this result is to establish a 'gold standard' to be used as the basis for evaluating existing mapping techniques, as well as the newly developed technique.

Chapter 4 presents the calibration of the proposed spatial description-based solution based on four parameters. These parameters are the number of fiducial points used, number of fiducial lines used, area size of the query region and selection of fiducial point location. An evaluation of mapping using 14 well-defined fiducial points reviewed in the literature is also provided.

Chapter 5 describes the experiment which was carried out to evaluate the issues associated with image region mapping when the following three types of images were used: (1) similar images which are not identical in their morphologies, (2) non-identical images which are not identical in their morphologies, and (3) non-identical images with the same morphology. The chapter then presents an evaluation of image region mappings in identical images, as well as in non-identical images. The application of techniques for gene expression queries is then discussed.

Finally, Chapter 6 concludes the thesis and proposes examples for future research.

1.5 Publications

Zaizi, N. J. M. and Burger, A. Towards Spatial Description-Based Integration of Biomedical Atlases. In: *4th ICST International Conference on eHealth (eHealth 2011)*, Malaga, Spain, November 21 - 23, 2011, Kostkova, P., Szomszor, M. and Fowler, D (Eds.), Lecture Notes of the Institute for Computer Sciences, Social Informatics and Telecommunication Engineering, ISBN 978-3-642-29261-3, vol. 91, Springer-Verlag, Heidelberg, 2012, 196-203.

Zaizi, N. J. M. and Iskandar, D. N. A. Using image mapping towards biomedical and biological data sharing. *GigaScience*, 2(12), 2013.

Zaizi, N. J. M. and Burger, A. Biomedical Image Mapping: Issues and Challenges. *International Journal of Computer and Information Technology*, 3(6), 2014.

Chapter 2

Literature Review

2.1 Introduction

This thesis proposes image-based data integration to facilitate the sharing of data across biomedical atlases. The field of image-based data integration is primarily concerned with the study and design of techniques related to image representation and mapping.

This chapter is organised as follows: Section 2.2 provides an overview of three examples of biomedical atlases. Section 2.3 discusses two types of mapping primitives, namely spatial relations and fiducial points. Section 2.4 describes existing image mapping techniques, specifically ontology-based and image processing-based techniques. A brief review of similarity measure functions is provided in Section 2.5. These functions are useful for measuring the extent to which one region of one image matches a region in another image. Section 2.6 presents the formal logic for representation of spatial rules used within the thesis. Section 2.7 provides descriptions on the woolz image processing system for processing 2D image space used within experiments. Categorisation of the issues associated with image mapping is discussed in Section 2.8. Section 2.9 summarises the chapter.

2.2 Biomedical Atlases

This section presents an overview of biomedical atlases. In particular, the focus is on the examples of biomedical atlases within the context of mouse atlas applications. The section describes the following biomedical atlases: (1) The e-Mouse Atlas of Gene Expression (EMAGE); (2) The Allen Developing Mouse Brain Atlas; and (3)

The GENSAT Brain Atlas. EMAGE uses the EMAP (the Edinburgh Mouse Atlas) to index gene expression data. Therefore, this section begins with an overview of the Edinburgh Mouse Atlas.

2.2.1 The Edinburgh Mouse Atlas

The Edinburgh Mouse Atlas Project, also known as EMAP, is a digital atlas of mouse development, a project of the MRC Human Genetics Unit (HGU), Edinburgh. The development of the atlas was based on an object-oriented architecture and includes three-dimensional models corresponding to a series of developmental stages of the mouse embryo [21; 22; 23; 24]. These developmental stages are based on Theiler's staging [25] of embryo mouse development. The atlas uses the three-dimensional embryo model as a framework to map experimental results. In addition, the atlas allows users to navigate the three-dimensional embryo space which correspond to viewing parameters and define arbitrary two-dimensional sections at any orientation. Figure 2.1 depicts the user interface of the application. The embryo image seen in the atlas corresponds to the two-dimensional section selected from the three-dimensional embryo model. The tree-structured listing represents the anatomical structure nomenclature corresponding to the selected area of the embryo image. The EMAP is linked to the EMAGE, an online database of gene expression data for the developing mouse embryo.

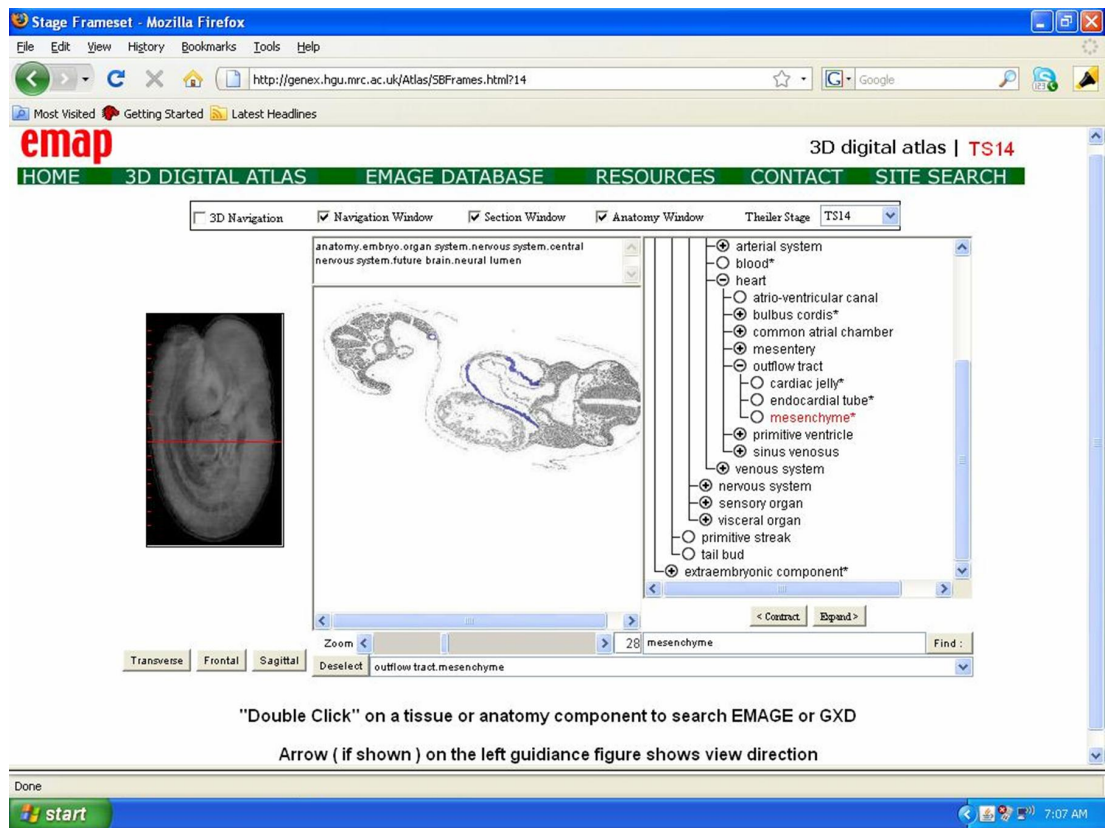


Figure 2.1: Excerpt from the 3D Digital Atlas of the EMAP. The application allows users to navigate in the three-dimensional embryo space corresponding to viewing parameters, and to define arbitrary two-dimensional sections.

2.2.2 The e-Mouse Atlas of Gene Expression

The e-Mouse Atlas of Gene Expression (EMAGE) is an online database of mouse development, based at the MRC Human Genetics Unit (HGU), Edinburgh [1; 20; 26]. The purpose of the system is to store gene expression data on the developing mouse embryo and to allow for gene expression queries. EMAGE consists of a set of three-dimensional models, corresponding to a series of developmental stages of the mouse embryo. The user interface allows users to search interactively and analyse the data. EMAGE stores the gene expression data according to anatomical structures corresponding to the EMAP Anatomy Ontology [7]. Gene expression data in EMAGE are queried by painting appropriate regions in the EMAP embryo images, or by text-based descriptions using the gene name or terms in the anatomy ontology. Data in EMAGE include mRNA in situ hybridisation, protein immunohistochemistry and transgenic reporters. Figure 2.2 depicts the user interface of EMAGE for querying gene expression data by painting appropriate regions in the embryo image. The listings show search results of possibly detected genes corresponding to the painted location in the embryo image.

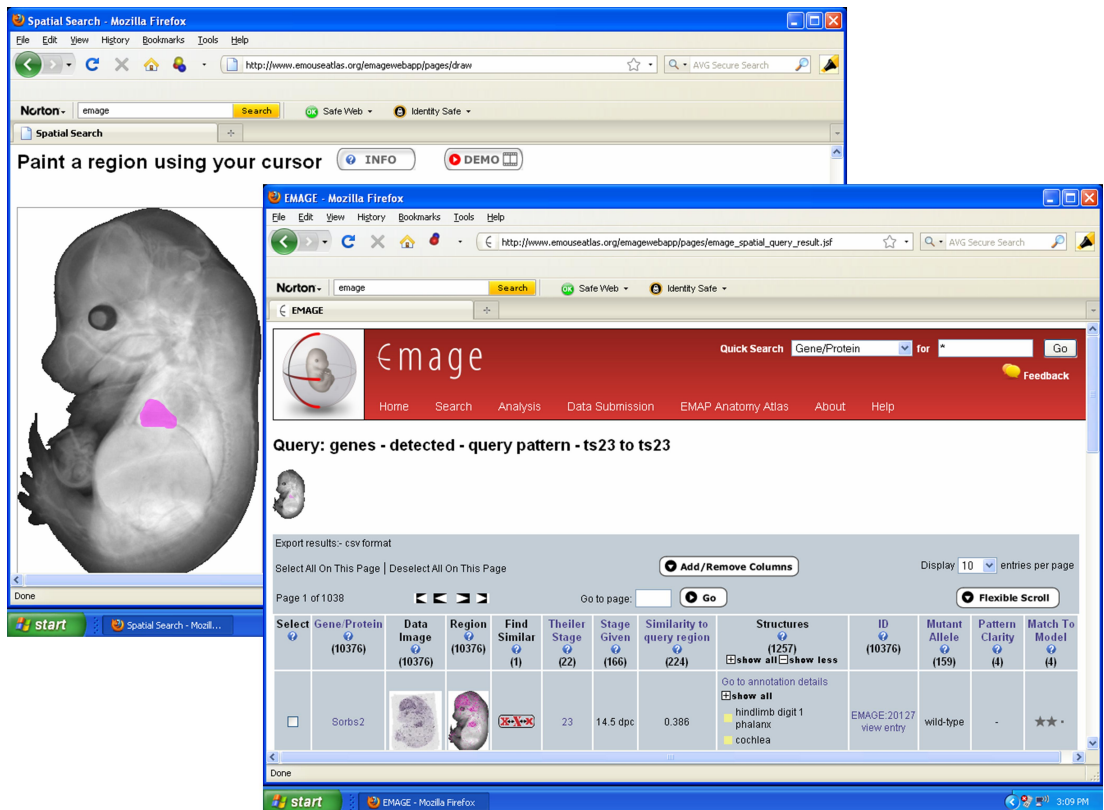


Figure 2.2: Excerpt from the EMAGE mouse atlas. The listings are the results of possibly detected genes corresponding to the painted location in the mouse embryo image.

2.2.3 Allen Developing Mouse Brain Atlas

The Allen Developing Mouse Brain Atlas is an online database of gene expression data for the mouse brain. The atlas is a project developed within the Allen Institute for Brain Science. The Allen Developing Mouse Brain Atlas provides gene expression data for the developing mouse brain from the embryo to the young adult. The purpose of the atlas is to serve as a neuroanatomical foundation to support informatics-based analysis tools and to allow for gene expression queries on the developing mouse brain [2]. Querying gene expression data can be carried out using text-based descriptions using the gene name, symbol, category or terms in the anatomy ontology. At present, the atlas contains seven developmental stages for the mouse brain. Each developmental stage has its own representative section corresponding to a mouse brain image. Figure 2.3 depicts the user interface of the Allen Developing Mouse Brain Atlas for viewing gene expression annotations corresponding to location in the mouse brain image. The tree-structured listing represents the anatomical structure nomenclature corresponding to annotated locations of the image. The gene expression annotations corresponding to annotated locations in the embryo image can be viewed by clicking on the annotated location, or by selecting a component of the anatomical structure nomenclature.

2.2.4 The GENSAT Brain Atlas

The GENSAT (Gene Expression Nervous System Atlas) Brain Atlas, a project at Rockefeller University, funded by the National Institutes of Health (NIH), is a gene expression atlas of both the developing and adult mouse. Data held in the atlas correspond to gene expression data for anatomical structures corresponding to the brain and spinal cord. The purpose of the atlas is to provide tools to catalogue, map, and electrophysiologically record gene expression data. The atlas includes a collection of images of gene expression maps of the mouse nervous system [3]. The atlas allows users to navigate in the atlas image, and select any region of interest to view gene expression annotations corresponding to the selected region. Figure 2.4 depicts the user interface of GENSAT for querying gene expression data by selecting appropriate regions in the mouse brain image. The listings show results of gene expression annotations corresponding to the selected location in the mouse brain image.

Chapter 2. Literature Review

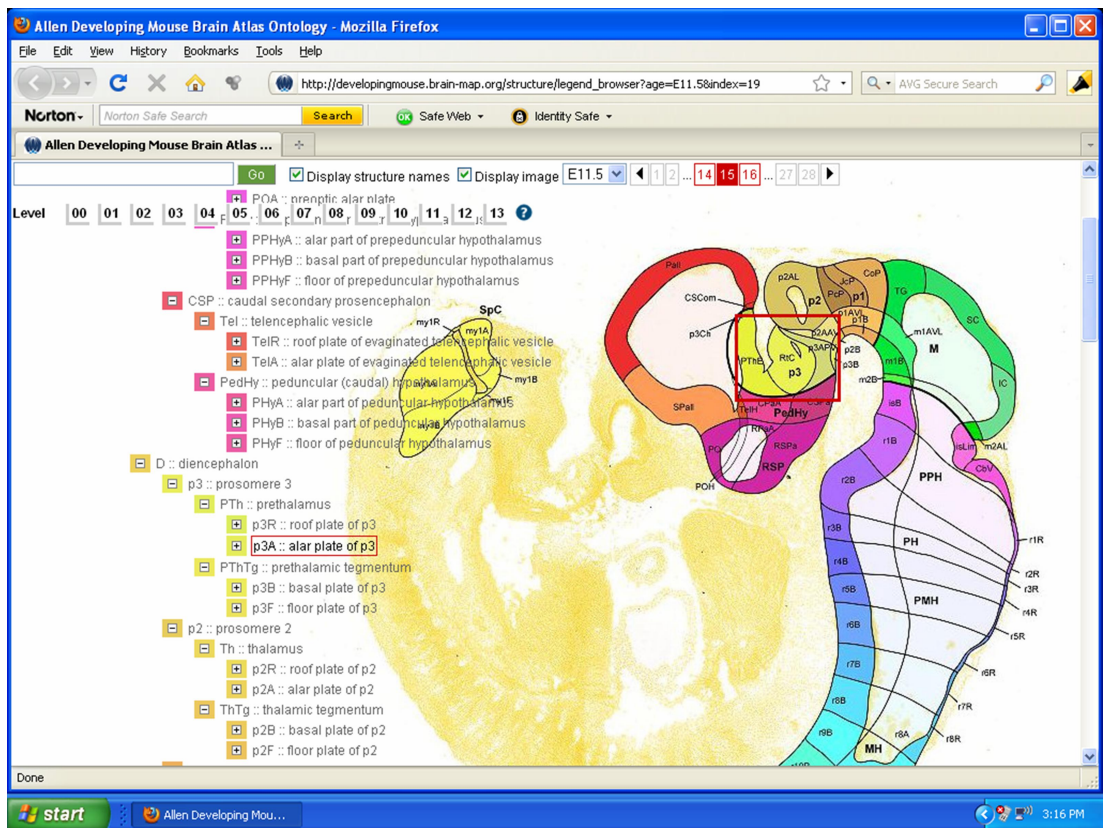


Figure 2.3: Excerpt from the Allen Developing Mouse Brain Atlas. The application allows users to navigate in the anatomical structure nomenclature and annotated space of the image to search for gene expression annotations.

Chapter 2. Literature Review

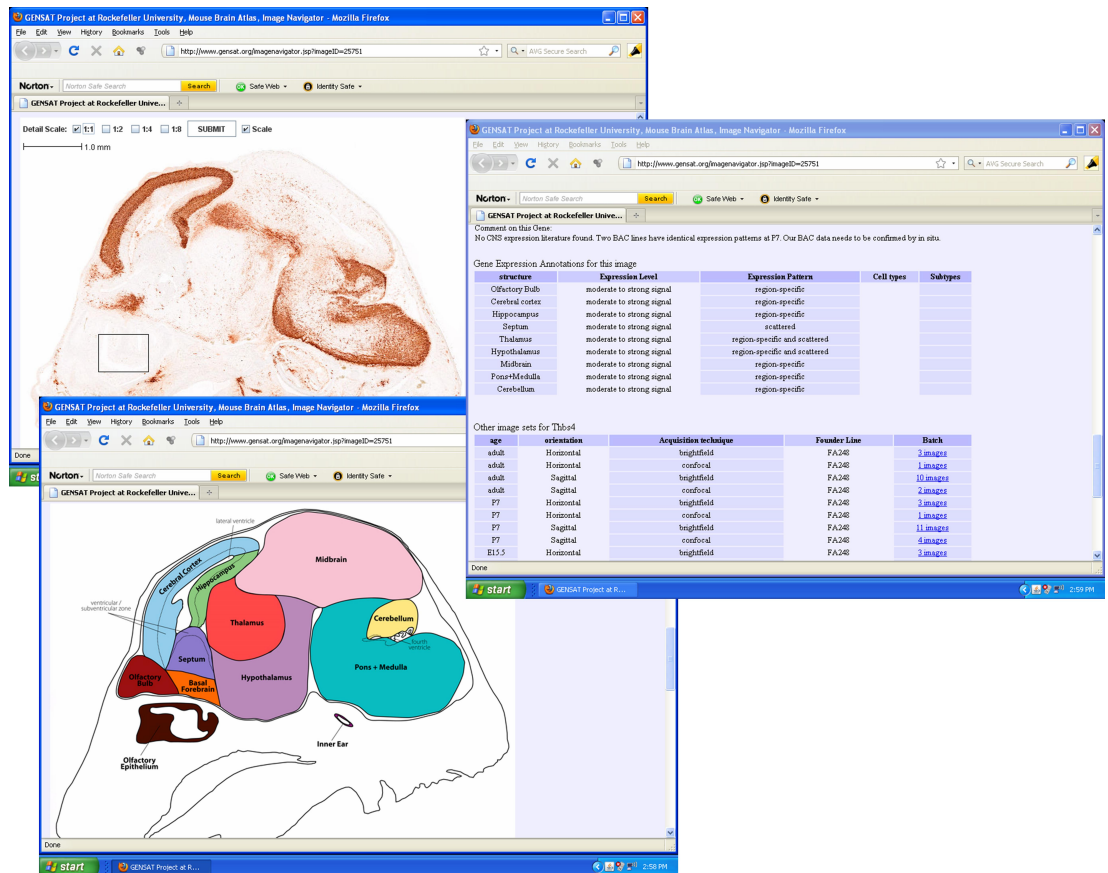


Figure 2.4: Excerpt from the GENSAT Brain Atlas. The listings are the results of gene expression annotations corresponding to the selected location in the mouse brain image.

2.3 Mapping Primitives

This section discusses two types of mapping primitives. These are spatial relations and fiducial points. These two types of mapping primitives are used to determine corresponding anatomical regions across images.

2.3.1 Spatial Relations as Mapping Primitives

Spatial relations describe the spatial relationships between spatial entities. The term 'spatial' refers to the location in anatomical space occupied by the anatomical entity. The term 'entity' refers to the individual anatomical structure, such as liver, heart and kidney. Spatial entities can be either material or immaterial. Material anatomical entities are here understood as anatomical structures with positive mass, such as the liver and brain, whereas immaterial anatomical entities are those anatomical structures with no mass, such as the stomach cavity [27]. This thesis focuses on spatial entities of type material and the thesis work is in the context of the mouse embryo anatomical domain. Thus, this thesis refers to spatial entities as anatomical structures of type material within the mouse embryo.

Spatial entities share spatial relationships. Spatial relationships include topological, directional and metric relations [28; 29]. These relations can be defined by specifying conditions between entities such as distance or relative position. Topological relations describe topological properties such as connectivity, disjointness and containment between spatial regions. Within the context of the study, spatial regions are assumed to be parts of an independent background space in which all individuals are located. The eight basic topological relations between two spatial regions according to Egenhofer and Herring [30] are *disjoint*, *externallyConnected*, *overlap*, *contains*, *equal*, *coveredBy*, *inside*, and *covers*. Figure 2.5 depicts the illustration of these eight basic topological relations.

Metric relations describe the value of the quantitative distance between two spatial entities. Distance can be measured, and it specifies how far the entity is from the reference entity. Based on distance, a relation by means of preposition near, far or adjacency can be defined. For example, near can be defined when the spatial regions, suitably enlarged, exhibit a nonempty intersection. Each spatial region's width can be enlarged by a fraction of its own height, and vice versa. According to Abella and Kender [31], based on human psychology studies, the value of this fraction is approximately 0.6, particularly, in the case, for long narrow, parallel entities. The relation far, on the other hand, is not the complement of the relation near [31]. Far may be defined as when the distance between the two enlarged spatial









disjoint 	externally connected 	overlap 	contains 
equal 	coveredBy 	inside 	covers 

Figure 2.5: Topological relations between two spatial regions according to Egenhofer and Herring [31].

regions x and y , in either x or y extent, is greater than the maximum dimension of the two spatial regions in that same x or y extent. The adjacency relation can be defined between two material anatomical entities that are close, but not connected. More precisely, the distance between them is a small but non-zero positive distance apart [32].

Directional relations are usually described between two spatial entities that do not overlap [33]. These relations can be approximated by comparing the entities' representative points (also called centroids) or their minimum bounding boxes. These relations are often described in terms of the cardinal directions between two spatial entities [34; 35]. Frank [36]; Freksa [37]; Ligozat [38] use the concept of centroids of spatial entities to define directional relations between two entities. Figure 2.6 depicts the model of directional relation between a and b where c_a is the centroid of a and c_b is the centroid of b .

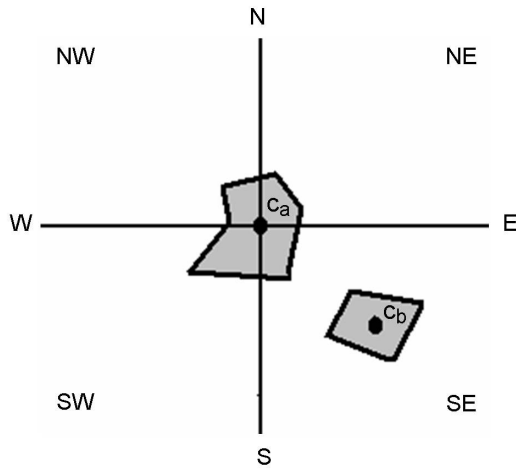


Figure 2.6: Directional relations between entities a and b where c_a is the centroid of a and c_b is the centroid of b .

Papadias and Sellis [39] represent each spatial entity using two coordinate points corresponding to the lower-left and upper-right corners of the entity's minimum bounding box. Figure 2.7 depicts the model of directional relations between a and b , which has been defined using minimum bounding boxes.

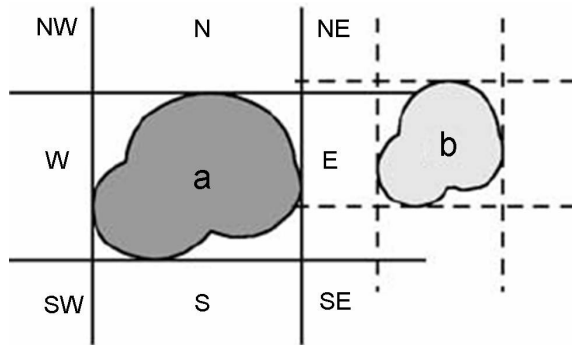


Figure 2.7: Directional relations between entities a and b defined using minimum bounding boxes.

Defining directional relations depends upon a frame of reference. A frame of reference can be established by assigning a 2D coordinate system to the centroid of the spatial entity. The x-axis can then be defined as the west-east axis of the entity. The negative region represents the west of the entity, while the positive region represents its east. Assigning the y-axis to describe the north and south of the entity, it is then possible to determine directional relations for every spatial entity corresponding to the spatial entity that has the frame of reference. The frame of reference guarantees that the directional relations between two spatial entities remain the same regardless of their viewpoint.

Topological relations are invariant under continuous transformations such as translation, rotation, and scaling. Directional relations are also invariant under such transformations where a frame of reference can be established [29]. Two spatial entities with a metric distance measure could also change upon scaling but be preserved under translation and rotation. As spatial relations are invariant under continuous transformation, their persistence is fundamental to recognition of anatomical regions in images.

2.3.2 Fiducial Points as Mapping Primitives

A fiducial point is a point in space in either 2D or 3D, typically an anatomical landmark, which is easily recognisable in an image, usually identified by human experts and possibly assisted by auto/semi-automated image processing algorithms. These fiducial points are typically located at the contours or points of high curvature of objects, like the tip of the lung, corners of the eyes. Two images are then aligned by determining pairs of corresponding fiducial points in each image.

Potesil *et al.* [40] and Seifert *et al.* [41] provide recent examples of research involving segmentation of fiducial points and the corresponding anatomical regions. Potesil *et al.* [40] proposed a method to detect 22 fiducial points based on dense matching of parts-based graphical models. These fiducial points are C2 vertebra, C7 vertebra, top of the sternum, top of the right lung, top of the left lung, aortic arch, carina, lowest point of sternum (ribs), lowest point of sternum (tip), Th12 vertebra, top of right kidney, bottom of right kidney, top left of kidney, bottom left of kidney, L5 vertebra, right spina iliaca anterior superior, left spina iliaca anterior superior, right head of femur, left head of femur, symphysis, os coccygeum, and center of bladder. Figure 2.8 depicts these fiducial points in a sagittal view. Seifert *et al.* [41] proposed a method for the localisation of 19 fiducial points for whole-body scan. These fiducial points are left and right lung tips, left and right humerus heads, bronchial bifurcation, left and right shoulder blade tips, inner left and right clavicle tips, sternum tip bottom, aortic arch, left and right endpoints of rib 11, bottom front and back of the L5 vertebra, coccyx, pubic symphysis (top and the left and right front corners of the hip bone). They also identified ten anatomical region centres. These are four heart chambers, liver, kidneys, spleen, prostate and bladder. Figure 2.9 depicts the illustration for these fiducial points and the segmented regions. These fiducial points are useful to estimate anatomical regions that are present as well as their most probable locations and boundaries in an image [41]. Subsequently, these fiducial points can be used to establish reliable correspondences between anatomical

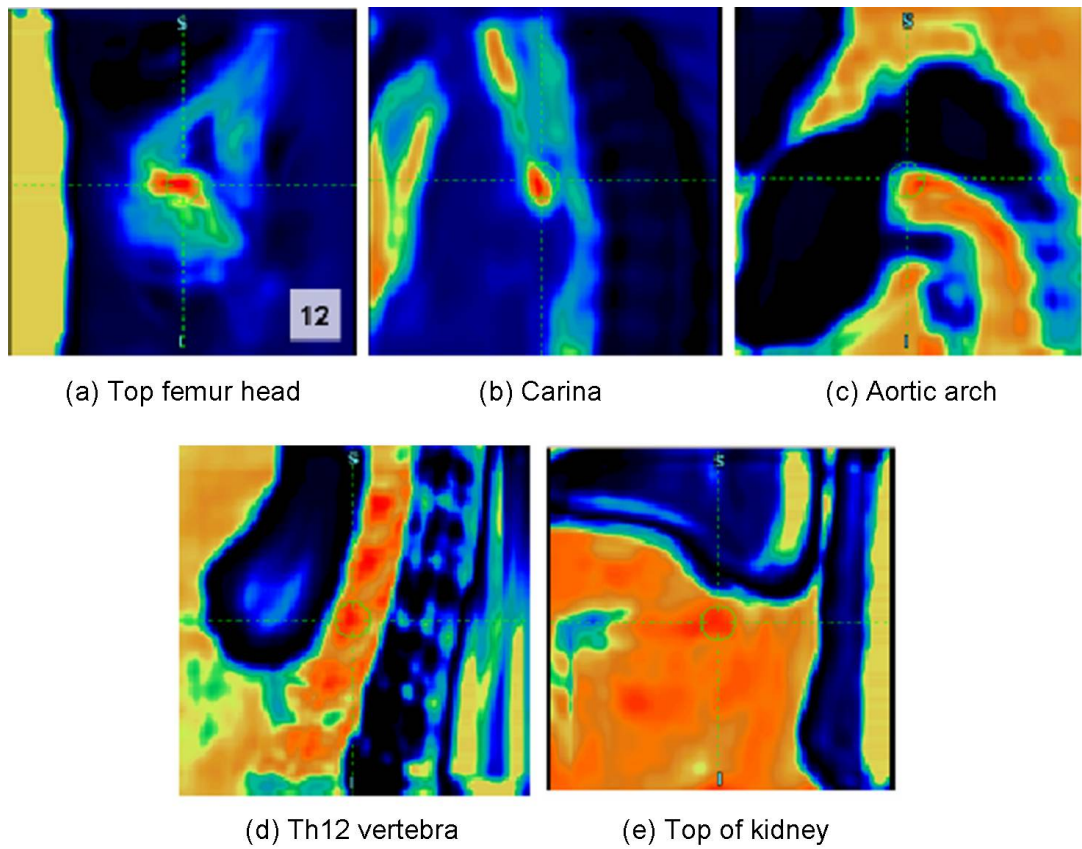


Figure 2.8: Example fiducial points probability maps of top femur head, carina, aortic arch, Th12 vertebra and top of kidney in sagittal view [41].

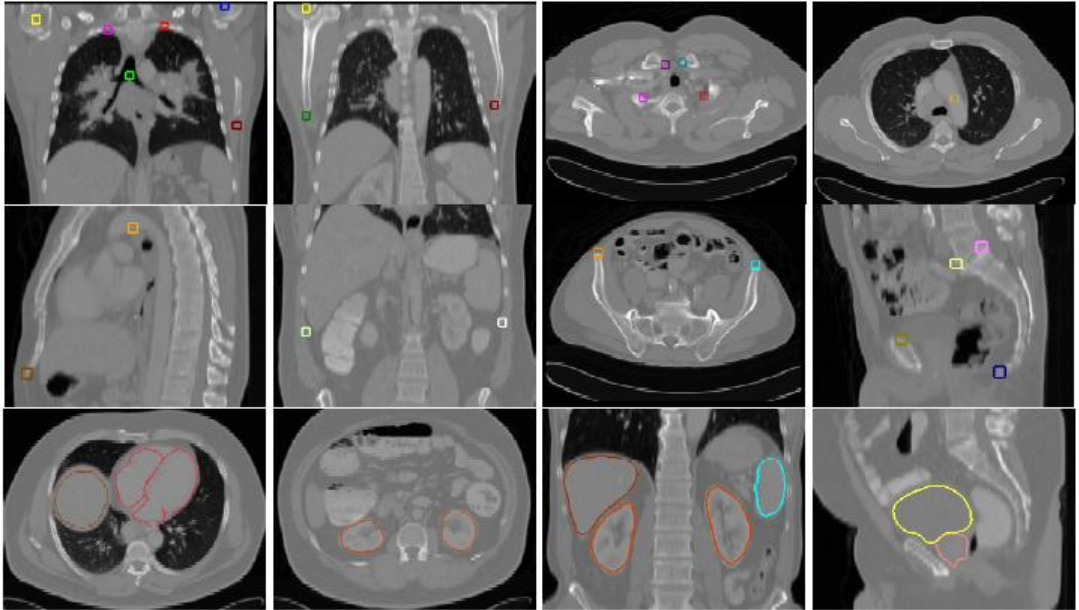


Figure 2.9: Example fiducial points and segmented anatomical regions: heart(red), liver(brown), kidneys(orange), spleen(light blue), bladder(yellow) and prostate (pink) [42].

regions across different images. Figure 2.10 depicts two images with 5 fiducial point correspondences. Based on these fiducial points, the two images can be aligned to one another; enabling anatomical space mapping between the two images.

2.4 Image Mapping Techniques

This section provides an overview of existing methods in image mapping using the following techniques: (1) ontology, and (2) image processing. The discussion focuses on ontology-based mappings using spatial relations and image processing-based mappings using fiducial points.

2.4.1 Ontology-based Mappings

An ontology consists of a list of domains and a set of spatial relationships between domains. The first step in mapping-based ontology is to segment the image according to its anatomical regions. Next, the regions are linked to the appropriate concepts in the atlas' anatomy ontology. Regions from two different images are then mapped according to the similarity of their spatial relationships. For example, if region $a1$ with relationships $a1$ is adjacent to $b1$, and $a1$ is adjacent to $c1$ then its equivalent region, $a2$, must be adjacent to $b2$ and $c2$. The integration of anatomical space can

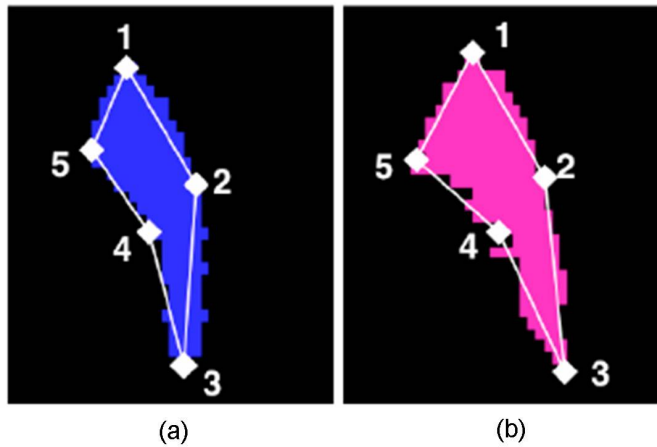


Figure 2.10: 2D illustration of image processing-based mapping with 5 fiducial point correspondences between the two images for anatomical space mapping.

then be achieved by linking between their respective anatomy ontologies.

The concepts of spatial relations have been employed successfully in ontologies by Bittner [32] and Rosse and Mejino [42] to describe anatomical space in the biomedical domain. In general, spatial relations between anatomical entities are described using relationships from the following categories:

Mereological relations describe the concept of parthood between the whole and its parts, e.g. finger is *part of* hand, hand is *part of* the arm.

Topological relations describe the concept of connectedness among entities, e.g. two entities are externally connected if the distance between them is zero and do not overlap. For example, in humans major parts of the joint, e.g. the synovial cavity, is externally connected to the synovial membrane [32].

Location relations describe the concept of relative location between entities that may coincide wholly or partially without being *part of* one another, for example, the brain is located in (but not *part of*) the cranial cavity.

A heavily used spatial relation ontology is the OBO (Open Biomedical Ontologies) Foundry, which includes various life science disciplines such as anatomy, health, biochemistry or phenotype [43]. OBO enables the sharing of controlled vocabularies across different biological and medical domains. OBO consists of the Relations Ontology (RO), which models the types of relationships between entities. The Relations Ontology (RO) is used to distinguish relationships between the types of entities. Relations such as *is_a* and *part_of* are used to model foundational relations. Relations such as *located_in*, *contained_in* and *adjacent_to* are used to model

connecting entities in terms of relations between the spatial regions they occupy. Temporal relations such as *transformation_of*, *derives_from* and *preceded_by* are used to model connecting entities, existing at different times. Participation relations such as *has_participant* and *has_agent* may be used to model connecting processes to their bearers.

This thesis focuses on the ability of topological relations to describe anatomical space in the biomedical domain, particularly on adjacency, discreteness, and connectedness relations. Two entities are described as being *adjacent* when they are close but not connected. *Discrete* entities are not connected. If two entities have a common anatomical space, such that they partially coincide or are externally attached to one another, they are said to be *connected*. The relations *located_in*, *contained_in* and *adjacent_to* as defined in the Relations Ontology (RO) can be adopted within this work to describe the location of an anatomical entity in space with respect to other entities. Such relations allow conceptualisation of anatomical space, thus facilitating the mapping of corresponding regions across images.

Nevertheless, images often contain ambiguous regions. These regions may be isolated or disconnected from the rest of the image. The limitation of topological relations (such as *located_in*, *contained_in*) as used in RO is that these relations cannot be used to model relative positions of ambiguous anatomical regions. The relation *adjacent_to* can model adjacency between two anatomical regions that are located very close to one another. However, as for anatomical regions that are isolated or disconnected, such that the relative position involving these regions cannot be described as adjacent because of distance constraints, more investigation is required.

Mechouche *et al.* [44] proposed an ontology to describes the sulci and gyri of the brain cortical structure using spatial relations of the following terms: *anteriorTo*, *posteriorTo*, *superiorTo*, *inferiorTo*, *lateralTo* and *medialTo*. Hudelot *et al.* [45] proposed an ontology to describe the brain cerebral by implementing spatial relations of the following terms: *right_Of*, *left_Of*, *close_to*, *very_close_to*, *external boundary* and *internal boundary*. Du *et al.* [46] proposed a method involving topological and directional relations to define some natural language spatial relations. They proposed the following directional natural-language terms: *EP* to denote natural language *east part of a region*, *WP* to denote natural language *west part of a region*, *SP* to denote natural language *south part of a region* and *NP* to denote natural language *north part of a region*. These sources demonstrate that the recognition of spatial entities depends on the entities' spatial relationships in an image.

Chang and Wu [47] proposed a technique known as a 9DLT matrix, which applies

nine directional codes to represent spatial relationships. They define directional code as follows: 0 to denote *east*, 1 to denote *northeast*, 2 to denote *north*, 3 to denote *northwest*, 4 to denote *west*, 5 to denote *southwest*, 6 to denote *south*, 7 to denote *southeast*, and 8 to denote *equal*. A single triple (x, y, r) denotes a spatial relation between two spatial entities. The two spatial entities are represented by x and y . The directional code is represented by r . For example, a single triple $(A, B, 0)$ represents that an entity A is to the east of an entity B . Subsequently, a set of triples represents an image. Two images are then mapped according to the similarity of their spatial relationships based on the corresponding set of triples. However, the 9DLT matrix has a significant drawback under rotation of direction. Assuming that a mapping is performed between two identical images, where the first image is a 90-degree rotated version of the second image, although these two images represent the same image, according to 9DLT matrix, the two images do not match, their corresponding sets of triples being completely different due to the 90-degree rotation of direction.

Guru and Punitha [48] proposed addressing the limitation of the 9DLT matrix by modelling directional relations between two spatial entities using a directed line segment. A directed line segment is a line joining two distinct entities. For example, the line joining the entity x to entity y becomes the line of reference, and the corresponding direction from entity x to entity y becomes the direction of reference for the image. Their approach computes the direction of the line joining x to y using Euclidean distance prior to obtaining the direction of reference. The relative pairwise spatial relationships between each pair of entities are perceived with respect to the direction of the line of reference. In order to make the system invariant to image transformations, the direction of reference is conceptually aligned with that of the positive x-axis of the coordinate system. The proposed improvement method by Guru and Punitha [48] successfully overcomes the deficiency in the 9DLT matrix; however, the method only covers directional information, which means topological information is lost.

Karouia and Zagrouba [49] proposed representing spatial relationships between two spatial entities of an image using entity relative positioning vectors. The set of these vectors provides information about the disposition of different entities of the image. This approach defines this disposition based on five component vectors. These vectors include positioning degree on the left, on the right, on top, below and of inclusion. Each of these elements expresses a degree of positioning by a numeric value between 0 and 1. This method is intended to represent images containing only isolated entities. Hence, information on topology is not required, so the approach

does not contain any concept of connectedness among spatial entities.

Zhou *et al.* [50] proposed a method called Augmented Orientation Spatial Relationship (AOSR) to describe a range of directions between two spatial entities of an image. Assume that two images $C1$ and $C2$ both have the same entities x and y , however, the relative distance between these entities in both images is different. If one simply says for image $C1$, entity x is at the *northeast* of entity y (according to the centroid of x and y), then there will be no difference between entities x and y in image $C2$. Therefore, the focus of AOSR is capturing the relative distance between spatial entities prior to describing the directional relations between them. Although topological information is also not covered in AOSR, Zhou *et al.* [50] claimed that the approach may simply be combined with Egenhofers topological representation, to cover topological information.

Kulkarni and Joshi [51] and Majumdar *et al.* [52] proposed a method, which combines both topological and directional relations. However, their method does not capture the notion of distance between spatial entities, such that there is no difference between two entities which may be quite near or far to one another.

Wang [53] proposed a method of using spatial operator Σ to capture the interval between the minimum bounding boxes of two spatial entities. This method apparently removes the precise spatial description, between entities. The operator indicates there is a space between the two entities that could be either disjoint, near or far. A description such as $\Sigma femur \Sigma metanephros \Sigma$, provides the spatial knowledge that *femur* and *metanephros* are disjoint, but leaves uncertainty as to whether these two spatial entities are near to or far from one another.

Yang and Zhong [54] proposed an image representation structure using a Mixed Graph Structure (MGS). They demonstrated their method on medical images. The method first extracts spatial entities as primitives. These spatial entities are then organised into a mixed graph structure according to their spatial relations. The approach uses only two types of spatial relations, which are *inclusion* and *adjacency*.

Overall, most image description and mapping approaches in [48; 50; 53] use spatial relations of entities in an image. The method in [51; 52] accounts for both topological and directional relations of spatial entities. The approaches in [49; 52; 54; 55] represent images as graphs. The graphs conceptualise spatial relations between entities and then solve the mapping as a graph-matching problem.

The approach proposed in this thesis should improve previous work by addressing many of the limitations. For example, some of the mapping approaches presented in this section used only one category of spatial relations, either topological or directional relations. Using only topological relations, spatial information regarding

direction will be lost. Likewise, using only directional relations, spatial information on topology will be lost. Consequently, using only one category of spatial relations may limit the descriptive power of a mapping algorithm. Combining the two categories of spatial relations (i.e. topological or directional relations) may be sufficient to capture wider spatial information. Nevertheless, images often have ambiguous regions that are isolated or disconnected from the rest of the image. Even by combining the two categories of spatial relations, the problem still arises as to how to capture spatial information for these isolated regions. For example, using topological relations to describe isolated regions using *disjoint* relation does not capture relative position between these regions. Although spatial information for these regions can be captured using directional relations, these regions could be affected by rotation direction. Rotation direction has a significant impact on object recognition because directional relations for a region differ according to position. These limitations are addressed by the proposed approach. Chapter 3 presents the proposed approach in detail.

2.4.2 Image Processing-based Mappings

There are several image processing algorithms which perform mapping based on fiducial points. Izard and Jedynak [56] described a registration algorithm, which employs a Bayesian approach to detect these points. First, the algorithm measures the intensity distribution of each pixel in the source image in order to detect the fiducial points. To ensure an affine transformation mapping the source image onto the target image, given a set of fiducial points, each target image is searched for the fiducial points that are mapped onto the same location.

Khaissidi *et al.* [57] proposed a feature-based, fully non-supervised methodology dedicated to fast medical image registration using the Hough Transform algorithm. First, the fiducial points are extracted from both images. Then, the Hough Transform algorithm provides a rigid transformation, which allows information transfer between both images in order to align these images based on the point correspondences. Guest *et al.* [58] proposed the use of a Gaussian-based algorithm to achieve a similar outcome. The algorithm calculates the point correspondences between images by determining the sensitivity of a correspondence to movement of the point being matched.

Wong and Orchard [59] proposed an image registration algorithm which extracts points of interest from only one of the two images. For each point of interest, the other image is exhaustively searched to find its best-matching location, in hopes of

matching the two compared images.

Park *et al.* [60] described an affine estimator registration approach. First, the algorithm extracts an arbitrary number of invariant points that latch onto significant structural features in both images. Next, each estimated invariant point is refined by taking the phase-gradient information into account. Finally, the source and the target images are matched based on these points.

The image processing algorithm, called ASIFT as proposed by Yu and Morel [61], performs mappings based on similar points of interest in the compared images. Similar points of interest are first detected between images by measuring the transition tilts based on the amount of distortion, followed by selecting a region around each point prior to establish mappings. Two images are then mapped onto one another by aligning pairs of corresponding points in each image.

Zeng *et al.* [62] proposed a topology-cuts algorithm to detect point of interests at the boundaries of image features. Since the anatomy of human tissues provides important topological constraints that ensure the correctness in biomedical image segmentation, the approach incorporates topology priors as global constraints. First, the algorithm labels each point to explicitly handle the topology constraints. Next, a distance map is created to record the points that are closest to the boundary. Finally, a bucket priority queue data structure is used to record the points of equal distance and also to efficiently extract the point with minimal distance value. Mapping between objects in two images is then performed based on these points.

2.5 Similarity Measures

The definition for best match criteria is particularly crucial in any mapping algorithm. Since anatomical structures exist at different ranges of scale, arrangement and position, there is the possibility that an exact copy of the location corresponding to the query region in one image is unavailable in another image. Therefore, there is a possibility of error (mismatch) in the corresponding mapped location. Thus, a search for the locations of best match is appropriate.

A similarity measure is a function to determine the degree of similarity between pairs of images. Under image retrieval perception, ranking the most similar image to the query image uses the similarity measure function. The higher the similarity measure, the more similar the two images will be. When applied to image mapping, given two anatomical regions, a similarity measure determines the extent to which one anatomical region matches another. The following sections discuss two similarity measures: Hausdorff distance and Overlay distance.

2.5.1 Hausdorff Distance

Hausdorff distance is a way to measure the similarity between two images [63; 64]. The function computes the extent of the distance to which each point of a region set lies near some points in an image and vice versa. The distance determines the degree of equivalence between two spatial entities. Thus, an estimation of similarity between two images may be determined based on distance computation. The smaller the distance between the two compared images, the more similar the two images are. Given two finite point sets $A=\{a_1, \dots, a_p\}$ and $B=\{b_1, \dots, b_q\}$, the Hausdorff distance is defined as follows:

$$H(A, B) = \max(h(A, B), h(B, A)) \quad (2.1)$$

where

$$h(A, B) = \max_{a \in A} \min_{b \in B} \|a - b\| \quad (2.2)$$

The Hausdorff distance $H(A, B)$ is the maximum of $h(A, B)$ and $h(B, A)$. Thus, it measures the degree of mismatch between two sets by measuring the distance of the point of A that is farthest from any point of B and vice versa. Intuitively, if the Hausdorff distance is d , then every point of A must be within a distance of d from some point of B and vice versa. Thus the notion of resemblance encoded by this distance is that each member of A be near some member of B and vice versa. To compute the Hausdorff distance for anatomical regions in images, the first step is to determine how to associate a point set with an anatomical region. One way to carry this out is to define this point set as the points that lie on the boundary of an anatomical region. However, computing the distance between point sets that consist of an unlimited number of points is quite expensive [65]. Another option to compute the similarity based on distance is the use of the Overlay distance.

2.5.2 Overlay Distance

The Overlay distance measures the similarity between two objects based on the degree of overlap between the two objects [65]. The Overlay distance $D_{Overlay}(I_1, I_2)$ between objects I_1 and I_2 is defined as:

$$D_{Overlay}(I_1, I_2) = 1 - \frac{Area(Intersection(I_1, I_2))}{Area(Union(I_1, I_2))} \quad (2.3)$$

Measuring the similarity between two anatomical regions can then be carried out by computing the degree of their overlap based on the Overlay distance function. $Area(Intersection(I_1, I_2))$ denotes the area of the actual region in one canonical image. $Area(Union(I_1, I_2))$ denotes the area in another image, which corresponds to the mapped location for the query region.

2.6 Representation of Spatial Rules

This section presents the formal logic for representation of spatial rules created in this thesis. The thesis proposes to use the first-order predicate logic in order to define the set of spatial rules. The purpose of such spatial rules is to determine corresponding regions across images.

2.6.1 Predicate Logic

Predicate logic has overcome the limited expressive power of propositional logic to encode the declarative statement [66]. Propositional logic is a sentence with components such as *not*, *and*, *or* and *if-then* and does not cover the logical aspects of universal quantification, such as a statement is true for everything, or a statement is true only for a certain thing, for example, the declarative statement [66]:

Not all birds can fly

Propositional logic is not able to represent the properties in this statement and their logical relationships, dependencies and truth. In contrast, predicate logic is capable of determining the relationship that exists between the objects and properties in this statement. Predicate logic (also called first-order logic) can be used to represent correlation between these properties that can be true or false. Two identified properties for the sentence are x is a bird and x can fly. The variable x is used to replace the bird's name, and quantifiers \forall and \exists to describe the notion of all and there exist in the statement. The statement can be represented as follows:

$$\neg(\forall x(B(x) \rightarrow F(x))) \tag{2.4}$$

Alternatively, the above statement may be rephrased as it is not the case that all things, which are birds, can fly, which gives the same meaning. This can be represented as follows:

$$\exists x(B(x) \wedge \neg F(x)) \tag{2.5}$$

2.6.2 Spatial Rules

The formation of the proposed spatial rules consists of a set of terms and formulas of first-order logic. These terms and formulas are a string of symbols, which comprise of variables, logical connectors and quantifiers. This thesis uses lower-case letters (e.g. x, y, z) as variables to denote individual spatial regions and upper-case letters (e.g. C, P, PP) as variables to denote functions or spatial relations. The logical connectors ($\neg, \wedge, \vee, \rightarrow, \leftrightarrow$) have their own definitions (not, and, or, if-then, and if and only if (iff), respectively). Given two statements $S1$ and $S2$, the statement $\neg S1$ is true if and only if $S1$ is false. The statement $S1 \wedge S2$ is true if both $S1$ and $S2$ are true; if both are false, the statement is false. The statement $S1 \vee S2$ is true if $S1$ or $S2$ (or both) are true; if both are false, the statement is false. $S1 \rightarrow S2$ means if $S1$ is true then $S2$ is also true; if $S1$ is false then nothing is said about $S2$. $S1 \leftrightarrow S2$ means $S1$ is true if and only if $S2$ is true. The symbol \equiv denotes a definition. The logical quantifiers (\forall, \exists) have their own quantifiable purpose. $\forall x$ denotes universal quantification for all x . $\exists x$ denotes existential quantification there is at least one x . The formation of spatial rules can be found in Chapter 3 of this thesis. A full exposition of spatial rules formation for biomedical domains can be found in the literature [27; 32].

2.7 Woolz Image Processing

The MRC Clinical Population and Cytogenetics Unit, now known as the Human Genetics Unit, developed the woolz image processing software [67]. The software comprises a java library, implemented in C, and the object store, implemented in C++ [68]. This java library (also called the woolz library) comprises interval coding functions for image processing operations such as set operations (e.g. union, intersection, difference), morphological operations (e.g. dilation, erosion) and domain operations (e.g. segmentation, labelling).

The scope of the thesis is within the 2D image space. Therefore, the thesis proposes to use woolz image processing because of the efficiency of the woolz library to perform various image processing operations on 2D image space. The 2D image space corresponds to a woolz object.

2.7.1 Woolz Objects

The woolz image processing includes both 2D and 3D woolz image structure. According to Baldock [69] the "3D image structure in woolz is a simple extension of

the 2D structure. In 2D an image (one of a number of possible woolz objects) is defined over an arbitrary region of a discrete 2D space with coordinates (k, l) where k is the column coordinate and l is the line coordinate. For each line in the image there is a list of intervals which give the start and end points of the image along that line. There is a list (possibly empty) of intervals for each line. It is clear that an arbitrarily complex region of the discrete space can be defined in this way. It is assumed that the discretisation in the x and y directions is at fixed regular intervals, constant in both directions but not necessarily equal. The 3D structure is simply a stack of 2D images again with the constraint that the planes are evenly spaced and that within the plane bounds there must be a 2D image for every plane, although the image could be the empty set. The plane coordinates are defined to be p . Figure 2.11 depicts a 3D image structure in woolz. A section view through this 3D image space corresponds to the 2D image space [70]. The 2D image space has values

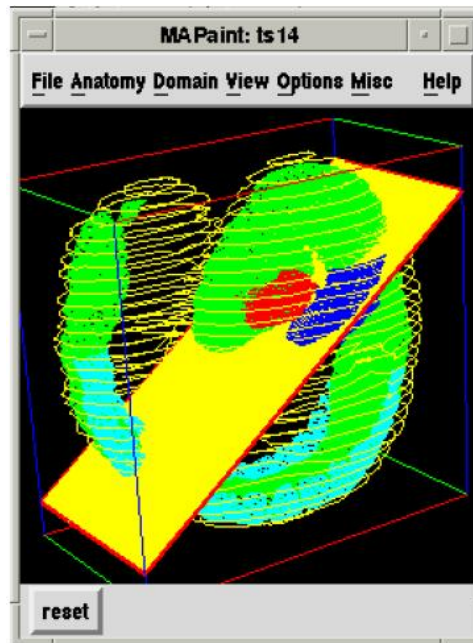


Figure 2.11: A 3D image structure in woolz [71].

selected by traversing a plane that cuts through the 3D image space. Figure 2.12 depicts an image in 2D. One of a number of possible woolz objects can be defined over an arbitrary region of a discrete 2D space with coordinates (k, l) , where k is the column coordinate and l is the line coordinate. This arbitrary region in 2D can be saved into a woolz object by using the MAPaint software [69]. MAPaint is a 3D painting program based on the woolz image processing library. The software allows the definition and saving of arbitrarily complex 2D spatial domains by painting over the appropriate region. The basic idea of painting is for image segmentation. The

purpose of segmenting an arbitrary region is to partition a 2D image space into multiple segments. The result of image segmentation is a set of regions that collectively cover the entire image. Each region can be saved into a woolz object. A

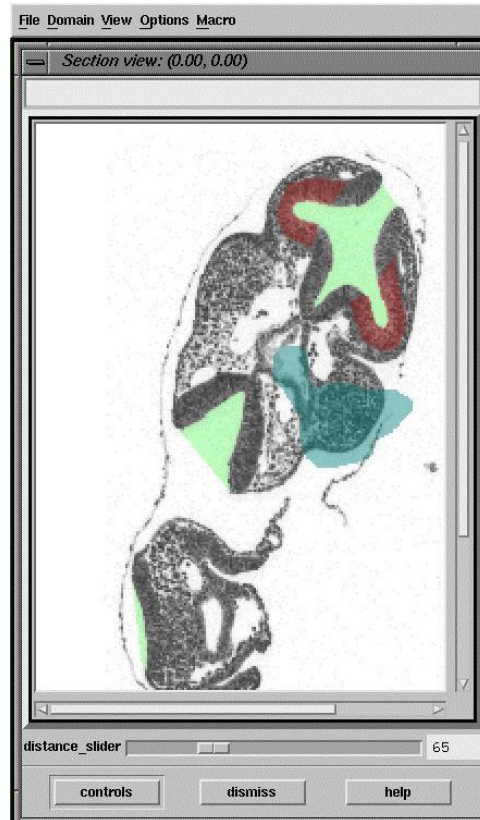


Figure 2.12: An image in 2D. The image corresponds to a section view through a 3D image space. One of a number of possible woolz objects can be defined over an arbitrary region of a discrete 2D space. The arbitrary region can be defined and saved into a woolz object by using the MAPaint software. Each woolz object corresponds to a discrete region of 2D space and has a coordinate (k, l) , where k is the column coordinate while l is the line coordinate [71].

woolz object consists of two structures: domain and values. The domain represents the name of the space region corresponding to the values and an arbitrarily complex region of 2D space. The values represent a set of coordinates corresponding to the location at each point in the domain.

2.7.2 Woolz Library

The woolz image processing system provides interval coding functions for processing woolz objects. In particular, focus is on image processing functions for computing set operations. To name a few, there are *WlzArea*, *WlzBoundingBox*, *WlzDilation*,

WlzDiffDomain, *WlzHasIntersect*, *WlzIntersect*. The *WlzArea* function calculates the area of the input 2D woolz object. The *WlzBoundingBox* function calculates the bounding box coordinate of the input woolz object. The *WlzDilation* function can perform dilation to a domain woolz object. The *WlzDiffDomain* function calculates the difference of the input woolz objects. The *WlzHasIntersect* function can test for a non-zero intersection between the input woolz objects. The *WlzIntersect* function calculates the intersection of the input woolz objects. A more detailed list for the woolz library can be found in [71]. The capability of the library for processing woolz objects to conduct sets operations, morphological operations and domain operations between the woolz objects is the main reason for using the system. A full exposition of woolz image processing system can be found in the literature [72; 73; 74; 75].

2.8 Image Mapping Problems Overview

This section provides an overview of image mapping problems and explains how existing solutions may be used to deal with these issues. Here, we use the words *mapping* and *matching* interchangeably.

2.8.1 Image Mapping Classification

There are two categories of image mappings, as depicted in Table 2.1. The first case involves a single query image and a set of potential target images and the matching process should return those images from the target set that match the query image by some notion of equivalence. The second case is given a drawn query region in one image, find the corresponding region in another image that matches the query region. Either of these cases can be classified into two sub-cases. The first sub-case is the images with painted domains. The second sub-case refers to images with no painted domain.

Table 2.1: Image Mapping Cases

Mapping Cases	Image Domains
1) Find a matching image	Painted
	Not painted
2) Find a matching region	Painted
	Not painted

2.8.1.1 Image Matching vs Region Mapping

Figure 2.13 depicts the visual example of mapping one query image and a set of potential target images. The query image is the midline image of an embryo. The

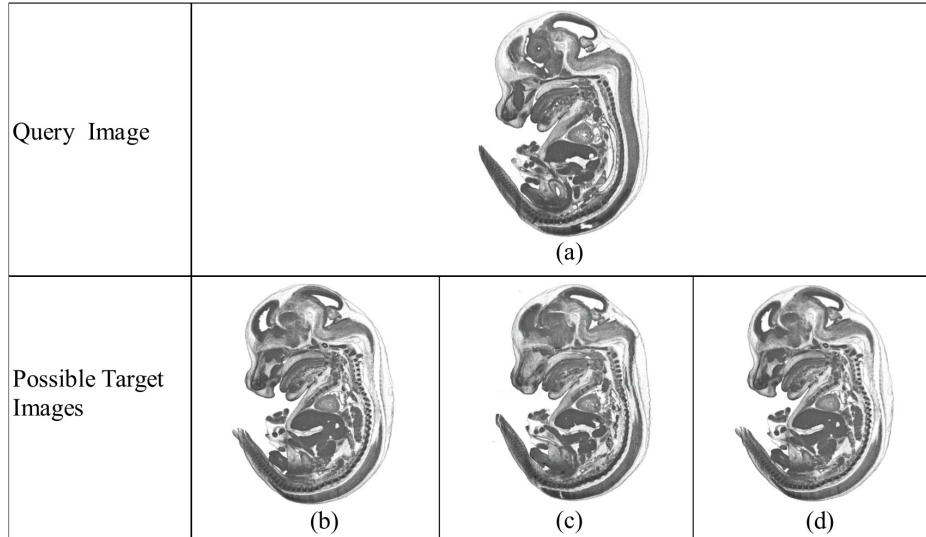


Figure 2.13: The mapping of (a) one query image (i.e. the midline image of an embryo) onto three potential target images: (b) the image slice at 0.100mm distance from midline, (c) the image slice at 0.200mm distance from midline, and (d) the image slice at 0.300mm distance from midline.

target images are the image slices near to the midline. These images are similar, just not identical in their morphologies. However, in principle they should match. Figure 2.14 depicts the visual example of image region mappings. The *liver* in Figure 2.14(a) is drawn as the query region. This query region has the following possible result regions as highlighted in Figure 2.14(b) to (d). These *livers* are different in their morphologies, but are the biologically meaningful matching areas.

2.8.1.2 Image Segmentation

Image segmentation involves breaking an image down into its basic components or regions. Before we can use the anatomy ontology to label the painted domains, we must perform image segmentation. The common methods of image segmentation are segmenting an image based on colour, boundary and shape. (Here we use the words *painted* and *segmented* interchangeably). The term *paint* denotes a technique of drawing on an image region. The purpose of painting is to tag a region according to an anatomy ontology. MApaint software provides the painting mechanism. This has been discussed in Section 2.7.1. Figure 2.15 depicts an embryo image which

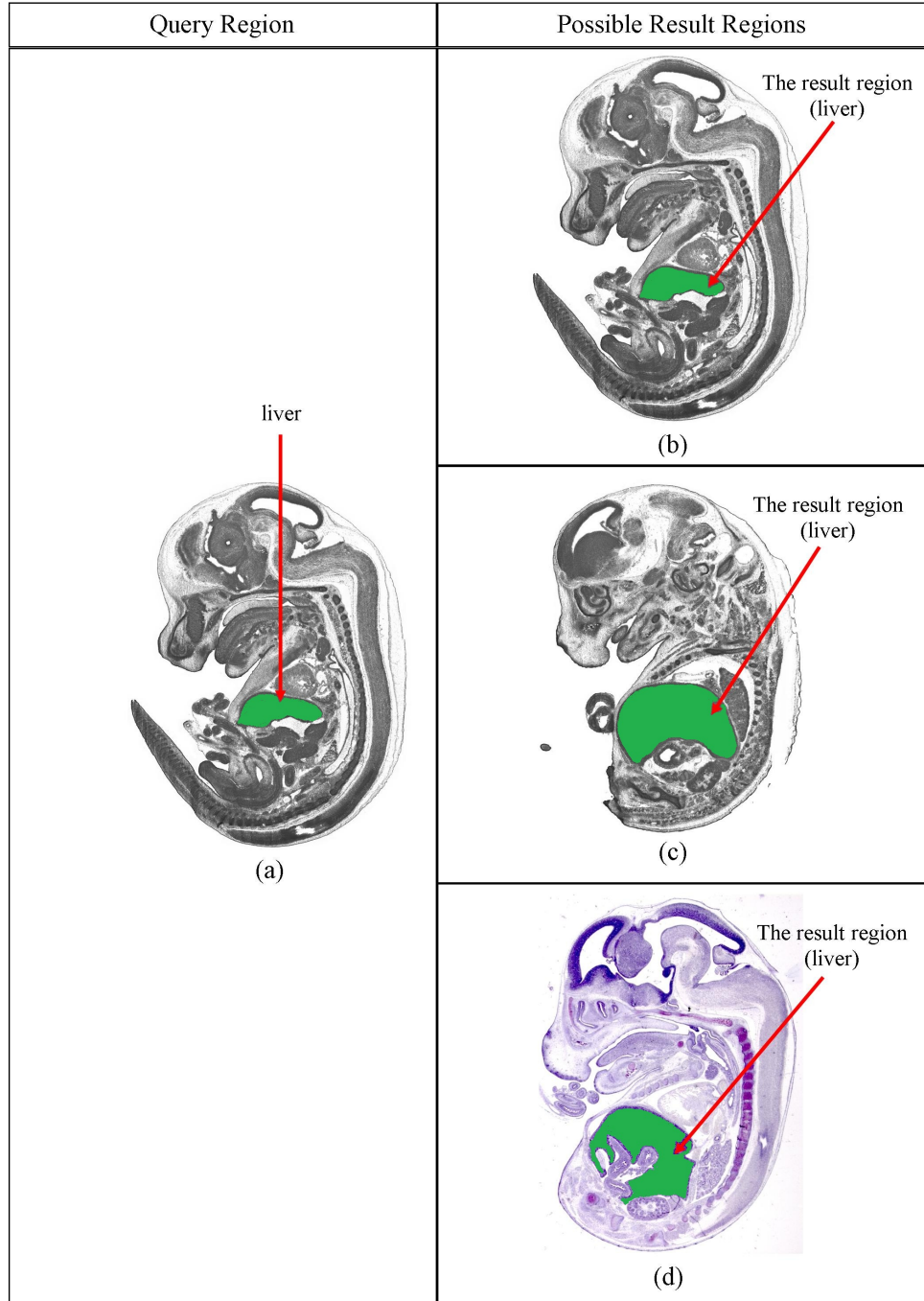


Figure 2.14: The mapping of region *liver* from (a) the midline image onto the following possible result regions: (b) the *liver* in an image with exactly the same morphology (i.e. identical images), (c) the *liver* in an image with a different morphology (i.e. the image slice near to the midline), and (d) the *liver* in another example of an image with a different morphology (i.e. the image of a different embryo at the same developmental stage).

has been segmented (painted) into 49 regions. Each region is labelled using its anatomical name.

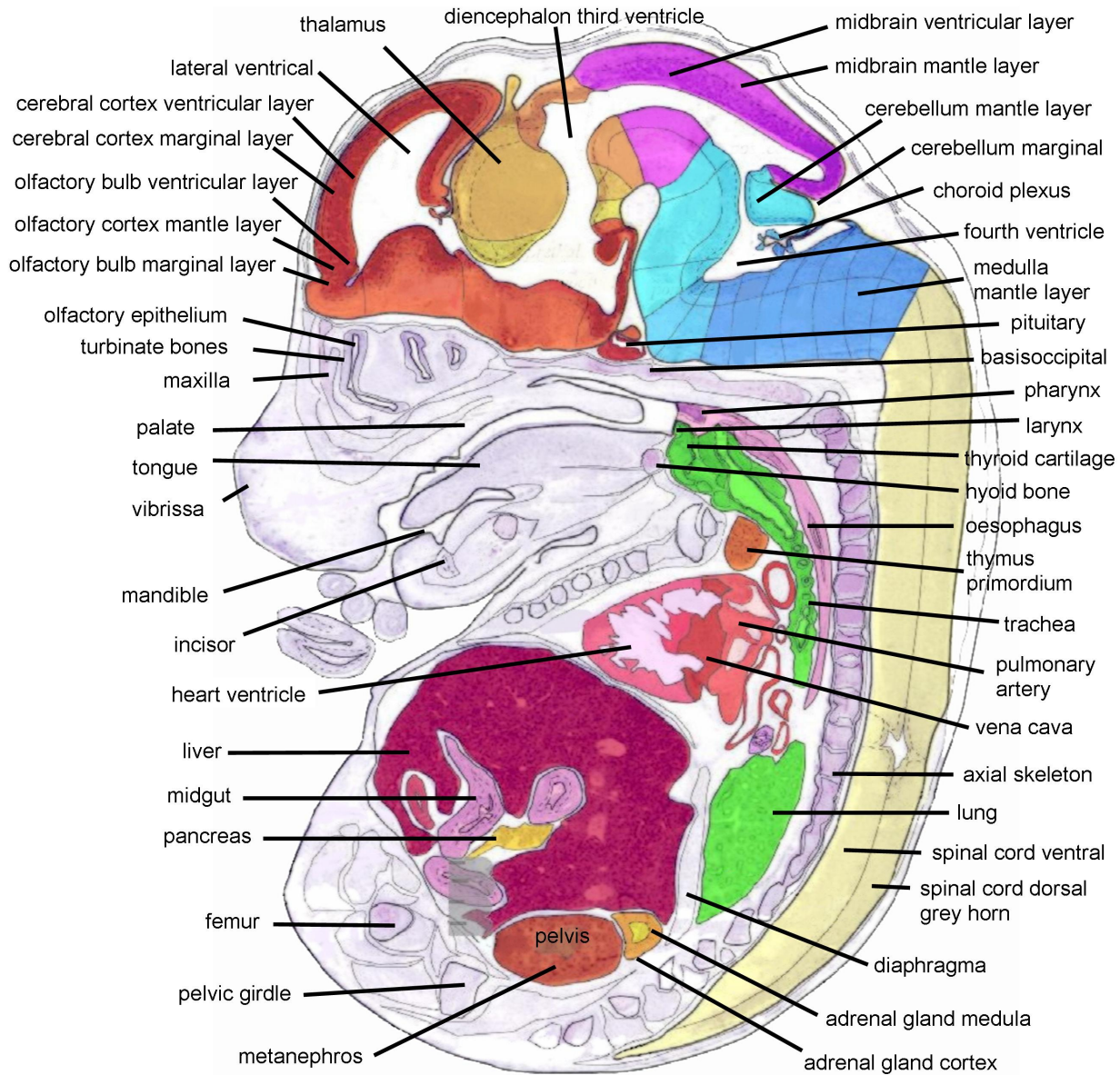


Figure 2.15: The image consists of 49 segmented regions (painted domains) and is labelled according to the anatomical names.

2.8.1.3 Variation of Morphology

In general, the two cases of image mappings can be carried out between images that have exactly the same morphologies, as well as between images that have different underlying morphologies. Morphology concerns the different formation of a particular anatomical structure in terms of scale, orientation and position.

Figure 2.16 depicts two image slices of an embryo. These images are good representatives for non-identical images with different morphologies. Both images have the following structures: *liver*, *heart*, and *lung*. However, these structures are different in terms of their scales and positions. For example, in terms of scale, the *liver* in Figure 2.16(a) appears slightly smaller compared to the *liver* in Figure 2.16(b). In terms of position, the *heart* in Figure 2.16(a) is located above the *liver* and the *lung*. In contrast, the *heart* in Figure 2.16(b) is located between the *liver* and the *lung*.

Figure 2.17 depicts two images of an embryo across different visual domains. The image in Figure 2.17(a) is the clip art graphic version of the image in Figure 2.17(b). The visual content of both images is similar at the higher scene level, but both images are entirely different at the pixel-level. These images are a good representation of non-identical images with the same morphology. Although the two images are dissimilar at the pixel-level, both images are morphologically the same set of structures in terms of their scale, orientation and position.

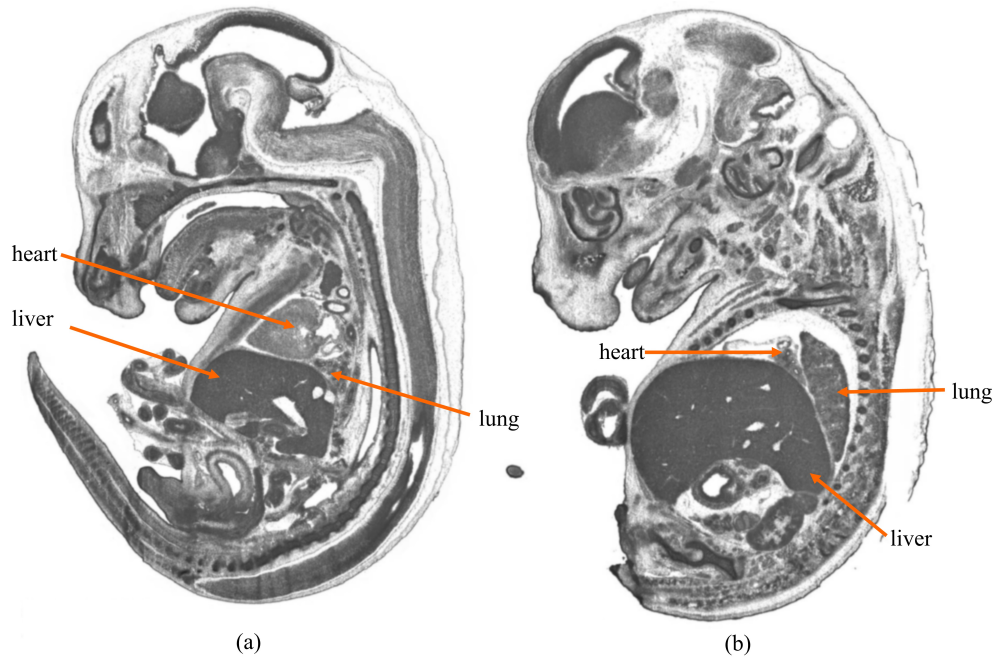


Figure 2.16: Two non-identical mouse embryo images with the same structures: *liver*, *heart*, and *lung*. However, these structures are different in their morphologies.

2.8.1.4 Criteria for Matching Images/Regions

In a case in which images are lacking painted domains, the criteria to consider whether two images match or two regions match can be based on the equivalence of

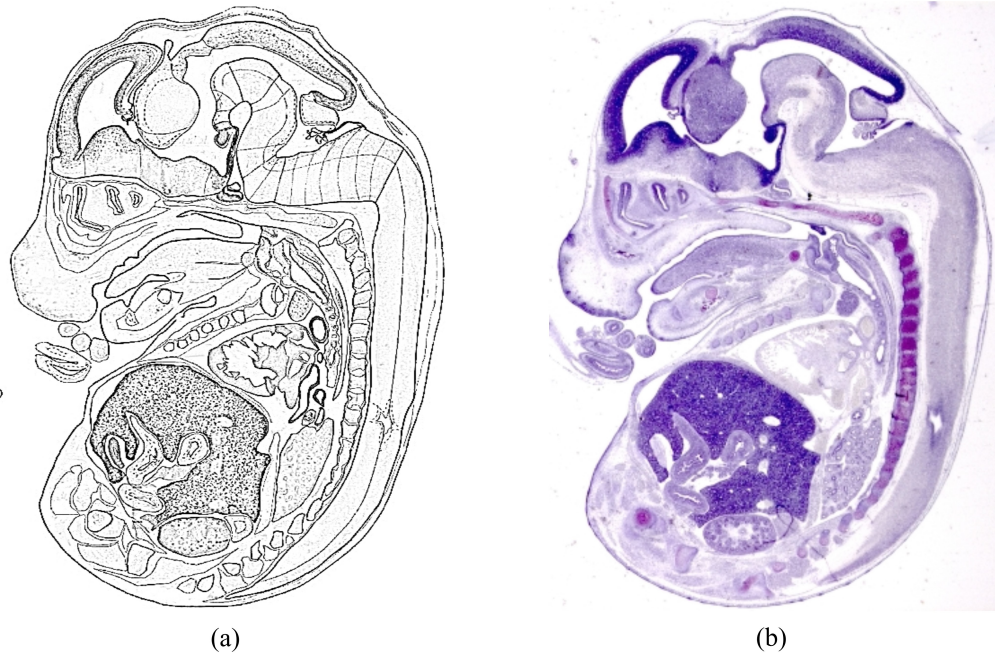


Figure 2.17: Two non-identical mouse embryo images with morphologically the same set of structures in terms of scale, orientation and position. The visual content of both images is only similar at the higher scene level: both images are entirely different at the pixel-level.

their low-level image features. Commonly extracted features include colour, texture and shape. These low-level image features can either represent a whole image or a specific region. A notion of equivalence is quantified using either the combination of several low-level features or making use only of a particular feature.

Colour information can be extracted from an image and represented as a colour histogram [76; 77]. A global colour histogram can be used to define the number of pixels that have colours in each of a fixed list of colour ranges for a whole image. Two images match when their colour histograms match. Similarly, image region matching can also be performed using colour histograms. A local colour histogram can be used to define the colour information for a specific region of an image. An image can be divided into several regions and a colour histogram can be created for each region. Two regions match when their local colour histograms match.

Texture is defined as properties related to the appearance and feel of a surface. It can be categorised into two types. The first is stochastic, meaning rough, grainy and irregular; the second is structural, or having a regular and smooth surface. The main characteristics of the texture are distinctive and repetitive over a region. Texture features are useful in the comparison of equivalence between two images. The equivalence between two images can be compared on the basis of texture match-

ing. Texture matching is performed by extracting the texture features from the images and the images are segmented into regions; each containing a homogeneous texture pattern [78; 79]. Two images match or two regions match when they are homogeneous in terms of their texture patterns.

Shape matching is performed by comparing the region-based edge features. Edge features extracted from images are considered as point sets. For a point on the first image, it is expected to find the best matching point on the second image according to the edge features. Two images match when their feature point correspondences match. Similarly, image region matching can also be performed by comparing the region-based edge features. Edge features extracted from one specific region are considered point sets. A region matches another when a point on a region in one image is found on the region in the other image, according to the edge features.

In the case of images with painted domains, the criteria to consider whether two images match or two regions match can be based on the equivalence of their high-level semantic classifications based on the painted regions; an image or a specific region in one image can be classified into categories which are intended to distinguish semantically meaningful differences [80]. Spatial knowledge representations are useful for describing the spatial relationships among the painted regions in an image. Commonly used spatial knowledge representation is the topological properties. Topological properties include the number of sub-regions and the relationships between the properties of the sub-regions and the regions [81]. These topological properties are examples of meaningful semantics which may be derived from the content of an image. For example, if a structure is seen, it can be connected to some previously learned spatial concepts (e.g. lies to the right of the *stomach* and overlies the *gallbladder*), which can be used to recognise that this structure is a *liver*. Besides spatial concepts, the types of shared semantic attributes which might describe common structure properties are such as parts of a structure (e.g. has four chambers, two superior atria and two inferior ventricles which can be used to recognise this structure is a *heart*), common materials (e.g. material with positive mass which can be used to recognise anatomical structures with positive mass, such as *liver* and *brain*), and common immaterial (e.g. material with no mass which can be used to recognise anatomical structures with no mass such as the *cavity of the stomach*).

In the context of finding a matching image, two images match when a region-matching scheme that integrates the semantic properties of all the regions in one image matches the semantic properties of all the regions in the other image. Similarly, in the context of finding a matching region, two regions match when the

semantic properties of a region match with the semantic properties of the other region.

Since the gene expression data in biomedical atlases are queried by painting or drawing arbitrary regions in the canonical images, this thesis focuses on image region mappings. Therefore, the case of mapping to find a matching image is not further explored in subsequent chapters because it was not a part of the dissertation. In general, there is no literature that provides the definition of criteria to determine if two regions match biologically. Within the context of this research, when the region mappings are between identical images, we used the Overlay distance to determine whether two regions match. The Overlay distance measures the similarity between two objects based on the degree of overlap between the two objects. The discussion on the Overlay distance is presented in Section 2.5.2. In the case of region mappings between non-identical images, we used the mappings from a biologist as the golden standard. The details are provided in Chapter 3.

2.8.2 Overview of Mapping Solutions

In general, image mappings can be carried out using image processing and ontology-based methods.

2.8.2.1 Image Processing-based Method

There are several examples of image processing algorithms that perform mapping based on fiducial points. These are proposed by Khaissidi *et al.* [57], Guest *et al.* [58], Wong and Orchard [59], Park *et al.* [60], Yu and Morel [61], and Zeng *et al.* [62]. Note that these algorithms have been described in Section 2.4.2. There is also one exemplary work on image processing algorithm, which makes use of semantic concepts. Liu *et al.* [85] presented an algorithm, which segments an image into different regions. Each region is extracted together with its low-level features. These features are linked to the semantic concepts obtained in a proposed decision tree-based learning algorithm. The matching algorithm combines both query by keyword and query by region of interest. However, this algorithm does not include the notion of fiducial points, which makes the method irrelevant to the scope of this thesis.

Note that only the image processing algorithms in [61; 62] are available with source codes and executable by us. Mappings resulting from using the image processing algorithm proposed by Yu and Morel [61] provides better accuracy compared to the algorithm proposed by Zeng *et al.* [62]. For this reason, we used the image

processing algorithm called ASIFT proposed by Yu and Morel [61] in order to perform the evaluation, results of which are summarised in Table 2.2.

Table 2.2 provides the two categories of image mappings, the different available data conditions and the criteria for a mapping failure resulting from using image processing-based solutions. The first case of mapping is to find a matching image. An image processing algorithm may provide the mapping of one image against another to determine whether the two images match, regardless of whether the image domains are painted or not. Since the image processing technique depends on a pixel-based system, therefore, this method does not require semantic knowledge of an image.

An image processing algorithm may not be able to cope with the mapping between images that are similar but not identical in their underlying morphologies. An exemplary case is when the mapping is between two midline images from two consecutive Theiler Stages of the same embryo. Different morphologies are represented with different pixel intensity distributions. Consequently, an image processing algorithm may have difficulty when the mapping is between images with large variations in pixel intensity distributions [59; 86]. This also applies to non-identical images that are not identical in their morphologies. An exemplary case is when the mapping is between midline images of different embryos at the same developmental stage.

An image processing algorithm may have difficulty coping with mappings between non-identical images with the same morphology. This is the case when the visual content of both images is only similar at the higher scene level, but entirely different at the pixel-level. These are the types of images taken across different visual domains, such as clip art graphics, photographs taken in different kinds of light, and sketches. Since the image processing technique relies on being a pixel-based system, this method may fail when two images have different pixel distributions.

The second case of mapping as depicted in Table 2.2 is to find a matching region. An image processing algorithm may have difficulty coping with mapping regions between images that are similar but not identical in their morphologies. Differences in morphologies and regions between two images can cause different

Table 2.2: The categories of image mappings, the different available data conditions and the criteria for a mapping failure resulting from using image processing-based solutions.

Mapping Cases	Image Domains	Criteria for a mapping failure
1) Find a matching image	Painted/ Not painted	Similar images but are not identical in their morphologies (e.g. the mapping between two midline images from two consecutive Theiler Stages of the same embryo).
		Non-identical images that are not identical in their morphologies (e.g. midline images of different embryos at the same developmental stage).
		Non-identical images with same morphology (e.g. images of an embryo across different image modalities).
2) Find a matching region	Painted/ Not painted	Regions in similar images but are not identical in their morphologies (e.g. the mapping between two midline images from two consecutive Theiler Stages of the same embryo).
		Regions in non-identical images that are not identical in their morphologies (e.g. midline images of different embryos at the same developmental stage).
		Regions in non-identical images with same morphology (e.g. images of an embryo across different image modalities).

pixel intensity distributions, with which the image processing technique is unable to cope. An exemplary case is when the regions are mapped between two midline images from two consecutive Theiler Stages of the same embryo. This also applies to non-identical images which are not identical in their morphologies.

Similarly, an image processing algorithm may have difficulty coping with the mapping of regions between non-identical images with the same morphology. The morphology of an animal can be represented in different sets of pixel distributions. This is the case when the visual content of both images is only similar at the higher scene level, but entirely different at the pixel-level.

Nevertheless, in the case of mapping a region from one image onto another where the two images have exactly the same morphologies, and these morphologies have exactly the same pixel intensity distribution, an image processing algorithm may provide image region mappings with good precision.

2.8.2.2 Ontology-based Method

Table 2.3 provides the two categories of image mappings, the different available data conditions and the criteria for a mapping failure resulting from using ontology-based solutions. It is the requirement of the ontology-based method that an image be painted according to its anatomical regions, and these regions are linked to specific terms in the ontology. Image mappings may use either the exact same ontology or different but aligned (mapped) ontologies.

In the case of finding a matching image using either the same or different ontologies, this method may find a match between the source and the target image if both images are painted according to their anatomical regions, both images have exactly the same number of regions, and these regions are linked to specific terms in the ontology. This applies to images with exactly the same morphology as well as images that are morphologically different.

In general, an ontology-based method may be unable to find a match between the source and the target image if both images have a different number of regions, or if dissimilar regions are segmented in both images. This applies in both cases either using the exact same ontology or using different, but aligned ontologies.

Table 2.3: The categories of image mappings, the different available data conditions and the criteria for a mapping failure resulting from using ontology-based solutions.

Mapping Cases	Image Domains	Morphology	Criteria for a mapping failure	
			Same ontology	Different ontologies
1) Find a matching image	Painted	Same	Mapping fails when images have a different number of painted regions, or dissimilar regions are painted in both images.	Mapping fails when images have a different number of painted regions, or dissimilar regions are painted in both images. Mapping also fails when there are terms associated with regions which cannot be mapped from one ontology to another.
		Different		
	Not painted	Same	An ontology-based mapping does not work if the images are not annotated with the ontological concepts.	
		Different		
2) Find a matching region	Painted	Same	Mapping is low in precision if there are regions painted in one image but not in the other.	Mapping is low in precision if there are terms associated with regions which cannot be mapped from one ontology to another. Mapping is also low in precision if there are regions painted in one image but not in the other.
		Different		
	Not painted	Same	An ontology-based mapping does not work if the images are not annotated with the ontological concepts.	
		Different		

In the case of mapping image regions using the same ontology, this method may provide a mapping with good precision if the regions being mapped are painted in both images and the ontology has a definition for this particular region. This applies to images with exactly the same morphology as well as images that are morphologically different.

In the case of mapping image regions using different ontologies, this method may provide a mapping with good precision if the regions being mapped are painted in both images, these regions have their definitions in the ontologies, and the term associated with each region can be mapped from one ontology to another one. This applies to images with exactly the same morphology as well as images that are morphologically different. In general, an ontology-based method may provide an image region mapping which is low in precision if the region to be mapped is visible in one image but not in the other. This applies in both cases, either using the exact same ontology or using different, but aligned ontologies.

As a conclusion, the approach proposed in this thesis should improve on existing techniques by addressing many of their limitations. For example, the ontology-based method requires the image to be painted according to anatomical regions. The proposed approach should not require the image to be painted in order to perform the mapping. Hence, mappings should work regardless of one region being segmented in one image and not in the other, or when one term is defined in one ontology but not in the other. In addition, the proposed approach should be able to perform mapping between images that are morphologically different. Hence, the mappings should work regardless of having varying orientation and position of the structure nor having a different number of regions in the two images. These are the issues with existing solutions. We demonstrated each of these issues using the mouse embryo images in the evaluation.

2.9 Summary

This chapter provides a literature review regarding image representation and mapping. In particular, it focused on the following approaches: ontology-based and image processing-based mappings. Ontology-based mappings may use spatial relations as the mapping primitive. Image processing-based mappings may use fiducial points as the mapping primitive. These two types of mapping primitives are able to guide the mapping of corresponding anatomical regions across images.

A background on spatial relations which can be distinguished between topological, metric, and directional relations, has also been presented. These spatial relations are useful to describe the location of anatomical space in an image. Related work on image representation and mapping, and the types of spatial relations that they employ, have also been discussed. In addition, we have demonstrated their deficiencies.

Furthermore, examples of well-defined fiducial points segmented by image processing algorithms have been presented. These fiducial points are useful for determining corresponding anatomical regions across images.

An overview relating to image mapping problems was then presented and how existing solutions deal with these issues has been discussed. Finally, areas for research and the problems to be addressed has been highlighted.

Chapter 3

Developing Spatial Description-Based Integration

3.1 Introduction

Requirements analysis involves the investigation, scoping and definition of a new mapping technique prior to the design and implementation of any new mapping approaches. In the case of the research project described in this thesis, the review of literature has shown that the existing image mapping techniques have several drawbacks. In addressing these drawbacks, research was conducted in five phases. The requirements analysis will thus be discussed in five phases.

The literature review has shown that the spatial relationships between entities are significant aspects in describing the location of spatial entities in an image prior to establishing an image mapping. Therefore, the first phase involves identifying the categories of spatial relations necessary to describe the location of anatomical regions in an image. The literature review has also provided evidence that fiducial points can help to identify anatomical regions that are present in an image. Therefore, the second phase involves identifying a new mechanism with fiducial points to describe the location of spatial entities in an image prior to establishing mappings. The third phase involves the study of a combined approach to identify the advantages of describing the location of anatomical regions using fiducial points and a set of spatial relations as well as spatial relations between segmented regions. The fourth phase discusses the final approach proposed, which is to be compared against the existing approaches discussed previously in the literature review in the evaluation chapter. Finally, the fifth phase describes manual mapping from a biologist to obtain a 'gold

standard'. The result is then used as the basis for evaluating the existing mapping techniques and the newly-developed technique.

3.2 Spatial Descriptions Based on Spatial Relationships between Segmented Regions

This section describes the proposed mapping approach in the context of finding a matching region using spatial descriptions based on spatial relationships between segmented regions. Many existing approaches of image mapping take into account the similarity of spatial relationships among spatial entities of an image. Spatial entities in an image are identified along with the spatial relationships among them to represent the image. Most image representation and mapping as proposed by [48; 50; 53; 87; 88] use spatial relations of objects in an image. Methods proposed by [51; 52] consider both topological and directional relations of objects. Work by [49; 52; 54; 55] represents images using graphs to conceptualise entities' spatial relationships and the mappings are resolved using graph matching. Spatial relations between entities are widely used in the process of identification of spatial entities. This has inspired the idea of image region mappings using anatomical regions' spatial relationships.

The first phase of the study involved the investigation and scoping of a new mapping technique, which is designed based on the following research question: What is the best set of spatial relations necessary to describe the location of anatomical regions in an image to guide the mapping of regions between images?

3.2.1 Design Rationale

This section presents the rationale of choosing the concepts of spatial relations explicitly for biomedical domains. More specifically, we explore closely the modelling of the mouse embryo domain. The analysis provides background knowledge of the proposed mapping approach, which relies on anatomical regions' spatial relationships.

3.2.1.1 Representation of Topology

To describe topological information for anatomical structures within the mouse embryo, we restrict these anatomical structures to be embedded in 2D space. These

include representations of anatomical structures of type material with appreciable mass, such as liver, heart, and kidney. A spatial region for an anatomical structure is enclosed in a Minimum Bounding Rectangle (MBR for short) in an image. An MBR is the smallest enclosing box of a region which can be described by x-y coordinate of the upper-left corner and by the x-y coordinate of the lower-right [89]. This information can be used to determine topological relations between two spatial regions. For that reason, eight topological relations between two spatial regions according to Egenhofer and Herring [30] have been adopted to represent spatial information concerning connectivity, disjointness and containment. These relations are referred to as *disjoint*, *partiallyOverlap*, *externallyConnected*, *inside*, *contains*, *coveredBy*, *covers*, and *equal*. Region Connection Calculus (RCC-8) uses a similar approach based on this set of eight binary topological relations to describe the topological relationships between two spatial regions [90]. Section 3.2.3 gives a definition for each of these topological relations.

3.2.1.2 Representation of Arrangement

For anatomical structures that are disjoint from one another, topological information does not capture the relative position between them. A spatial relation called an 'arrangement' was proposed by Tagare *et al.* [91] to describe part embeddings, which implement Voronoi modelling to capture spatial arrangement between disjoint regions. The Voronoi modelling is the nearest-neighbour map for a set of parts. It captures boundary information between disjoint parts based on triangulation between three Voronoi polygons [92]. The critical issue in implementing Voronoi is to capture the spatial arrangement between disjoint anatomical regions within the mouse embryo and decide which boundaries are to be preserved to form the boundary triangulation. This is dissimilar to Tagare *et al.* [91] who implemented Voronoi modelling to describe arrangement. We proposed to include the relation *adjacent* to describe spatial *arrangement* between disjoint anatomical regions into the proposed approach. Following Bittner [32], adjacent holds exist among material anatomical structures that are a small but non-zero positive distance apart. As long as the distance between spatial objects can be measured, spatial arrangement by means of adjacency can be defined. Section 3.2.3 provides the definition for this relation.

3.2.1.3 Representation of Direction

Per the example of the positioning between midbrain mantle layer and lung, in terms of topological information, midbrain mantle layer and lung are disjoint. However, in terms of spatial arrangement, the midbrain mantle layer and lung cannot be described as adjacent because of the distance constraint. Therefore, we need a solution to deal with spatial arrangement between disjoint anatomical regions that are far apart and cannot be described using adjacency. We include directional relations that express north, east, south, and west into the proposed approach. These four directional terms can be used to describe anatomical regions, within the mouse embryo, since a reference frame to describe directional relations can be established for the image.

Although this approach can be used to deal with the problem of spatial arrangement between disjoint anatomical regions that are far apart such that they cannot be described as adjacent, this approach has a drawback. The drawback of this approach is that directional relations between two anatomical regions change at each of their movements. The movement of anatomical structures for example, fingers bending or the jaw opening and closing causes a wide range of positions for these structures. Anatomical structure movements, which cause changes in directional information, affect anatomical region recognition.

Directional relations corresponding to an anatomical region differs according to the position. If the same anatomical region appears at two different positions between the two compared images, directional relations may fail to provide anatomical space mappings. Regardless of such a drawback, the mapping of anatomical space based on directional relations is sufficient as directional relations that express north, east, south, and west are capable of describing images that are not too different. Section 3.2.3 provides a definition for each of these directional relations.

3.2.2 Mapping Method

The approach to finding a matching region begins with segmenting the images according to their anatomical regions. A query region is then described using its spatial relationships with respect to other anatomical regions. The mapping of a query region in the first image onto the query result region in the second image is carried out based on the satisfaction of exact same spatial relationship constraints. To illustrate this approach, given two images $C1$ and $C2$, if anatomical region $A1$ in image $C1$ has the relationships $A1$ is adjacent to $B1$, and $A1$ is adjacent to $C1$, then its equivalent anatomical region, $A2$, in image $C2$, must be adjacent to $B2$ and $C2$,

where the latter two correspond to $B1$ and $C1$, respectively. The mapping of region $A1$ in image $C1$ onto region $A2$ in image $C2$ may then be achieved by mapping their respective spatial descriptions.

We propose *SpaRTAD* (Spatial Relations based on Topological, Arrangement and Directional relations) as an efficient representation structure to describe a query region in an image based on spatial relationships between anatomical regions. Spatial relationships may be described using topological, arrangement, and directional relations. A query region is then mapped onto the query result region, based on the satisfaction of exact same spatial constraints.

3.2.3 Formalism

We have defined *SpaRTAD* in first-order logic formulation. We use lower-case letters (*e.g.* x, y, z) as variables to denote individual spatial regions and upper-case letters (*e.g.* C, P, PP) as variables to denote spatial relations or function. The logical connectors ($\neg, \wedge, \vee, \rightarrow, \leftrightarrow$) have their own definitions (not, and, or, if-then, and if and only if (iff), respectively). The logical quantifiers (\forall, \exists) have their own quantification definitions (for all, there exist, respectively). The formalism is summarised below:

DEFINITION 1. *We define topological relations as*

$$T = \{disjoint, overlap, externallyConnected, inside, contains, coveredBy, covers, equal\} \quad (3.1)$$

The definitions for these topological relations and the first-order logic formulations are consistent with Region Connection Calculus (RCC-8) [90]. Relation *disjoint* occurs between two regions x and y , if and only if they are not connected, in the sense that x and y do not share any interior point and do not have any common point in the boundaries. The rule for this relation is presented as:

$$DISJOINTxy \leftrightarrow \neg Cxy \quad (3.2)$$

In the intended interpretation, the connection relation C holds between regions x and y if and only if they share a common point.

Relation *overlap* occurs between two regions x and y if and only if there is a region z such that z is part of x and z is part of y , in the sense that x and y share common

interior points. The rule for this relation is presented as:

$$OVERLAPxy \leftrightarrow (\exists z)(Pzx \wedge Pzy) \quad (3.3)$$

In the intended interpretation, the part of relation P holds between two regions x and y , when for all z , if z is connected to x then z is connected to y , which means x is part of y . The rule for this relation is presented as:

$$Pxy \leftrightarrow (\forall z)(Czx \rightarrow Czy) \quad (3.4)$$

In the intended interpretation, the proper part of relation PP holds between regions x and y if and only if x is part of y and y is not part of x .

$$PPxy \leftrightarrow Pxy \wedge \neg Pyx \quad (3.5)$$

Relation *externallyConnected* occurs between two regions x and y if and only if they share a common point and do not overlap. The rule for this relation is presented as:

$$EXTERNALLY_CONNECTEDxy \leftrightarrow (Cxy \wedge \neg OVERLAPxy) \quad (3.6)$$

Relation *inside* occurs between two regions x and y , for example, x is *inside* y if and only if the spatial region x is a part of spatial region y , in the sense that x 's location is included in y 's location and there is no common point z such that z is in boundaries of x and y . The rule for this relation is presented as:

$$INSIDExy \equiv PPxy \wedge \neg(\exists z)[EXTERNALLY_CONNECTED_{zx} \wedge EXTERNALLY_CONNECTED_{zy}] \quad (3.7)$$

Relation *contains* occurs between two regions x and y , for example, y *contains* x is defined by the inverse of *inside*. The rule for this relation is presented as:

$$CONTAINSyx \equiv INSIDExy \quad (3.8)$$

Relation *coveredBy* occurs between two regions x and y , for example, x is *coveredBy* y in the sense that x 's location is included in y 's location and there is a point z such

that z is in boundaries of x and y . The rule for this relation is presented as:

$$\begin{aligned} COVERED_BYxy \equiv PPxy \wedge (\exists z)(EXTERNALLY_CONNECTED_{zx} \\ \wedge EXTERNALLY_CONNECTED_{zy}) \end{aligned} \quad (3.9)$$

Relation *covers* occurs between two regions x and y , for example, y covers x , is defined by the inverse of *coveredBy*. The rule for this relation is presented as:

$$COVERS_{yx} \equiv COVERED_BYxy \quad (3.10)$$

Relation *equal* occurs between two regions x and y if and only if x is part of y and y is part of x . The rule for this relation is presented as:

$$EQUALxy \equiv (Pxy \wedge Pyx) \quad (3.11)$$

DEFINITION 2. We define spatial arrangement as

$$A = \{adjacent\} \quad (3.12)$$

The definition and the corresponding first-order logic formulation for relation *adjacent* is consistent with OBO relation ontology [27; 32]. Two regions x and y are *adjacent* if and only if x and y are not connected and there is a region z such that z is connected to both x and y , and z is negligible in size with respect to x and y . The rule for this relation is presented as:

$$ADJACENTxy \equiv \neg Cxy \wedge (\exists z)(Czx \wedge Czy \wedge z \ll x \wedge z \ll y) \quad (3.13)$$

We compute adjacency between two regions by dilating one of the regions by two units, and then computing the intersection between them. Adjacency holds between the two regions if they have a non-empty intersection.

DEFINITION 3. We define directional relations as

$$D = \{northOf, eastOf, southOf, westOf\} \quad (3.14)$$

We define directional relations between regions by comparing their Minimum Bounding Rectangles (MBR for short) on a 2D coordinate system that has 0,0 at the top-left corner. An MBR is the smallest enclosing box of a region, which can be described by x-y coordinate of the upper-left corner and by the x-y coordinate of

the lower-right.

Relation *northOf*, for example, *a* is north of *b* if the y-coordinate lower-right for MBR of region *a* is smaller or equal to the y-coordinate upper-left for MBR of region *b*. The rule for this relation is presented as:

$$NORTH_OF(a, b) \equiv Y_LOWER_RIGHT(a) \leq Y_UPPER_LEFT(b) \quad (3.15)$$

Relation *eastOf*, for example, *a* is east of *b* if the x-coordinate upper-left for MBR of region *a* is greater or equal to the x-coordinate lower-right for MBR of region *b*. The rule for this relation is presented as:

$$EAST_OF(a, b) \equiv X_UPPER_LEFT(a) \geq X_LOWER_RIGHT(b) \quad (3.16)$$

Relation *southOf*, for example, *a* is south of *b* is defined by the inverse of *northOf*. The rule for this relation is presented as:

$$SOUTH_OF(a, b) \equiv NORTH_OF(b, a) \quad (3.17)$$

Relation *westOf*, for example, *a* is west of *b* is defined by the inverse of *eastOf*. The rule for this relation is presented as:

$$WEST_OF(a, b) \equiv EAST_OF(b, a) \quad (3.18)$$

DEFINITION 4. We define anatomical regions in an image as

$$R = (P, S) \quad (3.19)$$

where *R* contains a set of anatomical parts $P = \{p_1, p_2, \dots, p_n\}$ with spatial information $S = \{r(p_i, p_j) \mid r \in (T \cup A \cup D) \text{ and } p_i, p_j \in P\}$

Figure 3.1 illustrates two images of an embryo. However, anatomical structure *x* in image *A* is not segmented in image *B*. The simplified spatial description for anatomical region *x* in Figure 3.1(a) is as below:

$$adjacent(x, liver), adjacent(x, pancreas), southOf(x, heart), westOf(x, lung)$$

The above descriptions map anatomical region *x* in Figure 3.1(a) to a location somewhere inside the area labelled as result region *y* in Figure 3.1(b).

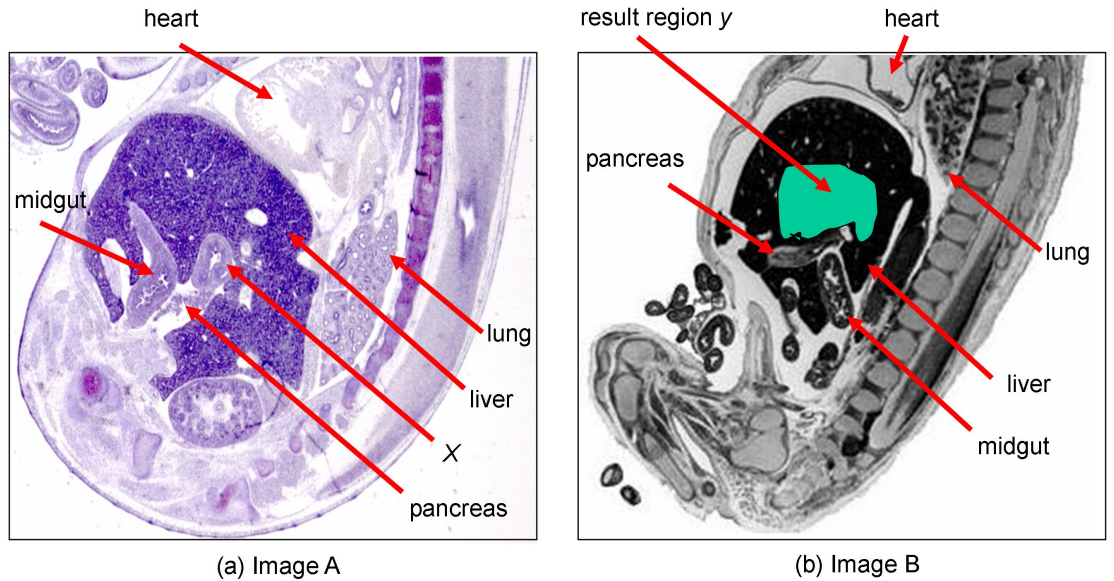


Figure 3.1: The mapping method using spatial relationships between segmented regions maps (a) query region x to (b) a location somewhere inside the area highlighted in green (the result region y).

3.2.4 Algorithm

This section presents the mapping algorithm combining topological, arrangement, and directional relations. The algorithm is first described in the context of finding a matching image. Note that the case of finding a matching image is beyond the scope of the thesis. Future research work might use this type of mapping case for experimentation to extend the scope of the thesis. This section later discusses modification of the algorithm in order to perform an image region mapping.

Assuming that the mapping is performed between two images $C1$ and $C2$, topological relations describe the position of connectedness, containment, overlap and disjointness between two anatomical regions. Therefore, all anatomical regions in image $C1$ and $C2$ must be topologically matched. Anatomical regions in image $C1$ and $C2$ are topologically matched if they have exactly the same topological information involving connectedness, containment and overlap. Though image $C1$ and $C2$ could have exactly the same disjoint anatomical regions, this does not guarantee that anatomical regions in image $C1$ and $C2$ are topologically equivalent. In the case of disjoint anatomical regions, topological information does not capture the relative position between them. Directional relations are usually described between two spatial regions that do not overlap [33]. Therefore, the algorithm uses directional relations only to capture relative position between disjoint anatomical regions. In conclusion, not all anatomical regions in image $C1$ and $C2$ must be matched in

terms of directional relations. Anatomical regions that are connected, contained, or overlap must be topologically equivalent. On the other hand, all disjoint anatomical regions must be matched in terms of directional relations.

Nevertheless, in the case of disjoint anatomical regions that do not match in terms of directional relations, these anatomical regions may be affected by rotation direction. Rotation direction has a significant impact on object recognition [100]. Therefore, our algorithm uses spatial arrangement based on adjacency to capture relative position between disjoint anatomical regions that do not match in terms of directional relations. In conclusion, not all anatomical regions in image $C1$ and $C2$ are required to be directionally matched. Anatomical regions that are connected, contained or overlap must be topologically equivalent. On the other hand, for disjoint anatomical regions that do not match in terms of directional relations, these regions must be matched in terms of their adjacency.

Figure 3.2 depicts the flow diagram of the proposed algorithm. The phase called *Topological Relations Classification* classifies anatomical region representations $R = (P, S)$ for image $C1$ and image $C2$ based on topological information involving connectivity, containment and overlap. If $C1$ and $C2$ are not topologically equivalent, then $C1$ and $C2$ do not match. Otherwise, the algorithm proceeds to check for disjoint anatomical regions (anatomical regions that are not connected to any other regions). If $C1$ and $C2$ do not have disjoint anatomical regions, then $C1$ matches $C2$. If $C1$ and $C2$ contain disjoint anatomical regions, the algorithm proceeds to the next phase.

The phase called *Directional Relations Classification* classifies disjoint anatomical region representation $R = (P, S)$ for image $C1$ and image $C2$ based on directional information. If $C1$ and $C2$ have exactly the same directional information between disjoint anatomical regions, the algorithm simply says that $C1$ matches $C2$. Otherwise, the algorithm proceeds to the next phase.

The phase called *Arrangement in terms of Adjacency Classification* classifies disjoint anatomical region representation $R = (P, S)$ for image $C1$ and image $C2$ based on adjacency information. If $C1$ and $C2$ have exactly the same arrangement in terms of adjacency information, the algorithm simply says that $C1$ matches $C2$. Otherwise; the algorithm simply says that $C1$ and $C2$ do not match. Given anatomical regions as in Figure 3.3(a) to (f), applying *SpaRTAD* algorithm will give the following result: anatomical regions in (a)~(b) are not equivalent, anatomical regions in (c)~(d) are equivalent, and anatomical regions in (e)~(f) are equivalent.

The above algorithm can be modified in order to accomplish an image region mapping. To illustrate this approach, assume that mapping is performed between

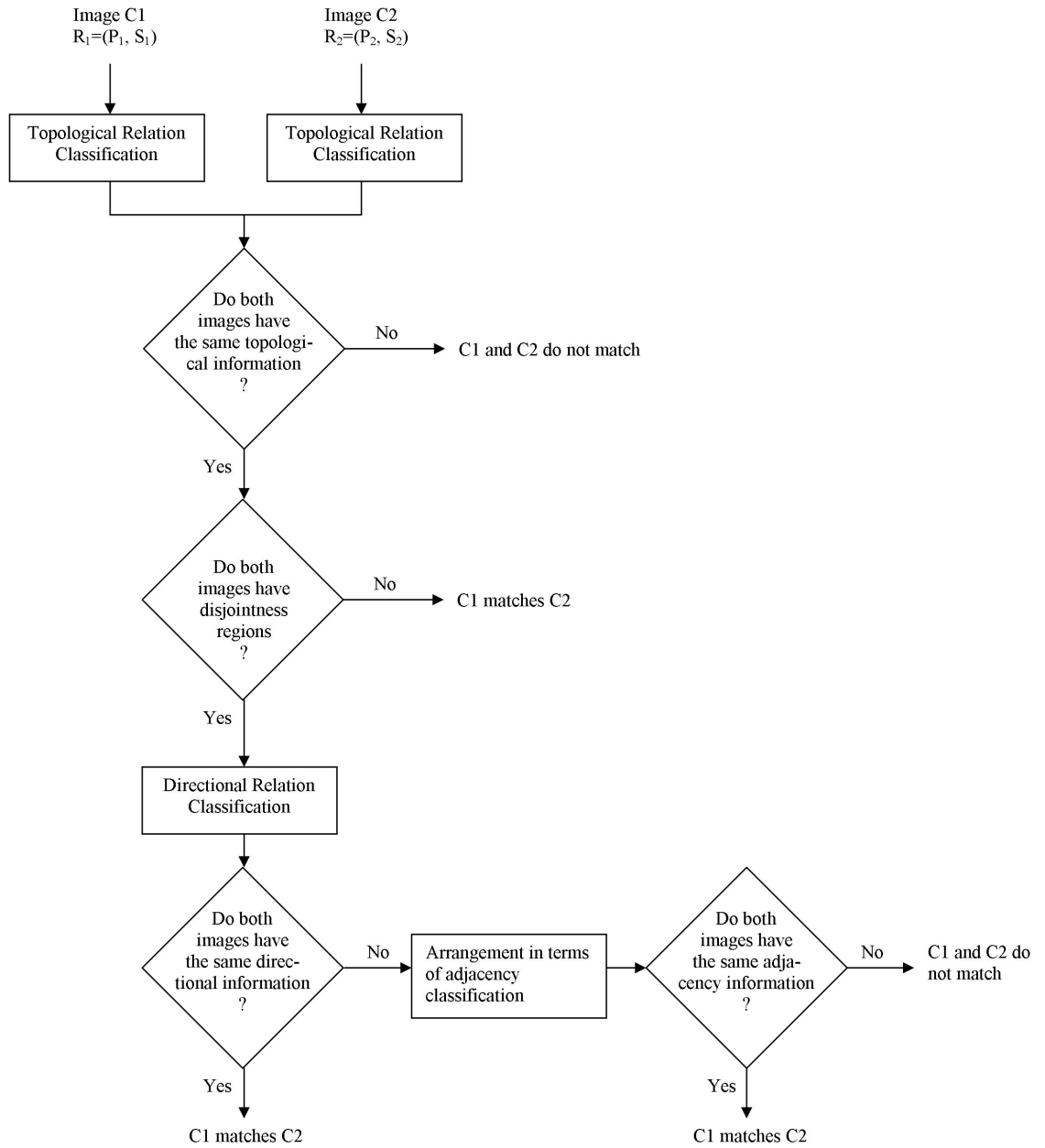


Figure 3.2: Flow diagram of the proposed *SpaRTAD* algorithm

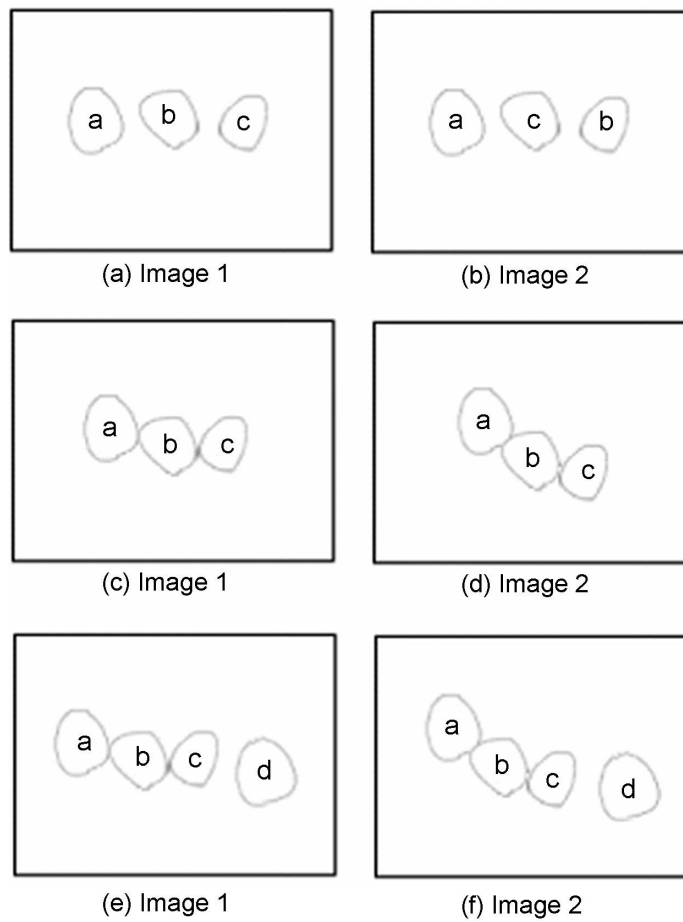


Figure 3.3: Anatomical regions in Image 1 and Image 2 with (a)~(b) disjointness, (c)~(d) connectedness, (e)~(f) disjointness and connectedness

two images $I1$ and $I2$: image $I1$ contains the part of heart and this corresponding part contains subregions. On the other hand, image $I2$ contains a full image of an embryo. Assume that a query region x is selected in image $I1$: we describe query region x using its spatial relationships with respect to other segmented regions in image $I1$ as:

$$R_Q(x) = \{r(x, p_i) \mid r \in (T \cup A \cup D) \text{ and } x, p_i \in P\} \quad (3.20)$$

$R_Q(x)$ is the spatial description for query region x with respect to a set of anatomical regions $P = \{p_1, p_2, \dots, p_n\}$. T , A and D are defined using Equations 3.1, 3.12 and 3.14 respectively. Query region x in image $I1$ are then mapped to the corresponding region in image $I2$ based on the satisfaction of the exact same spatial constraints.

3.3 Spatial Descriptions Based on Fiducial Points and a Set of Spatial Relations

This section describes the proposed mapping approach in the context of finding a matching region using Spatial Descriptions Based on Fiducial Points and a Set of Spatial Relations. This approach uses fiducial points to describe locations in an image. The study in the second phase involves the investigation and scoping of a new mapping technique, which has been designed based on the following research question: How to incorporate the fiducial points in a new mapping technique, which would support image region mappings independently of anatomical structures' spatial relationships?

3.3.1 Design Rationale

The idea of using fiducial points is inspired by the image processing mapping approach. Since a fiducial point can become a point of reference for an anatomical location, the location of a query region is described based on these points. The idea of using spatial relations has been inspired by the ontology mapping approach, but using less detailed ontologies by implementing the best set of spatial relations to describe anatomical domains. Since a spatial relation may be used to describe the location of a region in anatomical space, we propose to describe a query region using fiducial points and a set of spatial relations. A query region is any region in one image which is to be mapped onto another image.

This approach involves the following concepts: (1) a query region, (2) fiducial points, and (3) fiducial lines. Figure 3.4 depicts the illustration of a fiducial point, a fiducial line and a region. A fiducial point is a point in space. A fiducial line is made

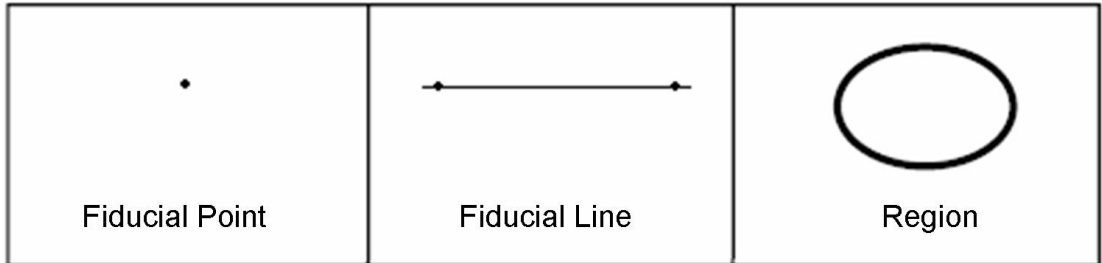


Figure 3.4: A fiducial point, a fiducial line and a query region.

by creating a straight line through a pair of fiducial points. A query region is made of connected multiple single-elements within a closed boundary. We define the goal of mapping as finding a corresponding region of one image and mapping it onto another region in another image which has the same intended meaning. This approach describes the relations between a query region and a fiducial point/line using directional relations of the following four terms: *northOf*, *eastOf*, *southOf* and *westOf*. By describing the query region with respect to the fiducial points/lines by using the directional relations we can overcome the problem relating to different anatomical names associated with regions in an image. Section 3.3.3 provides a definition for each of said directional relations.

3.3.2 Mapping Method

Given two images $I1$ and $I2$, mapping one image onto another begins by selecting the same fiducial points in both images. A query region is then described using spatial relations between the query region with respect to the fiducial points and the fiducial lines. Two regions from different images are then mapped based on the satisfaction of exact same constraints. For example, if query region x in image $I1$ is described as x is north of fiducial point $P1$ and x is west of fiducial point $P2$, then its equivalent region in image $I2$ must be a region that is located north of fiducial point $P1$ and west of fiducial point $P2$. This enables anatomical space mapping between images to facilitate the integration of biomedical atlases.

Figure 3.5 depicts the framework of our approach. Because the proposed spatial description approach employs both fiducial points and spatial relations, the approach fits in between ontology-based and image processing-based mapping techniques. The approach does not intend to include a large number of concepts in spatial relations

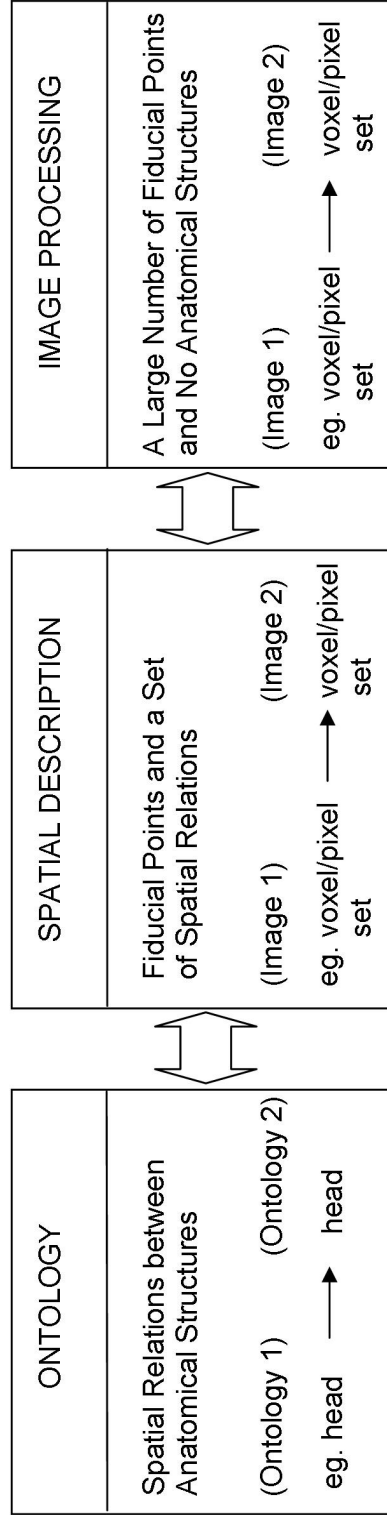


Figure 3.5: Ontology-based mappings identify corresponding elements between two ontologies (mapping of structure *head* from Ontology 1 to structure *head* in Ontology 2) based on spatial relations between anatomical structures. The image processing-based mappings align images (mapping of a voxel from Image 1 to the corresponding voxel in Image 2) based on equivalent voxel/pixel intensities and image warping algorithms using fiducial points (landmarks). The proposed spatial description fiducial points-based method fits in between these two as it employs both fiducial points and spatial relations.

as that replicates the ontology mapping approach. Subsequently, the entire spatial area of an image should be conceptualised with a set of fiducial points, where this set of fiducial points must not involve a large number of fiducial points, such that the approach essentially ends up as an image warping algorithm as used in image processing. High accuracy with a large number of fiducial points is not the end goal.

3.3.3 Formalism

We define the goal of mapping as being to find a corresponding region of one image and match it with another region in another image which has the same intended meaning, based on spatial description S_Q . The formalism of the Spatial Descriptions Based on Fiducial Points and a Set of Spatial Relations is summarised as:

DEFINITION 1. We define directional relations as

$$D = \{northOf, eastOf, southOf, westOf\} \quad (3.21)$$

Relation *northOf* between a region r and a fiducial point p , for example, r *northOf* p if the y-coordinate lower-right for MBR of region r is smaller or equal to y-coordinate of p . The rule for this relation is presented as:

$$NORTH_OF(r, p) \equiv Y_LOWER_RIGHT(r) \leq Y_COORDINATE(p) \quad (3.22)$$

Relation *northOf* between a region r and a fiducial line l can be defined as follows: Initially, a pair of fiducial points $p1$ and $p2$ define a fiducial line l . Subsequently, there exists two new points $p3$ and $p4$ with coordinates $x1-y1$ and $x2-y2$, respectively, on fiducial line l (these new points are not the initial fiducial points that define the fiducial line). Relation *northOf* between a region r and a fiducial line l , for example, r *northOf* l if the y-coordinate lower-right for MBR of region r is smaller or equal to $y1$ and $y2$ of fiducial line l . Both $y1$ and $y2$ are values of $x1-y1$ and $x2-y2$, which are two new points on fiducial line l such that two vertical lines can be created through: (1) $x1-y1$ and x-y coordinate upper-left for MBR of r (2) $x2-y2$ and x-y coordinate lower-right for MBR of r . The rule for this relation is presented as:

$$NORTH_OF(r, l) \equiv Y_LOWER_RIGHT(r) \leq Y1_COORDINATE(l) \wedge Y_LOWER_RIGHT(r) \leq Y2_COORDINATE(l) \quad (3.23)$$

Relation *eastOf* between a region r and a fiducial point p , for example, r *eastOf* p if the x-coordinate upper-left for MBR of region r is greater or equal to the x-coordinate of p . The rule for this relation is presented as:

$$EAST_OF(r, p) \equiv X_UPPER_LEFT(r) \geq X_COORDINATE(p) \quad (3.24)$$

Relation *eastOf* between a region r and a fiducial line l can be defined as follows: Initially, a pair of fiducial points $p1$ and $p2$ define a fiducial line l . Subsequently, there exists two new points $p3$ and $p4$ with coordinates $x1-y1$ and $x2-y2$, respectively, on fiducial line l (these new points are not the initial fiducial points that define the fiducial line). Relation *eastOf* between a region r and a fiducial line l , for example, r *eastOf* l if the x-coordinate upper-left for MBR of region r is greater or equal to $x1$ and $x2$ of fiducial line l . Both $x1$ and $x2$ are values of $x1-y1$ and $x2-y2$, which are two points on fiducial line l such that two horizontal lines can be created through: (1) $x1-y1$ and x-y coordinate upper-left for MBR of r (2) $x2-y2$ and x-y coordinate lower-right for MBR of r . The rule for this relation is presented as:

$$EAST_OF(r, l) \equiv X_UPPER_LEFT(r) \geq X1_COORDINATE(l) \wedge X_UPPER_LEFT(r) \geq X2_COORDINATE(l) \quad (3.25)$$

Relation *southOf* between a region r and a fiducial point p , for example, r *southOf* p if the y-coordinate upper-left for MBR of region r is greater or equal to y-coordinate of p . The rule for this relation is presented as:

$$SOUTH_OF(r, p) \equiv Y_UPPER_LEFT(r) \geq Y_COORDINATE(p) \quad (3.26)$$

Relation *southOf* between a region r and a fiducial line l can be defined as follows: Initially, a pair of fiducial points $p1$ and $p2$ define a fiducial line l . Subsequently, there exists two new points $p3$ and $p4$ with coordinates $x1-y1$ and $x2-y2$, respectively, on fiducial line l (these new points are not the initial fiducial points that define the fiducial line). Relation *southOf* between a region r and a fiducial line l , for example, r *southOf* l if the y-coordinate upper-left for MBR of region r is greater or equal to $y1$ and $y2$ of fiducial line l . Both $y1$ and $y2$ are values of $x1-y1$ and $x2-y2$, which are two points on fiducial line l such that two vertical lines can be created through: (1) $x1-y1$ and x-y coordinate upper-left for MBR of r (2) $x2-y2$ and x-y

coordinate lower-right for MBR of r . The rule for this relation is presented as:

$$\begin{aligned} SOUTH_OF(r, l) \equiv & Y_UPPER_LEFT(r) \geq Y1_COORDINATE(l) \wedge \\ & Y_UPPER_LEFT(r) \geq Y2_COORDINATE(l) \end{aligned} \quad (3.27)$$

Relation *westOf* between a region r and a fiducial point p , for example, r *westOf* p if the x-coordinate lower-right for MBR of region r is smaller or equal to x-coordinate of p . The rule for this relation is presented as:

$$WEST_OF(r, p) \equiv X_LOWER_RIGHT(r) \leq X_COORDINATE(p) \quad (3.28)$$

Relation *westOf* between a region r and a fiducial line l can be defined as follows: Initially, a pair of fiducial points $p1$ and $p2$ define a fiducial line l . Subsequently, there exist two new points $p3$ and $p4$ with coordinates $x1-y1$ and $x2-y2$, respectively, on fiducial line l (these new points are not the initial fiducial points that define the fiducial line). Relation *westOf* between a region r and a fiducial line l , for example, r *westOf* l if the x-coordinate lower-right for MBR of region r is smaller or equal to $x1$ and $x2$ of fiducial line l . Both $x1$ and $x2$ are values of $x1-y1$ and $x2-y2$, which are two points on fiducial line l such that two horizontal lines can be created through: (1) $x1-y1$ and x-y coordinate upper-left for MBR of r (2) $x2-y2$ and x-y coordinate lower-right for MBR of r . The rule for this relation is presented as:

$$\begin{aligned} WEST_OF(r, l) \equiv & X_LOWER_RIGHT(r) \leq X1_COORDINATE(l) \wedge \\ & X_LOWER_RIGHT(r) \leq X2_COORDINATE(l) \end{aligned} \quad (3.29)$$

DEFINITION 2. We describe a query region x in an image as

$$S_Q(x) = \{r(x, f_i) \mid r \in D \text{ and } f_i \in (F_{point} \cup F_{line})\} \quad (3.30)$$

where $S_Q(x)$ is the spatial description for query region x with respect to a fiducial point $F_{point} = \{p_1, p_2, \dots, p_n\}$ or a fiducial line $F_{line} = \{l_1, l_2, \dots, l_n\}$

3.3.4 Algorithm

This section presents the algorithm for mapping based on fiducial points and a set of spatial relations. Assuming that a mapping is performed between two images $C1$ and $C2$: the algorithm begins by processing S_Q , which is the spatial description for query region x in image $C1$. The algorithm to find the result region y corresponding

to S_Q in image $C2$ consists of the following steps:

- 1: Start with all possible fiducial lines.
- 2: Exclude fiducial lines that cut through the query region x in image $C1$.
- 3: Fiducial lines left around query region x must be considered.
- 4: Find the smallest polygon that contains the whole of x .
- 5: Return the smallest polygon as the result region y in image $C2$.

3.3.5 Mapping Identical, Scale Changed, Rotated and Morphologically Different Images

This section discusses the applicability of the proposed approach with respect to the problem of mapping identical images, scale-changed and rotated images, and images with the same anatomical structures but with differing arrangement and orientation of spatial structures. Figure 3.6 illustrates two identical images of 2D mouse embryo with six fiducial points and 15 fiducial lines.

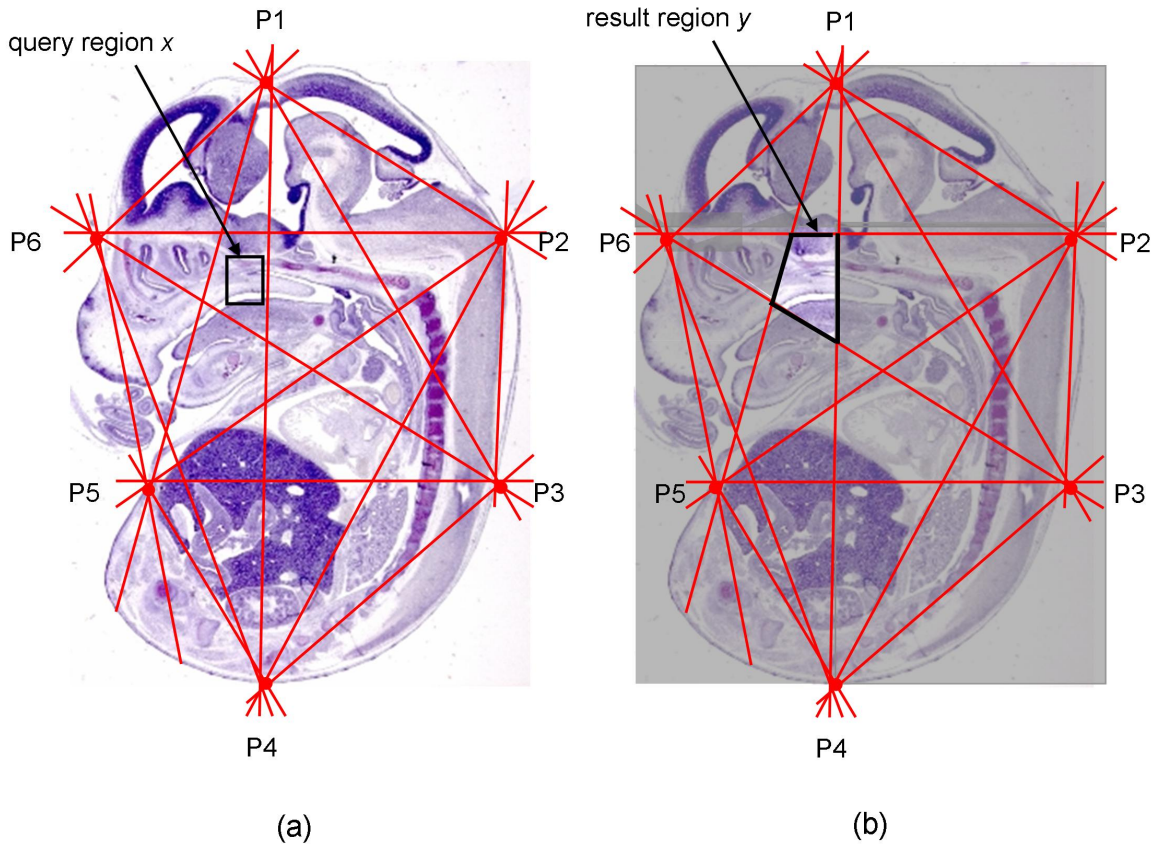


Figure 3.6: The spatial description fiducial points-based method maps (a) the query region x to (b) the result region y .

The simplified description for query region x is described as:

$$SOUTH_OF(x, P6P2), NORTH_OF(x, P6P3), EAST_OF(x, P1P5), WEST_OF(x, P1P4)$$

The above description maps the query region x to the result region y . We label a fiducial line according to its pair of fiducial points.

In addition, anatomical structures in an image may appear in various orientations and positions. Figure 3.7 depicts an example of two rotated structures. Structure x in Figure 3.7(a) is equivalent to structure x in Figure 3.7(b) if region x is described using *betweenness* relation. This relation can be defined as:

$$\begin{aligned} BETWEEN(x, L1, L2) \equiv & SOUTH_OF(x, L1) \wedge NORTH_OF(x, L2) \vee \\ & WEST_OF(x, L1) \wedge EAST_OF(x, L2) \vee \\ & (NORTH_OF(x, L1) \wedge SOUTH_OF(x, L2)) \vee \\ & EAST_OF(x, L1) \wedge WEST_OF(x, L2) \end{aligned} \quad (3.31)$$

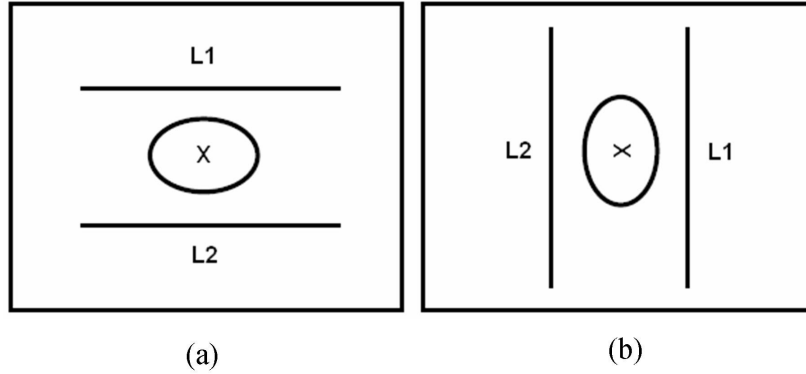


Figure 3.7: Example of rotated images. Region x is *between* fiducial lines $L1$ and $L2$.

The notion of *betweenness* is the way to deal with rotated direction and orientation. However, this approach is not pursued further in this thesis. We do not implement this relation in the mapping algorithm because we have used spatial adjacency to deal with rotated direction and orientation. However, future research work might use the notion of *betweenness* to extend the scope of the thesis. Figure 3.8 illustrates three exact same anatomical structures, however, the structure in the middle has different positions. The method to attempt this problem requires some fiducial lines to be relaxed. The method is described as follows:

1. Select the centroid of the structure that has various positions as a fiducial point.
2. Link that fiducial point to the centroid of any other structures that remain in the same position.

Description for query region x of Figure 3.8(a) is described as:

$$NORTH_OF(x, L1), SOUTH_OF(x, L2)$$

The white coloured areas in all three images of Figure 3.8 denote the corresponding match location based on this description.

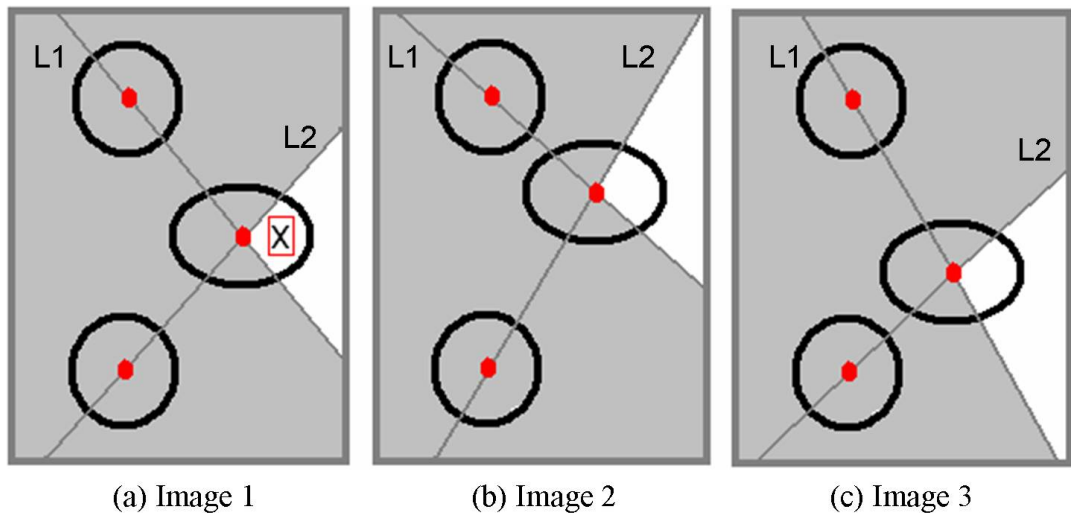


Figure 3.8: In all three images, the centroid of the structure in the middle denotes a fiducial point. This particular fiducial point is then linked to the centroids of two other structures which remain in the same position. The white areas denote the acceptable location for query region x .

The approach for solving this problem requires marking points or lines to specific regions of the image. In practice, experts such as radiologists [93; 94] and surgeons [95; 96] annotate images to associate a specific region with medical opinion. The annotation includes placing a circle or a rectangle, identifying a set of salient points, and drawing lines and arrows. For that reason, the requirement of marking a centroid [97; 98; 99] prior to specific lines on an image region should not be an impediment to implementation.

The definition for best match criteria is important in any mapping algorithm. Since anatomical structures exist at different ranges of scale, arrangement and position, there is the possibility of an exact copy of the location corresponding to the

query region in one image being unavailable in another image. The proposed spatial description fiducial points-based method at the current state perform mappings by returning a location that satisfies all spatial relation constraints corresponding to a query region. However, this may not be necessary. Consider the difference between the images in Figure 3.9(a) and Figure 3.9(b). The blue circle in Figure 3.9(a) is entirely below the line drawn between two fiducial points. However, the blue circle in Figure 3.9(b) lies a little above the line. By enforcing an exact mapping, part of the blue circle will be missing in the image of Figure 3.9(b). Therefore, some form of google-like matching can be considered. An easy google-like matching can be performed by matching as many constraints as possible as a criterion for finding the next best mapped location. Another option for google-like matching is specifying a range; for example, allowing for a distance limit from a fiducial line, which will return a location given by the range.

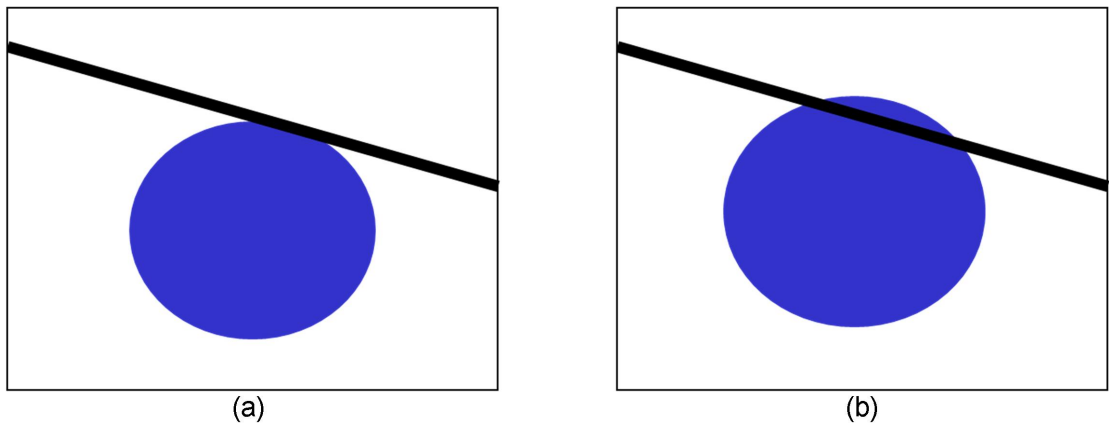


Figure 3.9: The blue circle in (a) is entirely below the line drawn between two fiducial points. However, part of the blue circle in (b) lies a little above the line.

3.4 Spatial Descriptions Based on Fiducial Points and a Set of Spatial Relations, Integrated with Spatial Relations between Segmented Regions

This section describes the proposed mapping approach in the context of finding a matching region using Spatial Descriptions Based on Fiducial Points and a Set of Spatial Relations, Integrated with Spatial Relations between Segmented Regions. This approach uses both the spatial relationships between entities, as well as spatial relationships between the entity and the fiducial points to describe locations in an

image. The study's third phase involves identifying the advantages of a combined mapping technique, inspired by the approaches designed under phases one and two.

3.4.1 Mapping Method

The approach of mapping using the fiducial points-based method can be integrated with spatial relations between segmented regions. This combined approach describes a query region using spatial relations between the query region with respect to other anatomical regions as well as spatial relations between the query region with respect to fiducial points and fiducial lines.

An image region mapping is performed based on the following steps: (1) firstly, the query region is mapped onto the result region according to the Spatial Descriptions Based on the Fiducial Points and a Set of Spatial Relations, (2) secondly, the result region is narrowed down using the approach of Spatial Descriptions Based on Spatial Relationships between Segmented Regions. To illustrate this combined approach, Figure 3.10 depicts an embryo with anatomical regions a , b , c , d , e , f and g , with four fiducial points $P1$, $P2$, $P3$ and $P4$. In this example, all fiducial lines are coloured in red. The simplified description of query region X according to the spatial description fiducial points-based method is as follows:

'X is southOf P1P2, X is eastOf P1P3, X is northOf P2P4'

On the other hand, the simplified description of query region X based on the spatial relationships between segmented regions is as below:

'X is southOf b, X is westOf d, X is northOf f'

The integration between the spatial description fiducial points-based method with spatial relationships between segmented regions is achieved by combining descriptions from these two approaches. Therefore, mapping of query region X in Figure 3.10(a) first uses the spatial relations based on the fiducial points, which mapped the query region X to the result region Y (the grey coloured area as depicted in Figure 3.10(b)). The result region Y was then narrowed down using spatial relationships between segmented regions, which mapped the query region X to the result region Z (the yellow coloured area as depicted in Figure 3.10(c)).

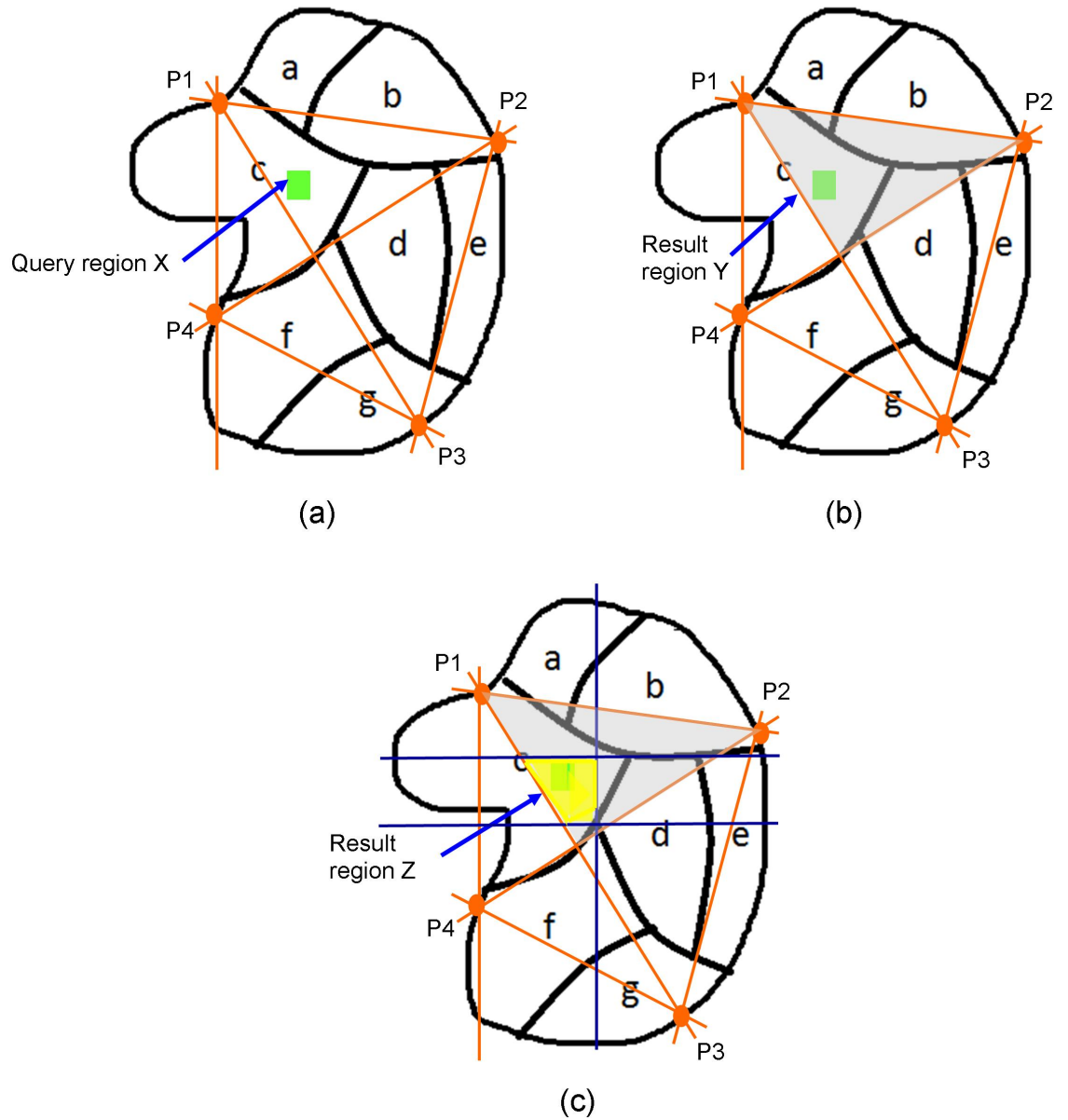


Figure 3.10: An embryo with anatomical regions *a*, *b*, *c*, *d*, *e*, *f* and *g*, with four fiducial points *P1*, *P2*, *P3* and *P4*. The spatial description fiducial points-based method maps (a) the query region *X* to (b) the result region *Y*. Then, the spatial description using spatial relationships between segmented regions make the result region *Y* narrower as in (c) the result region *Z*.

3.4.2 Formalism

Since this is a combined approach, we have integrated both R_Q and S_Q to describe a query region in an image. The formalism of the approach is presented as $C_Q(x)$ and is defined below:

$$C_Q(x) = R_Q(x) \cup S_Q(x) \quad (3.32)$$

$R_Q(x)$ and $S_Q(x)$ are defined using Equations 3.20 and 3.30 respectively.

3.5 Selected Mapping Approach

The different methods which could be used in the case of image region mappings are:

- Method One: Spatial Descriptions Based on Spatial Relationships between Segmented Regions.
- Method Two: Spatial Descriptions Based on Fiducial Points and a Set of Spatial Relations.
- Method Three: Spatial Descriptions Based on Fiducial Points and a Set of Spatial Relations, Integrated with Spatial Relations between Segmented Regions.

A significant advantage of method one is that it enables mapping between two images which contain a different number of anatomical regions, but associates the same anatomical name for these regions. Given two images $I1$ and $I2$, where image $I1$ contains anatomical regions A , B , C , and D , and image $I2$ contains only anatomical regions A , B , and C . This approach may determine the location for anatomical region D in image $I2$ by using spatial descriptions based on spatial relationships between anatomical region D with respect to anatomical regions A , B , and C in image $I1$. Overall, this approach is domain-dependent, such that mapping depends on spatial relationships between regions segmented in an image. Both mapping method one and three depend on the spatial relationships between segmented regions. One major problem associated with these two methods is that it becomes difficult, or perhaps impossible, to map regions between two images that use different names for their structures, or to divide the anatomy in different ways. In addition, problems could arise when different biomedical atlases have images with a different number

of segmented regions, causing one structure to correspond to parts of several structures, and vice versa. The consequence is that mapping of image regions in order to achieve biomedical atlas integration may require alignment representations of anatomy differing in structure and domain coverage. Furthermore, this approach requires spatial knowledge of every anatomical structure in an image in order to do the mappings. Although these images may have the same structures, the morphology may vary with orientation and the position of the structure causing different spatial relationships between them. In conclusion, a mapping method which works independently of anatomical structures' spatial relationships seems to be a solution to these problems.

Method two uses directional relations to describe the location of a query region with respect to the fiducial points and the fiducial lines. This method enables mappings without the tedious task of aligning a different number of segmented regions and domain coverage. More importantly, it overcomes the interoperability problem caused by different anatomical names and vocabularies used between different atlases. For this reason, method two has been selected as the best solution to facilitate image region mappings.

As discussed in the literature review, the selected approach within this thesis should overcome the limitations of ontology and image processing-based techniques by addressing many of the image region mapping issues. For example, there are images without painted domains. In this case, the spatial description fiducial points-based method is more capable of supporting an image region mapping than the ontology-based method. Moreover, in the case where the images are painted and annotated with ontological concepts, the ontology-based method cannot be considered as the only best solution. There are cases where some regions are painted in one image but not in the other and also cases where there exist terms associated with regions which cannot be mapped from one ontology to another. In these cases, the spatial description fiducial points-based method may be another option for mapping.

Furthermore, the selected approach should be able to perform image region mappings between similar but not identical images in their morphologies (e.g. image slices of an embryo, midline images from two consecutive Theiler Stages of the same embryo, and so on). The selected approach should also be capable of performing image region mappings between non-identical images that are not identical in their morphologies (e.g. midline images of different embryos at the same developmental stage). In addition, the selected approach should be capable of performing image region mappings between non-identical images with the same morphology (e.g. images of an embryo taken across different imaging modalities). Images with different

morphologies are subject to different voxel/pixel distributions. This also applies to images with the same morphology but taken from different imaging modalities. Since the spatial description fiducial points-based method describes a query region with respect to the fiducial points and the fiducial lines by using directional relations, this method resolves the issue of voxel/pixel intensities variation between images. Therefore, the spatial description fiducial points-based method may be able to overcome the limitations of the image processing-based mapping.

3.6 Biologist Mapping Results

The fifth phase involved an experienced biologist with a background in anatomical science, particularly in the annotation of mouse embryo images to produce mapping samples. The purpose of acquiring this result was to establish a 'gold standard' to be used as the basis for evaluating existing mapping techniques, as well as the proposed technique developed in this research.

Two studies were carried out: (1) selection of fiducial points, and (2) image region mappings. Table 3.1 describes the types of images, the type of region mappings and the source of images used in these two studies.

Table 3.1: Description of Images

Type of Images	Type of Region Mappings	Source of Images
1) Different morphologies of an embryo model (i.e. images with different morphologies because they are from the same embryo model at different developmental stages)	Identifiable Region	Same source (i.e. Kaufman Atlas)
	Random Region	
2) Different embryo morphologies (i.e. images with different morphologies because they are derived from different atlases)	Identifiable Region	Different sources (i.e. e-Mouse Atlas and Kaufman Atlas)
	Random Region	
3) Different image modalities (i.e. images with the same morphology because one image is the clip art graphic version of the original image)	Identifiable Region	Same source (i.e. Kaufman Atlas)
	Random Region	

The two studies used three types of image. For each image type, mappings were carried out on two types of region: (1) identifiable region, and (2) random region. An identifiable region is a region in an image which is easily recognisable and identified by human experts, such as liver, lung, heart etc. A random region is an arbitrary

region of interest in an image.

The first type is images with different morphologies caused by using images from the same embryo model at different developmental stages. In this example, the comparison between two midline images from two consecutive Theiler Stages of the same embryo from the Kaufman Digital Atlas represents the problem of different morphologies of an embryo model.

The second type is images with different morphologies caused by using images from different atlases (i.e. midline images of different embryos at the same developmental stage). In this example, the comparison between the e-Mouse Atlas and the Kaufman Digital Atlas represents the problem of different embryo morphologies.

The third type is images with the same morphology because one image is the clip art graphic version of the original image. In this example, the comparison between an original image from the Kaufman Atlas with its clip art graphic version exposes the problem of different image modalities.

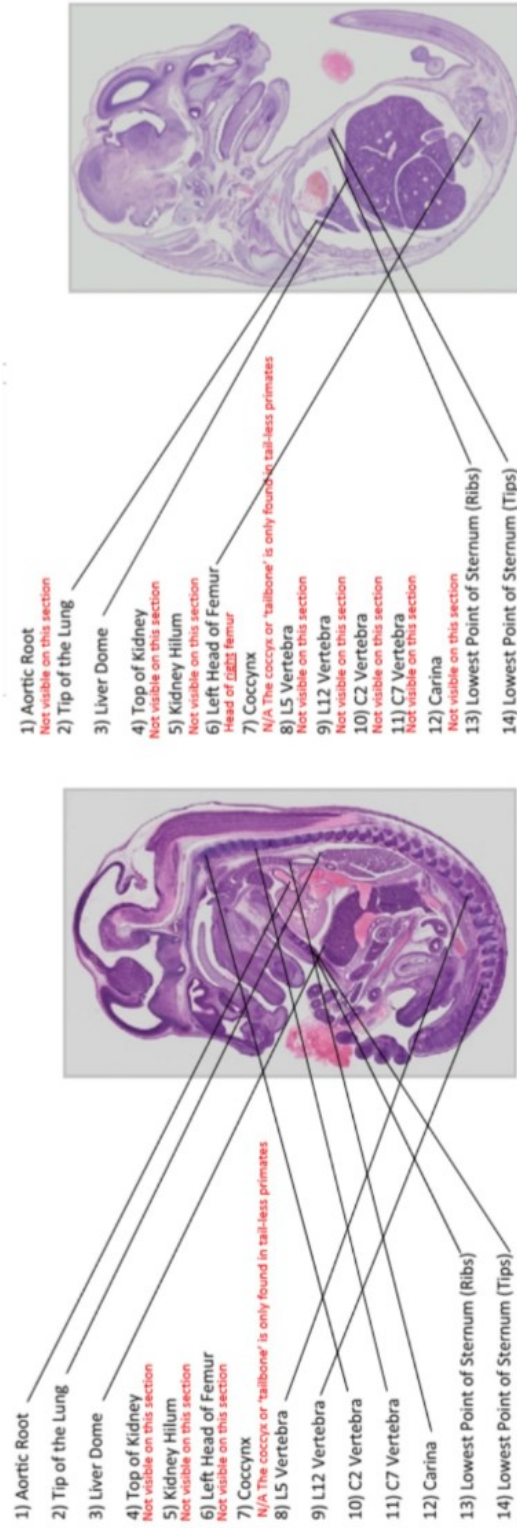
The spatial description fiducial points-based method uses fiducial points as the pre-requisite for any mapping of regions. Therefore, the first study was carried out by selecting fiducial points in the images as described in Table 3.1.

3.6.1 Selection of Fiducial Points

The purpose of the study was to obtain three sets of fiducial points, where two sets were selected by a biologist and one set was selected by a non-biologist. In the evaluation, we demonstrate that the difference between selection by a biologist and selection by a non-biologist has a significant impact on the results.

The first set of fiducial points selected by a biologist is based on the 14 fiducial points identified in the literature review: *Aortic Root*, *Tip of the Lung*, *Liver Dome*, *Top of Kidney*, *Kidney Hilum*, *Left Head of Femur*, *Coccyx*, *L5 Vertebra*, *L12 Vertebra*, *C2 Vertebra*, *C7 Vertebra*, *Carina*, *Lowest Point of Sternum (Ribs)*, and *Lowest Point of Sternum (Tips)*. A biologist was asked to identify the locations of these fiducial points in the images as described in Table 3.1. This study involved three image pairs. Figure 3.11 depicts one example of these image pairs.

The second set of fiducial points is an extended version of the first set, where it contains additional fiducial points of a biologist's own choice. The third set of fiducial points was selected by a non-biologist. Once the three sets of fiducial points have been selected, the result regions according to the fiducial points selected by both a biologist and a non-biologist can then be identified.



(a) TS22-23, Plate 33a, Subplate a,
Kaufman Digital Atlas

(b) TS24, Plate 36a, Subplate a,
Kaufman Digital Atlas

Figure 3.11: A biologist was asked to identify the location of 14 fiducial points in a pair of images. This example shows the mapping of fiducial points between two midline images from two consecutive Theiler Stages of the same embryo. The material for the exercise in this section is provided in Appendix C.

3.6.2 Image Region Mappings

The second study was carried out to obtain image region mappings involving identifiable regions and random regions in the images as described in Table 3.1. The study involved 12 image pairs. Figure 3.12 depicts one example of these image pairs at the mapping of an identifiable region. A biologist was given the left image with the blue area as the query region, then asked to find the matching region in the right image that corresponds to the query region. Figure 3.13 depicts an example of mapping a random region denoted as query region x .

For the evaluation, the exercise in this section was used to evaluate the accuracy resulting from using existing mapping approaches and the newly proposed technique in the mapping of image regions in three cases: (1) similar images but not identical in their morphologies (i.e. two midline images from two consecutive Theiler Stages of the same embryo), (2) non-identical images that are not identical in their morphologies (i.e. midline images of different embryos at the same developmental stage), and (3) non-identical images with the same morphology (i.e. images of an embryo from different imaging modalities).

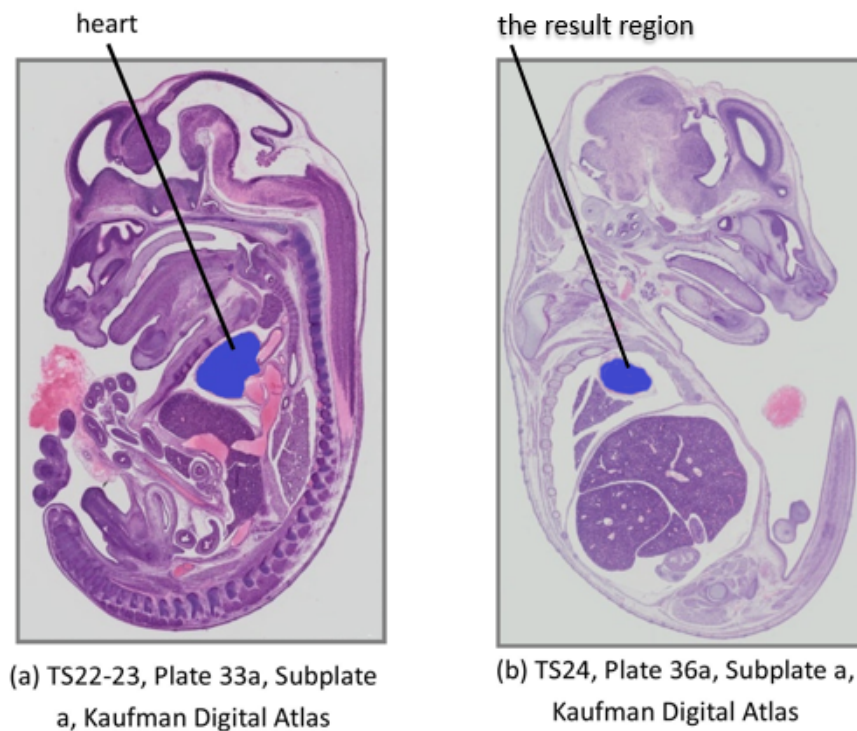


Figure 3.12: The mapping of an identifiable region, for example, the *heart* between two midline images from two consecutive Theiler Stages of the same embryo. A biologist was given the left image with the blue area as the query region. He was then asked to draw the area in the right image that matches the query region. In the above example, the blue area in the right image was drawn by a biologist as the query result region corresponding to the query region in the left image. The material for the exercise in this section is provided in Appendix C.

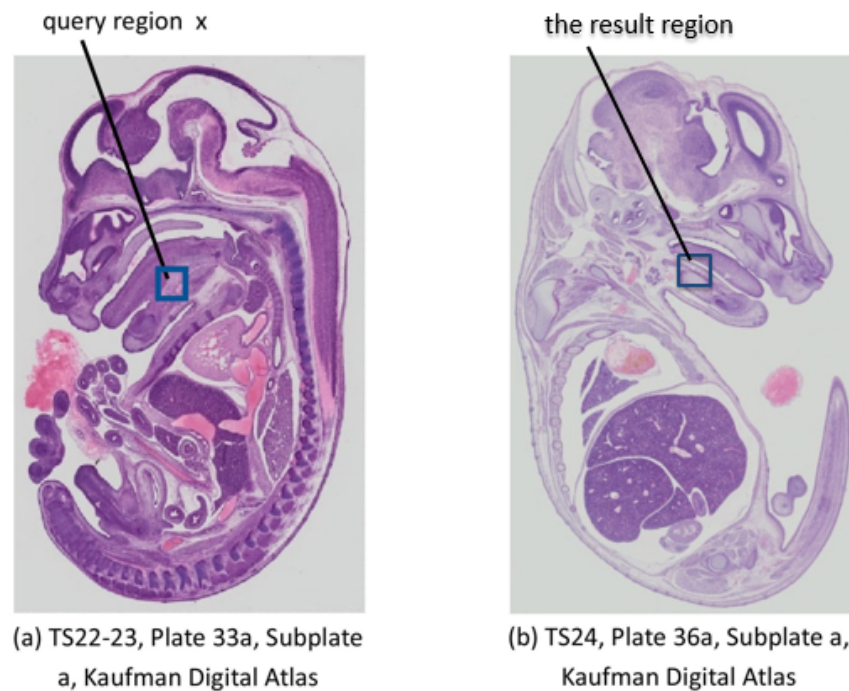


Figure 3.13: The mapping of a random region denoted as query region x between two midline images from two consecutive Theiler Stages of the same embryo. A biologist was given the left image with the blue area as the query region. Then, he was asked to draw the area in the right image that matches the query region. In the above example, the blue area in the right image was drawn by a biologist as the query result region corresponding to the query region x in the left image. The material for the exercise in this section is provided in Appendix C.

3.7 Summary

This chapter has presented three different approaches to spatial description to facilitate anatomical space integration. These approaches are: (1) Spatial Descriptions Based on Spatial Relationships between Segmented Regions, (2) Spatial Descriptions Based on Fiducial Points and a Set of Spatial Relations, and (3) Spatial Descriptions Based on Fiducial Points and a Set of Spatial Relations, Integrated with Spatial Relations between Segmented Regions.

The research project began with an investigation of what information each category of spatial relations provides. To address the problem of biomedical atlas integration, we have proposed *SpaRTAD* for conceptualising anatomical space based on spatial relations between segmented regions using three categories of spatial relations. These are topological, arrangement and directional relations. Anatomical regions between two images are then mapped onto one another based on the satisfaction of exact same spatial constraints. Nevertheless, different biomedical atlases may have images with a different number of segmented regions causing one structure to correspond to parts of several structures, and vice versa. The mapping of images in order to achieve biomedical atlas integration may require alignment representations of anatomy differing in structure and domain coverage. Moreover, even if the biomedical atlases have the same segmented regions in their images, they may associate different anatomical names with the segmented regions causing an interoperability problem with finding corresponding anatomical regions between these images.

We attempted to solve these problems by exploring the independent mapping of spatial relationships between segmented regions. In addressing this problem, we have proposed and implemented a spatial description approach that conceptualises anatomical space based on fiducial points and a set of spatial relations. The approach describes a query region using spatial relations with respect to fiducial points and fiducial lines. Mapping is then performed based on the satisfaction of exact same constraints in the target image. A novel property of the approach is that the method is not voxel/pixel intensity dependent and mapping is performed independently of spatial relationships between segmented regions of an image. However, there is no restriction for this approach to be used on its own. Given available resource, the approach of mapping using the Spatial Descriptions Based on Fiducial Points and a Set of Spatial Relations can be integrated with the Spatial Descriptions Based on Spatial Relationships between Segmented Regions.

Chapter 3. Developing Spatial Description-Based Integration

The approach of Spatial Descriptions Based on Fiducial Points and a Set of Spatial Relations has been selected as the best solution to facilitate image region mappings. Chapter 5 provides the evaluation of this approach in comparison with existing image mapping techniques discussed in the literature review above. The following chapter provides a calibration of the selected spatial description-based solution in detail.

Chapter 4

The Calibration of Spatial Description-Based Integration

4.1 Introduction

This chapter presents the calibration of the proposed spatial description-based solution. Calibration results were evaluated based on the number of fiducial points, number of fiducial lines, area of query region and selection of fiducial point location. An evaluation of mapping using 14 well-defined fiducial points reviewed in the literature is also provided.

This chapter is organised as follows: Section 4.2 provides the experiments to analyse the criteria for fiducial point parameters to improve the mapping process in terms of accuracy. The problem of having a variety of experts' definitions for a particular fiducial point location is also discussed. An overview of well-defined fiducial points, and an evaluation of mapping using these points, is presented in Section 4.3. Section 4.4 summarises the chapter.

4.2 Analysis of Spatial Descriptions Based on Fiducial Points and a Set of Spatial Relations

The purpose of the experiments was to demonstrate how fiducial points and a set of spatial relations may be used to describe locations. Figure 4.1 depicts the image used for the experiments. The image is designed as the abstract representation of a mouse embryo. The purpose of an abstract representation is to evaluate mapping

performance of a conceptual model such that the parameters can be used to evaluate the actual model. This defines the initial model structural properties. First,

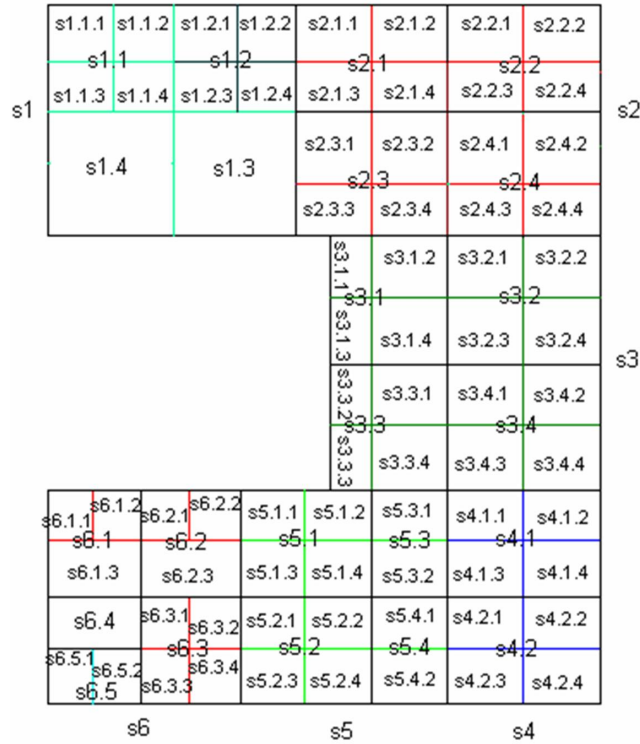


Figure 4.1: Abstract representation for evaluation of mapping using fiducial points.

the abstract representation is intended to provide more complex regions. Thus, the abstract representation consists of multiple subregions with 102 spatial regions annotated in the image. Second, the abstract representation is intended to have structural nomenclature. Thus, the 102 spatial regions are structured into three hierarchical levels. These hierarchical levels of structure represent the *part-of* relationship. Although this relation is not used further in this thesis, it is included in the abstract representation so that the model is generic enough to represent mereological relations in the mouse embryo anatomical domain. The *part-of* relationship is beyond the scope of the thesis. Future research work may use the *part-of* relationship for experimentation to extend the scope of research. Figure 4.2 depicts the tree structure corresponding to the nomenclature for the components of the abstract representation. This nomenclature mimics the *part-of* hierarchy of the actual anatomy. The evaluation in a later chapter uses real mouse embryo images, particularly for the gene expression evaluation.

The abstract representation generated 97,104 query regions each of size 50x50 squared pixels, 68,154 query regions each of size 100x100 squared pixels, 44,204 query regions each of size 150x150 squared pixels, and 25,254 query regions each of

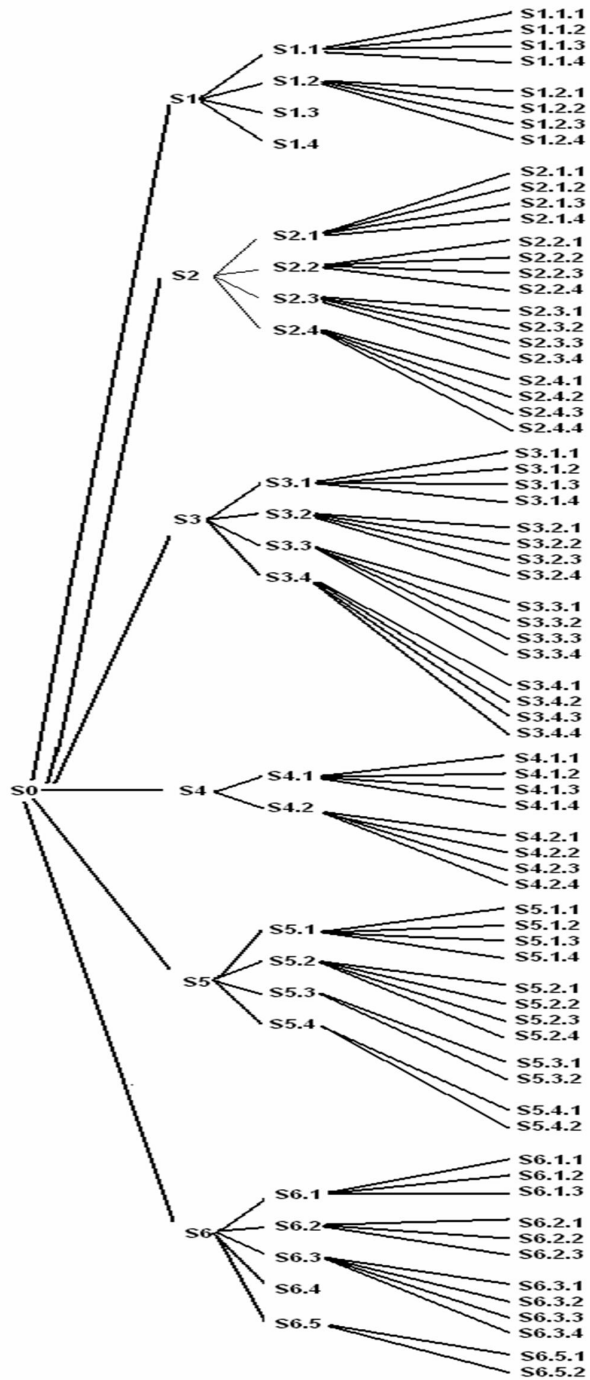


Figure 4.2: Tree structure corresponding to the nomenclature for the components in the abstract representation in Figure 4.1. This nomenclature mimics the *part-of* hierarchy of the actual anatomy.

size 200x200 squared pixels. For all query regions of size 50x50 squared pixels, the first query region starts at the top-left corner of the image and is increased every time by one pixel in order to generate the following query region and so on. Query regions of other sizes are also generated by following this one-pixel step. The idea of using query regions is to test the mappings of pixels in a query region of one image to pixels in a region of another image based on fiducial points. Five experiments were carried out in order to analyse the criteria of fiducial point parameters to increase the accuracy of the mapping process.

4.2.1 Impact of Number of Fiducial Points on Result Accuracy

The experiment was conducted to evaluate the impact of the number of fiducial points on average percentage of accuracy. First, the percentage of accuracy for a query region is calculated as:

$$Accuracy (\%) = \frac{Area\ of\ the\ query\ region}{Area\ of\ the\ query\ result\ region} \times 100 \quad (4.1)$$

Next, the average percentage of accuracy for a total number of query regions corresponding to the query region area is calculated as:

$$Average\ Accuracy (\%) = \frac{Sum\ of\ query\ region\ accuracies}{Number\ of\ query\ regions} \quad (4.2)$$

The area of the query region and the area of the query result region are not critical, but the overlap between the query region and the query result region are. The performance has been compared starting from two fiducial points and up to 880 fiducial points. Note that this method will in general involve selecting these fiducial points by hand. Mappings using 880 fiducial points are not realistic, but experimentation on such a large number of fiducial points has been carried out out of theoretical interest. These fiducial points were tested on 97,104 query regions each of size 50x50 squared pixels, 68,154 query regions each of size 100x100 squared pixels, 44,204 query regions each of size 150x150 squared pixels, and 25,254 query regions each of size 200x200 squared pixels.

Figure 4.3 depicts the average percentage of accuracy produced by a given number of fiducial points. The graph shows that the more fiducial points were used, the higher the accuracy. For example, the average percentage of accuracy for query regions of 50x50 squared pixels, 100x100 squared pixels, 150x150 squared pixels and

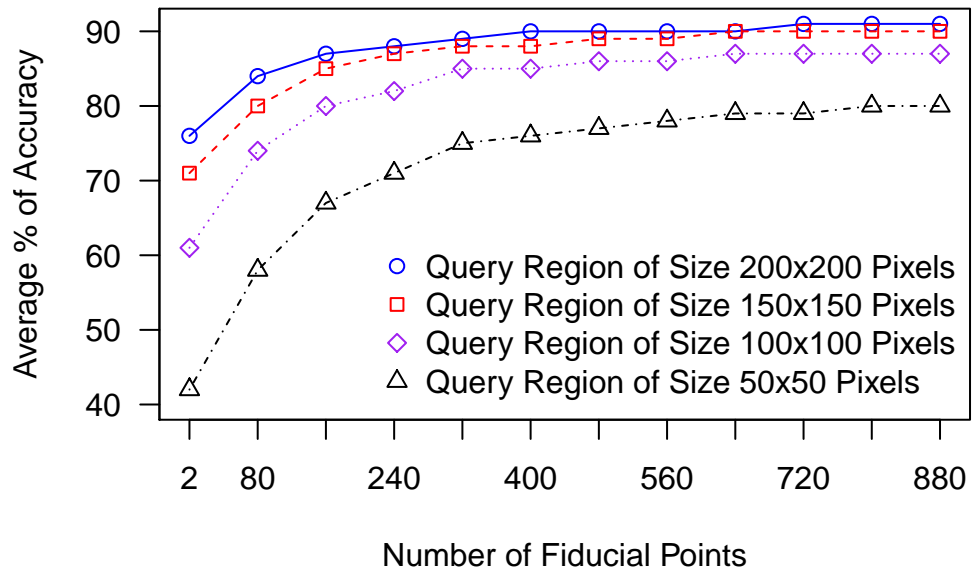


Figure 4.3: Average percentage of accuracy produced by different numbers of fiducial points. The more fiducial points are included the higher the average percentage of accuracy. Moreover, the query region area versus the number of fiducial points affects mapping accuracy.

200x200 squared pixels have significantly increased by 38%, 26%, 19% and 15% respectively, when the number of fiducial points was increased from two to 880.

In addition, the graph shows that the query region area versus the number of fiducial points affects mapping accuracy. For example, when a total of 80 fiducial points was used, the average percentage of accuracy was increased by 16%, 6%, 4% when the area of the query regions were increased from 50x50 to 100x100 squared pixels, from 100x100 to 150x150 squared pixels, and from 150x150 to 200x200 squared pixels, respectively. In principle, it is not the query region area by itself, but the relationship between the area of the query region and the area quotient that can be captured via the fiducial points.

Consequently, it is the query region size versus the number of fiducial points that matters. The more fiducial points are used, the more areas are captured, which increases accuracy.

4.2.2 Impact of Number of Fiducial Lines on Result Accuracy

An experiment was carried out to evaluate the impact of the number of fiducial lines on result accuracy. Figure 4.4 depicts the average percentage of accuracy involving 4 and 24 fiducial lines served by query region size. The graph shows that the average

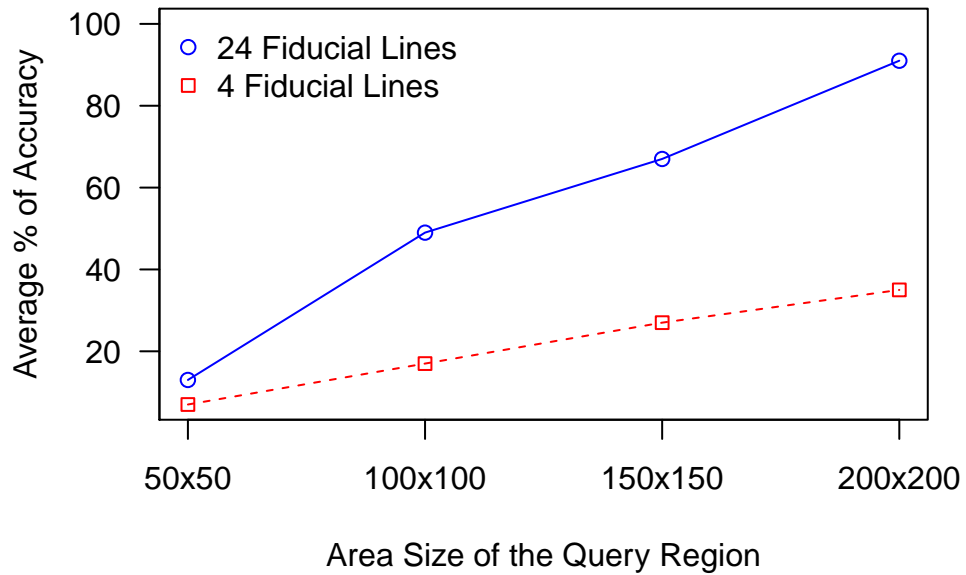


Figure 4.4: Average percentage of accuracy involving 4 and 24 fiducial lines served by query region size. The average percentage of accuracy is higher when more fiducial lines are used.

percentage of accuracy significantly increased when more fiducial lines were used. For example, the average percentage of accuracy for a query region of size 200x200 squared pixels is 35% in the image with 4 fiducial lines and 91% in the image with 24 fiducial lines. In principle, it is relatively easy to get a large number of fiducial lines. The number of fiducial lines increases quickly with the increase of the number of fiducial points.

4.2.3 Impact of Fiducial Point Positioning on Result Accuracy

An experiment was carried out to evaluate the impact of fiducial points positioning on result accuracy. The performance was compared in three different positioning sets of 8 fiducial points, as shown in Figure 4.5. Figure 4.6 depicts the average percentage of accuracy for the three positioning sets served by query region area. The graph shows that different placements of the same number of fiducial points produce different accuracies. For example, the average percentage of accuracy for a query region of size 200x200 squared pixels are 91%, 68%, 31% in set A, B, C respectively. As shown in Figure 4.5, different placement of the same number of fiducial points can create a different number of defined areas. We define a 'defined area' as a segment bounded by fiducial lines (a fiducial line is made by creating a straight line through a pair of fiducial points). Moreover, if the fiducial points

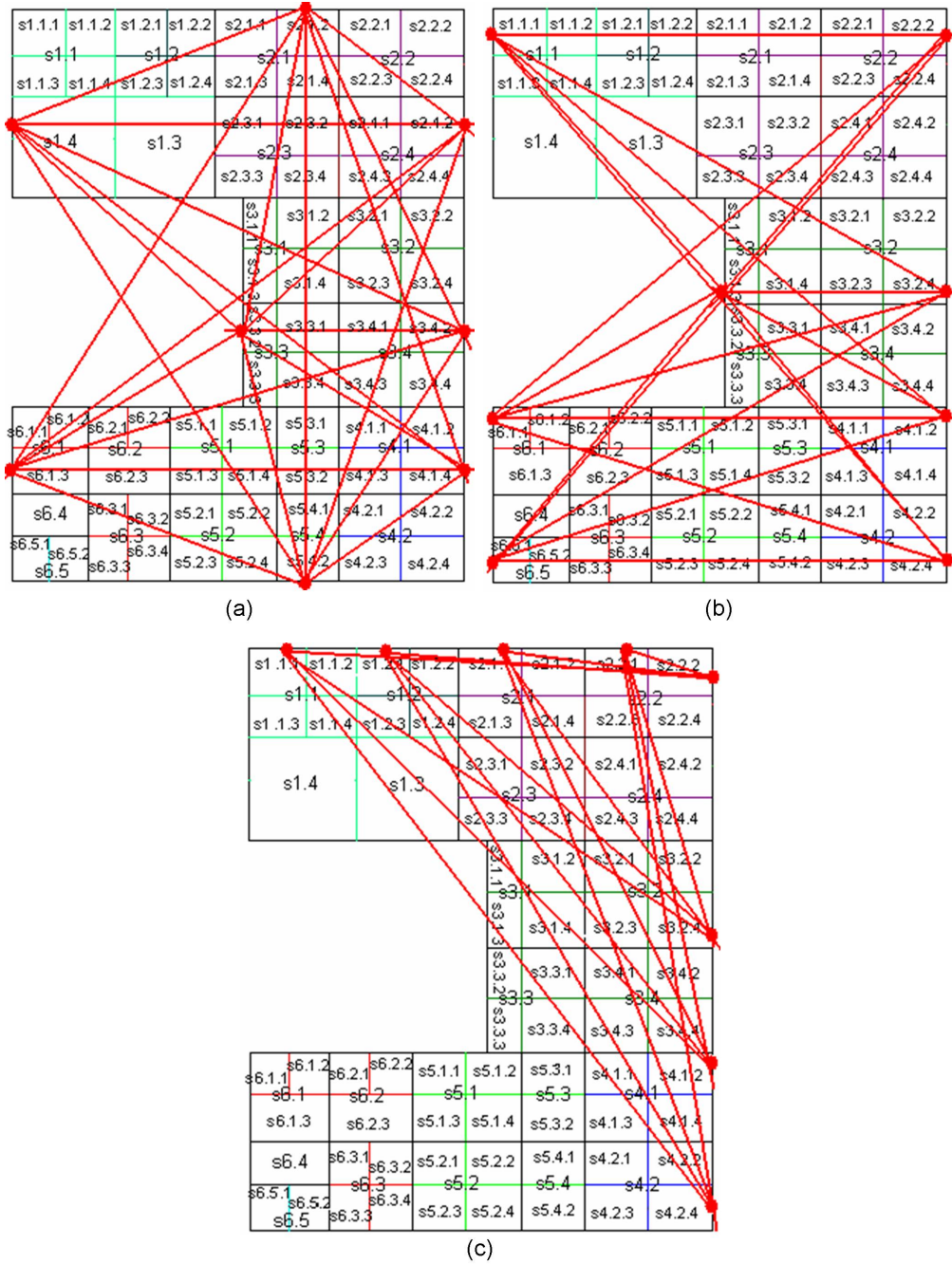


Figure 4.5: Positioning for 8 fiducial points in (a) Set A (b) Set B (c) Set C

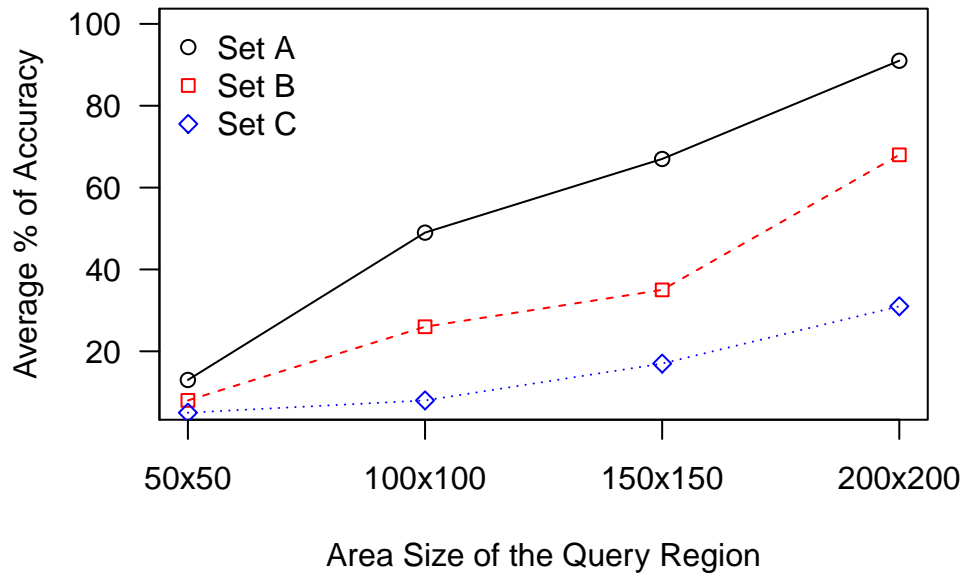


Figure 4.6: Average percentage of accuracy in three different positioning sets of 8 fiducial points served by query region area. The same number of fiducial points placed at different positions produces different average percentages of accuracy. Mapping accuracy gets better when fiducial points are in even distribution.

are distributed evenly, more defined areas can be created. Consequently, the more evenly distributed the fiducial points are, the more segments bounded by the fiducial lines are created, and thus the more areas are captured, which increases the average percentage of accuracy.

4.2.4 Impact on Result Accuracy of Fiducial Point Locations at the Boundary of the Embryo Part or a Location Inside the Embryo Part

An experiment was conducted to evaluate the effectiveness of choosing the boundary of the embryo part or a location inside the embryo part as the location for a fiducial point. The performance is compared in three different positioning sets of 8 fiducial points placed according to two types of locations as shown in Figure 4.7. The first set has all fiducial points at both boundary of the embryo part and inside the embryo part. The second set has all fiducial points located only inside the embryo part. The third set has all fiducial points located only at the boundary of the embryo part.

Figure 4.8 depicts the average percentage of accuracy by selecting 8 fiducial points at the boundary of the embryo part, inside the embryo part or combination of both, served by query region area size. The graph shows that the selection of fiducial points at the boundary of the embryo part or a location inside the embryo



Figure 4.7: Selection of 8 fiducial points (a) at both boundary of the embryo part and inside the embryo part (b) inside the embryo part (c) at the boundary of the embryo part.

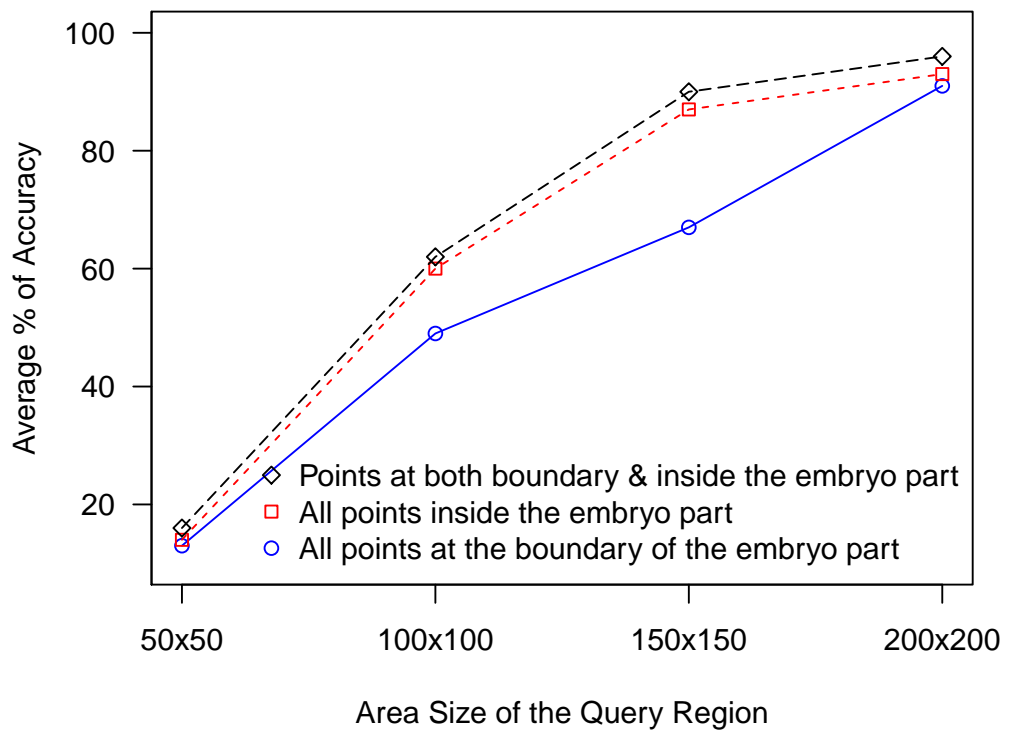


Figure 4.8: Average percentage of accuracy by selecting 8 fiducial points at the boundary of the embryo part, inside the embryo part or a combination of both, produced by query region area. Mapping accuracy increases when more definable areas are created through the fiducial points.

part produces varying average percentages of accuracy. For example, the average percentage of accuracy for a query region of size 200x200 squared pixels is 91% in a positioning set where all fiducial points are located at the boundary of the embryo part. This value is increased to 93% in a positioning set where all fiducial points are located inside the embryo part. This value is further increased to 96% in a positioning set where all fiducial points are located at both boundary and inside the embryo part.

In principle, when different placements of the same number of fiducial points create a different number of defined areas, the more defined areas created through the fiducial points, the better the accuracy. To illustrate this, Figure 4.9 depicts three images with three fiducial points: the first and the second image have all three fiducial points located inside the image, creating seven segments of different sizes. The third image has all three fiducial points at the boundary of the whole

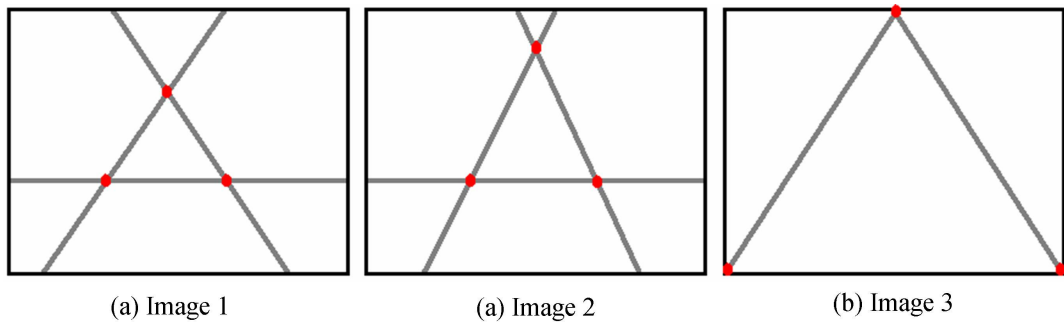


Figure 4.9: Three images (assume that this image represents a whole mouse embryo part) with the same number of fiducial points creating a different number of segments. The number of segments generated is influenced by fiducial point location. Images 1 and 2 have the same number of segments, but different sizes. Fiducial points located inside the embryo part created more segments than where fiducial points were all placed at the boundary of the embryo part. Again, mapping is more accurate when more segments are created through the fiducial points.

image creating only three segments. Assuming that this image represents a whole mouse embryo part, this example shows that the number of defined areas generated is influenced by the location of the fiducial points. Fiducial points located inside the embryo part create more segments than fiducial points located at the boundary of the embryo part. Consequently, when more segments are created, more areas can be captured, increasing accuracy. This result suggests that the best accuracy is achieved when the size of defined areas does not change too much. The following experiment was carried out to verify this finding.

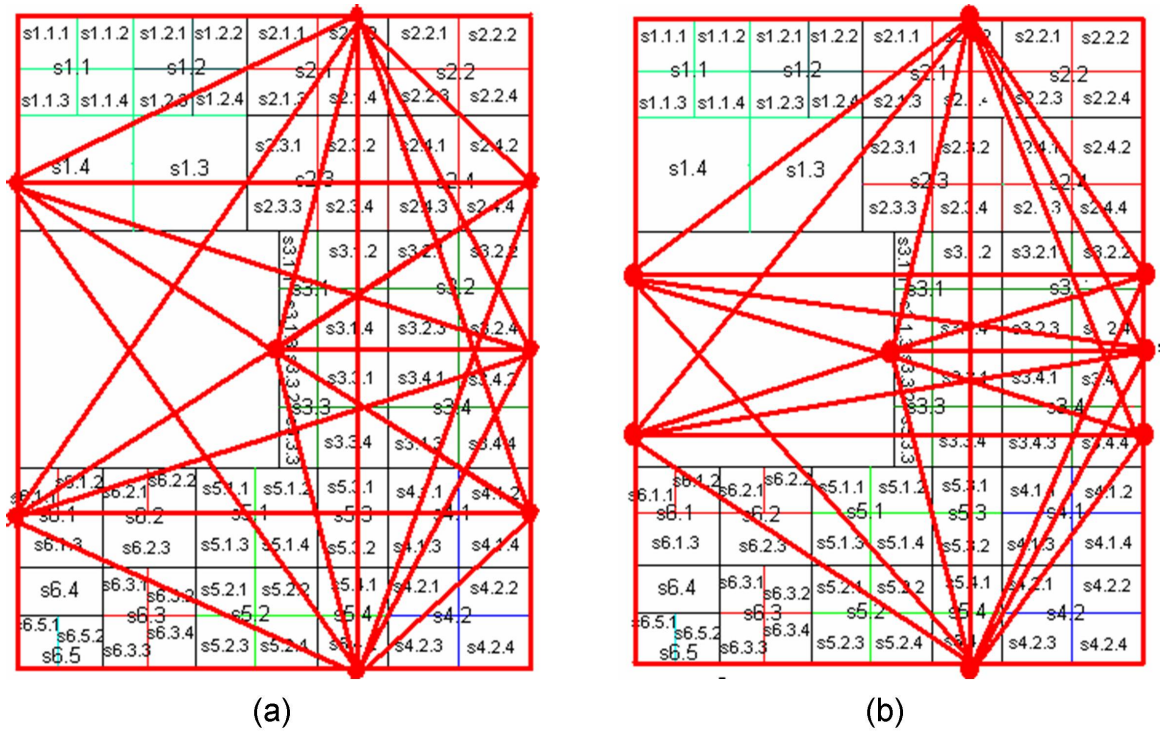


Figure 4.10: The placement of 8 fiducial points creating 54 definable areas on an (a) even distribution of different areas (b) strongly uneven distribution of different areas.

4.2.5 Impact of Distribution of Area Sizes Made by Fiducial Points on Result Accuracy

We believe that the previous four experiments affect the distribution of the size of the areas made by the fiducial points. The following experiment was carried out to evaluate the impact of the distribution of the size of the areas made by the fiducial points on result accuracy. The performance is compared in two images with the same number of defined areas, but varying in size as shown in Figure 4.10.

Figure 4.11 depicts the average percentage of accuracy based on these varying distributions of areas produced by query region size. The graph shows that an even distribution of the size of the defined areas made by the fiducial points produces greater accuracy. For example, the average percentage of accuracy for the query region of size 200x200 squared pixels for Figures 4.10(a) and 4.10(b) are 92% and 87%, respectively.

In principle, for two images with the same number of fiducial points (selected at different positions) and with the same number of defined areas, but varying in sizes, mapping is more accurate between images that have less variation in size.

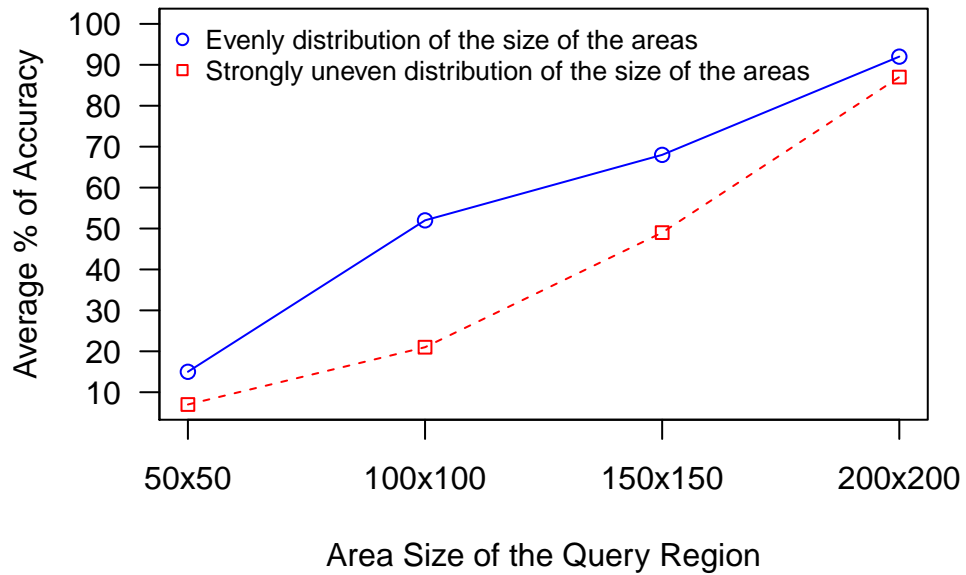


Figure 4.11: Average percentage of accuracy in two images with the same number of defined areas but varying in size produced by query region size. Mapping is more accurate where there is less variation in area size.

4.2.6 Results and Analysis

Fiducial points, fiducial lines, and their associated relations increase the average percentage of accuracy based on the following four parameters: (1) number of fiducial points, (2) number of fiducial lines, (3) area of the query region, and (4) selection of fiducial point location.

The evaluation of the experimental results suggests that the number of fiducial points has a significant influence on the average percentage of accuracy. The more fiducial points are used, the higher the average percentage of accuracy. Consequently, the more fiducial points are used, the more areas are captured, which increases the average percentage of accuracy. Eventually, each individual pixel can be captured by having a huge number of fiducial points; however, this is not a realistic approach.

The evaluation of the experimental results also suggests that different numbers of fiducial lines produce different average percentage of accuracy. These findings suggest the best accuracy can be achieved when more fiducial lines are used. Eventually, the more fiducial lines are included, the more definable areas (segments) are created to capture pixels, increasing the average percentage of accuracy.

Furthermore, the evaluation of the experimental results suggests that the same number of fiducial points located at different positions produces different average percentages of accuracy. A different positioning set for the same number of fiducial

points can create a different number of segments. The more segments are created through the fiducial points, the more pixels are captured, which increases the average percentage of accuracy. Hence, choosing a location for a fiducial point is a critical aspect of maximising accuracy.

More specifically, different placements of the same number of fiducial points can create either a different number of segments, or an exact same number of segments. When the same number of fiducial points located at different positions have created a different number of segments, the more segments created the greater the accuracy. Consequently, choosing a location for a fiducial point is a critical factor in improving accuracy, as it affects the number of segments created.

Evaluation of the experimental results also suggests that when the same number of fiducial points located at different positions creates an exact same number of defined areas (segments), the more even the distribution of the size of the areas, the more accurate the mappings. Figure 4.10 illustrates two images with a total of 8 fiducial points. The placement for this set of eight fiducial points is different in both images, but both placements create a total of 54 segments. Although these two images have an exact same number of segments, these segments vary in their sizes. We suggest that the more even the distribution of the size of these areas (segments), the more accurate the mappings. This may be tested through the standard deviation.

Standard deviation is useful for measuring the distribution of the size of these areas. Standard deviation is applied to the size of the defined areas for each image. The more even the distribution of the size of these areas, the smaller the standard deviation. Distribution of areas with a smaller standard deviation usually shows a comparatively fewer number of large areas/smaller areas. Therefore, the more even the distribution of the size of the areas created through the fiducial points, the smaller standard deviation, thus producing higher accuracy.

Table 4.1 depicts the standard deviation of the areas defined by the placement of 8 fiducial points in Figures 4.10(a) and 4.10(b). Although Figures 4.10(a) and 4.10(b) both contain a total of 54 definable areas, the standard deviations for each image are significantly different. The standard deviations of the size of the defined areas for Figures 4.10(a) and 4.10(b) are 2381.0 and 3421.6 respectively. This result show that the standard deviation for Figure 4.10(a) is smaller than the standard deviation for Figure 4.10(b). Based on this analysis, Figure 4.10(a) contains definable areas where the sizes of these areas are more evenly distributed compared to the areas for Figure 4.10(b).

Therefore, in the measurement of even distribution of the size of the defined areas, standard deviation is important. The lesser the standard deviation, the lesser

Table 4.1: Standard deviations of 54 areas defined through 8 fiducial points as arranged in Figures 4.10(a) and 4.10(b)

Image	The Size of the Defined Areas	Mean	Standard Deviation
Fig. 4.10(a)	7488.0, 2288.0, 1352.0, 1820.0, 2756.0, 2808.0, 2880.0, 1810.0, 2837.5, 2688.0, 2174.0, 2388.0, 635.0, 702.0, 1093.0, 1050.0, 1430.0, 1609.5, 1600.5, 850.0, 875.0, 532.5, 1050.0, 2022.0, 2283.0, 1461.5, 1195.0, 583.0, 508.0, 54.0, 50.5, 162.0, 216.0, 607.0, 702.0, 964.5, 2592.0, 816.0, 1296.0, 2160.0, 6816.0, 510.0, 1005.0, 566.0, 3673.5, 2798.5, 1925.5, 2705.0, 2485.0, 11128.0, 7135.5, 10272.0, 5564.0, 5136.0	2298.3	2381.0
Fig. 4.10(b)	6520.5, 7486.5, 3059.0, 5071.5, 1690.5, 2012.5, 17227.0, 3413.5, 526.5, 407.0, 1103.5, 2070.5, 1257.5, 3447.0, 1680.5, 1904.5, 423.0, 510.0, 6120.0, 15408.0, 1868.5, 1854.0, 6480.0, 2808.0, 4536.0, 1224.0, 1944.0, 7704.0, 602.5, 1291.5, 724.5, 475.0, 1000.5, 1407.0, 1256.0, 518.0, 400.0, 1468.5, 834.5, 1119.0, 1058.0, 40.0, 221.5, 91.0, 231.5, 264.0, 161.5, 50.0, 15.0, 321.5, 498.5, 143.0, 78.0, 81.0	2298.3	3421.6

the number of large areas/smaller areas. Therefore, the more even the distribution of the size of these areas, the more accurate the mappings. To conclude, given the same number of defined areas, the best results occur when these areas are of about the same size.

The area distribution, however, matters less when the query area is large. Consider the average percentage of accuracy for the query region of size 200x200 squared pixels in Figure 4.11, the average percentage of accuracy has a slight increase of only 5% when the size of the defined areas changed from strongly uneven to even distribution of the size of the areas. Figure 4.12 depicts the model parameter image and a query region of size 200x200 squared pixels in their actual sizes. The distribution of the size of the areas matters less when the area of the query region is large. This may be due to the mapping accuracy that depends on the relationship between the query region size and the size of the areas that are defined by the fiducial points. As shown in Figure 4.13, smaller query regions can easily be captured within the defined areas created by the fiducial points compared to larger query regions.

Overall, these evaluations have shown that the spatial description fiducial points-based method maximises accuracy depending on the variation of number and size of the areas defined by the approach. With an appropriate number of fiducial points used and better selection of fiducial point location, mappings can be improved in

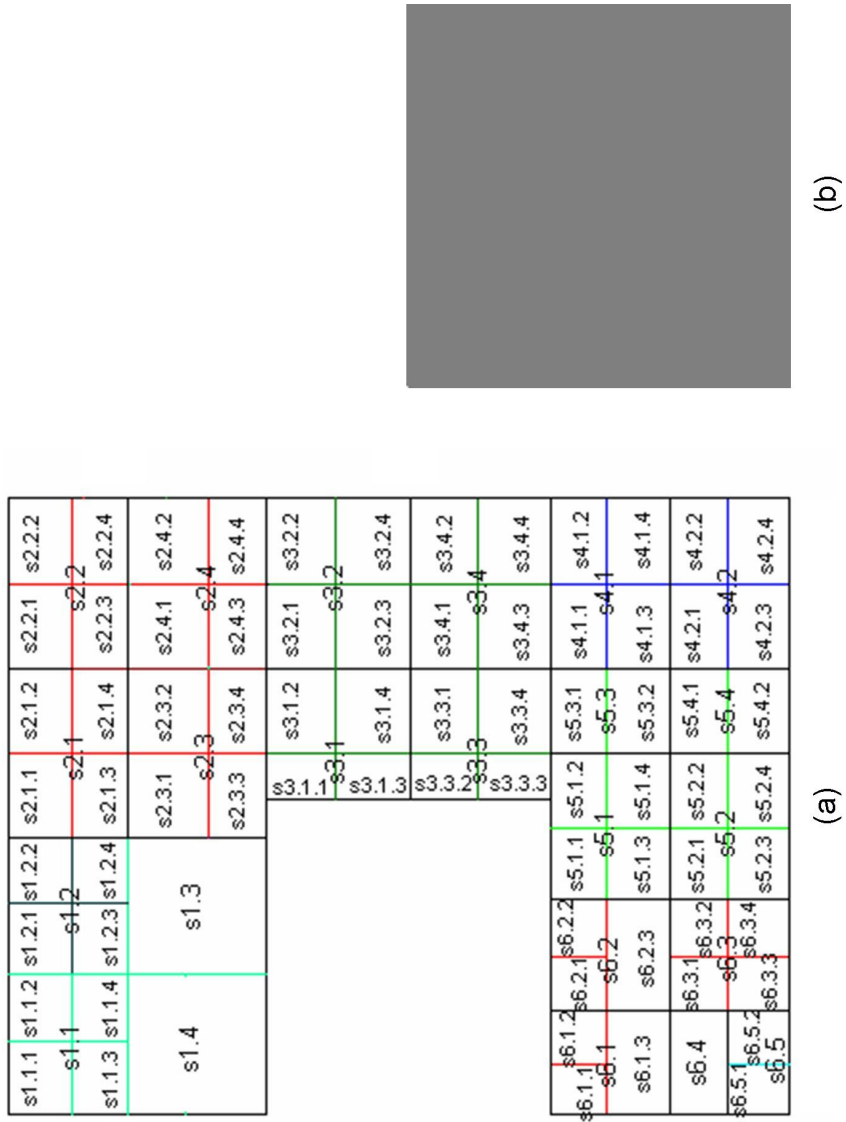


Figure 4.12: The actual size of the (a) model parameter image (b) query region of 200x200 squared pixels.

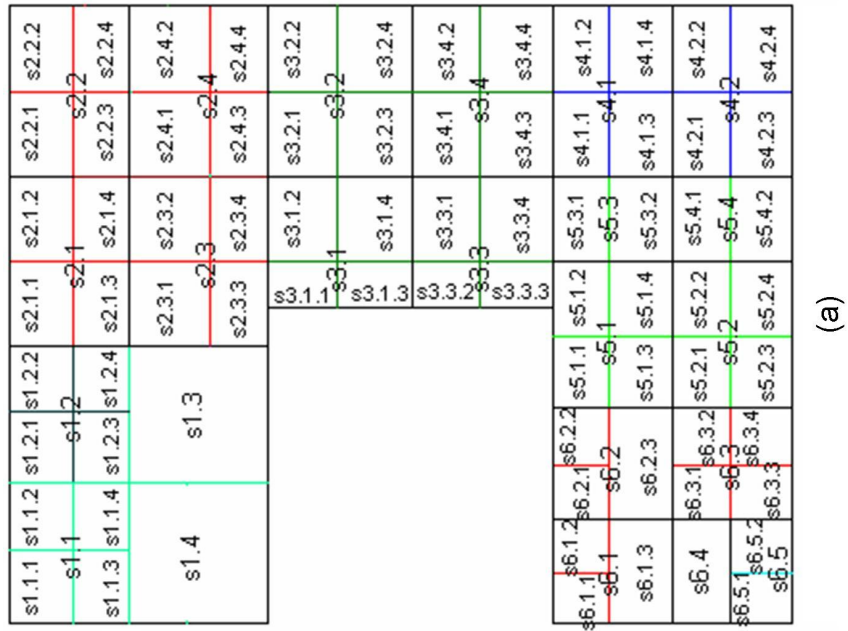


Figure 4.13: The actual size of the (a) model parameter image (b) query region of 50x50 squared pixels.

terms of accuracy. Specifically, the more evenly distributed the size of the definable areas created through the fiducial points, the more accurate the mappings. For these reasons, we have confirmed that the spatial description fiducial points-based method is useful to describe locations in the anatomical domain.

4.2.7 Discussion

This section has addressed the problem of biomedical atlas integration by linking the images of these atlases using the spatial description fiducial points-based method. This approach conceptualises anatomical regions independently of spatial relationships between segmented regions. Mapping is carried out based on spatial relations between the query region and the fiducial points or lines.

The evaluation of the experimental results suggests that our approach improves mapping accuracy with the appropriate number of fiducial points used and with better selection of fiducial point location. Specifically, the more evenly distributed the size of the definable areas created through the fiducial points, the more accurate the mappings.

Nevertheless, locating fiducial points on images is a challenging task even for experts. Depending on experience and the variance among experts' definitions, locations may be slightly different [102; 103]. This has motivated the development of several projects aiming for automatic landmarking. The purpose of automatic landmarking is to put fiducial points on surfaces and match fiducial points on different surfaces to each other. Project focuses range from detection of landmark in organs [41], cephalometry [104], skeletal [105; 106; 107] and brain [108; 109] images. Our proposed approach here, however, is not meant to involve a large number of fiducial points such that the estimation may require image processing. Getting high accuracy by using a large number of fiducial points is not the goal. Instead, we encourage selection of fiducial points that may be defined easily, without the need for image processing. This work will be demonstrated in the following section.

4.3 Overview of Well-defined Fiducial Points

The following experiments were undertaken to test 14 well-defined fiducial points surveyed in the literature (Chapter 2). These well-defined fiducial points can be selected manually in a canonical image, based on their definitions. These fiducial points are available for selection in the sagittal view of the Theiler Stage 23 mouse embryo image as shown in Figure 4.14. They are *Aortic Root*, *Tip of the Lung*, *Liver*

Dome, Top of Kidney, Kidney Hilum, Left Head of Femur, Coccyx, L5 Vertebra, L12 Vertebra, C2 Vertebra, C7 Vertebra, Carina, Lowest Point of Sternum (Ribs), and Lowest Point of Sternum (Tips). Figure 4.14 provides the illustration for these fiducial points.



Figure 4.14: Sagittal view of TS23 mouse embryo image with 14 well-defined fiducial points identified during literature review (Chapter 2)

Aortic root is described by Seifert *et al.* [41] as the "junction between the left ventricle and the aortic arch". The tip of the lung is the end of the pointed lung structure. The liver dome is described by Seifert *et al.* [41] as "the maximal point directing into the right lung". The kidney hilum has been described by Seifert *et*

al. [41] as the "recessed central fissure" in a kidney. The top of the kidney is the top-most part of the kidney.

The head of the femur is described by Hanumantharaju and Shivanand [110] as the "globular and forms rather more than a hemisphere, is directed upward, medialward, and a little forward, the greater part of its convexity being above and in front".

The coccyx is described as "the tailbone, which is the final segment of the ape vertebral column" [111].

L5 is described by Bhandutia *et al.*[112] as the "fifth lumbar vertebra of the spine". L12 is the 12th level of thoracic vertebra of the spine. The C2 vertebra is the second cervical vertebra of the spine. C7 vertebra is the seventh cervical vertebra of the spine. The carina of the trachea is described as "the ridge separating the openings of the right and left main bronchi at their junction with the trachea" [113].

The sternum is described by Rosdahl and Kowalski [114] as "a flat, sword-shaped bone in the middle of the chest". The top-most part and bottom-most part of the sternum are also denoted as fiducial points.

4.3.1 Analysis of Mapping Using Well-defined Fiducial Points

The purpose of the following experiments was to analyse the percentage of accuracy produced by the spatial description fiducial points-based method using 14 well-defined fiducial points identified during literature review. The experiments were conducted on the embryo image depicted in Figure 4.14 on the following anatomical regions: liver, midgut, lung, thalamus, pancreas, adrenal gland cortex, metanephros, and femur. These eight regions were chosen as an anatomical location test set to demonstrate examples of the resulting accuracy. The percentage of accuracy for every anatomical location is calculated using Equation 4.1. We measured the percentage of accuracy resulting from the combination of 7, 9 and 11 well-defined fiducial points. Each combination of fiducial points comes with its test sets in order to evaluate which combination of fiducial points can produce the highest accuracy for the eight anatomical locations tested for experimentation.

This series of experiments involved mapping from one image to the exact same image. The later chapter deals with mapping between images that are morphologically different. The actual area for every anatomical region involved in these experiments is computed using the woolz image processing system. The *WlzArea* function of woolz library was used to calculate the area for every input anatomical region in the 2D woolz object image format.

The effectiveness of mapping using 7 well-defined fiducial points was evaluated using the following 4 test sets:

- a) Test Set 1: Combination of 7 fiducial points which include *Liver Dome*, *C2 Vertebra*, *L5 Vertebra*, *Tip of the Lung*, *Left Head of Femur*, *Lowest Point of Sternum (Ribs)*, and *Coccynx*
- b) Test Set 2: Combination of 7 fiducial points which include *Lowest Point of Sternum (Ribs)*, *Tip of the Lung*, *L5 Vertebra*, *L12 Vertebra*, *C7 Vertebra*, *Coccynx*, and *Left Head of Femur*
- c) Test Set 3: Combination of 7 fiducial points which include *Kidney Hilum*, *Carina*, *Left Head of Femur*, *Liver Dome*, *L5 Vertebra*, *L12 Vertebra*, and *Lowest Point of Sternum (Ribs)*
- d) Test Set 4: Combination of 7 fiducial points which include *Tip of the Lung*, *Kidney Hilum*, *Aortic Root*, *Left Head of Femur*, *C2 Vertebra*, *C7 Vertebra*, and *Lowest Point of Sternum (Tips)*

The effectiveness of mapping using 9 well-defined fiducial points was evaluated using the following 4 test sets:

- a) Test Set 1: Combination of 9 fiducial points which include *Liver Dome*, *Lowest Point of Sternum (Tips)*, *Lowest Point of Sternum (Ribs)*, *C2 Vertebra*, *Carina*, *L12 Vertebra*, *L5 Vertebra*, *Top of Kidney*, and *Left Head of Femur*
- b) Test Set 2: Combination of 9 fiducial points which include *Aortic Root*, *Lowest Point of Sternum (Tips)*, *Lowest Point of Sternum (Ribs)*, *C7 Vertebra*, *Tip of the Lung*, *Kidney Hilum*, *L5 Vertebra*, *Left Head of Femur*, and *Coccynx*
- c) Test Set 3: Combination of 9 fiducial points which include *C2 Vertebra*, *Carina*, *Tip of the Lung*, *Liver Dome*, *Kidney Hilum*, *Lowest Point of Sternum (Ribs)*, *L5 Vertebra*, *Left Head of Femur*, and *Coccynx*
- d) Test Set 4: Combination of 9 fiducial points which include *Aortic Root*, *Lowest Point of Sternum (Tips)*, *Carina*, *Liver Dome*, *Top of Kidney*, *L5 Vertebra*, *L12 Vertebra*, *Left Head of Femur*, and *Coccynx*

The effectiveness of mapping using 11 well-defined fiducial points was evaluated using the following 4 test sets:

- a) Test Set 1: Combination of 11 fiducial points which include *Tip of the Lung, Liver Dome, Top of Kidney, Left Head of Femur, Coccynx, L5 Vertebra, L12 Vertebra, C2 Vertebra, C7 Vertebra, Carina, and Lowest Point of Sternum (Tips)*
- b) Test Set 2: Combination of 11 fiducial points which include *Aortic Root, Tip of the Lung, Liver Dome, Left Head of Femur, Coccynx, L5 Vertebra, L12 Vertebra, C2 Vertebra, C7 Vertebra, Carina, and Lowest Point of Sternum (Ribs)*
- c) Test Set 3: Combination of 11 fiducial points which include *Aortic Root, Liver Dome, Kidney Hilum, Left Head of Femur, Coccynx, L5 Vertebra, L12 Vertebra, C2 Vertebra, C7 Vertebra, Carina, and Lowest Point of Sternum (Ribs)*
- d) Test Set 4: Combination of 11 fiducial points which include *Aortic Root, Tip of the Lung, Kidney Hilum, Top of Kidney, Left Head of Femur, Coccynx, L5 Vertebra, C2 Vertebra, Carina, Lowest Point of Sternum (Tips), and Lowest Point of Sternum (Ribs)*

The accuracy resulting from using the spatial description fiducial points-based method based on the combination of 7, 9 and 11 well-defined fiducial points is shown in Figures 4.15, 4.16 and 4.17 respectively.

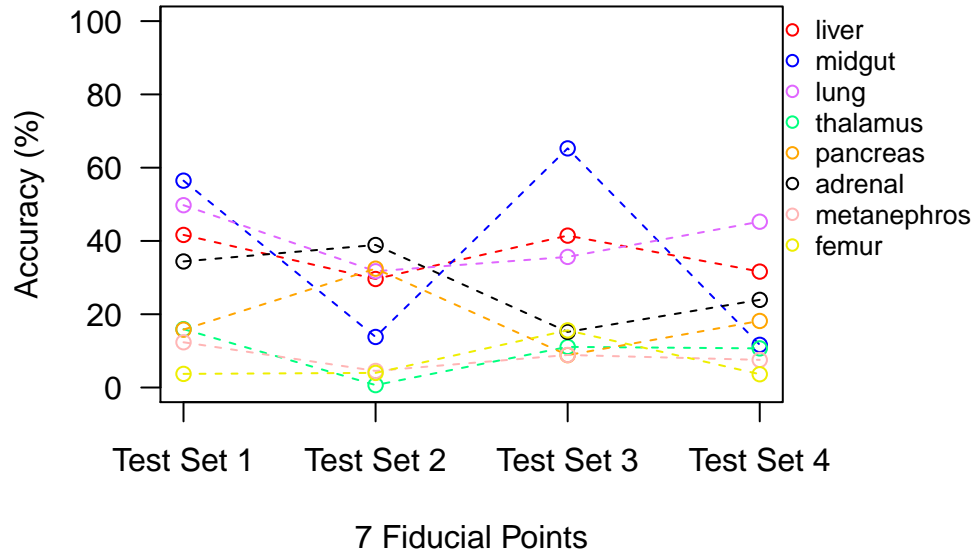


Figure 4.15: The percentage of accuracy served by the combination of 7 fiducial points. None of these combinations yielded the highest accuracy for all anatomical locations.

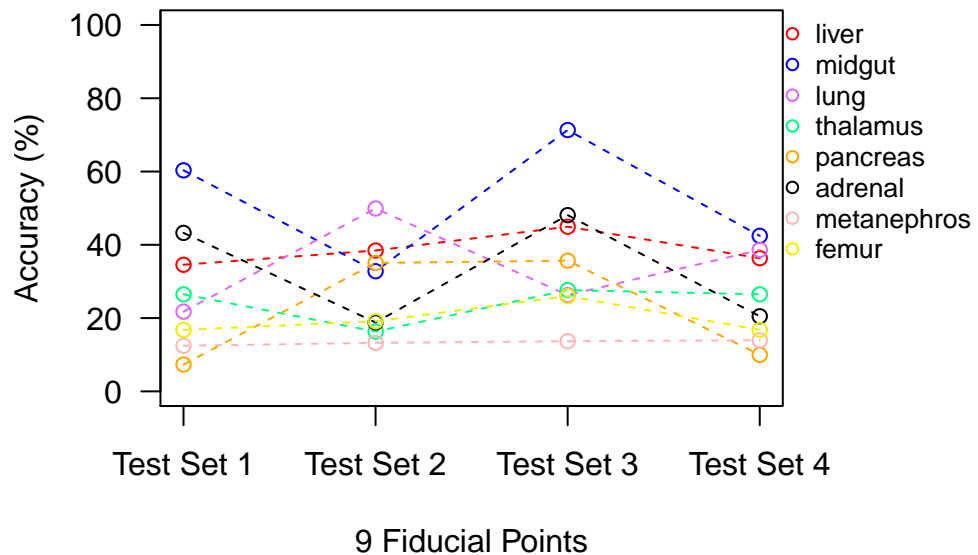


Figure 4.16: The percentage of accuracy served by the combination of 9 fiducial points. None of these combinations yielded the highest accuracy for all anatomical locations.

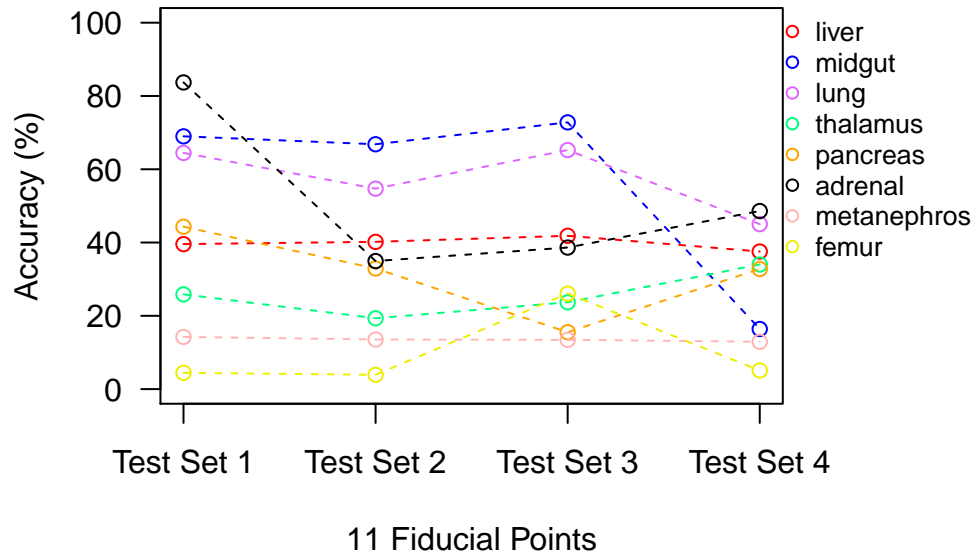


Figure 4.17: The percentage of accuracy served by the combination of 11 fiducial points. None of these combinations yielded the highest accuracy for all anatomical locations.

4.3.2 Discussion

The results of this study suggest that given the choice of a list of fiducial points, selecting a certain number of fiducial points and having different combinations of these, resulted in no one combination that gives the highest percentage of accuracy for all anatomical locations. The only method to improve the mapping accuracy is by increasing the number of fiducial points. Figure 4.18 shows the percentage of accuracy served by the number of fiducial points for all eight anatomical locations tested during this evaluation. The percentage of accuracy for each anatomical location plotted in this graph corresponds to the highest percentage of accuracy produced by the combination of 7, 9, 11 and 14 number of fiducial points. The graph shows that the percentage of accuracy increases with the increase number of fiducial points.

4.4 Summary

This chapter has presented the calibration results of the spatial description fiducial points-based method. This method conceptualises anatomical regions independently of spatial relationships between segmented regions. Mapping is performed based on the satisfaction of exactly the same constraints between the query region and the fiducial points, and also between the query region and the fiducial lines. The

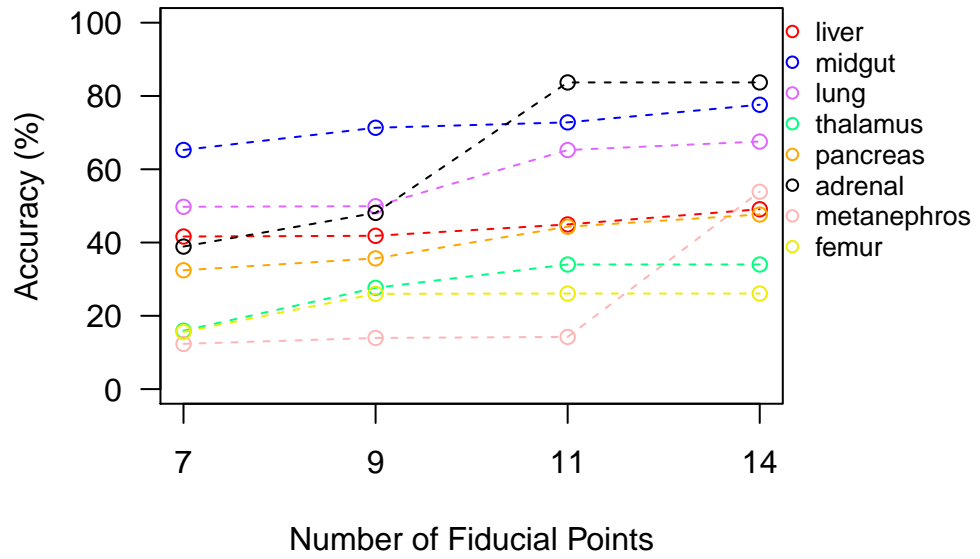


Figure 4.18: The percentage of accuracy served by the number of fiducial points. The more fiducial points are included the higher the percentage of accuracy.

evaluation of the experimental results suggests that the approach improves mapping accuracy with the appropriate number of fiducial points used and better selection of fiducial point location. Specifically, the more evenly distributed the size of the definable areas, which are created through the fiducial points, the more accurate the mappings are. The evaluation of the experimental results also suggests that given a list of fiducial points, using a certain number of fiducial points and selecting different combinations of these, there is no single combination that gives the highest accuracy for all anatomical locations. The only method to improve the accuracy is by increasing the number of fiducial points. We have demonstrated this using 14 well-defined fiducial points, as identified during the literature review.

Chapter 5

The Evaluation of Spatial Description-Based Integration

5.1 Introduction

This chapter presents a performance evaluation of the spatial description fiducial points-based method. Three sets of experiments were conducted.

The first set of experiments was carried out to evaluate problems associated with image region mappings. Since the gene expression data in biomedical atlases are queried by painting or drawing arbitrary regions in the canonical images, this thesis focuses on image region mappings. Therefore, the case of mapping to find a matching image was not further explored as it was not a part of the dissertation.

The second set of experiments was carried out to measure accuracy when using one ontology-based method and one method in image processing. The results were compared to the spatial description fiducial points-based method. This set of experiments was carried out to evaluate image region mappings in identical images.

The third set of experiments used mappings done by an expert biologist. The results were compared to one ontology-based method, one method in image processing, and the spatial description fiducial points-based method. This experiment was carried out to evaluate image region mappings in non-identical images. Finally, an evaluation of gene expression data was carried out to measure the spatial similarity between two mapped spatial regions.

This chapter is organised as follows: Section 5.2 presents the set of experiments to illustrate the categorisation of problems associated with image region mappings. Section 5.3 presents the set of experiments to measure accuracy when using one ontology-based method and one method in image processing and compares the results with the fiducial points-based method. Section 5.4 presents mappings done by an expert biologist, the results being compared to the image processing algorithm, the ontology-based method, and the spatial description fiducial points-based method. Section 5.5 presents an evaluation that measures the spatial similarity between two mapped spatial regions. Section 5.6 summarises the chapter.

5.2 Demonstration of Problems Associated with Image Region Mappings

There are three types of image which are relevant within the context of this study: (1) similar images which are not identical in their morphologies (e.g. image slices of an embryo, midline images from two consecutive Theiler Stages of the same embryo etc), (2) non-identical images which are not identical in their morphologies (e.g. midline images of different embryos at the same developmental stage etc), and (3) non-identical images with the same morphology (e.g. images of an embryo from different imaging modalities etc). The images used for this evaluation were chosen as good representatives to represent the natural variation of animals and for the approximation of dealing with different morphologies. In addition, these images are significant in the many different requirements of a mapping system, which would support the integration of biomedical atlases.

For this evaluation, the image processing algorithm used was the ASIFT algorithm. The reason for using this algorithm has been explained in the literature review. In the case of mapping image regions, the experiments started by cropping a query region from the original image. Next, the query region and the full image were uploaded into the ASIFT system to generate the mapping result.

The experiment which used the ontology-based method was carried out using the OBO and EMAP ontologies. These two ontologies have been chosen because both are relevant in the context of the images used within this evaluation. The experiment started by painting the image according to its anatomical regions. Each painted region is linked to the corresponding concept in the ontology. The two images *I1* and *I2* of Figures 5.1, 5.2 and 5.3 used the OBO and EMAP ontologies, respectively. Both OBO and EMAP define the structure of the *liver* as:

"liver is part_of visceral organ, visceral organ is part_of organ system, organ system is part_of embryo, embryo is part_of mouse"

Figure 5.1 depicts the mapping of region *liver* resulting from using the ontology-based method on two images similar but not identical in their morphologies.

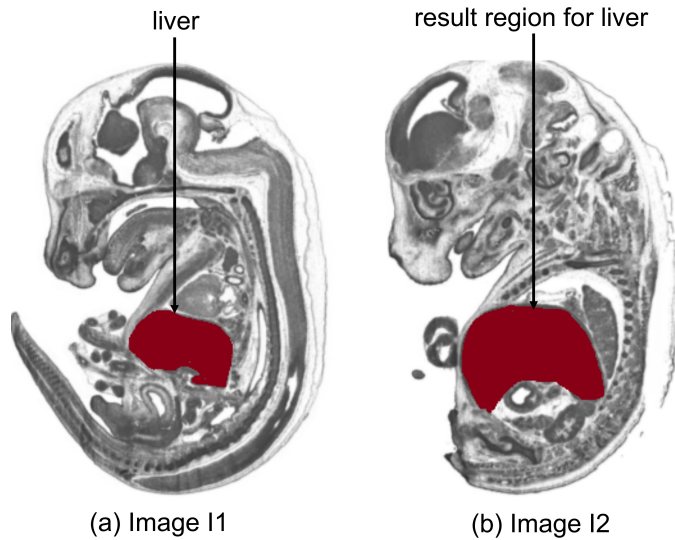


Figure 5.1: Image regions mapped between similar images but not identical in their morphologies. The ontology-based method has mapped the *liver* in (a) image *I1* to the (b) result region in image *I2*. In contrast, the image processing algorithm failed in this mapping.

Figure 5.2 depicts the mapping of the *liver* region using the ontology-based method on non-identical images that are not identical in their morphologies.

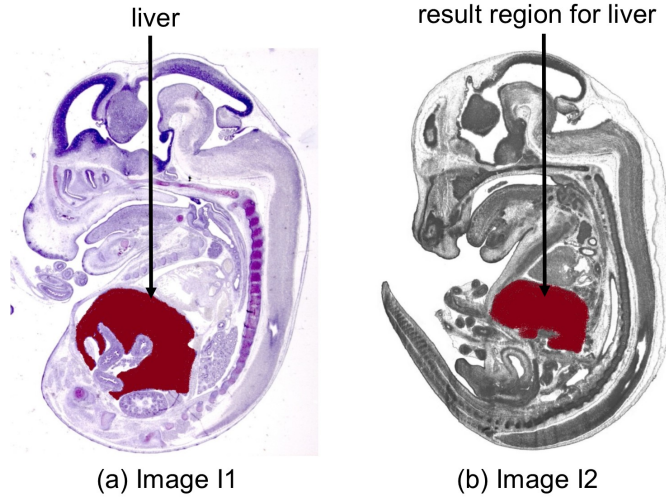


Figure 5.2: Image regions mapped between non-identical images that are not identical in their morphologies. The ontology-based method has mapped the *liver* in (a) image *I1* to the (b) result region in image *I2*. In contrast, the image processing algorithm has failed in this mapping.

Figure 5.3 depicts the mapping of the *liver* region using the ontology-based method on non-identical images with same morphology. The image in Figure 5.3(a) is the clip art graphic version of the image in Figure 5.3(b) in which the visual content of both images is only similar at the higher scene level, but both images are entirely different at the pixel-level.

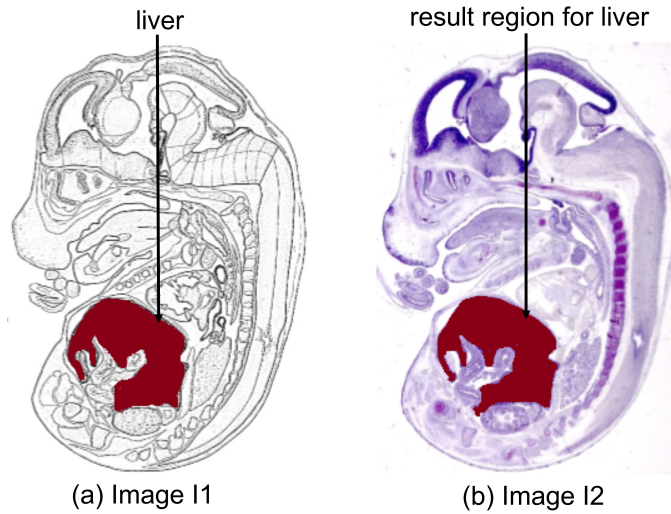


Figure 5.3: Mappings of image regions between non-identical images with the same morphology. The ontology-based method has mapped the *liver* in (a) image *I1* to the (b) result region in image *I2*. In contrast, the image processing algorithm failed in this mapping.

Although two different ontologies were used, the mapping of region *liver* in Figures 5.1, 5.2 and 5.3 were successful because the *liver* was segmented in both images, and both ontologies have exactly the same definition for the *liver*. This also applies when the mappings use two same ontologies. In contrast, the image processing algorithm has failed in these three cases of mappings because the two regions are different in their morphologies. In principle, the ontology-based method may provide a mapping with good precision if mapping is between same regions. This region is segmented in both images and is defined in the ontologies. Nevertheless, the ontology-based method may not be able to provide a mapping with good precision if the mapping is between a region that is segmented in one image but not in the other. For example, assume that the *pituitary* is segmented in image *I1*, but not in image *I2*: Image *I1* used the OBO ontology and image *I2* used the EMAP ontology. OBO describes the *pituitary* as:

"pituitary is part_of stomatodaeum, stomatodaeum is part_of alimentary system, alimentary system is part_of visceral organ, visceral organ is part_of organ system, organ system is part_of embryo, embryo is part_of mouse"

This term is linked to region *pituitary*, which is segmented in image *I1*. EMAP describes the *pituitary* as:

"*pituitary is part_of gland, gland is part_of diencephalon, diencephalon is part_of forebrain, forebrain is part_of brain, brain is part_of central nervous system, central nervous system is part_of nervous system, nervous system is part_of organ system, organ system is part_of embryo, embryo is part_of mouse*"

Image *I2* does not have the segmentation of region *pituitary*; therefore, this term is not linked to any region in the image. Since the ontology-based method was carried out by identifying structure correspondences between the two ontologies, the consequence is that no result region was found because the term *pituitary* in EMAP is not linked to any region in image *I2*. This also applies when the mappings use two same ontologies. The ontology-based method was unable to provide a mapping because one term is linked to a region in one image but not in the other.

Semantic interoperability problems arise when images have different image region annotations. Ontology matching is a process to determine the correspondences between heterogeneous annotated data. James *et al.* [115] describe a similarity measure for two concepts *A* and *B*, where *A* is a term defined in ontology *O1* and *B* is a term defined in ontology *O2*. Both *A* and *B* can be equated with their corresponding sets. The similarity between *A* and *B* can be determined based on the intersection of these sets. Assuming that *A* represents the *pituitary* in OBO and *B* represents the *pituitary* in EMAP, the sets for these two concepts are as follows:

$$\begin{aligned} pituitary_{OBO} = \{ & part_of(pituitary, stomatodaeum), \\ & part_of(stomatodaeum, alimentary\ system), \\ & part_of(alimentary\ system, visceral\ organ), \\ & part_of(visceral\ organ, organ\ system), \\ & part_of(organ\ system, embryo), part_of(embryo, mouse)\} \end{aligned}$$

$$\begin{aligned} pituitary_{EMAP} = \{ & part_of(pituitary, gland), part_of(gland, diencephalon), \\ & part_of(diencephalon, forebrain), part_of(forebrain, brain), \\ & part_of(brain, central\ nervous\ system), \\ & part_of(central\ nervous\ system, nervous\ system), \\ & part_of(nervous\ system, organ\ system), \\ & part_of(organ\ system, embryo), part_of(embryo, mouse)\} \end{aligned}$$

The intersection between these two sets is:

$$\begin{aligned} pituitary_{OBO} \cap pituitary_{EMAP} = \\ \{ part_of(organ\ system, embryo), part_of(embryo, mouse)\} \end{aligned}$$

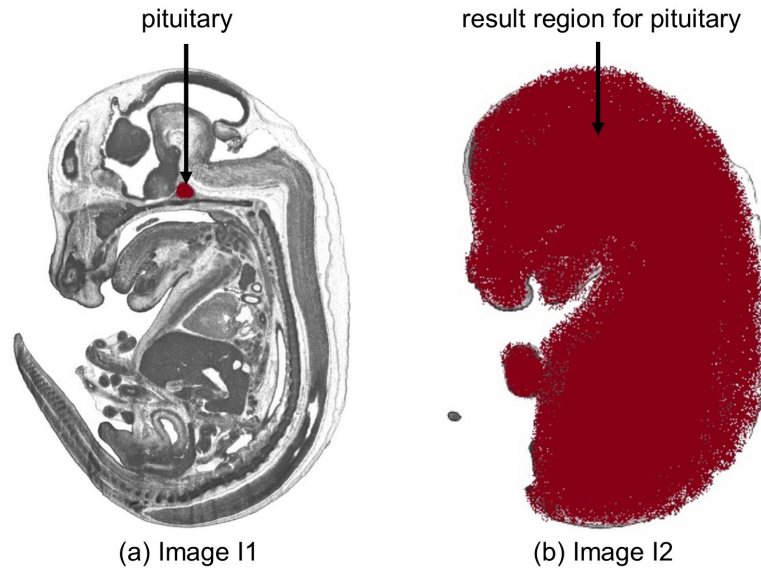


Figure 5.4: The mapping of image regions between two slices of an embryo. The ontology-based method has mapped the *pituitary* in (a) image *I1* to the (b) result region in image *I2*. Region *pituitary* is annotated in image *I1* but not in image *I2*. The two ontologies provide different definitions for the *pituitary*. Defining the similarities between these two definitions using an ontology matching approach based on the set intersection have resulted in a low mapping precision.

Figure 5.4 depicts the mapping resulting from using the ontology-based method on two image slices of an embryo, in which the first is the midline and the second is the sliced image at 0.800mm distance from the midline. This kind of ontology matching has mapped the *pituitary* in image *I1* to the whole embryo region in image *I2* to consider both the organ system and the embryo as the result region. Mapping was successful; however, the results of this approach are low in terms of spatial precision.

5.3 Analysis of Image Region Mappings in Identical Images

The purpose of the following experiments was to analyse the accuracy produced by one ontology-based method and one method in image processing and to compare the results with the spatial description fiducial points-based method. The experiment was conducted on an embryo image as depicted in Figure 4.14 in Chapter 4, on the following anatomical regions: liver, midgut, lung, thalamus, pancreas, adrenal gland cortex, metanephros, and femur. These eight regions were chosen for this anatomical location test set in order to demonstrate examples of the resulting accuracy when mappings between these structures were performed using the three approaches. This

experiment was carried out at the mapping of regions between two identical images considering that this is the kind of case where all techniques are able to cope with the mapping. The evaluation in a later section deals with the mapping of image regions between non-identical images. The percentage of accuracy for every anatomical location was calculated using Equation 4.1.

5.3.1 Ontology-Based Method

An ontology-based method consists of a collection of anatomical domains and relations between those domains. We used the 49 segmented spatial regions (as depicted in Figure 2.15 in Chapter 2) as a collection of anatomical domains. The relations between these anatomical domains were based on spatial relationships following *SpaRTAD*. We used these two resources for the ontology-based method considering that the 49 anatomical domains of the embryo image had been painted according to the ontology. Moreover, relations between these anatomical domains have been determined according to three categories of spatial relations; topological, arrangement and directional relations. This simplification allowed us to concentrate in this experiment on evaluating the accuracy resulting from using the fiducial points-based method and comparing the results with one ontology-based method and one method in image processing. Moreover, it is a time-consuming task to implement an ontology-based method developed by other researchers considering that the anatomical domain in the mouse embryo Theiler Stage 23 image had to be painted according to the ontology and there were differences in terms of the anatomical names and domain coverage causing difficulty in the implementation. Table 5.1 depicts the results in accuracy and detection time when mapping used the ontology-based method. Visual results of mapping using the ontology-based method are shown in

Table 5.1: The resulting accuracy and the detection time when mapping used the ontology-based method.

Anatomical Location	Actual Area (Woolz)	Area (Ontology-based Method)	Detection Time	Accuracy (%)
Liver	46920	76302	0.375s	61.49
Midgut	9216	12768	0.375s	72.18
Lung	9729	18576	0.375s	52.37
Thalamus	12206	25092	0.375s	48.64
Pancreas	1275	12325	0.375s	10.34
Adrenal Gland Cortex	1320	3132	0.375s	42.15
Metanephros	5381	6432	0.375s	83.66
Femur	1068	2268	0.375s	47.09

Figures 5.5 to 5.12. Figure 5.5 is used to demonstrate how the result region was generated. Figure 5.5 depicts five anatomical regions in their bounding boxes: liver, pelvic girdle, vibrissa, pulmonary artery and lung. These bounding boxes were used to determine spatial relations between these anatomical regions. For example, the

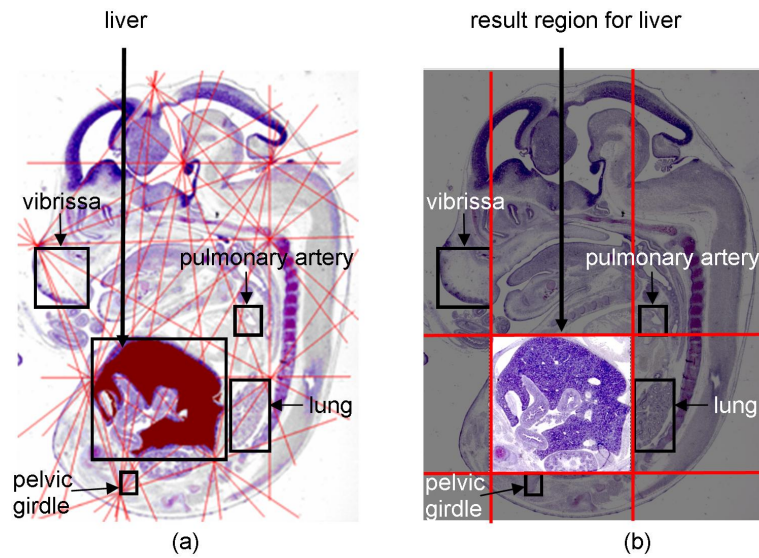


Figure 5.5: Anatomical location of liver (a) in its actual location, and (b) the corresponding match location resulting from the ontology-based method.

simplified description for liver in Figure 5.5(a) can be described as follows:

'liver is northOf pelvic girdle, liver is eastOf vibrissa, liver is southOf pulmonary artery, liver is westOf lung'

This description mapped liver in Figure 5.5(a) to the result region as shown in Figure 5.5(b).

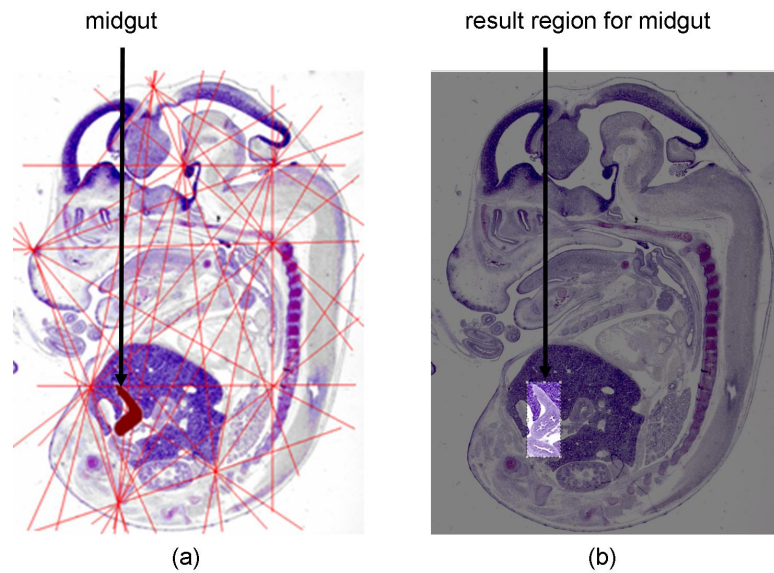


Figure 5.6: Anatomical location of midgut (a) in its actual location, and (b) the corresponding match location resulting from the ontology-based method.

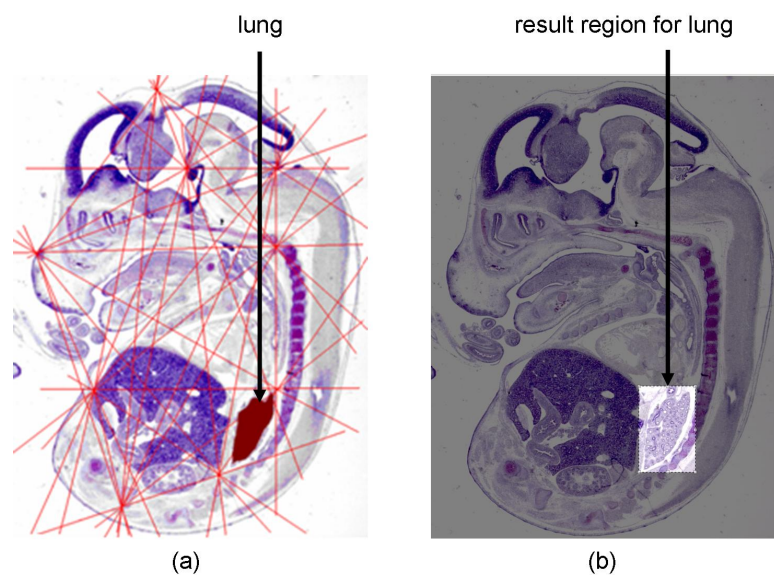


Figure 5.7: Anatomical location of lung (a) in its actual location, and (b) the corresponding match location resulting from the ontology-based method.

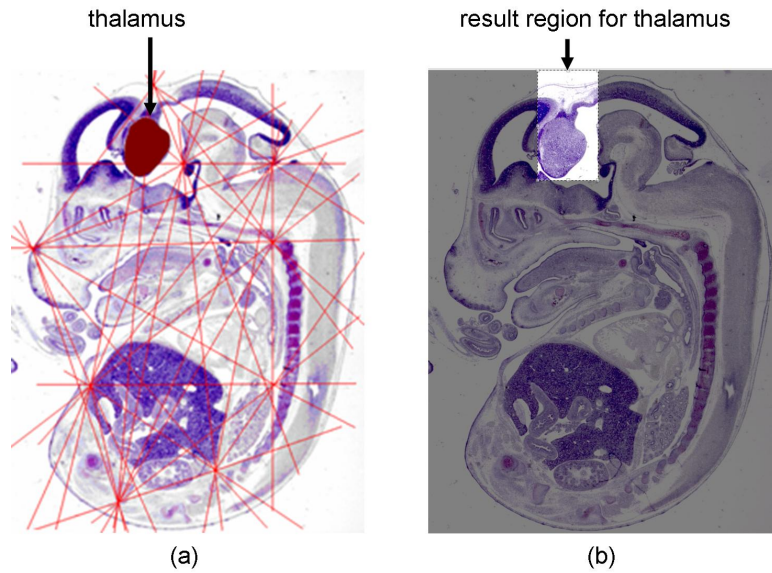


Figure 5.8: Anatomical location of thalamus (a) in its actual location, and (b) the corresponding match location resulting from the ontology-based method.

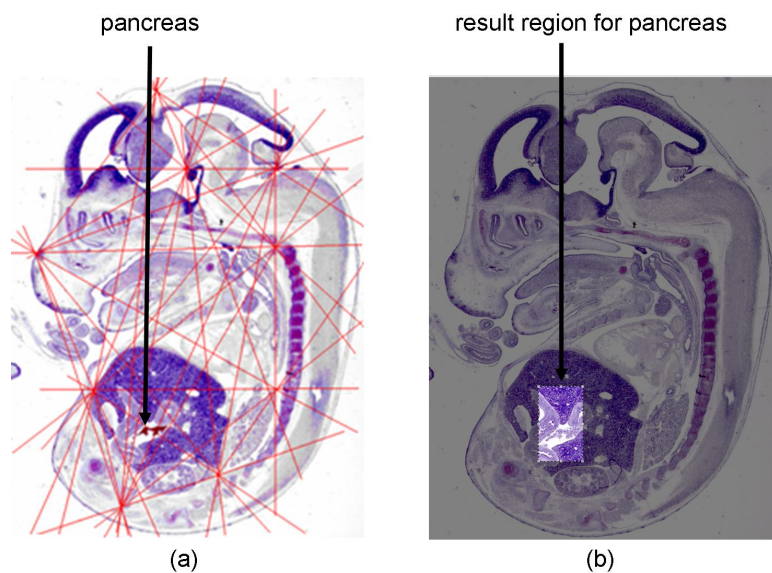


Figure 5.9: Anatomical location of pancreas (a) in its actual location, and (b) the corresponding match location resulting from the ontology-based method.

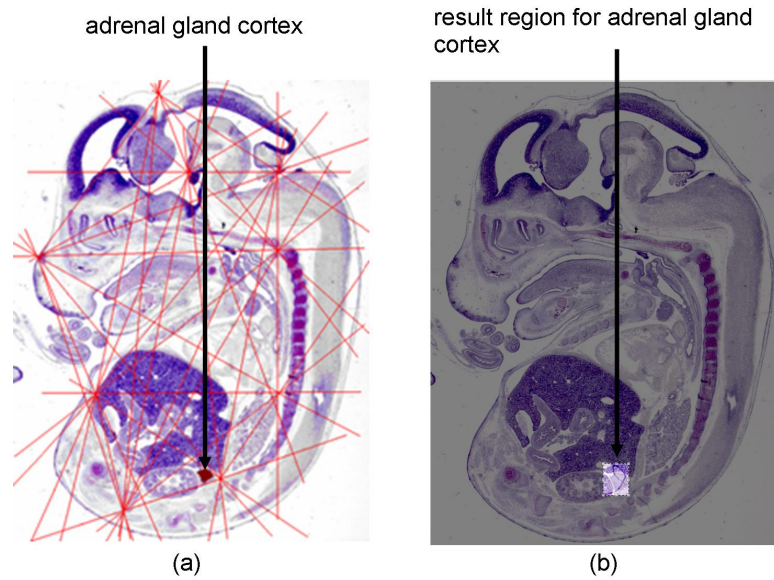


Figure 5.10: Anatomical location of adrenal gland cortex (a) in its actual location, and (b) the corresponding match location resulting from the ontology-based method.

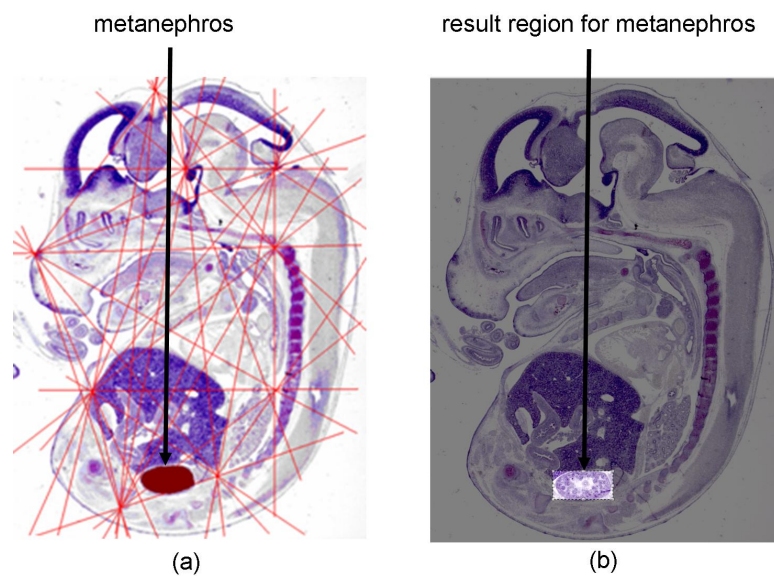


Figure 5.11: Anatomical location of metanephros (a) in its actual location, and (b) the corresponding match location resulting from the ontology-based method.

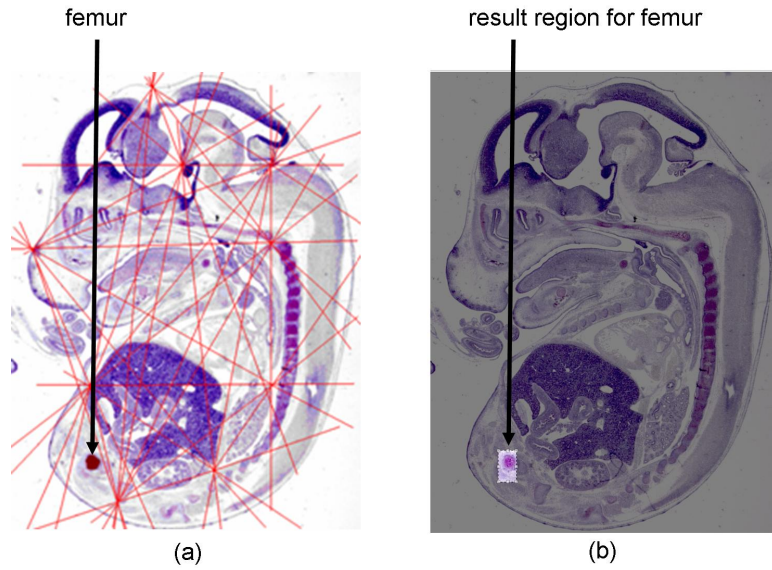


Figure 5.12: Anatomical location of femur (a) in its actual location, and (b) the corresponding match location resulting from the ontology-based method.

5.3.2 Image Processing Algorithm

The image processing-based mapping used the ASIFT [61] image processing algorithm. Conducting the experiment using the ASIFT is described above in Section 5.2. Table 5.2 depicts the accuracy and the detection time when mapping used the image processing algorithm. Visual results of mapping produced by the image pro-

Table 5.2: The resulting accuracy and the detection time when mapping used the image processing algorithm.

Anatomical Location	Actual Area (Woolz)	Area (Image Processing Algorithm)	Detection Time	Accuracy (%)
Liver	46920	56967	36s	82.36
Midgut	9216	10876	52s	63.55
Lung	9729	16187	65s	60.10
Thalamus	12206	19240	42s	63.44
Pancreas	1275	3612	32s	35.30
Adrenal Gland Cortex	1320	4835	32s	27.30
Metanephros	5381	12345	30s	43.59
Femur	1068	1527	30s	69.94

cessing algorithm are shown in Figures 5.13 to 5.20. The mapping of an anatomical region query image onto the full embryo image was based on a set of point correspondences between the two compared images. The lines going from one image to the other illustrate the mapping of points between these images.

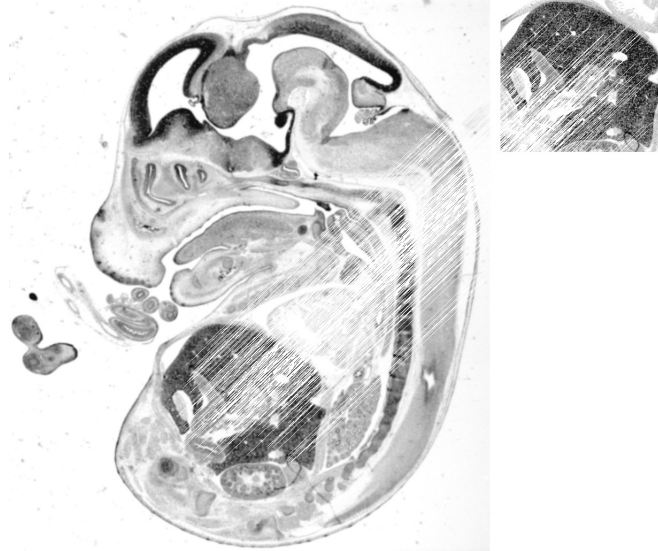


Figure 5.13: Mapping of anatomical location of liver resulting from the ASIFT image processing algorithm.

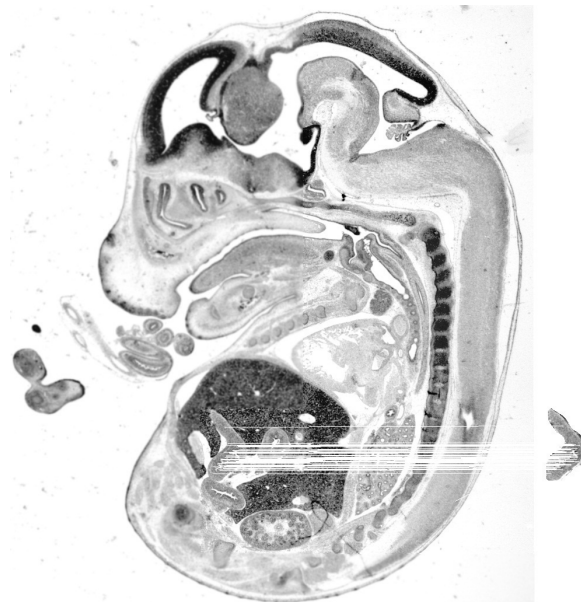


Figure 5.14: Mapping of anatomical location of midgut resulting from the ASIFT image processing algorithm.

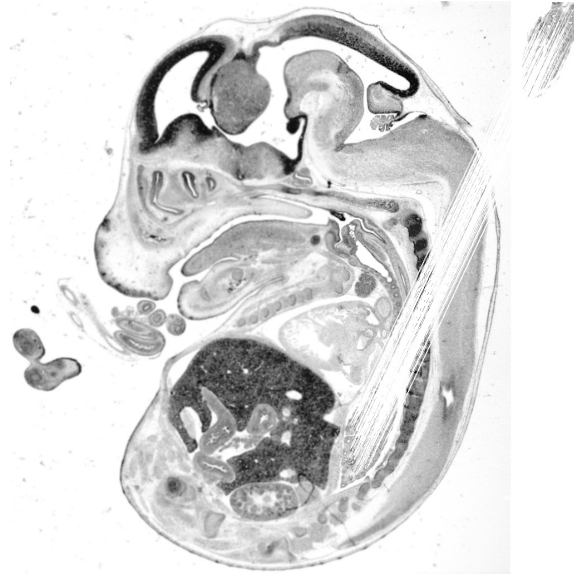


Figure 5.15: Mapping of anatomical location of lung resulting from the ASIFT image processing algorithm.



Figure 5.16: Mapping of anatomical location of thalamus resulting from the ASIFT image processing algorithm.

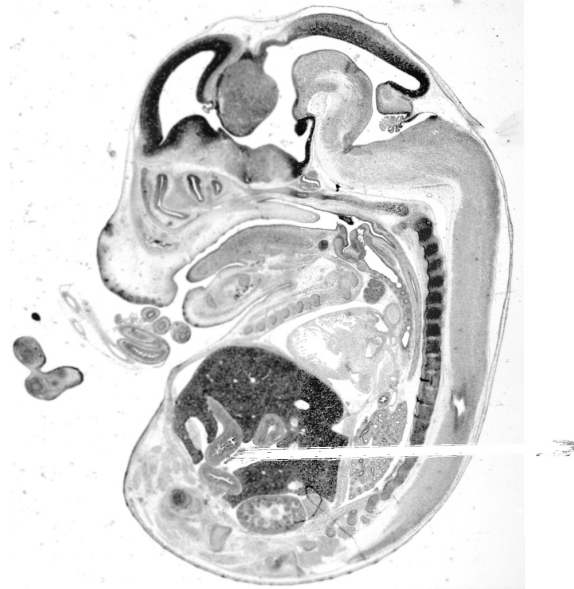


Figure 5.17: Mapping of anatomical location of pancreas resulting from the ASIFT image processing algorithm.

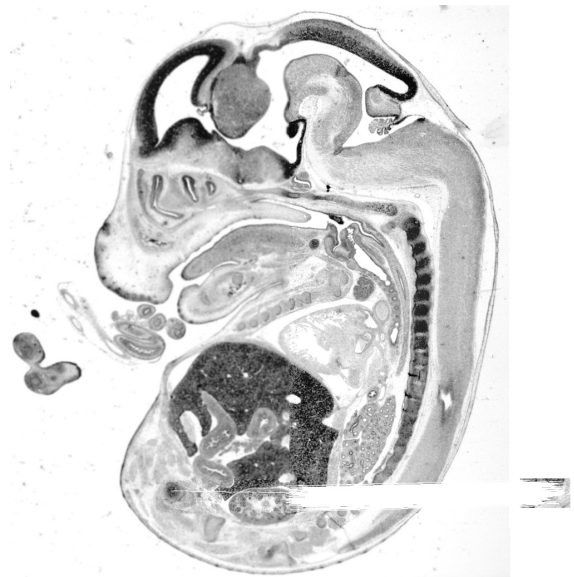


Figure 5.18: Mapping of anatomical location of adrenal gland cortex resulting from the ASIFT image processing algorithm.

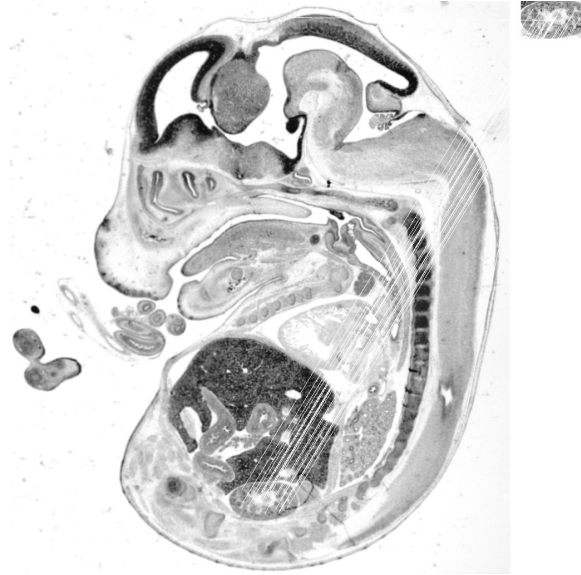


Figure 5.19: Mapping of anatomical location of metanephros resulting from the ASIFT image processing algorithm.



Figure 5.20: Mapping of anatomical location of femur resulting from the ASIFT image processing algorithm.

5.3.3 Spatial Description Fiducial Points-Based Method

The purpose of the experiment was to demonstrate that there is a small number of fiducial points where the combination can provide mapping accuracy as effective as both the ontology-based method and the image processing algorithm. More importantly, it is possible to select a set of fiducial points with such performance without depending on image processing. Table 5.3 depicts accuracy and detection time results when mapping is carried out used the spatial description fiducial points-based method, using all 14 well-defined fiducial points.

Table 5.3: Accuracy and detection time results when mapping using the spatial description fiducial points-based method.

Anatomical Location	Actual Area (Woolz)	Area (SD Fiducial Points-Based Method)	Detection Time	Accuracy (%)
Liver	46920	95575	0.375s	49.09
Midgut	9216	11874	0.375s	77.61
Lung	9729	14399	0.375s	67.57
Thalamus	12206	35889	0.375s	34.01
Pancreas	1275	2675	0.375s	47.66
Adrenal Gland Cortex	1320	1577	0.375s	83.70
Metanephros	5381	9989	0.375s	53.87
Femur	1068	4095	0.375s	26.08

These results were compared to the accuracy of the ontology and image processing-based mappings as depicted in Tables 5.1 and 5.2 respectively. Figure 5.21 depicts the accuracy resulting from using these three techniques. Based on the eight anatomical locations that were tested, when comparing the accuracy produced by the image processing algorithm and the fiducial points-based methods, five out of eight anatomical locations with the highest percentage of accuracy resulted from using the spatial description fiducial points-based method. The image processing algorithm managed to produce only three anatomical locations with the highest accuracy. These results suggest that the spatial description based-solution is sufficient to provide mapping accuracy as good as the image processing algorithm. When comparing the accuracy of the fiducial points-based method with the ontology-based method, four out of eight anatomical locations with the highest percentage of accuracy resulted from using the ontology-based method. Likewise, the fiducial points-based method also managed to produce four anatomical locations with the highest accuracy. These results suggest that the spatial description based-solution is sufficient to provide mapping accuracy as effective as the ontology-based method.

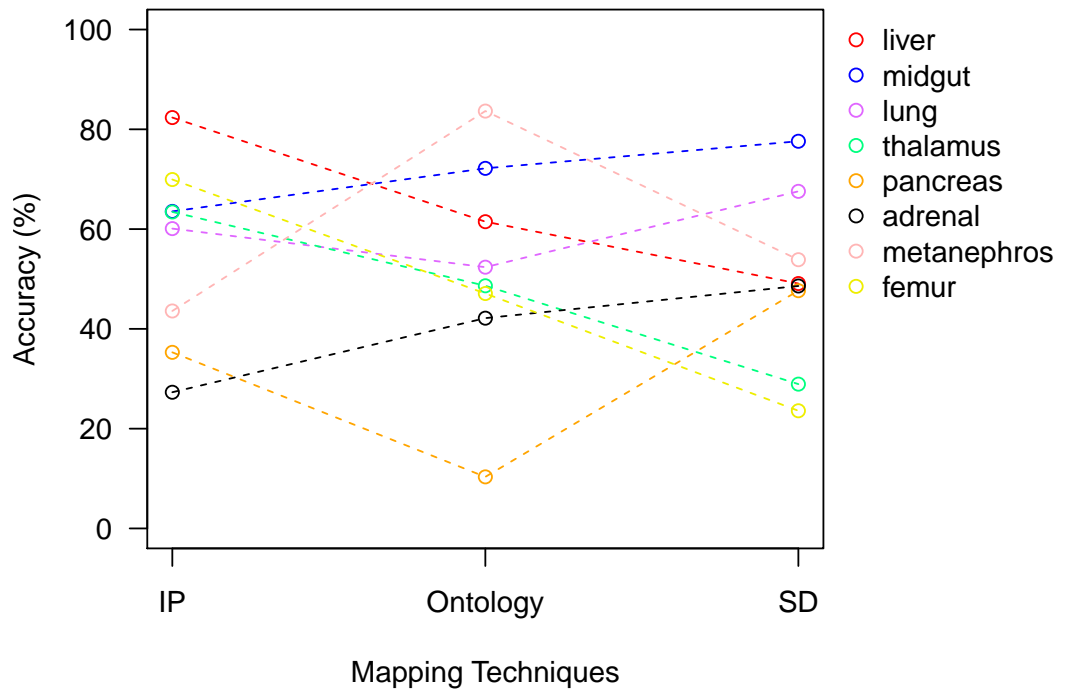


Figure 5.21: Percentage accuracy for the eight anatomical locations produced by the image processing algorithm, the ontology-based method, and the fiducial points-based method involving all 14 well-defined fiducial points. The results suggest that the spatial description fiducial points-based method can provide mapping accuracy as good as both the image processing algorithm and the ontology-based method. *IP* denotes the image processing algorithm, *Ontology* denotes the ontology-based method and *SD* denotes the spatial description fiducial points-based method.

5.3.4 Results and Analysis

The evaluation of the experimental results suggests that there exists, at least in the cases that have been tested, a small number of fiducial points where the combination can provide performance as effective as both the ontology-based method and the image processing algorithm. One example of fiducial points combination with such performance are *Aortic Root*, *Tip of the Lung*, *Liver Dome*, *Top of Kidney*, *Kidney Hilum*, *Left Head of Femur*, *Coccyx*, *L5 Vertebra*, *L12 Vertebra*, *C2 Vertebra*, *C7 Vertebra*, *Carina*, *Lowest Point of Sternum (Ribs)*, and *Lowest Point of Sternum (Tips)*. This finding is, however, based on the set of eight anatomical locations and the set of well-defined fiducial points tested within this series of experimentation.

In terms of detection speed, the spatial description-based solution is faster than the image processing algorithm. Detection speed is related to the computational complexity of the mapping algorithm. A spatial description mapping algorithm examines the isomorphism between the compared spatial description. An isomorphism [116] is a one-to-one correspondence between the elements of the two compared spatial descriptions. These elements correspond to textual description representing the image via spatial relations. On the other hand, the image processing mapping algorithm examines pixels in the corresponding images. Images are large in the number of pixels. Computational complexity for an algorithm that examines image pixels is time consuming, as more pixels are involved [60; 84]. Searching for the correspondences anatomical regions, between canonical images, based on a textual description, is faster than searching for the corresponding pixels between images. This is because the number of textual description is shorter compared to the number of pixels in an image. Furthermore, spatial description is structured according to object/relationship pairs. Hence, mappings based on spatial descriptions are faster than those based on the image processing algorithm. On the other hand, the spatial description is equally as fast as the ontology and both methods are not really problematic from the speed point of view. Detection speeds for these two methods are equally fast because both approaches do not search for image pixels, but are instead searched by a textual description.

5.4 Analysis of Image Region Mappings in Non-Identical Images

This section presents mappings by an expert biologist, with the results comparing the following: (1) the image processing algorithm, (2) the ontology-based method,

and (3) the spatial description fiducial points-based method. The mapping results produced by an expert biologist were used as the 'gold standard'. The purpose of the experiment was to evaluate image region mappings in the following three cases: (1) non-identical images that are not identical in their morphologies, (2) similar images but not identical in their morphologies and (3) non-identical images with the same morphology.

The experiment was conducted on the following anatomical regions: liver, heart, lung, and three arbitrary query regions denote as query regions x , y and z . These six regions were chosen as an anatomical location test set to assess the accuracy resulting from using the three approaches against the 'gold standard'. The percentage accuracy for every anatomical location was calculated using Equation 4.1.

The image processing-based mapping used the ASIFT [61] algorithm. Conducting the experiment using this algorithm has been described in Section 5.2. The spatial description fiducial points-based method used three sets of fiducial points. Set 1 contains a list of fiducial points, as presented in the literature review. A biologist was asked to identify these fiducial points in the images used in the experiment. Set 2 is an extended version of fiducial points in Set 1 by adding a biologist's own choice of fiducial points. Set 3 is also an extended version of fiducial points in Set 1 by adding the non-biologist's own choice of fiducial points.

5.4.1 Mapping between Non-Identical Images that are Not Identical in Their Morphologies

The purpose of the experiments was to demonstrate the mapping of regions between two different embryos. These embryos are at the same developmental stage. Two midline images at Theiler Stage 23 were used. The first is derived from the Kaufman Digital Atlas and the second is derived from the Edinburgh Mouse Atlas as shown in Figure 5.22. The spatial description fiducial points-based method used three sets of fiducial points. Figures 5.22, 5.23 and 5.24 depict the fiducial points in Set 1, Set 2 and Set 3, respectively.

Figure 5.25 depicts the accuracy resulting from using six approaches at the mapping of the six regions. The biologist defined gold standard mappings, demonstrating that there exists a result region for every query region. Unfortunately, the image processing algorithm used in this experiment has failed. On the other hand, an ontology-based method is not available to provide mappings in these experiments because the Kaufman Atlas's image is not available with painted domains. This provides evidence that the ontologies may have difficulty with images without painted

domains.

The graph shows that the spatial description fiducial points-based method is sufficient to provide mappings. The accuracy resulting from using this method depends on the choice of fiducial points and the number of fiducial points used. For example, the accuracy resulting from using the fiducial points in Set 2 is higher than with the fiducial points in Set 1, because Set 2 contains more fiducial points than Set 1.

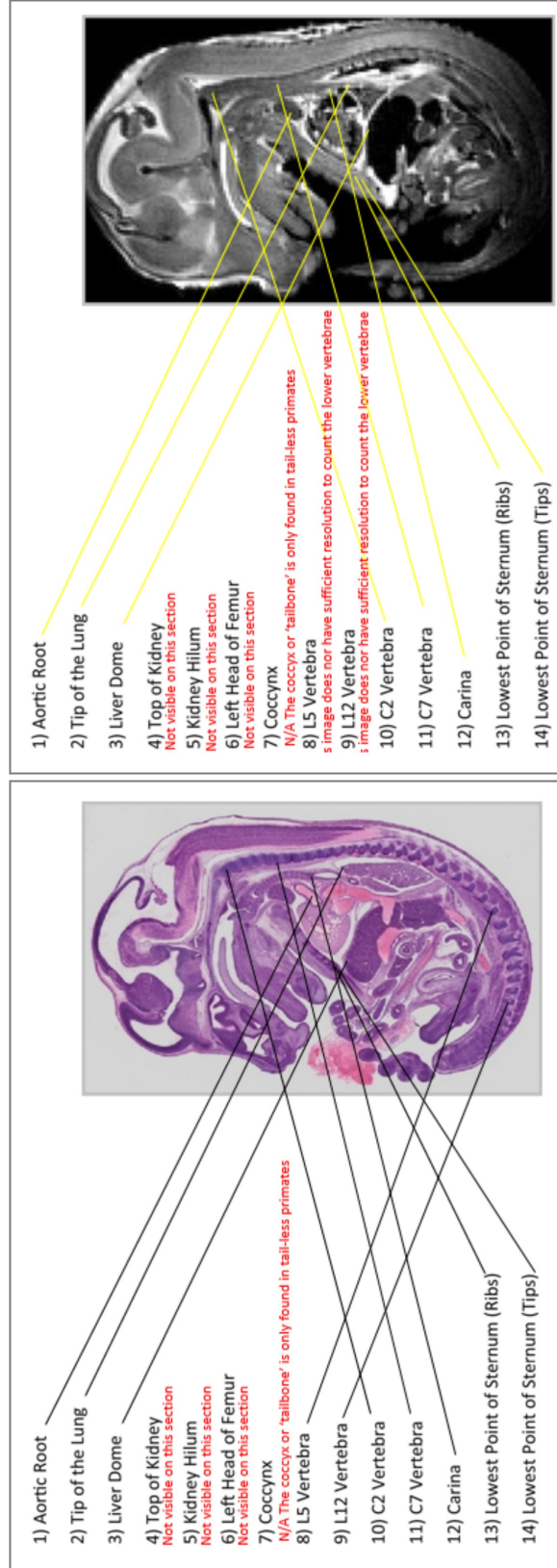


Figure 5.22: Mapping of fiducial points between two midline images of different embryos at Theiler Stage 23 based on 14 fiducial points, as identified in the literature review, selected by a biologist. There are only eight relevant fiducial points between the two images.

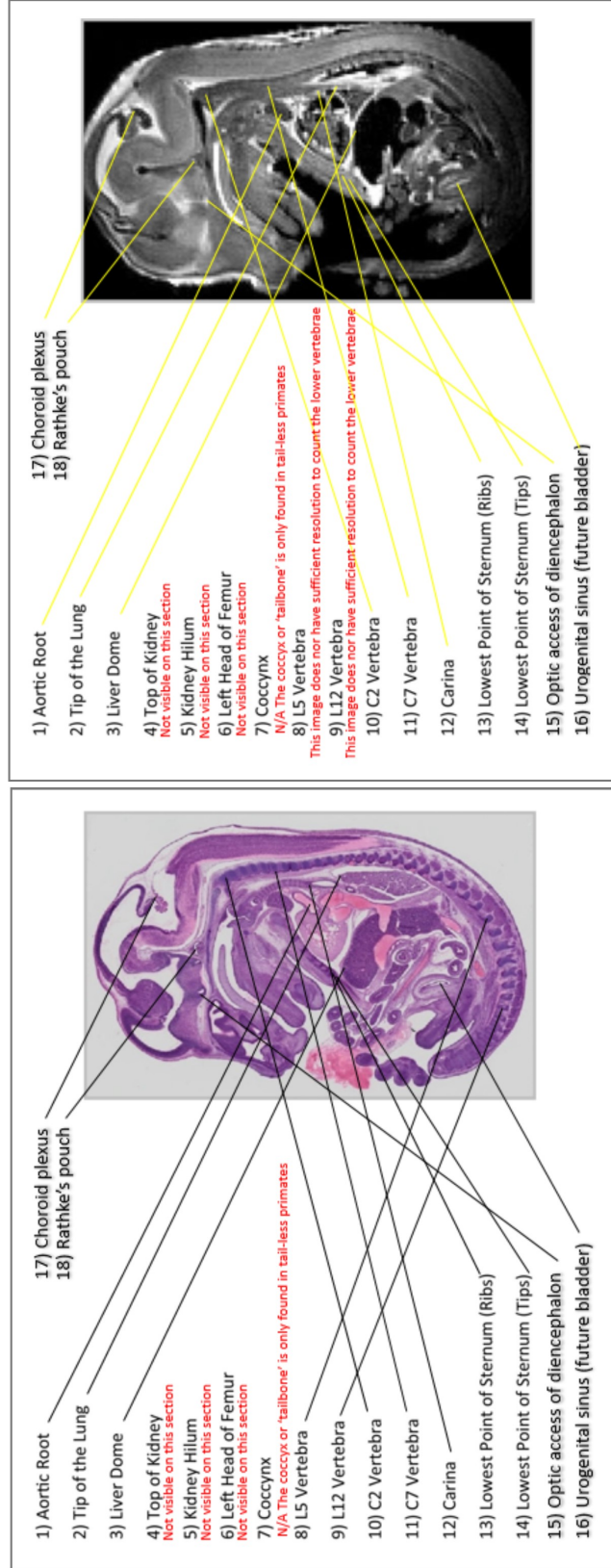
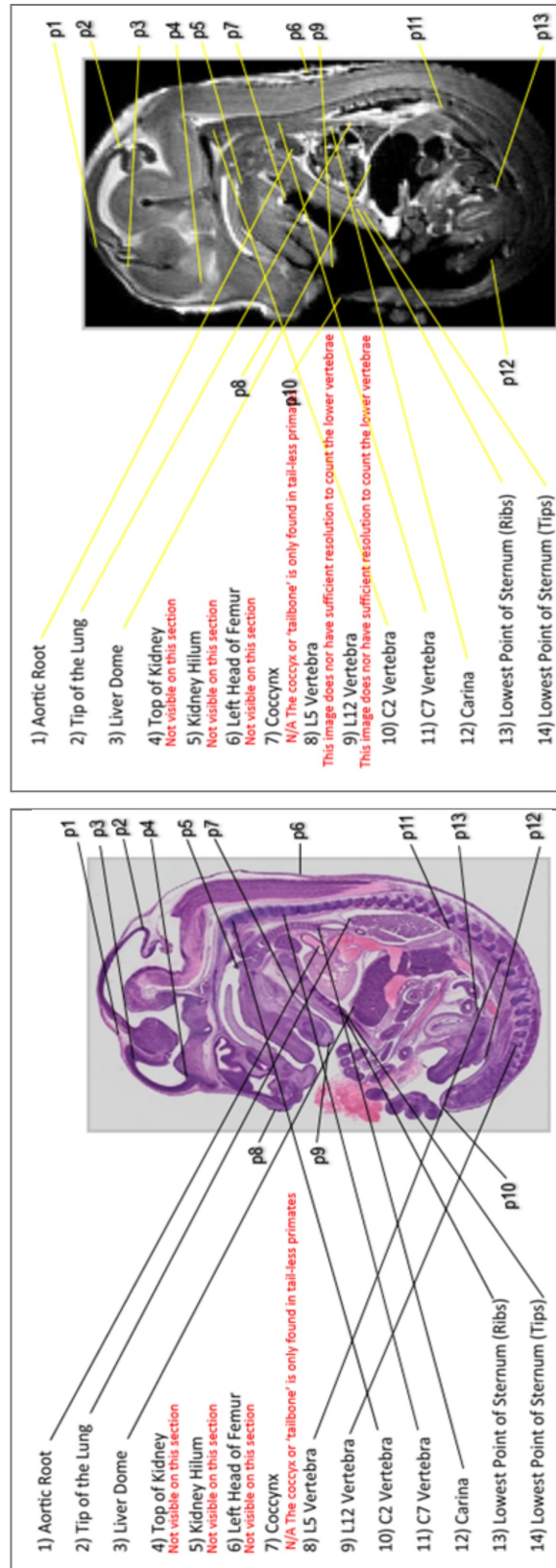


Figure 5.23: Extended selection of fiducial points between two midline images of different embryos at Theiler Stage 23 selected by a biologist. There are four additional fiducial points selected. Thus, the images have 12 relevant fiducial points between them.



(a) An embryo image at TS22-23, Kaufman Digital Atlas

(b) An embryo image at TS23, Edinburgh Mouse Atlas

Figure 5.24: Extended selection of fiducial points between two midline images of different embryos at Theiler Stage 23 selected by a non-biologist. There are 13 additional fiducial points selected (labelled as p1 to p13). Thus, the images have 21 relevant fiducial points between them.

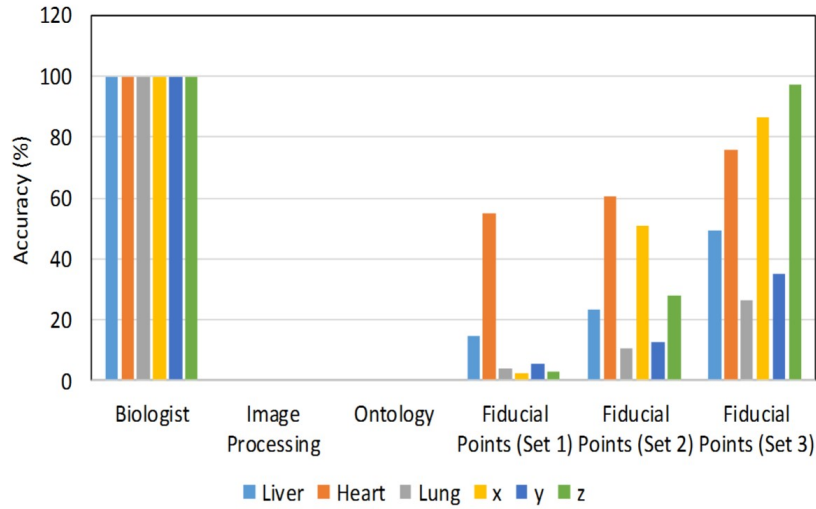


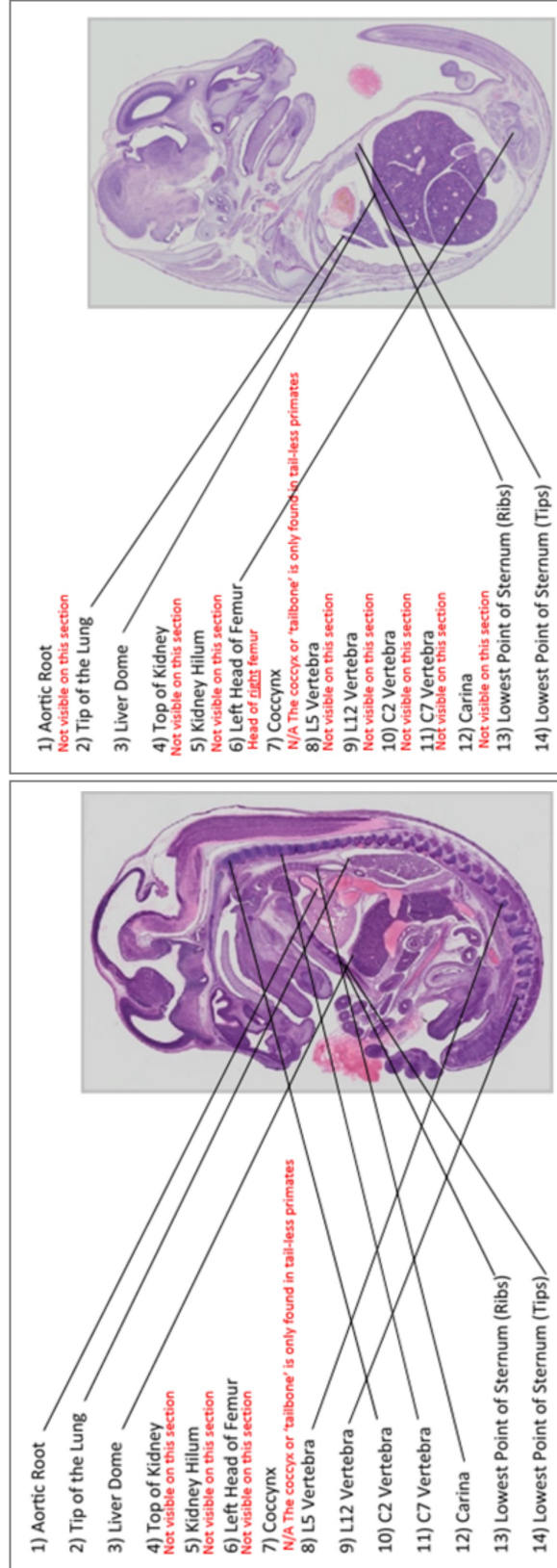
Figure 5.25: The percentage of accuracy for regions mapped between two midline images of different embryos at the same developmental stage served by six mapping approaches.

5.4.2 Mapping between Similar Images Not Identical in Morphology

The purpose of the experiment was to demonstrate the mapping of regions between two midline images from two consecutive Theiler Stages of the same embryo. The first image is taken at Theiler Stage 23. The second image is taken at Theiler Stage 24. Both are derived from the Kaufman Digital Atlas as shown in Figure 5.26. The spatial description fiducial points-based method used two sets of fiducial points. Figures 5.26 and 5.27 depict the fiducial points in Set 1 and Set 2, respectively. Note that in this experiment, there is no extended version of fiducial points in Set 1 by adding the biologist’s own choice of fiducial points because the biologist was unable to find additional points in the TS24 image that matched the images at TS23 of the Edinburgh Mouse Atlas and the Kaufman Digital Atlas.

Figure 5.28 depicts the accuracy resulting from using five approaches at the mapping of the six regions. The biologist defined gold standard mappings proven that there exist a result region for every query region. Unfortunately, the image processing algorithm used in this experiment has failed. On the other hand, an ontology-based method is not available to provide mappings in this experiment because the two images from the Kaufman Digital Atlas are not available with painted domains. This provides evidence that the ontologies may have difficulty when images are not painted.

The graph shows that the spatial description fiducial points-based method is



(a) An embryo image at TS22-23, Kaufman Digital Atlas

(b) An embryo image at TS24, Kaufman Digital Atlas

Figure 5.26: Mapping of fiducial points between two midline images from two consecutive Theiler Stages (TS23 to TS24) of the same embryo based on 14 fiducial points identified in the literature review, selected by a biologist. There are only four relevant fiducial points between the two images.

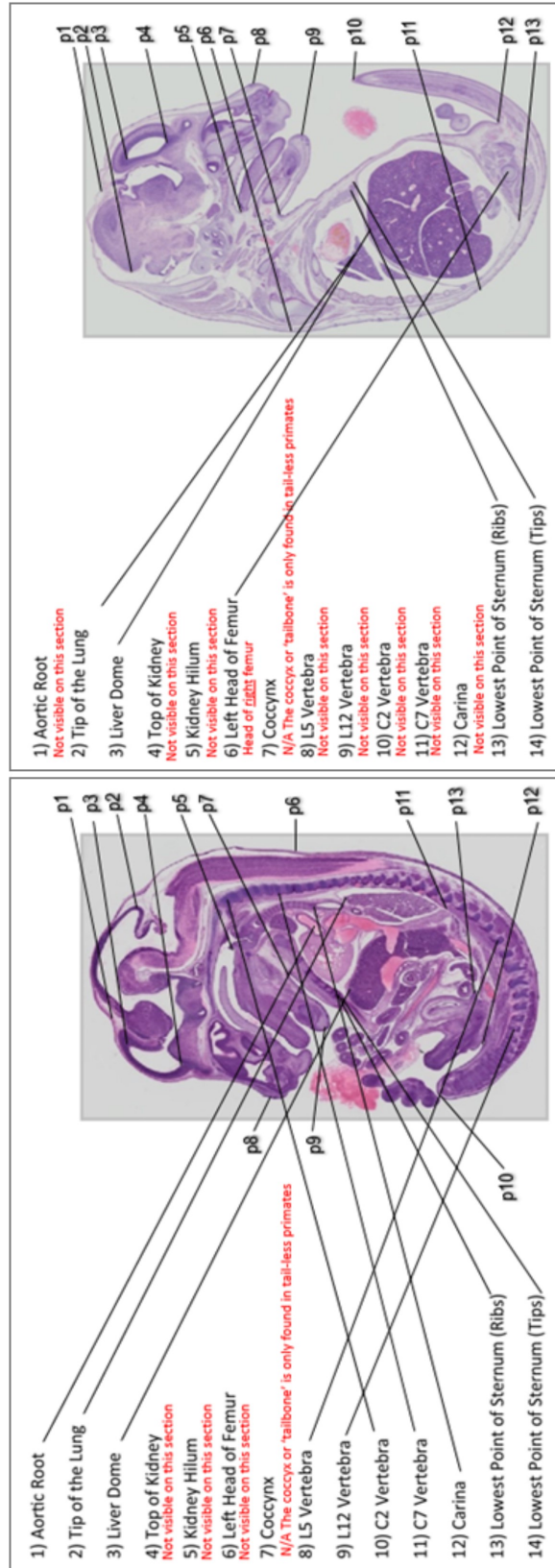


Figure 5.27: Extended selection of fiducial points between two midline images from two consecutive Theiler Stages (TS23 to TS24) of the same embryo, selected by a non-biologist. There are 13 additional fiducial points selected (labelled as p1 to p13). Thus, the images have 17 relevant fiducial points between them.

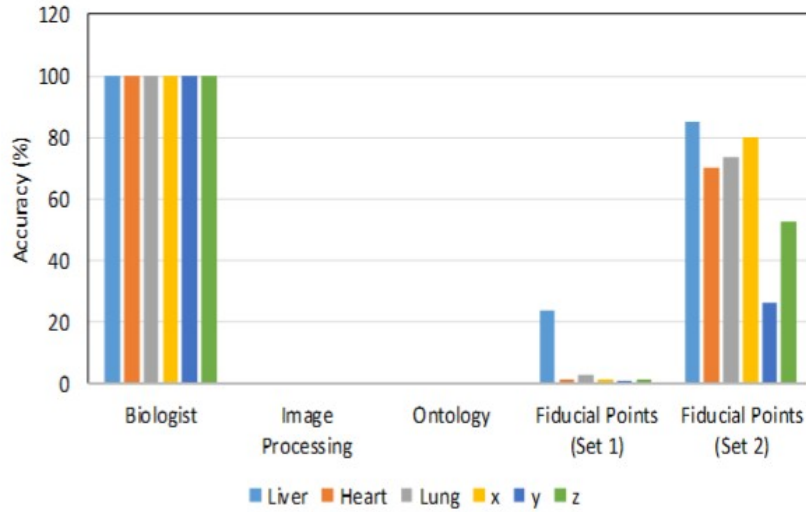


Figure 5.28: The percentage of accuracy for regions mapped between two midline images from two consecutive Theiler Stages of the same embryo served by five mapping approaches.

sufficient to provide mappings. The accuracy resulting from using this method depends on the choice of fiducial points and the number of fiducial points used. For example, the accuracy resulting from using the fiducial point in Set 2 is higher than with the fiducial points in Set 1 because Set 2 contains more fiducial points compared to Set 1.

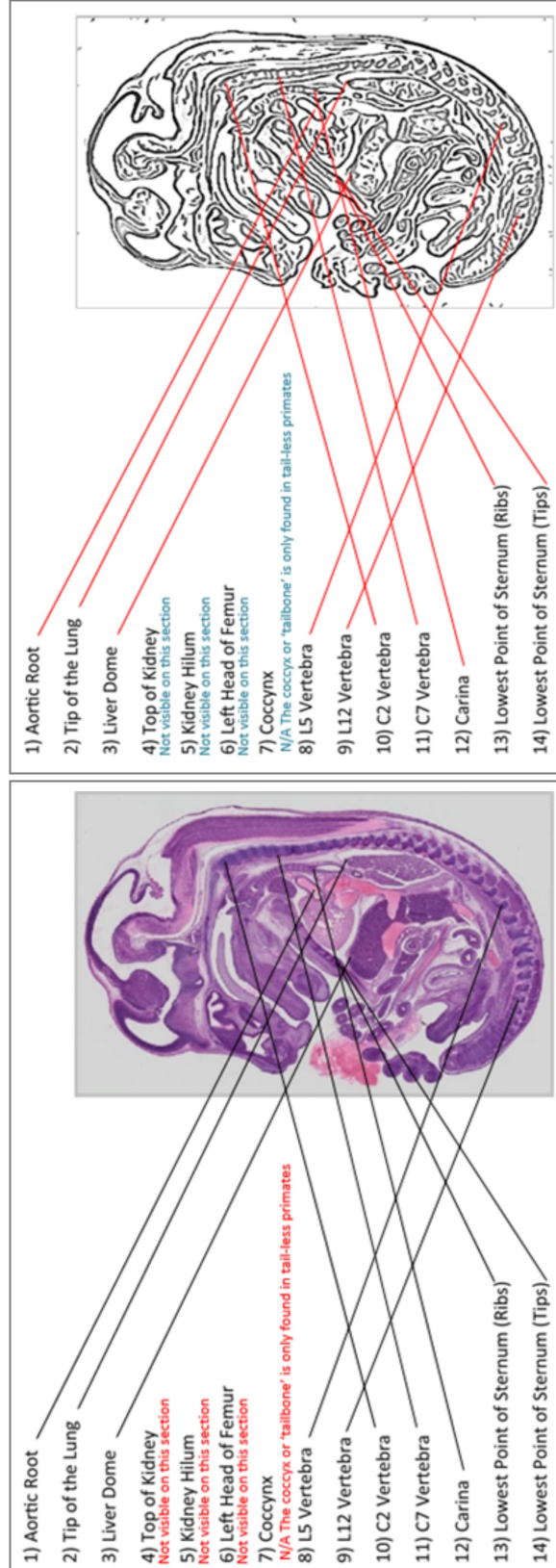
5.4.3 Mapping between Non-Identical Images with Same Morphology

The purpose of the experiment was to demonstrate the mapping of regions between two midline images of an embryo from different imaging modalities. This evaluation used two images as shown in Figure 5.29. The image in Figure 5.29(b) is the clip art graphic version of the image in Figure 5.29(a). The visual content of both images is only similar at the higher scene level, but both images are entirely different at the pixel-level. The spatial description fiducial points-based method used three sets of fiducial points. Figures 5.29, 5.30 and 5.31 depict the fiducial points in Set 1, Set 2 and Set 3, respectively.

Figure 5.32 depicts the accuracy resulting from using six approaches at the mapping of the six regions. The biologist defined gold standard mappings proven that there exist a result region for every query region. Unfortunately, the image processing algorithm used in this experiment has failed.

On the other hand, an ontology-based method is not available to provide mappings in this experiment because the Kaufman Atlas's image is not available with painted domains. This provides evidence that the ontologies may have difficulty with images without painted domains.

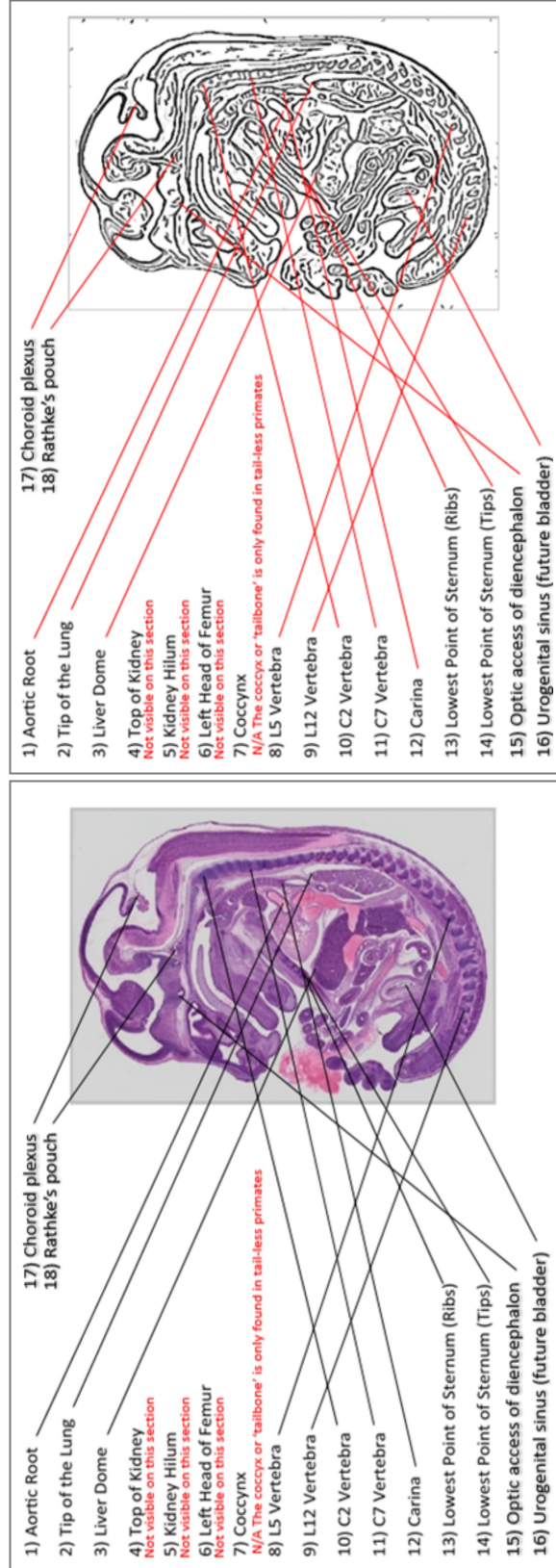
The graph shows that the spatial description fiducial points-based method is sufficient to provide mappings. The accuracy resulting from using this method depends on the choice of fiducial points and the number of fiducial points used. For example, the accuracy resulting from using the fiducial point in Set 2 is higher compared to the fiducial points in Set 1, because Set 2 contains more fiducial points than with Set 1.



(a) An embryo image at TS22-23, Kaufman Digital Atlas

(b) A clip art version of embryo image at TS22-23, Kaufman Digital Atlas

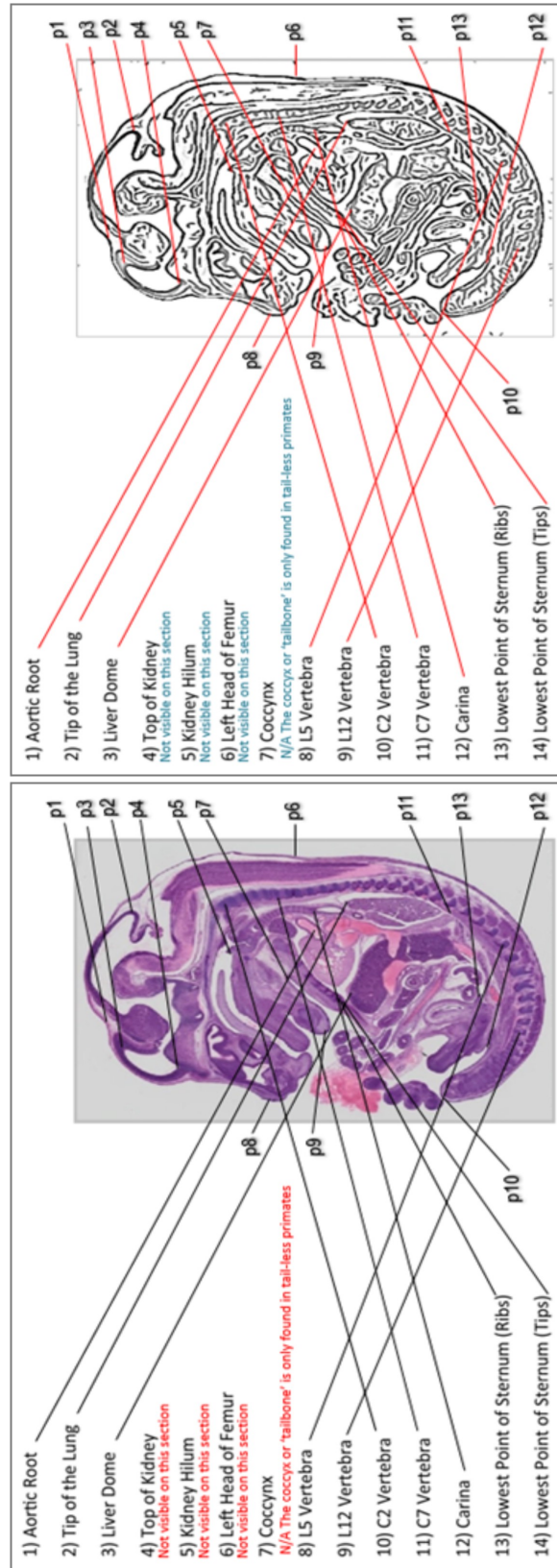
Figure 5.29: Mapping of fiducial points between two exact same images of different image modalities, selected by a biologist. There are 10 relevant fiducial points between the two images.



(a) An embryo image at TS22-23, Kaufman Digital Atlas

(b) A clip art version of embryo image at TS22-23, Kaufman Digital Atlas

Figure 5.30: Extended selection of fiducial points between two exact same images of different image modalities, selected by a biologist. There are four additional fiducial points selected. Thus, the images have 14 relevant fiducial points between them.



(a) An embryo image at TS22-23, Kaufman Digital Atlas

(b) A clip art version of embryo image at TS22-23, Kaufman Digital Atlas

Figure 5.31: Extended selection of fiducial points between two exact same images of different image modalities, selected by a non-biologist. There are 13 additional fiducial points selected (labelled as p1 to p13). Thus, the images have 23 relevant fiducial points between them.

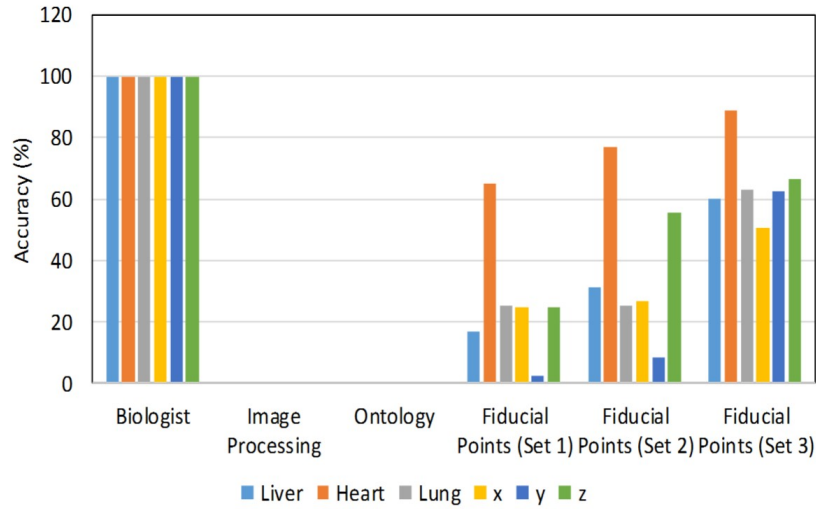


Figure 5.32: The percentage of accuracy for regions mapped between two same images of different image modalities served by six mapping approaches.

5.4.4 Results and Analysis

The evaluation of the experimental results suggests that the image processing algorithm is unable to cope with the mapping of images, which are at the same developmental stage, but from different embryo models. Different embryo models have different morphologies. Consequently, the image processing-based solution fails when the images have different underlying morphologies.

The evaluation of the experimental results suggests that the image processing algorithm is unable to cope with the mapping of images, which are from the same embryo model but are at different developmental stage. Images at different stages are different in their morphologies, although they are from the same embryo model. Consequently, the image processing-based solution fails when the images are morphologically different.

The evaluation of the experimental results suggests that the image processing algorithm is unable to cope with the mapping of the same images acquired in different modalities. The image processing-based mapping examines pixels. Thus, this method fails when the visual content of both images is similar only at the higher scene level, but both images are entirely different at the pixel-level.

Evaluation of these experimental results suggests that the ontologies may have difficulties when the images are not painted. Although we can argue that a biologist can paint an image according to its anatomical regions, this is a hard task for biologists and is expensive to acquire.

The evaluation of the experimental results suggests that the spatial description

fiducial points-based method has the capability to provide mappings in all three cases: (1) the mapping of images at the same developmental stage but come from different embryo models, (2) the mapping of images from the same embryo model but are at different developmental stage, and (3) the mapping of the same images acquired in different modalities. The accuracy resulting from using this method varies as it depends on the choice of fiducial points and the number of fiducial point used. A significant advantage of this method is that there were no cases in which a query region was mapped onto the whole embryo region in the target image, suggesting that the method has addressed one of the limitations of ontology-based solutions. Moreover, the method overcomes the drawbacks of an ontology-based solution that may not be available for images without painted domains, or when there are no matching ontologies.

In the following section, we demonstrate that selections of fiducial points by a biologist as opposed to a non-biologist may have a significant impact on the evaluation of gene expression results. In conclusion, the spatial description fiducial points-based method is a middle approach that could be attempted when the image processing-based solution is unavailable or when the ontology-based solution encounters difficulties.

5.5 Application of Techniques for Gene Expression Queries

Here, we focus on two regions and the spatial similarity between them. The first region is the biologist-defined gold standard region. The second region is generated by applying the spatial description fiducial points-based method. Comparing the two gene expression profiles enables the spatial similarity to be measured. The gene expression queries were carried out on the following regions: *lung*, *heart*, *liver*, and three arbitrary query regions denoted as query regions x , y and z . First, the genes expression results corresponding to the gold standard areas and the areas resulting from using the spatial description fiducial points-based method were retrieved. The retrieved data were then analysed using precision and recall metrics in order to measure the quality of query search results. Precision is the ratio of the number of relevant genes retrieved to the total number of irrelevant and relevant genes retrieved. It is typically expressed using a percentage. Precision can be defined

mathematically using the following formula:

$$P = \frac{A}{A + C} \times 100 \quad (5.1)$$

In the above formula, P represents precision, A is the number of relevant genes retrieved and C is the number of irrelevant genes retrieved. Recall is the ratio of the number of relevant genes retrieved to the total number of relevant genes in the database and is usually expressed as a percentage.

$$R = \frac{A}{A + B} \times 100 \quad (5.2)$$

In the above formula, R represents recall, A is the number of relevant genes retrieved and B is the number of relevant genes not retrieved. Figure 5.33 depicts the gene expression data query for region *lung* retrieved from EMAGE. Note that the Edinburgh Mouse Atlas is linked to the EMAGE, an online database of gene expression data in the developing mouse embryo. In this example, the number of genes detected in the gold standard region corresponds to the number of relevant genes retrieved for region *lung*. Meanwhile, the number of genes detected in the areas resulting from using the fiducial points-based method corresponds to the total number of irrelevant and relevant genes retrieved for region *lung*.

Figure 5.34 depicts the recall of gene expression data resulting from using the spatial description fiducial points-based method based on the fiducial points as selected in Sets 1, 2 and 3. Since the area of the result regions resulting from using the spatial description fiducial points-based method are larger than the area of the gold standard result region, all three sets of fiducial points achieved 100% recall for every query. Nevertheless, there will be cases in which 100% recall does not apply. Consider a mapping between two images A and B where anatomical regions in these two images are morphologically different. For instance, assume that an anatomical region X in image A is entirely below the line drawn between two fiducial points $P1$ and $P2$. On the other hand, an anatomical region X in image B lies a little above the line drawn between two fiducial points $P1$ and $P2$. In consequence, part of anatomical region X will be missing in image B , and thus 100% recall is not applicable. This kind of scenario is likely to happen when the mapping is between embryos that are very different. When some part of a structure is missing, one might not retrieve a gene that is actually important. It is not critical if one gets extra genes, since those which are not of interest may be filtered out later. Some form of google-like matching can be considered to avoid a result region to loose pixels.

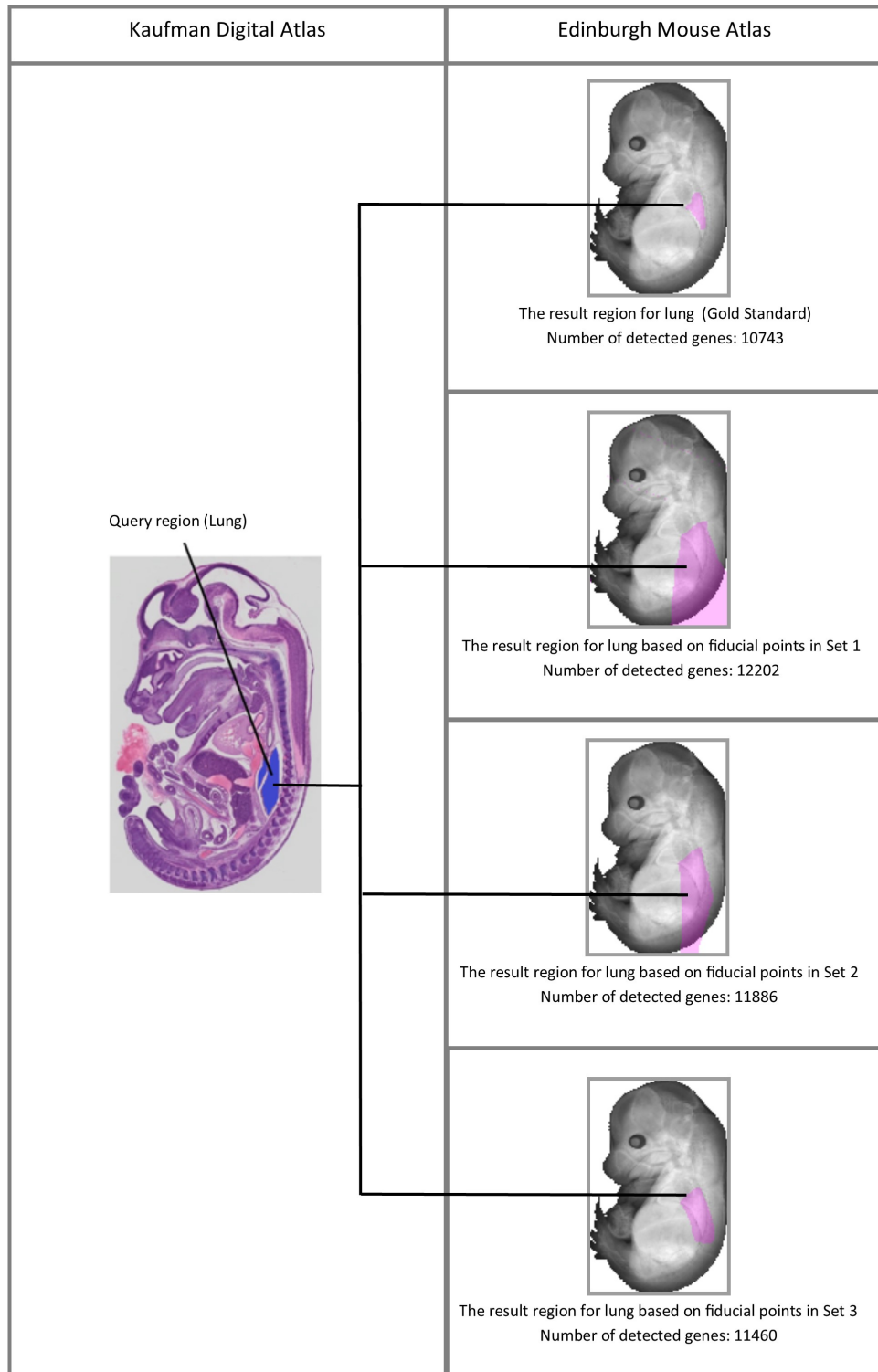


Figure 5.33: Mapping of region *lung* from the Kaufman Digital Atlas to the Edinburgh Mouse Atlas and the number of detected genes retrieved for region *lung* from EMAGE.

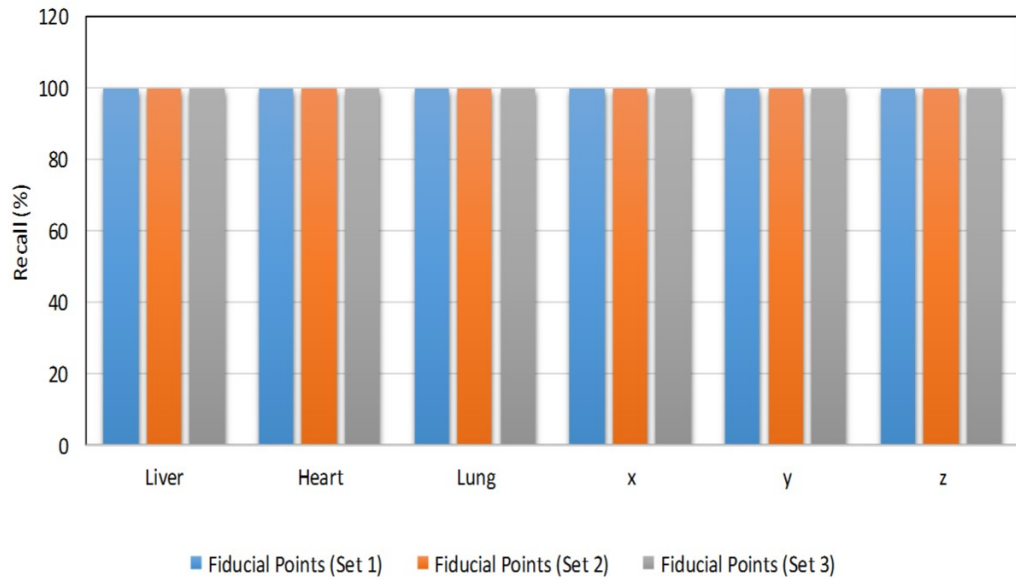


Figure 5.34: The recall of genes expression query results for six anatomical locations resulting from using the spatial description fiducial points-based method based on the fiducial points as selected in Sets 1, 2 and 3 (See Figures 5.22 to 5.24 for these sets of fiducial points).

For example, specifying a range to allow a distance limit from a fiducial line, which will return a location given by the range.

Nevertheless, this does raise questions as to which direction to extend or not to extend in that particular direction. Extending a result region could increase the recall but may damage the precision. A detailed study of this has not been further explored because the case of extending a result region is beyond the scope of the thesis.

Figure 5.35 depicts the precision of gene expression data resulting from using the spatial description fiducial points-based method based on the fiducial points as selected in Sets 1, 2 and 3. Set 1 and Set 2 were selected by a biologist and the images consist of 8 and 12 relevant fiducial points respectively. The graph shows that these two sets of fiducial points have achieved good precision for every query. Set 3 was selected by a non-biologist and the images consist of 21 fiducial point correspondences when this set was used. The number of fiducial points was considerably larger when Set 3 was used. Thus, it is an expected result to see that the precision achieved by this set was the highest. In the following, we demonstrate how the choices of fiducial points made by a biologist and a non-biologist affect the results. The number of fiducial points is used as the parameter in this evaluation.

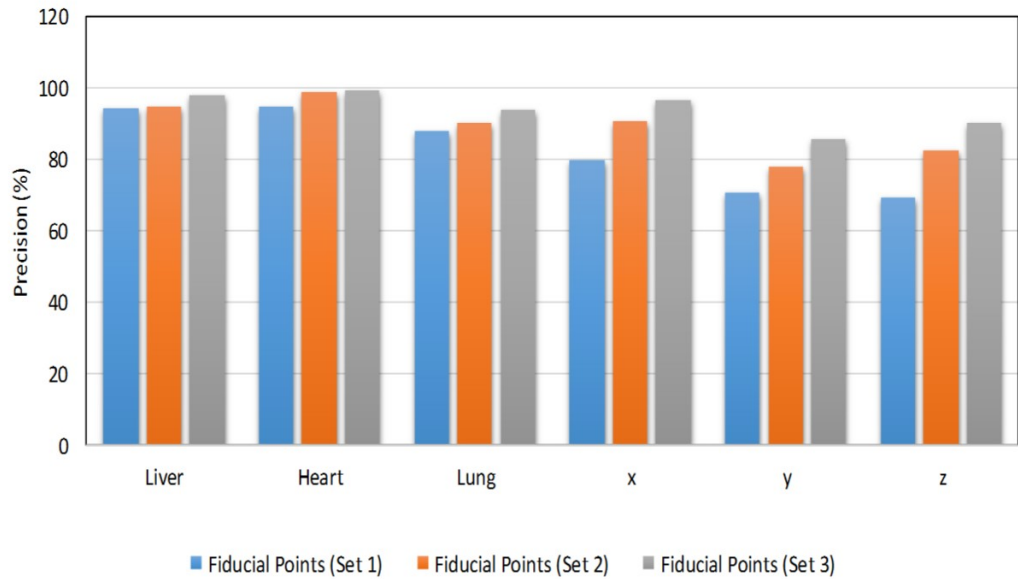


Figure 5.35: The precision of genes expression query results for six anatomical locations resulting from using the spatial description fiducial points-based method based on the fiducial points as selected in Sets 1, 2 and 3 (See Figures 5.22 to 5.24 for these sets of fiducial points).

Figure 5.36 depicts the precision of gene expression query results for six anatomical locations based on the number of fiducial points, where the selection of these points was made by a biologist and a non-biologist. It can be concluded that the selection of fiducial points made by a biologist and a non-biologist did not have a significant impact on the results. The graph shows that both a biologist and a non-biologist can select a set of fiducial points, which provides a gene expression query with good precision. However, the biologist is able to achieve this using a smaller number of fiducial points. The non-biologist has to use quite a large number of fiducial points to achieve similar results. For example, when a total of 12 fiducial points was used, the selection made by the biologist has successfully achieved good precision. In contrast, when the same number of fiducial points was used by the non-biologist, the result of the gene expression queries is relatively low in precision. Nevertheless, as more fiducial points were added by the non-biologist, the precision increases and reaches the biologist’s precision results, suggesting that inaccuracies in the location of fiducial points can at least partially compensated by using a larger number of such points.

Although the method may yield extra nor loose pixels in a result region, the experimental results provide evidence that we have built a useful integration approach

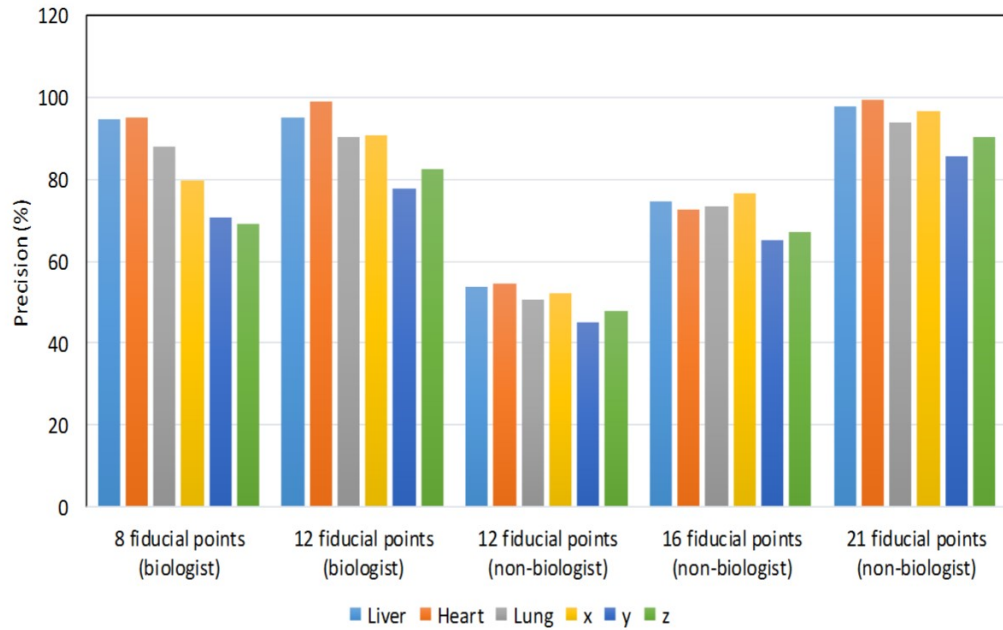


Figure 5.36: The precision of genes expression query results for six anatomical locations resulting from using the spatial description fiducial points-based method based on the number of fiducial points selected by a biologist and a non-biologist.

given gene expression data which are good representatives of spatial data. In conclusion, when there are no matching ontologies or when the image processing-based techniques are not available, the spatial description fiducial points-based method can provide sufficient results.

In general, the spatial description fiducial points-based method can provide a mechanism for image-based data integration, which may benefit medical applications. For example, a radiogenomics strategy integrates gene expression and patients' medical images. The correlation between imaging features and gene expression from multiple patients with the same disease can yield useful information for diagnosis and prediction; for example, to make automated stratification of patients into different risk categories, or to compare the range of abnormalities in patients. The ability to integrate and compare such image-based data has developed into an increasingly critical component in the life sciences and eHealth domain.

5.6 Summary

This chapter has presented an analysis of the performance of the spatial description-based method in comparison with one ontology-based method and one method in image processing. Performance was measured in terms of accuracy. Within the

context of this evaluation, the experimental results have suggested that there exists, at least in the cases that had been tested, a small number of fiducial points where the combination can give performance as effective as both the ontology-based method and the image processing algorithm. Note that this was an analysis of image region mappings between identical images.

The performance of the three mapping techniques (i.e. spatial description-based solution, ontology-based method and image processing algorithm) was then analysed in mapping of image regions involving three types of images. These are: (1) similar images but not identical in morphology, (2) non-identical images that are not identical in morphology, and (3) non-identical images with same morphology. The result was compared to the result obtained from a biologist. Evaluation from experimental results suggested that the image processing-based solution may fail when images are morphologically different. On the other hand, the ontology-based solution does not work when images are not annotated with the ontological concepts. The proposed spatial description-based solution provides an alternative to the image processing-based technique that may fail when the images have different underlying morphologies. In addition, the spatial description-based solution overcomes the limitations of an ontology-based solution that may not be available when there are no matching ontologies, or in the case when images lack painted domains. Painting an image according to its anatomy is a hard task for biologists and is expensive to acquire.

The results of the gene expression evaluation indicate that the extra pixels in a result region resulting from using the spatial description fiducial points-based method do not matter when it comes to gene expression data. In conclusion, the precision results provide evidence that we have built a useful integration approach given gene expression data which are good representatives of spatial data. The following chapter provides a summary, with suggestions for future research.

Chapter 6

Conclusions and Future Work

6.1 Introduction

The main outcome of the research undertaken for this thesis was the development of a new technique using spatial description to integrate image-based data towards the integration of biomedical atlases. The main benefit of spatial description is that it allows the mapping of regions in the following three types of images: (1) similar images but not identical in morphology, (2) non-identical images that are not identical in morphology, and (3) non-identical images with same morphology.

In general, the spatial description technique addresses the many different requirements of a mapping system which would support the integration of biomedical atlases. Eight main areas in this context were investigated. The first area emphasises the conceptualisation of anatomical space using spatial relations between anatomical spaces. Therefore, the first stage involved the implementation of an approach called *SpaRTAD*, which maps anatomical regions between images using spatial descriptions based on spatial relationships between segmented regions of an image.

The second area emphasises the conceptualisation of anatomical space based on fiducial points and a set of spatial relations, so as to overcome issues arising in the first area. Therefore, the second stage involved the development of a mapping technique using the spatial description fiducial points-based method.

The third area emphasises the conceptualisation of anatomical space using the spatial description fiducial points-based method, integrated with spatial relations between segmented regions. Therefore, the third stage emphasises determining the advantages of mapping by combining the previous two approaches of spatial descriptions.

The fourth area discusses the final approach proposed (i.e. the spatial description

fiducial points-based method) which was compared against the existing approaches as discussed in the literature review.

The fifth area is the biologist-defined gold standard mappings, the results of which were used as the basis for evaluating the existing mapping techniques and the newly developed technique.

The sixth area involved an optimisation strategy for the spatial description fiducial points-based method based on the number of fiducial points, number of fiducial lines, area size of the query region and selection of fiducial point location.

The seventh area was an evaluation of the accuracy resulting from using one ontology-based method, one method in image processing and the proposed spatial description-based method in the mapping of image regions in both identical and non-identical images.

The eighth area involved the validation of the proposed spatial description-based solution using precision and recall metrics. The purpose of validation was to quantify spatial description as a valid approach for integrating gene expression data. This chapter summarises the eight stages of work conducted throughout this research, as well as their main results, whilst also providing a discussion regarding future research.

6.2 Summary

This thesis has proposed the mapping of image-based data between biomedical atlases to enable the integration of these data sources. The integration of these resources is needed because data from these atlases are often inconsistent and incomplete. Integrating heterogeneous and distributed biomedical atlases by linking their image-based data involves a number of issues. These issues have been investigated in the context of mouse atlas applications. To be precise, the work in this thesis was undertaken in the context of the Edinburgh Mouse Atlas Project [6; 7; 20] and the e-Mouse Atlas of Gene Expression [1; 20], digital atlases of mouse embryo development. This section summarises each issue within each mapping technique developed in this research.

This thesis has explored existing image mapping approaches. These approaches can be categorized according to their mapping primitives. These mapping primitives are spatial relations and fiducial points. Spatial relations are used in ontology-based mapping. Fiducial points are used in image processing-based mapping. Furthermore, three different kinds of integration technology have been explored. These

technologies include image processing-based integration, ontology-based integration and spatial description-based integration. The image processing-based solutions may not work in the mapping of images that are too different due to variance of anatomical structures' morphology or variation in pixel intensity distributions. Ontology-based solutions often lack spatial precision. The spatial description-based solution is a middle approach that could be attempted when an image processing-based solution is unavailable, or when the ontology-based solution has difficulties.

This research has developed three approaches of spatial descriptions. Since spatial relations can be used to describe the location of an anatomical region and the fact that two anatomical regions can be mapped onto one another according to their spatial similarity, thus, the focus of the research was on a mapping approach using spatial descriptions based on spatial relations between anatomical regions. Three categories of spatial relations were employed: topological, arrangement and directional relations. We proposed *SpaRTAD* as an efficient representation structure to conceptualise anatomical space based on the combination of these three categories of spatial relations. However, there are a number of problems with this approach, such as the use of different segmented images between atlases, different domain coverage between images of atlases, and the use of different anatomical names or vocabulary causing interoperability issues in finding corresponding anatomical regions between images. These issues encouraged this research project to develop a new technique, which can provide the mapping of image regions independently of anatomical structures' spatial relationships.

The mapping approach using spatial descriptions based on fiducial points and a set of spatial relations was developed to overcome the problems found in the first approach. This approach describes a query region using spatial relations with respect to fiducial points and fiducial lines. Mapping was performed based on the satisfaction of exactly the same constraints in the target image. A novel property of the approach is that the method is not voxel/pixel intensity dependent, and mapping is carried out independently of spatial relationships between segmented regions of an image. The evaluation of the experimental results suggests that this approach improves mapping accuracy when the appropriate number of fiducial points is used, given better selection of fiducial point location. Specifically, the more evenly distributed the size of the definable areas which are created through the fiducial points, the more accurate the mappings. Subsequently, the mapping approach using spatial descriptions based on fiducial points and a set of spatial relations can be integrated with spatial descriptions based on spatial relationships between segmented regions. The evaluation of the experimental results suggests that the integration of these two

approaches, although it may require an alignment of segmented regions and domain coverage, can yield significantly higher accuracy compared to using either approach alone.

The selected mapping approach within this thesis is the spatial description fiducial points-based method. This method overcomes the limitations of ontology-based and image processing-based techniques by addressing many of the image region mapping issues. The performance of this method was analysed in terms of mapping accuracy with one ontology-based method and one method in image processing. The evaluation of the experimental results suggests that there exists, at least in the cases that have been tested, a small number of fiducial points in which the combination can perform as effectively as both ontology-based methods and image processing algorithms. More importantly, it is possible to select sets of fiducial points producing such performances without depending on image processing. This evaluation also suggests that these three mapping techniques are not really problematic from the speed point of view. Note that this was an analysis of image region mappings between identical images.

The performance of the three mapping techniques (i.e. spatial description-based solution, ontology-based method and image processing algorithm) was then analysed in the mapping of regions between morphologically different images, the results being compared with the mapping results produced by an expert biologist. The evaluation from experimental results suggests that the image processing-based solution fails when the images are morphologically different. However, ontology-based solutions often lack spatial precision and do not work when the images are not annotated with the ontological concepts. The proposed spatial description-based solution overcomes the limitations of existing solutions by addressing the issue of images without painted domains such that the ontology-based solution is unable to cope, and provides an alternative to the image processing-based solution that may fail when the images have different underlying morphologies.

In order to determine the spatial similarity between two mapped spatial areas, validation was performed through the comparison of gene expression data observed from EMAGE. The genes expression results corresponding to the gold standard areas and the areas resulting from using the spatial description fiducial points-based method were retrieved. The retrieved data were then analysed using precision and recall metrics to measure the quality of query search results. It can be concluded that the spatial description fiducial points-based method can provide a high level of precision. For these reasons, we conclude that spatial description is a useful integration approach given gene expression data, which are good representatives of

spatial data.

This study was carried out on gene expression data because of the availability of these data and considering that we were looking at image data with biological meaning. Note that the gene expression data are representative of many other image data. In conclusion, the spatial description-based solution is a middle approach that may be attempted when an image processing-based solution is unavailable or when the ontology-based solution encounters difficulties.

6.3 Future Work

The scope of this thesis lies within 2D image space. In principle, this research can also be applied within 3D image space using the same approach as in 2D image space. Extending the proposed approach from 2D to 3D image space requires all three concepts of fiducial point, fiducial line and query region to be defined in the 3D image space. A fiducial point associated with a coordinate (x, y, z) can be plotted in a 3D image space. In a 3D image space, a fiducial line can be transformed into a fiducial plane. Likewise, a 2D image region can be transformed into a 3D image region. There will be spatial relations to describe anatomical space in 3D, which have been determined by this research. This study has decided to use 2D image space as the focal point.

Overall, the spatial description-based solution can provide successful mechanisms to guide mapping between images across biomedical atlases in order to facilitate data integration among these data sources. However, this work covers a specific domain, namely mapping between images of biomedical atlases. Vigorous effort is needed to facilitate data integration between biomedical atlases with other resources, such as natural-language description of space (i.e. free text from biomedical literature) [117; 118; 119] and database warehouses (i.e. structured databases of biomedical facts) [120; 121; 122; 123; 124]. Research is needed in order to compile spatial descriptions of user-provided images and spatial descriptions of user-supplied documents, for instance; and how a user can compile such descriptions.

In principle, this research provides a number of indications that the proposed solution works. However, it would be helpful if research that extends the analysis into a number of other image domains (not just gene expression examples) are carried out. Additionally, one could investigate the use of other or additional spatial relations and the impact that this may have on the results.

A general conclusion to be drawn from this thesis is that the spatial description-

based solution not only complements the other methods (i.e. ontology-based methods and image processing algorithms), but it also adds a new mechanism for integrating data from various information structures. For example, the spatial description-based solution may be adapted to support the mapping of satellite imagery generated from Digital Elevation Models (DEM). Stereo radar images are used to match multiple coverage from sequential image acquisition cycles [125]. Radar images do not promise clear edge information. Therefore, the edge or feature-based methods are not suitable. One of the radar mapping techniques operates on a reference and a search window. In this technique, for each position of the search window, a match value is computed from grey level values in the reference window. A match is accomplished if the match value at a certain position of the search window has a local maximum when compared to the match values at all other positions of the search windows. This local maximum corresponds to a tie point. Thus, the use of the spatial description fiducial points-based method in radar mapping studies is one of the opportunities for future research that could be based on the study presented in this thesis.

Further research could also involve further development of the spatial description-based solution as a technique for content-based image retrieval systems to retrieve visual similarity between images across different visual domains, such as clip art graphics, photographs taken in different seasons, paintings, and sketches. The problem with matching cross-domain images is that the visual content is only similar at the higher scene level, but quite dissimilar at the pixel-level [126]. The spatial description-based solution has enormous potential to support searches in a large dataset to find visually similar matches to a given query, be it an image patch, a full image, or a spatio-temporal block, considering that this technique is capable of providing mappings even if images are different at the pixel-level.

The Geographical Information System (GIS) is a useful tool for disaster prevention. For example, using the spatial database of slope failure to map disaster areas on GIS [127]. An image database on slope failure can be developed using GPS digital cameras. GPS cameras can log the coordinates of their locations. The coordinates, which correspond to the view point position of the camera can be stored in the GIS data. The coordinates can be converted to the actual location information of the slope failure area based on object points. These object points are calculated from the view point of the GPS camera. The slope failure area in the photograph is then converted as GIS data. To retrieve the actual location information of the slope failure area, future research could further develop spatial description-based solutions for generating GIS image data to map disaster areas.

Appendix A Table Results

Number of Fiducial Points	Average Percentage of Accuracy (%)			
	Size50x50	Size100x100	Size150x150	Size200x200
2	42	61	71	76
80	58	74	80	84
160	67	80	85	87
240	71	82	87	88
320	75	85	88	89
400	76	85	88	90
480	77	86	89	90
560	78	86	89	90
640	79	87	90	90
720	79	87	90	91
800	80	87	90	91
880	80	87	90	91

Table A.1: Results corresponding to fig. 4.3

Number of Fiducial Lines Used	Average Percentage of Accuracy (%)			
	Size50x50	Size100x100	Size150x150	Size200x200
4	7	17	27	35
24	13	49	67	91

Table A.2: Results corresponding to fig. 4.4

Positioning Set	Average Percentage of Accuracy (%)			
	Size50x50	Size100x100	Size150x150	Size200x200
Set A	5	8	17	31
Set B	8	26	35	68
Set C	13	49	67	91

Table A.3: Results corresponding to fig. 4.6

Positioning Set	Average Percentage of Accuracy (%)			
	Size50x50	Size100x100	Size150x150	Size200x200
All points at the boundary of the whole image	13	49	67	91
All points inside the image	14	60	87	93
Points at both boundary & inside image	16	62	90	96

Table A.4: Results corresponding to fig. 4.8

Types of Areas Distribution	Average Percentage of Accuracy (%)			
	Size50x50	Size100x100	Size150x150	Size200x200
Strongly uneven areas distribution	7	21	49	87
Evenly areas distribution	15	52	68	92

Table A.5: Results corresponding to fig. 4.11

Method	Accuracy (%)							
	Liver	Midgut	Lung	Thalamus	Pancreas	Adrenal Gland Cortex	Metanephros	Femur
SD Fiducial Points-Based (Test Set 1)	41.65	56.46	49.76	15.94	15.80	34.41	12.35	3.72
SD Fiducial Points-Based (Test Set 2)	38.45	32.80	49.92	16.32	35.05	18.82	13.24	19.13
SD Fiducial Points-Based (Test Set 3)	44.94	71.33	26.26	27.64	35.68	48.10	13.69	26.00
SD Fiducial Points-Based (Test Set 4)	36.35	42.45	38.62	26.49	9.98	20.50	13.96	16.78

Table A.6: Results corresponding to fig. 4.15

Method	Accuracy (%)							
	Liver	Midgut	Lung	Thalamus	Pancreas	Adrenal Gland Cortex	Metanephros	Femur
SD Fiducial Points-Based (Test Set 1)	34.56	60.33	21.76	26.49	7.32	43.26	12.45	16.78
SD Fiducial Points-Based (Test Set 2)	160.05	204.85	100.34	512.64	185.33	431.29	655.36	422.60
SD Fiducial Points-Based (Test Set 3)	122.53	40.19	280.78	261.79	180.24	107.88	630.59	283.43
SD Fiducial Points-Based (Test Set 4)	175.10	135.57	158.95	277.56	901.73	387.73	616.24	495.88

Table A.7: Results corresponding to fig. 4.16

Method	Accuracy (%)							
	Liver	Midgut	Lung	Thalamus	Pancreas	Adrenal Gland Cortex	Metanephros	Femur
SD Fiducial Points-Based (Test Set 1)	39.57	68.99	64.46	25.86	44.32	83.70	14.24	4.44
SD Fiducial Points-Based (Test Set 2)	40.19	66.83	54.71	19.33	32.92	34.95	13.54	3.91
SD Fiducial Points-Based (Test Set 3)	41.84	72.8	65.25	23.69	15.53	38.64	13.45	26.08
SD Fiducial Points-Based (Test Set 4)	37.55	16.41	45.03	34.01	32.78	48.60	12.92	5.09

Table A.8: Results corresponding to fig. 4.17

Anatomical Location	Accuracy (%)			
	7 Fiducial Points	9 Fiducial Points	11 Fiducial Points	14 Fiducial Points
Metanephros	12.35	13.96	14.24	53.87
Femur	15.6	26	26.08	26.08
Thalamus	15.94	27.64	34.01	34.01
Pancreas	32.44	35.68	44.32	47.66
Adrenal Gland Cortex	38.90	48.10	83.70	83.70
Liver	41.65	41.84	44.94	49.09
Lung	49.76	49.92	65.25	67.57
Midgut	65.27	71.33	72.80	77.61

Table A.9: Results corresponding to fig. 4.18

Method	Accuracy (%)							
	Liver	Midgut	Lung	Thalamus	Pancreas	Adrenal Gland Cortex	Metanephros	Femur
Image Processing Algorithm	82.36	63.55	60.10	63.44	35.30	27.30	43.59	69.94
Ontology-Based Method	61.49	72.18	52.37	48.64	10.34	42.15	83.66	47.09
SD Fiducial Points-Based (14 FP)	49.09	77.61	67.57	34.01	47.66	83.70	53.87	26.08

Table A.10: Results corresponding to fig. 5.21

Method	Accuracy (%)					
	liver	heart	lung	x	y	z
Biologist	100	100	100	100	100	100
Image Processing	0	0	0	0	0	0
Ontology	0	0	0	0	0	0
Fiducial Points (Set 1)	14.81	54.70	3.86	2.59	5.41	2.87
Fiducial Points (Set 2)	23.12	60.77	10.54	50.90	12.52	27.76
Fiducial Points (Set 3)	49.22	75.71	26.32	86.41	35.13	97.53

Table A.11: Results corresponding to fig. 5.25

Method	Accuracy (%)					
	liver	heart	lung	x	y	z
Biologist	100	100	100	100	100	100
Image Processing	0	0	0	0	0	0
Ontology	0	0	0	0	0	0
Fiducial Points (Set 1)	23.44	1.29	2.61	0.99	0.39	1.15
Fiducial Points (Set 2)	84.82	70.30	73.37	80.09	26.00	52.81

Table A.12: Results corresponding to fig. 5.28

Method	Accuracy (%)					
	liver	heart	lung	x	y	z
Biologist	100	100	100	100	100	100
Image Processing	0	0	0	0	0	0
Ontology	0	0	0	0	0	0
Fiducial Points (Set 1)	16.77	64.86	25.28	24.52	2.39	24.69
Fiducial Points (Set 2)	31.07	76.71	25.28	26.53	8.31	55.64
Fiducial Points (Set 3)	60.25	88.89	63.02	50.75	62.42	66.67

Table A.13: Results corresponding to fig. 5.32

Method	Recall (%)					
	liver	heart	lung	x	y	z
Fiducial Points (Set 1)	100	100	100	100	100	100
Fiducial Points (Set 2)	100	100	100	100	100	100
Fiducial Points (Set 3)	100	100	100	100	100	100

Table A.14: Results corresponding to fig. 5.34

Method	Precision (%)					
	liver	heart	lung	x	y	z
Fiducial Points (Set 1)	94.55	94.89	88.04	79.60	70.82	69.18
Fiducial Points (Set 2)	94.87	98.93	90.38	90.69	77.85	82.44
Fiducial Points (Set 3)	97.75	99.19	93.74	96.60	85.69	90.47

Table A.15: Results corresponding to fig. 5.35

Method	Precision (%)					
	liver	heart	lung	x	y	z
8 Fiducial Points (Biologist)	94.55	94.89	88.04	79.6	70.82	69.18
12 Fiducial Points (Biologist)	94.87	98.93	90.38	90.69	77.85	82.44
12 Fiducial Points (Non-Biologist)	53.85	54.68	50.56	52.20	44.96	47.69
16 Fiducial Points (Non-Biologist)	74.47	72.57	73.42	76.60	65.28	66.92
21 Fiducial Points (Non-Biologist)	97.75	99.19	93.74	96.6	85.69	90.47

Table A.16: Results corresponding to fig. 5.36

Appendix B Spatial Queries

Figure B.1~B.7 depict visual results of mapping by using image processing algorithm developed by [62]. This algorithm is not used in the thesis for performance comparison because the mapping results are poor compared to algorithm as proposed by [61].

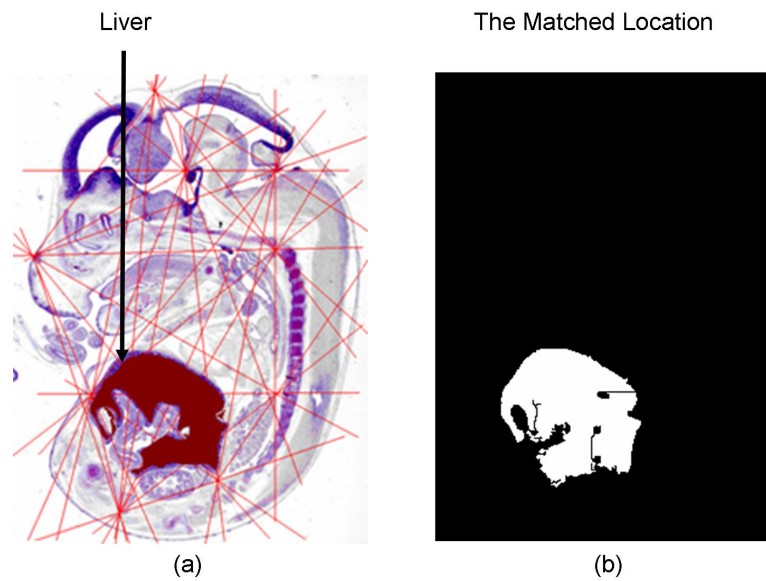


Figure B.1: Anatomical location of liver (a) in its actual location, and (b) the corresponding matched location resulting from image processing algorithm by [63].

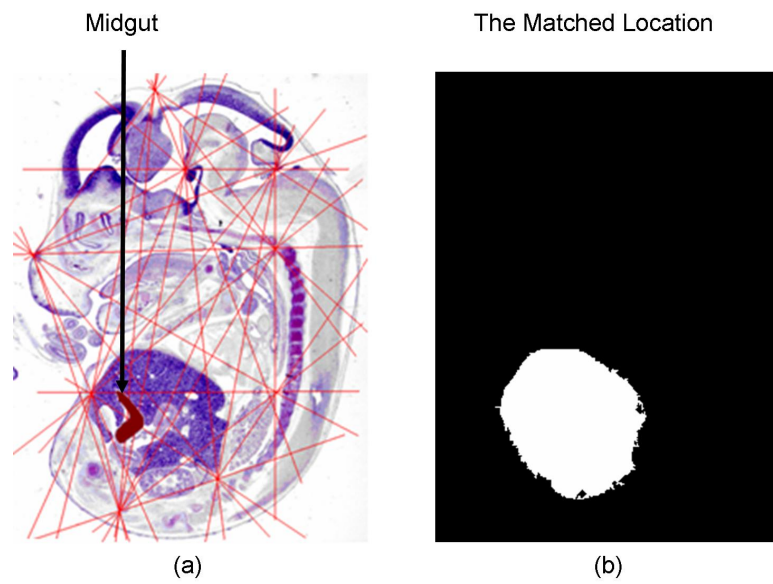


Figure B.2: Anatomical location of midgut (a) in its actual location, and (b) the corresponding matched location resulting from image processing algorithm by [63].

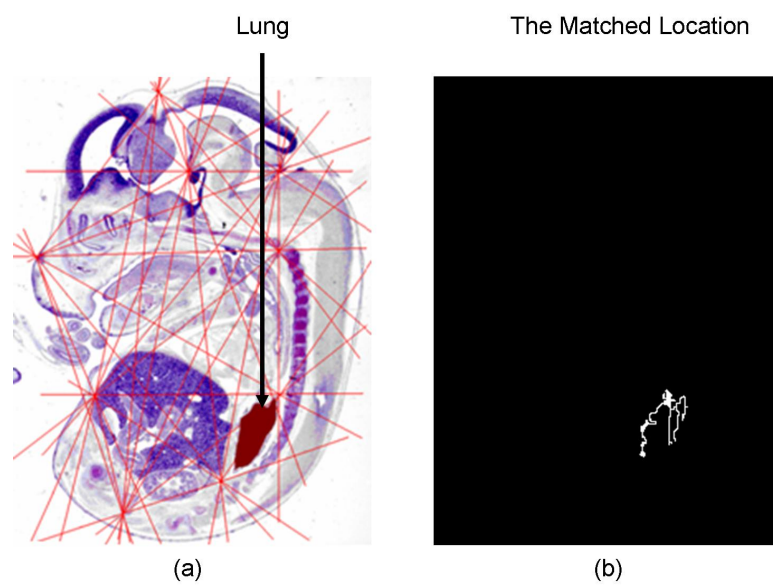


Figure B.3: Anatomical location of lung (a) in its actual location, and (b) the corresponding matched location resulting from image processing algorithm by [63].

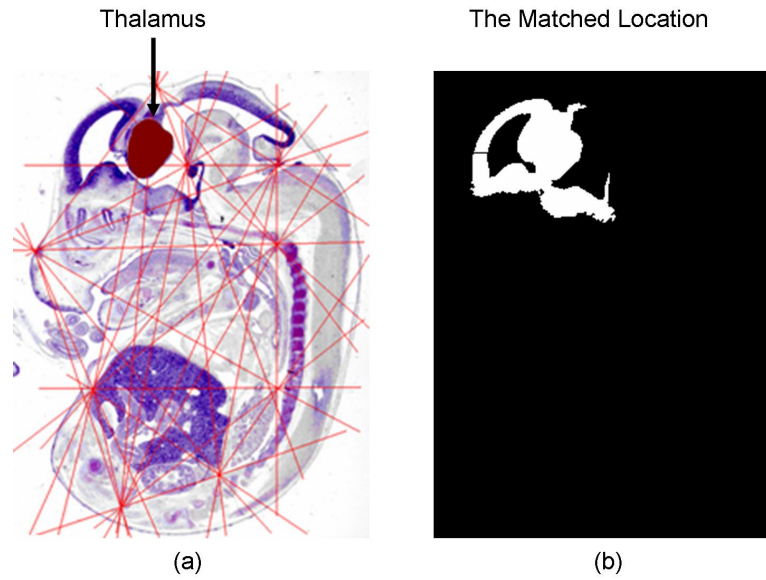


Figure B.4: Anatomical location of thalamus (a) in its actual location, and (b) the corresponding matched location resulting from image processing algorithm by [63].

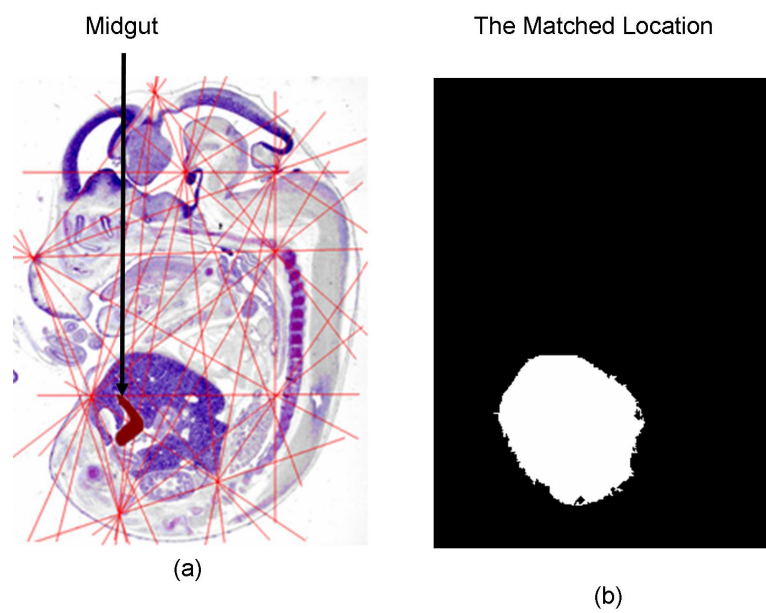


Figure B.5: Anatomical location of pancreas (a) in its actual location, and (b) the corresponding matched location resulting from image processing algorithm by [63].

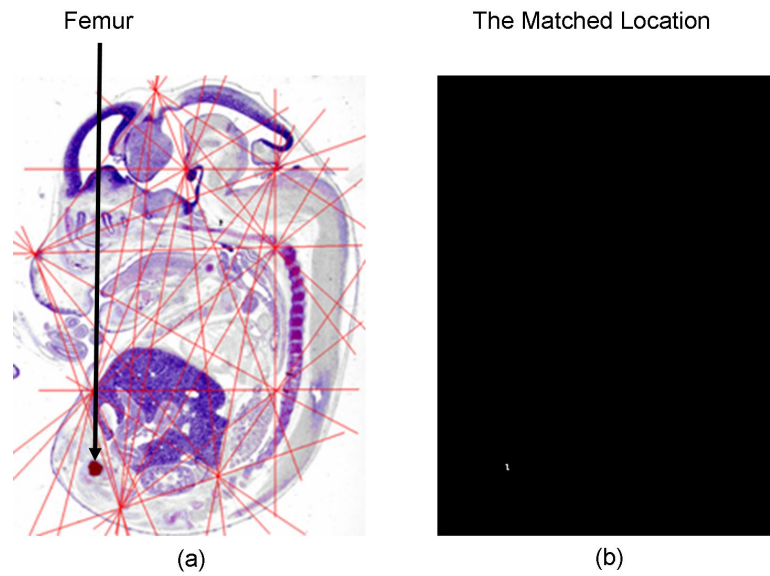


Figure B.6: Anatomical location of femur (a) in its actual location, and (b) the corresponding matched location resulting from image processing algorithm by [63].

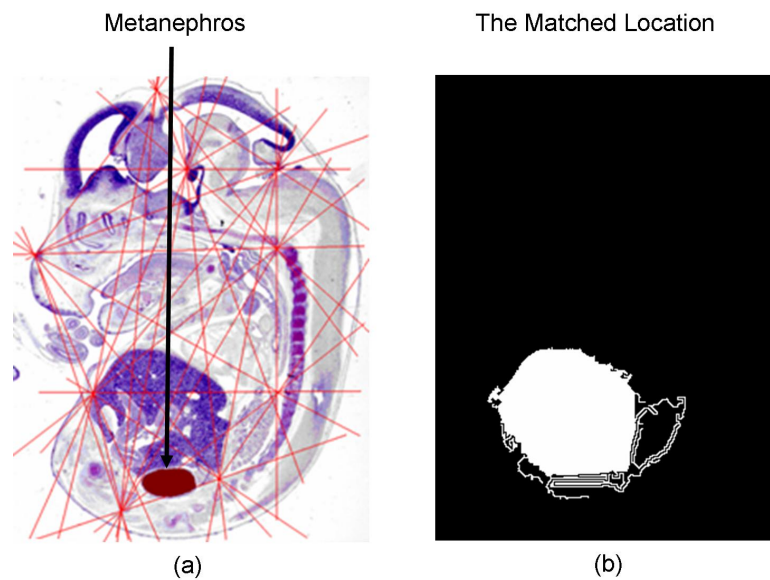
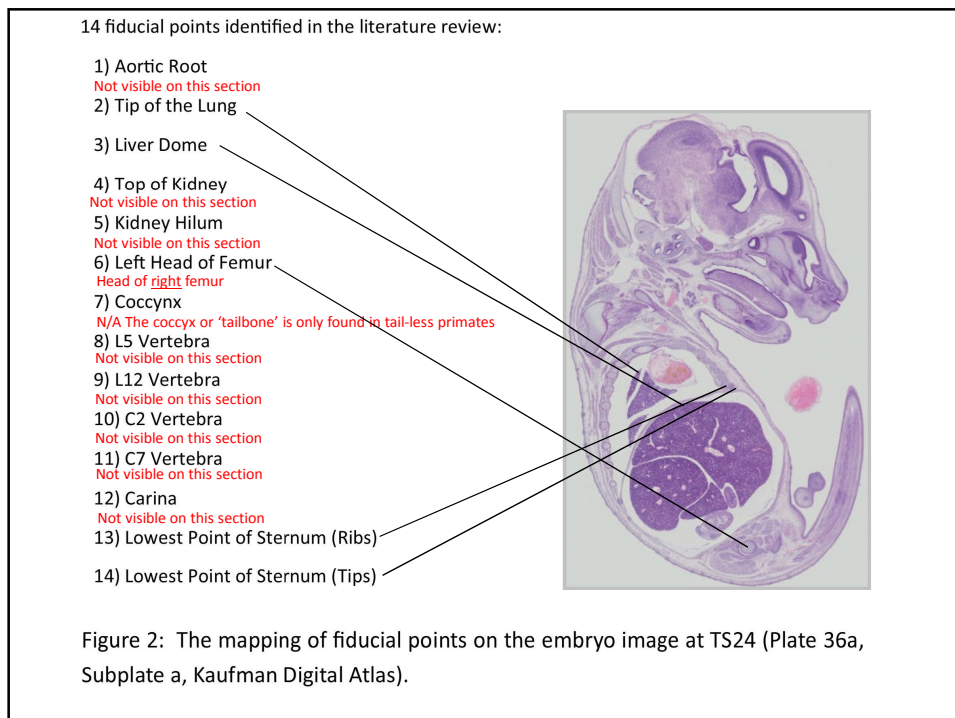
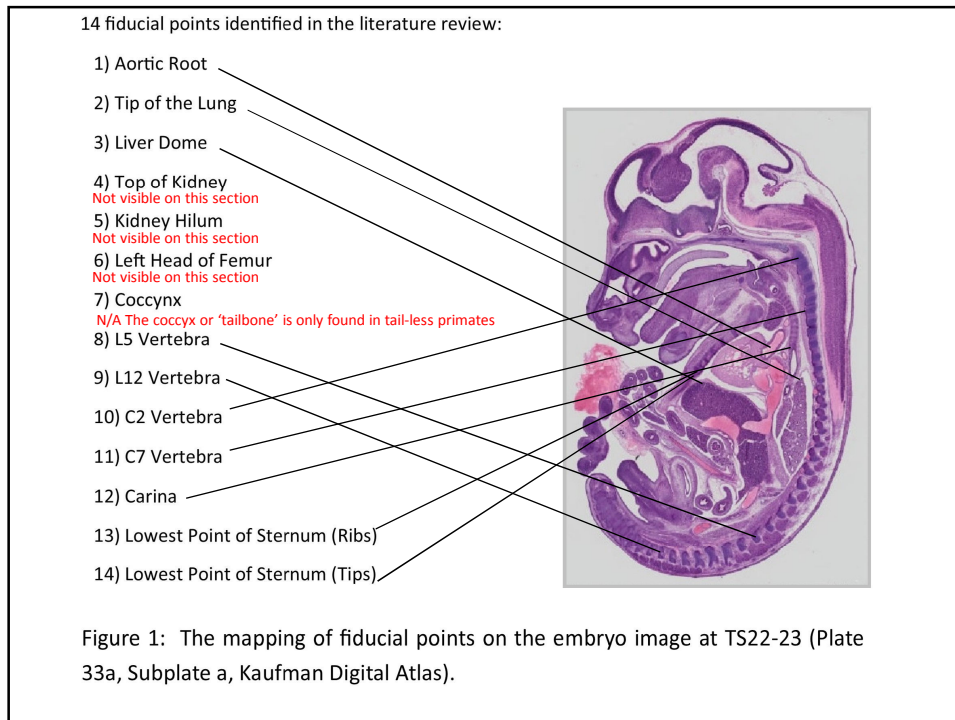
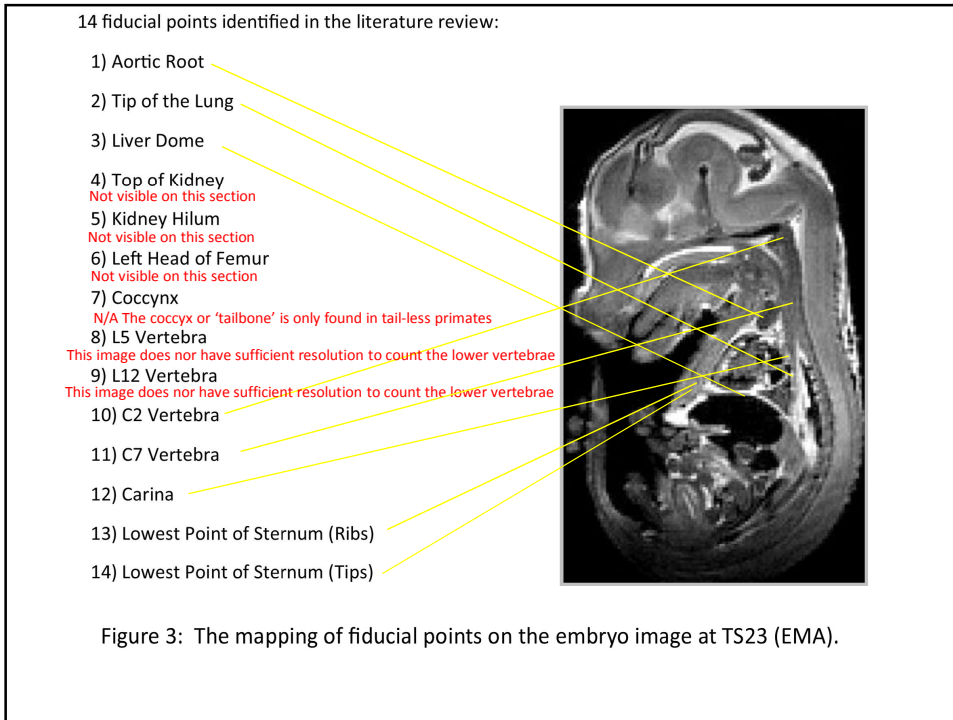
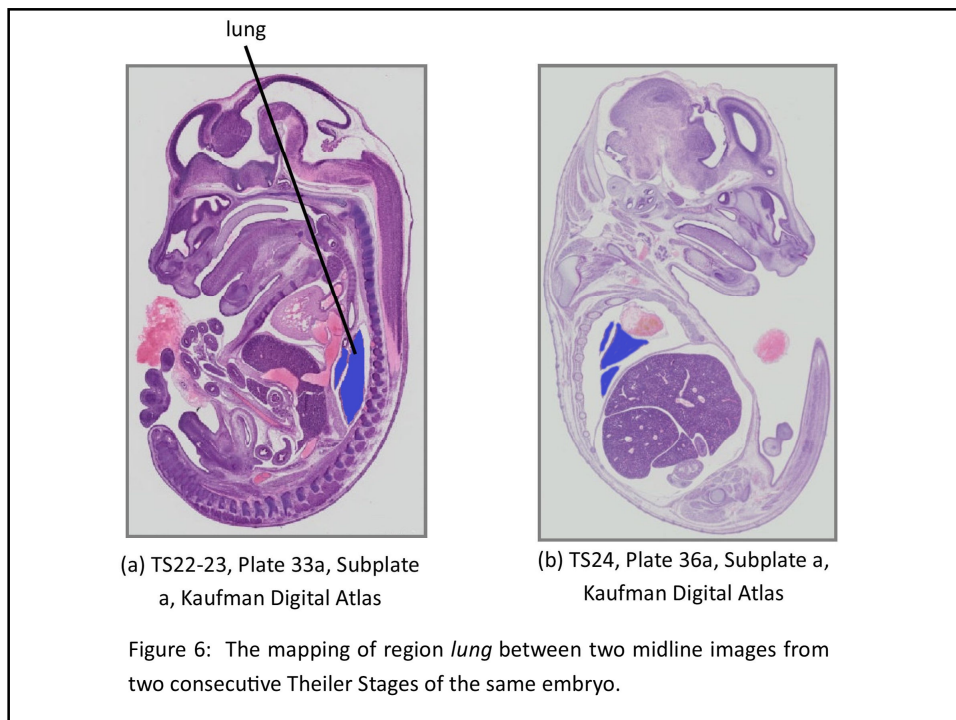
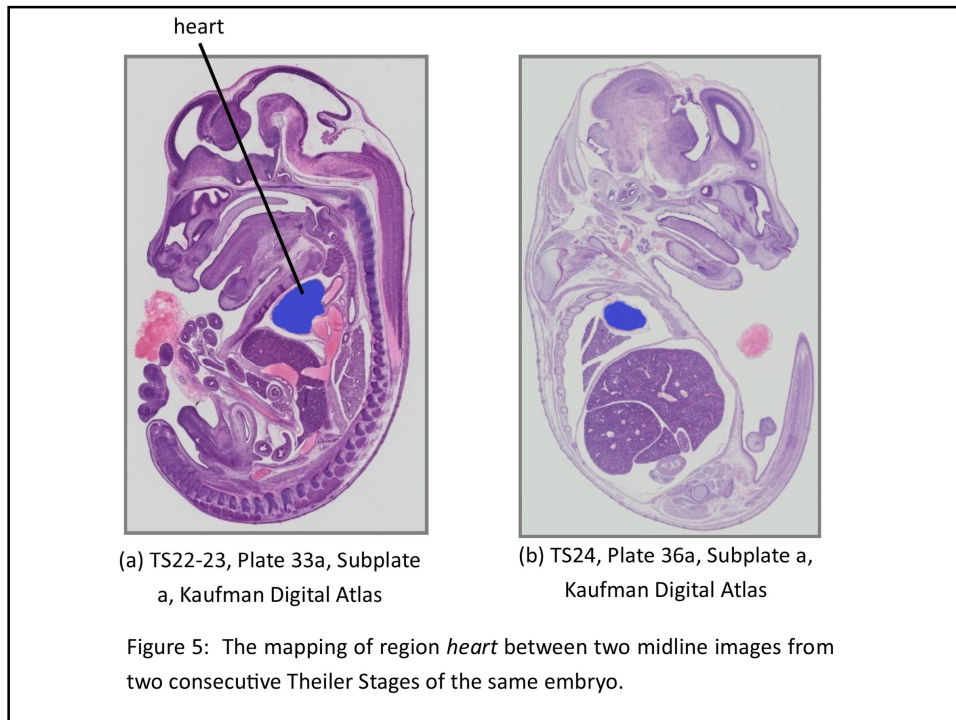


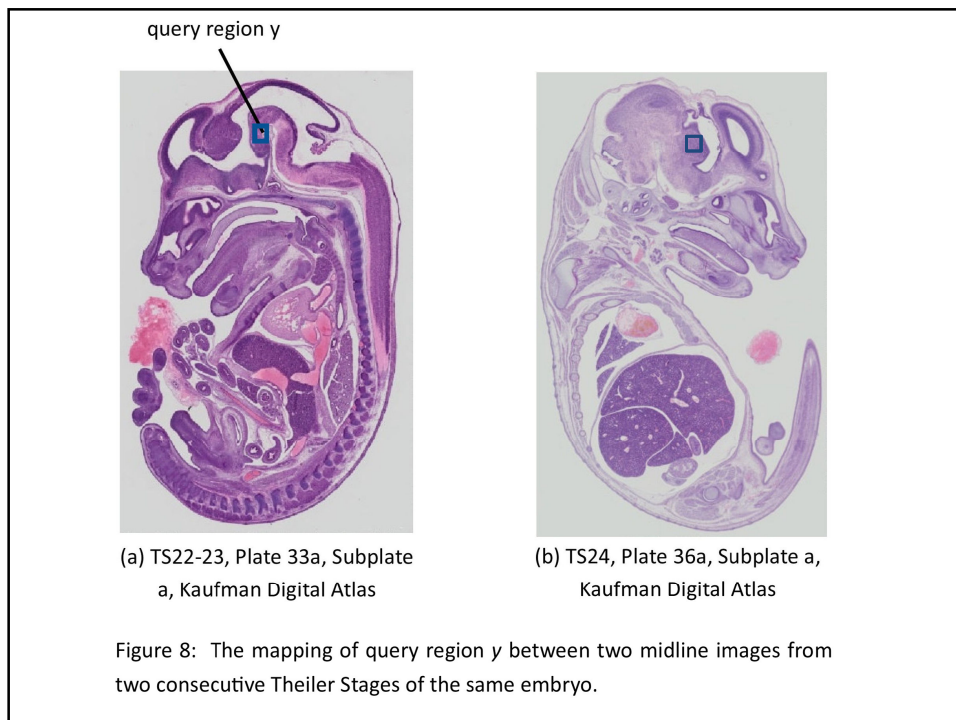
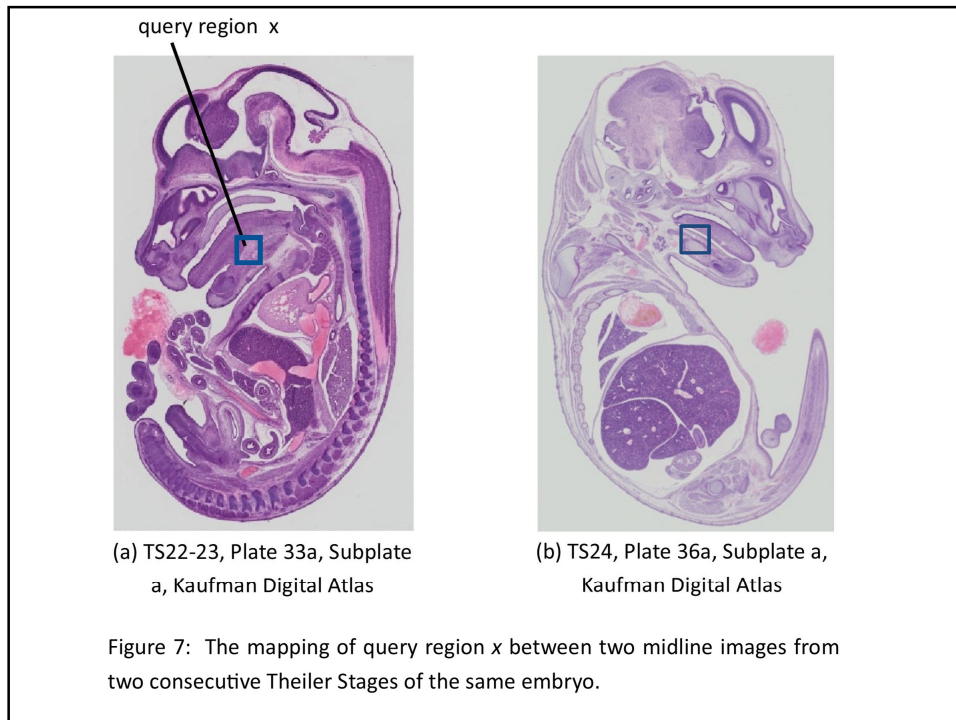
Figure B.7: Anatomical location of metanephros (a) in its actual location, and (b) the corresponding matched location resulting from image processing algorithm by [63].

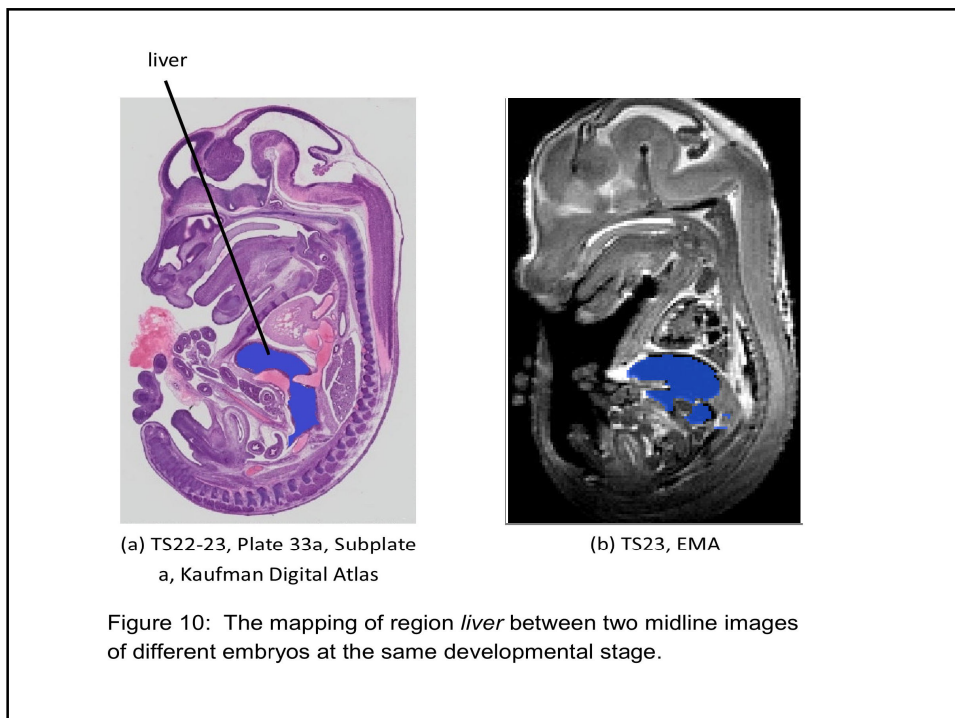
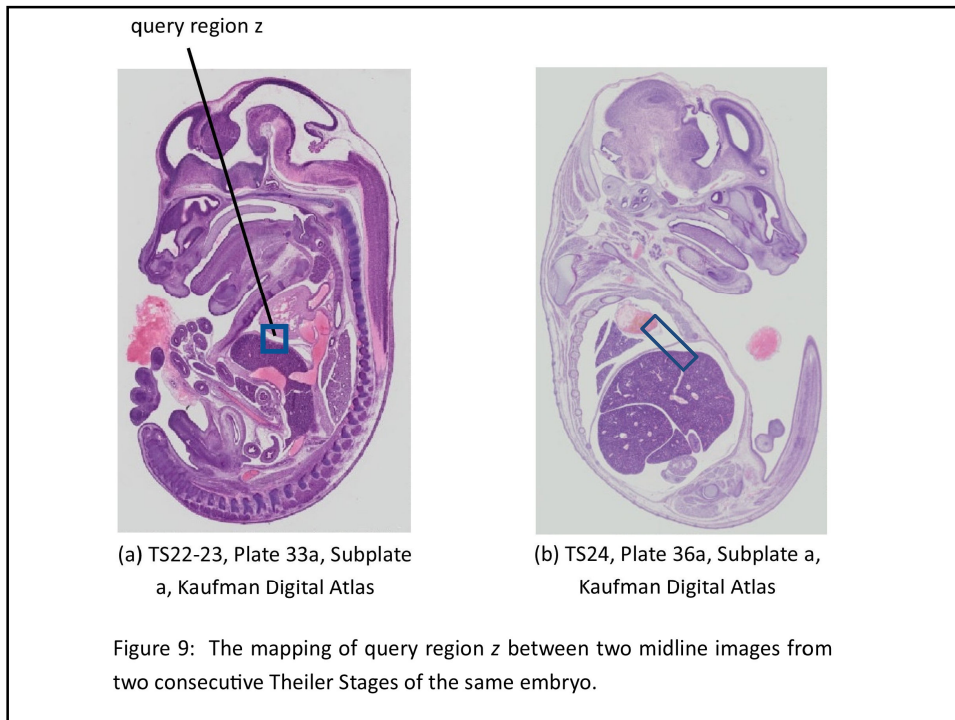
Appendix C Biologist Gold Standard

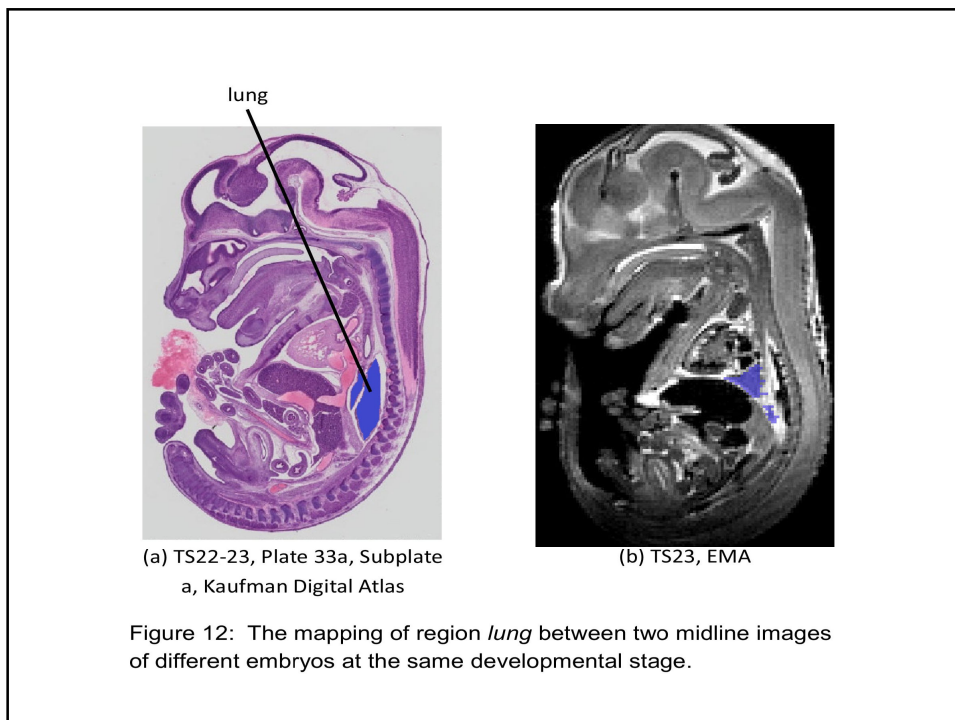
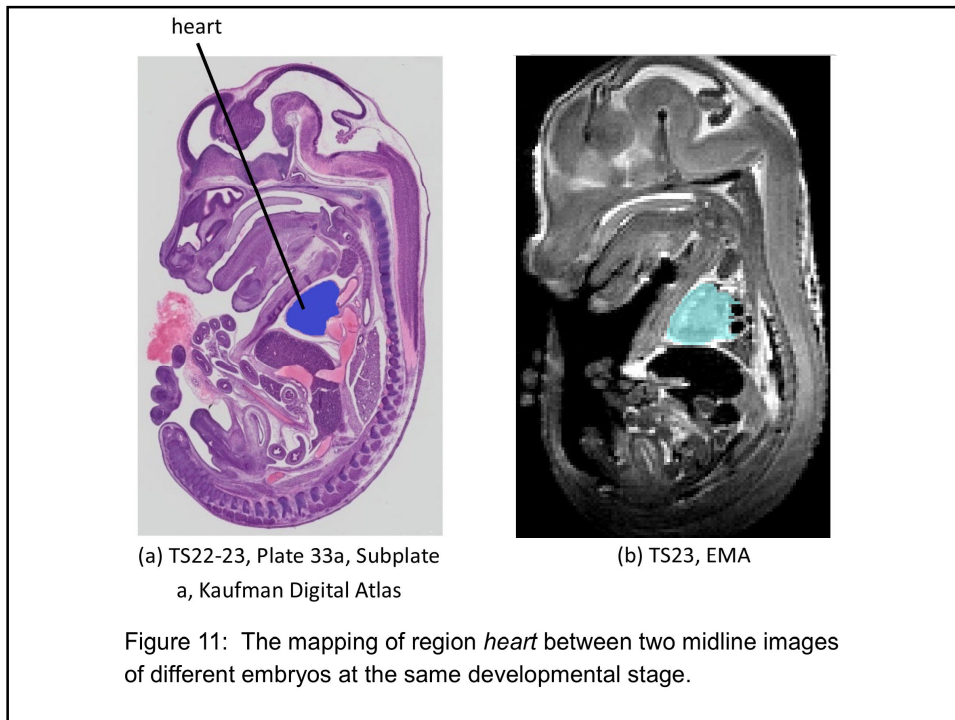


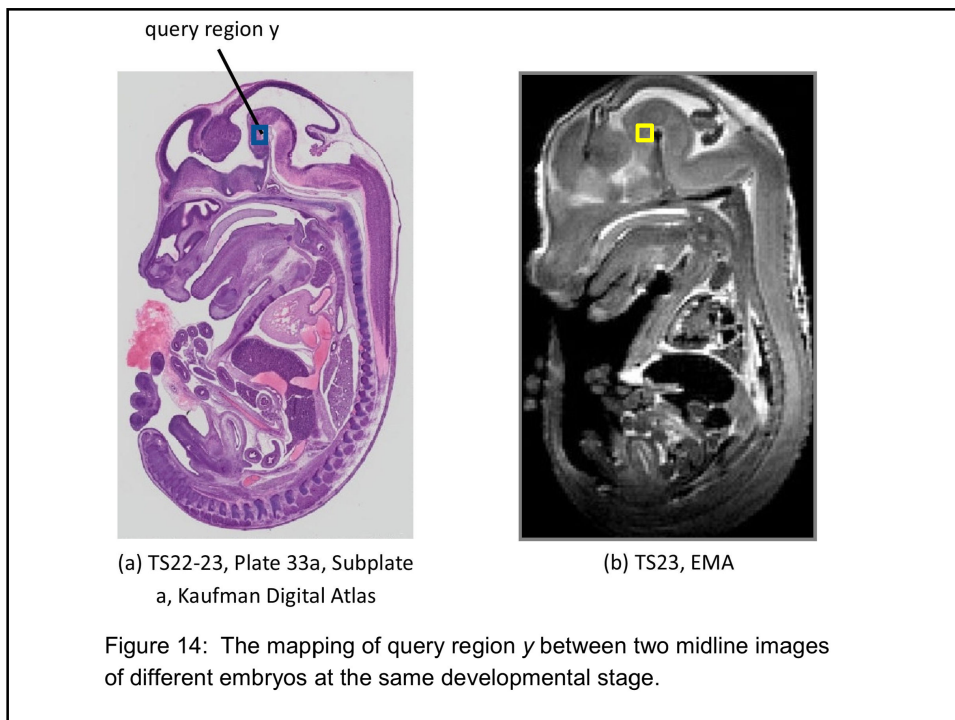
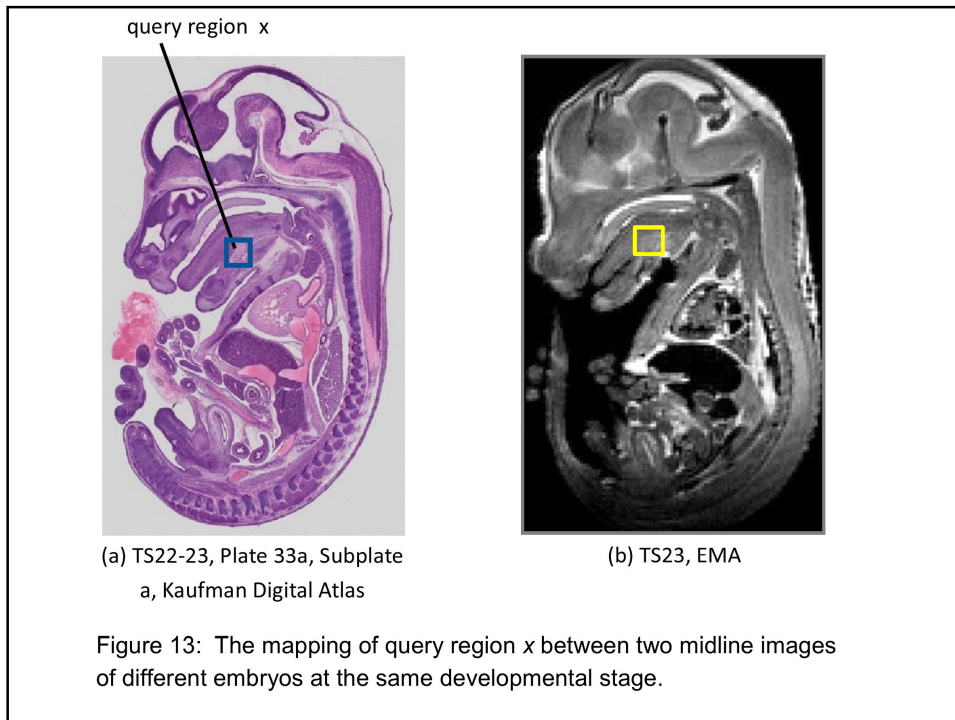


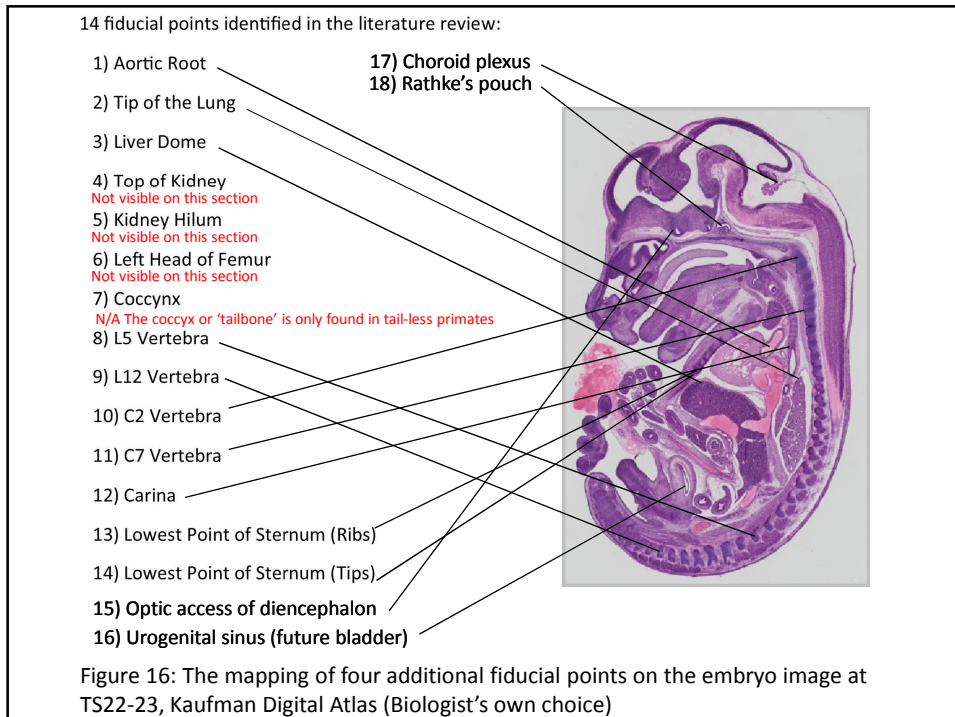
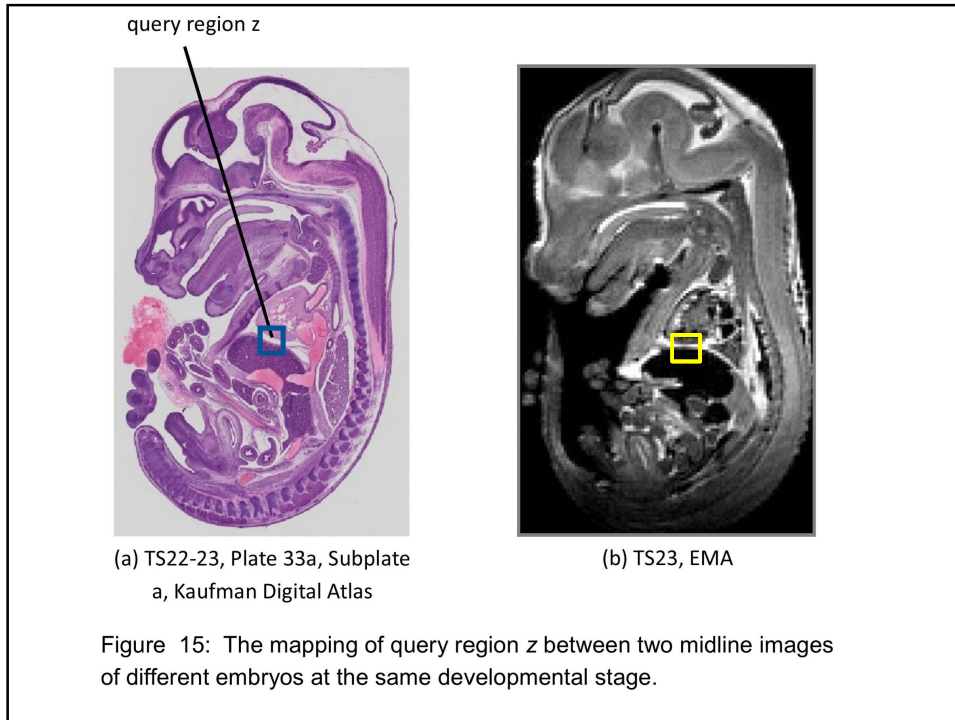


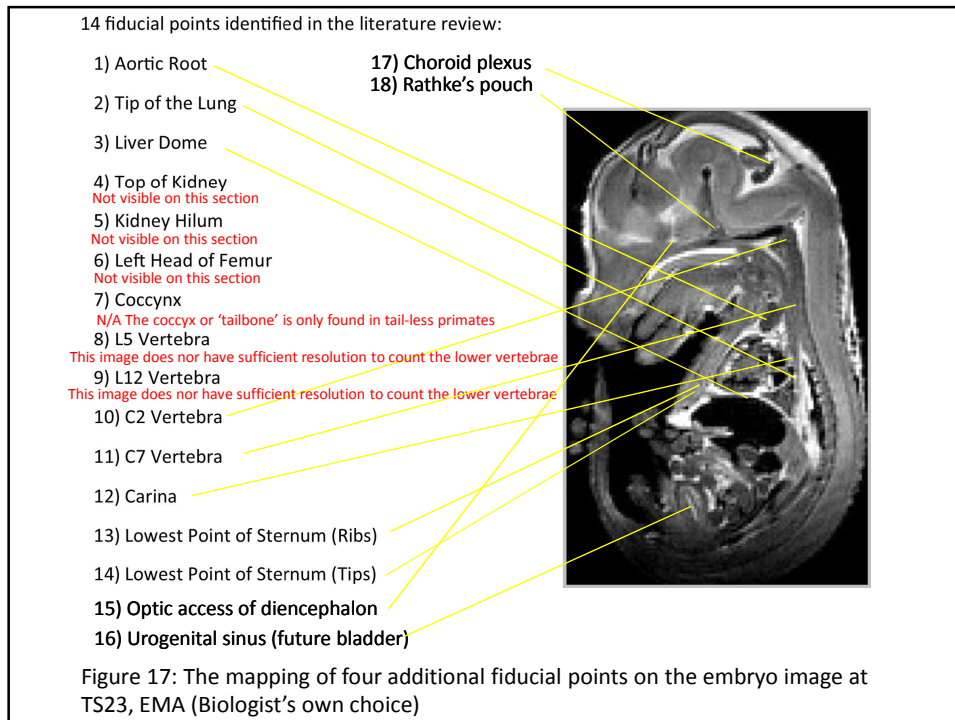












References

- [1] Emage. <http://www.emouseatlas.org/emage/home.php>. Accessed: 28/06/2012. 1, 5, 11, 147
- [2] Allen Developing Mouse Brain Reference Atlas. *Technical Report*, 2010. 1, 12
- [3] Gensat. gensat brain atlas of gene expression. gensat brain atlas of gene expression in egfp transgenic mice. <http://www.gensat.org/index.html>. Accessed: 28/06/2012. 1, 2, 12
- [4] S. Andrews and K. McLeod. Gene Co-Expression in Mouse Embryo Tissues *Int. J. Intell. Inf. Technol.*, 9(4):55–68, 2013. 1
- [5] Allen brain atlas: Developing mouse brain. <http://developingmouse.brain-map.org>. Accessed: 28/06/2012. 1
- [6] J. H. Christiansen, Y. Yang, S. Venkataraman, L. Richardson, P. Stevenson, N. Burton, R. A. Baldock, and D. R. Davidson. Emage: a spatial database of gene expression patterns during mouse embryo development. *Nucleic Acids Research*, 34(suppl 1):D637–D641, 2010. 1, 5, 147
- [7] R. A. Baldock, J. B. Bard, A. Burger, N. Burton, J. Christiansen, G. Feng, B. Hill, D. Houghton, M. Kaufman, J. Rao, J. Sharpe, A. Ross, P. Stevenson, S. Venkataraman, A. Waterhouse, Y. Yang, and D. R. Davidson. Emap and emage - a framework for understanding spatially organized data. *Neuroinformatics*, 4:309–325, 2003. 1, 5, 11, 147
- [8] K. McLeod and A. Burger. Towards the use of argumentation in bioinformatics: a gene expression case study. *Bioinformatics*, 24:304–312, 2008. 2
- [9] J. Boline, E. F. Lee, and A. W. Toga. Digital atlases as a framework for data sharing. *Front Neurosci*, 2(1):100–106, 2008. 2

References

- [10] K. McLeod, G. Ferguson, and A. Burger. Argudas: lessons for argumentation in biology based on a gene expression use case. *BMC Bioinformatics*, 13(Suppl 1):S8, 2012. 2
- [11] D. Davidson, J. Bard, R. Brune, A. Burger, C. Dubreuil, W. Hill, M. Kaufman, J. Quinn, M. Stark, and R. Baldock. The mouse atlas and graphical gene-expression database. *Seminars in Cell and Developmental Biology*, 8(5):509–517, 1997. 2
- [12] A. Burger and J. Bard. Xspan- a cross-species anatomy network. In A Burger, D Davidson, and R Baldock, editors, *Anatomy Ontologies for Bioinformatics: Principles and Practise*, volume 1, pages 163–175. Springer Verlag, 1st edition, 2008. 2
- [13] H. Nie, R. P. M. A. Crooijmans, A. Lammers, E. M. V. Schothorst, J. Keijer, P. B. T. Neerincx, J. A. M. Leunissen, H. J. Megens, and M. A. M. Groenen. Gene expression in chicken reveals correlation with structural genomic features and conserved patterns of transcription in the terrestrial vertebrates. *PLoS One*, 5(8), 2010. 2
- [14] W. Z. Wang, F. M. Oeschger, J. F. Montiel, F. Garcia-Moreno, A. Hoerder-Suabedissen, L. Krubitzer, C. J. Ek, N. R. Saunders, K. Reim, A. Villalon, and Z. Molnar. Comparative aspects of subplate zone studied with gene expression in sauropsids and mammals. *Cereb Cortex*, 2011. 2
- [15] P. Coumailleau and D. Duprez. Sim1 and sim2 expression during chick and mouse limb development. *International Journal of Developmental Biology*, 53:149–157, 2009. 2
- [16] The university of bath press release, 2008. chicks to give scientists clearer picture of fetal development. <http://www.bath.ac.uk/news/2008/11/14/chick-atlas.html>. Accessed: 28/06/2012. 3
- [17] A. A. Joshi, A. Chaudhari, C. Li, D. W. Shattuck, J. Dutta, R. M. Leahy, and A. W. Toga. Posture matching and elastic registration of a mouse atlas to surface topography range data. In *ISBI*, pages 366–369, 2009. 3
- [18] S. Zhang and O. Bodenreider. Experience in aligning anatomical ontologies. *Int. J. Semantic Web Inf. Syst.*, 3(2):1–26, 2007. 4

References

- [19] N. A. Chowdhury and D. Dejing. Improving the accuracy of ontology alignment through ensemble fuzzy clustering. In *Proceedings of the 2011th Confederated international conference on On the move to meaningful internet systems - Volume Part II*, OTM'11, pages 826–833, Berlin, Heidelberg, 2011. Springer-Verlag. 4
- [20] L. Richardson, S. Venkataraman, P. Stevenson, Y. Yang, N. Burton, J. Rao, M. Fisher, R. A. Baldock, D. R. Davidson, and J. H. Christiansen. Emage mouse embryo spatial gene expression database: 2010 update. *Nucleic Acids Research*, 38(suppl 1):D703–D709, 2010. 5, 11, 147
- [21] M. Ringwald, R. A. Baldock, J. Bard, M. Kaufman, J. T. Eppig, J. E. Richardson, J. H. Nadeau, and D. Davidson. A database for mouse development. *Science*, 265:2033–2034, 1994. 9
- [22] R. A. Baldock, C. Dubreuil, B. Hill, and D. Davidson. The edinburgh mouse atlas: Basic structure and informatics. In S Levotsky, editor, *Bioinformatics Databases and Systems*, volume 1, pages 102–115. Kluwer Academic Press, 1st edition, 1999. 9
- [23] A. Burger, D. Davidson, Y. Yang, and R. A. Baldock. Integrating partonomic hierarchies in anatomy ontologies. *BMC Bioinformatics*, 5:184, 2004. 9
- [24] R. A. Baldock and D. Davidson. The edinburgh mouse atlas. In A Burger, D Davidson, and R Baldock, editors, *Anatomy Ontologies for Bioinformatics: Principles and Practise*, volume 1, pages 249–265. Springer Verlag, 1st edition, 2008. 9
- [25] K. Theiler. *The house mouse: atlas of embryonic development*. Springer-Verlag, New York, 1989. 9
- [26] S. Venkataraman, P. Stevenson, Y. Yang, L. Richardson, N. Burton, T. P. Perry, P. Smith, R. A. Baldock, D. R. Davidson, and J. H. Christiansen. Emageedinburgh mouse atlas of gene expression: 2008 update. *Nucleic Acids Research*, 36(Database issue):D860–D865, 2008. 11
- [27] T. Bittner, M. Donnelly, L. J. Goldberg, and F. Neuhaus. Modeling principles and methodologies - spatial representation and reasoning. In A. Burger, D. Davidson, and R. Baldock, editors, *Anatomy Ontologies for Bioinformatics: Principles and Practise*, volume 1, pages 307–326. Springer-Verlag, London, 1st edition, 2008. 15, 29, 52

References

- [28] S. Li. Combining topological and directional information for spatial reasoning. In *Proceedings of the 20th international joint conference on Artificial intelligence, IJCAI'07*, pages 435–440, San Francisco, CA, USA, 2007. Morgan Kaufmann Publishers Inc. 15
- [29] A. Schwering. Evaluation of a semantic similarity measure for natural language spatial relations. In *Proceedings of the 8th international conference on Spatial information theory, COSIT'07*, pages 116–132, Berlin, Heidelberg, 2007. Springer-Verlag. 15, 18
- [30] M. J. Egenhofer and J. Herring. *Categorizing binary topological relations between regions, lines and points in geographic databases, Technical Report*. Department of Surveying Engineering, University of Maine, 1991. 15, 48
- [31] A. Abella and J. R. Kender. From images to sentences via spatial relations. In *Integration of Speech and Image Understanding, 1999. Proceedings*, pages 117–146, 1999. 15
- [32] T. Bittner. Logical properties of foundational mereogeometrical relations in bio-ontologies. *Applied Ontology*, 4(2):109–138, 2009. 16, 21, 29, 48, 52
- [33] Y. Liu, Q. Guo, and M. Kelly. A framework of region-based spatial relations for non-overlapping features and its application in object based image analysis. *ISPRS Journal of Photogrammetry and Remote Sensing*, 63(4):461 – 475, 2008. 16, 54
- [34] A. Isli. Combining cardinal direction relations and other orientation relations in qsr. In *Proc. of 8th International Symposium on Artificial Intelligence and Mathematics (AIM04)*, Fort Lauderdale, Florida, 2004. 16
- [35] J. Chen, H. Jia, D. Liu, and C. Zhang. Composing cardinal direction relations basing on interval algebra. In *Proceedings of the 4th international conference on Knowledge science, engineering and management, KSEM'10*, pages 114–124, Berlin, Heidelberg, 2010. Springer-Verlag. 16
- [36] A. U. Frank. Qualitative spatial reasoning: Cardinal directions as an example. *International Journal of Geographical Information Science*, 10(3):269–290, 1996. 16
- [37] C. Freksa. Using orientation information for qualitative spatial reasoning. In *Proceedings of the International Conference GIS - From Space to Territory:*

References

- Theories and Methods of Spatio-Temporal Reasoning on Theories and Methods of Spatio-Temporal Reasoning in Geographic Space*, pages 162–178, London, 1992. Springer-Verlag. 16
- [38] G. Ligozat. Reasoning about cardinal directions. *J. Vis. Lang. Comput.*, 9(1):23–44, 1998. 16
- [39] D. Papadias and T. Sellis. Qualitative representation of spatial knowledge in two-dimensional space. *The VLDB Journal*, 3(4):479–516, October 1994. 17
- [40] V. Potesil, T. Kadir, G. Platsch, and M. Brady. Improved anatomical landmark localization in medical images using dense matching of graphical models. *BMVC'2010*, pages 1–10, 2010. 18
- [41] S. Seifert, A. Barbu, K. S. Zhou, D. Liu, J. Feulner, M. Huber, M. Suehling, A. Cavallaro, and D. Comaniciu. Hierarchical parsing and semantic navigation of full body ct data. In *Proc. SPIE 7259, Medical Imaging 2009: Image Processing*, volume 725902, (March 27, 2009). 18, 97, 98, 99
- [42] C. Rosse and J. L. V. Mejino. The foundational model of anatomy ontology. In A. Burger, D. Davidson, and R. Baldock, editors, *Anatomy Ontologies for Bioinformatics: Principles and Practise*, volume 1, pages 59–117. Springer-Verlag, London, 1st edition, 2008. 21
- [43] B. Smith, M. Ashburner, C. Rosse, J. Bard, W. Bug, W. Ceusters, L.J. Goldberg, K. Eilbeck, A. Ireland, C. J. Mungall, OBI Consortium, N. Leontis, P. Rocca-Serra, A. Ruttenberg, S. A. Sansone, R. H. Scheuermann, N. Shah, P. L. Whetzel, and S. Lewis. The obo foundry: coordinated evolution of ontologies to support biomedical data integration. *Nat Biotechnol*, 25(11):1251–1255, 2007. 21
- [44] A. Mechouche, X. Morandi, C. Golbreich, and B. Gibaud. A hybrid system for the semantic annotation of sulco-gyral anatomy in mri images. In *Proceedings of the 11th international conference on Medical Image Computing and Computer-Assisted Intervention - Part I, MICCAI '08*, pages 807–814, Berlin, Heidelberg, 2008. Springer-Verlag. 22
- [45] C. Hudelot, J. Atif, and I. Bloch. Fuzzy spatial relation ontology for image interpretation. *Fuzzy Sets and Systems*, 159(15):1929 – 1951, 2008. 22
- [46] S. Du, Q. Qin, D. Chen, and L. Wang. Spatial data query based on natural language spatial relations. In *Proceedings of the Geoscience and Remote*

References

- Sensing Symposium, 2005. IGARSS '05. 2005 IEEE International*, volume 2, pages 1210 – 1213, 2005. 22
- [47] C. C. Chang and T. C. Wu. An exact match retrieval scheme based upon principal component analysis. *Pattern Recogn. Lett.*, 16(5):465–470, May 1995. 22
- [48] D. S. Guru and P. Punitha. An invariant scheme for exact match retrieval of symbolic images based upon principal component analysis. *Pattern Recogn. Lett.*, 25(1):73–86, January 2004. 23, 24, 47
- [49] I. Karouia and E. Zagrouba. New image matching method based on spatial region interrelationships. In *4th International Conference on Innovations in Information Technology, 2007. IIT '07*, pages 675–679, 2007. 23, 24, 47
- [50] X. M. Zhou, C. H. Ang, and T. W. Ling. Image retrieval based on object's orientation spatial relationship. *Pattern Recogn. Lett.*, 22(5):469–477, April 2001. 24, 47
- [51] M. A. Kulkarni and R. C. Joshi. Content-based image retrieval by spatial similarity. *Defence Science Journal*, 52(3):285–291, 2002. 24, 47
- [52] Arun K. Majumdar, I. Bhattacharya, and A. K. Saha. An object-oriented fuzzy data model for similarity detection in image databases. *IEEE Trans. on Knowl. and Data Eng.*, 14(5):1186–1189, September 2002. 24, 47
- [53] Y. H. Wang. Image indexing and similarity retrieval based on spatial relationship model. *Information Sciences*, 154(12):39 – 58, 2003. 24, 47
- [54] L. Yang and T. Zhongjian. A novel approach for image representation and matching based on mixed graph structure. In *Computational Intelligence and Software Engineering (CiSE 2009)*, CiSE 2009, pages 1–4, 2009. 24, 47
- [55] P. Dasigi and C. V. Jawahar. Efficient graph-based image matching for recognition and retrieval. In *Proceedings of National Conference on Computer Vision, Pattern recognition, Image Processing and Graphics, Gandhinagar, 2008*. 24, 47
- [56] C. Izard and B. Jedynek. Bayesian registration for anatomical landmark detection. In *3rd IEEE International Symposium on Biomedical Imaging: Nano to Macro, 2006.*, pages 856–859, 2006. 25

References

- [57] G. Khaissidi, H. Tairi, and A. Aarab. A fast medical image registration using feature points. *ICGST-GVIP Journal*, 9(3):19–24, 2009. 25, 39
- [58] E. Guest, E. Berry, R. A. Baldock, M. Fidrich, and M. A. Smith. Robust point correspondence applied to two and three dimensional image registration. *IEEE Transactions on Pattern Analysis and Machine Intelligence*, 23(2):1–15, 2001. 25, 39
- [59] A. Wong and J. Orchard. Efficient fft-accelerated approach to invariant optical-lidar registration. *IEEE T. Geoscience and Remote Sensing*, 46(11):3917–3925, 2008. 25, 39, 40
- [60] H. Park, G. R. Martin, and A. Bhalerao. Local affine image matching and synthesis based on structural patterns. *Trans. Img. Proc.*, 19(8):1968–1977, August 2010. 26, 39, 124
- [61] Y. Guoshen and J. M. Morel. Asift: An algorithm for fully affine invariant comparison. *Image Processing On Line*, 2011, 2011. 26, 39, 40, 117, 125, 158
- [62] Y. Zeng, D. Samaras, W. Chen, and Q. Peng. Topology cuts: A novel min-cut/max-flow algorithm for topology preserving segmentation in n-d images. *Comput. Vis. Image Underst.*, 112(1):81–90, October 2008. 26, 39, 158
- [63] J. Hangouet. Computing of the hausdorff distance between plane vector polylines. *AUTO-CARTO 12*, pages 1–10, 1995. 27
- [64] D. P. Huttenlocher, G. A. Klanderman, and W. J. Rucklidge. Comparing images using the hausdorff distance. *IEEE Pattern Analysis and Machine Intelligence*, 15(9):329–340, 1993. 27
- [65] S. Wang, C. S. Chen, V. Rinsurongkawong, F. Akdag, and C. F. Eick. A polygon-based methodology for mining related spatial datasets. In *Proceedings of the 1st ACM SIGSPATIAL International Workshop on Data Mining for Geoinformatics*, DMG '10, pages 1–8, New York, NY, USA, 2010. ACM. 27
- [66] S. Russell and P. Norvig. *Artificial Intelligence: A Modern Approach*. Prentice Hall, 3rd edition, 2010. 28
- [67] Woolz. http://www.emouseatlas.org/emap/analysis_tools_resources/software/woolz.html. Accessed: 28/06/2012. 29

References

- [68] K. Liakos. *Efficient Access to Distributed Biomedical Image Data*. PhD thesis, Heriot-Watt University, School of Mathematical and Computer Sciences, 2005. 29
- [69] R. Baldock. *EMAP Technical Report: A 3D Paint Program for the Mouse Atlas and Gene Expression Database*. MRC Human Genetic Unit, 2004. 29, 30
- [70] R. Baldock. *EMAP Technical Report. MAPaint User Manual and Help Pages*. MRC Human Genetic Unit, 2001. 30
- [71] Woolz library index. edinburgh mouse atlas project. 32
- [72] J. Piper and D. Rutovitz. Data structures for image processing in a c language and unix environment. *Pattern Recognition Letters*, 3:119–129, 1985. 32
- [73] J. Piper and D. Rutovitz. *MRC Technical Report: An Investigation of Object-Oriented Programming as the Basis for an Image Processing and Analysis System*. MRC Human Genetic Unit, 1988. 32
- [74] L. Ji, J. Piper, and J. Y. Tang. Data structures for image processing in a c language and unix environment. *Pattern Recognition Letters* 9, 3:201–209, 1989. 32
- [75] Z. L. Husz, T. P. Perry, B. Hill, and R. A. Baldock. Woolz iip: A tiled on-the-fly sectioning server for 3d volumetric atlases. In *ISVC (1)*, pages 924–933, 2009. 32
- [76] W. Jia, H. Zhang, X. He, and Q. Wu. A comparison on histogram based image matching methods. In *IEEE International Conference on Video and Signal Based Surveillance, 2006. AVSS '06.*, pages 97–97, Nov 2006. 37
- [77] A. Hanbury and B. Marcotegui. Colour adjacency histograms for image matching. In *Proceedings of the 12th International Conference on Computer Analysis of Images and Patterns, CAIP'07*, pages 424–431, Berlin, Heidelberg, 2007. Springer-Verlag. 37
- [78] W. K. Leow and S. Y. Lai. Invariant matching of texture for content-based image retrieval. In *Proc. Workshop on Texture Analysis in Machine Vision*, pages 119–125, 1999. 38

References

- [79] W. K. Leow and S. Y. Lai. Invariant matching of texture for content-based image retrieval. In *Texture Analysis in Machine Vision*, pages 151–163. World Scientific, 2000. 38
- [80] J. Z. Wang, J. Li, and G. Wiederholdy. Simplicity: Semantics-sensitive integrated matching for picture libraries. In R. Laurini, editor, *Advances in Visual Information Systems*, volume 1929 of *Lecture Notes in Computer Science*, pages 360–371. Springer Berlin Heidelberg, 2000. 38
- [81] S. Todorovic and N. Ahuja. Region-based hierarchical image matching. *International Journal of Computer Vision*, 78(1):47–66, 2008. 38
- [82] R. A. Baeza-Yates and B. A. Ribeiro-Neto. *Modern Information Retrieval*. ACM Press / Addison-Wesley, 1999.
- [83] J. Cai, Z. J. Zha, Y. Zhao, and Z. Wang. Evaluation of histogram based interest point detector in web image classification and search. In *ICME*, pages 613–618, 2010.
- [84] J. You, E. Pissaloux, T. Dahlinm, and W. Zhu. The parallel detection of interesting points in distance transform for image matching. In *MVA*, pages 151–154, 1994. 124
- [85] Y. Liu and G. Zhang, D.and Lu. Region-based image retrieval with high-level semantics using decision tree learning. *Pattern Recogn.*, 41(8):2554–2570, August 2008. 39
- [86] E. Walia and A. Suneja. A conceptual study on image matching techniques. *Global Journal of Computer Science and Technology*, 10(12):83–88, 2010. 40
- [87] F. Cannavale, A. Casanova, M. Fraschini, and V. Savona. Content image retrieval based on topological information. *J. Vis. Lang. Comput.*, 15(5):347–359, 2004. 47
- [88] Shu-Ming Hsieh and Chiun-Chieh Hsu. Retrieval of images by spatial and object similarities. *Inf. Process. Manage.*, 44(3):1214–1233, 2008. 47
- [89] D. Chaudhuri and A. Samal. A simple method for fitting of bounding rectangle to closed regions. *Pattern Recogn.*, 40(7):1981–1989, July 2007. 48
- [90] D. A. Randell, Z. Cui, and A. Cohn. A Spatial Logic Based on Regions and Connection. In Bernhard Nebel, Charles Rich, and William Swartout, editors,

References

- Proceedings of the 3rd International Conference on Principles of Knowledge Representation and Reasoning*, pages 165–176. Morgan Kaufmann, San Mateo, California, 1992. 48, 50
- [91] H. Tagare, F. Vos, C. C. Jaffe, and J. S. Duncan. Arrangement: A spatial relation between parts for evaluating similarity of tomographic section. *IEEE Trans. Pattern Anal. Machine Intell*, 17(9):880–893, 1995. 48
- [92] C. M. Gold. Problems with handling spatial data the voronoi approach. *CISM Journal*, 45:65–80, 1991. 48
- [93] T. Weninger, S. Ramachandran, D. Greene, J. Hart, A. Kancherlapalli, W. H. Hsu, and J. Han. Speech-assisted radiology system for retrieval, reporting and annotation. *Proceedings of the 16th ACM SIGKDD Conference on Knowledge Discovery and Data Mining (KDD 2010)*, 2010. 66
- [94] C. R. Meyer, T. D. Johnson, G. McLennan, D. R. Aberle, E. A. Kazerooni, H. MacMahon, B. F. Mullan, D. F. Yankelevitz, E. J. van Beek, M. F. Armato, S. G. 3rd McNitt-Gray, A. P. Reeves, D. Gur, C. I. Henschke, E. A. Hoffman, P. H. Bland, G. Laderach, R. Pais, D. Qing, C. Piker, J. Guo, A. Starkey, D. Max, B. Y. Croft, and L. P. Clarke. Evaluation of lung mdct nodule annotation across radiologists and methods. *Acad Radiol*, 13(10):1254–1265, 2006. 66
- [95] P. Mozer, A. Leroy, Y. Payan, J. Troccaz, E. Chartier-Kastler, and F. Richard. Computer-assisted access to the kidney. *The International Journal of Medical Robotics and Computer-Assisted Surgery*, 1(4):58–66, 2005. 66
- [96] P. Dumpuri, L. W. Clements, R. Li, J. M. Waite, J. D. Stefansic, D. A. Geller, M. I. Miga, and B. M. Dawant. Comparison of pre/post-operative ct image volumes to preoperative digitization of partial hepatectomies: a feasibility study in surgical validation, 2009. 66
- [97] J. Chen and L. Zhao. A new method for uncertainty evaluation of centroid detection. *2nd International Congress Image and Signal Processing, 2009. CISP '09*, pages 1–4, 2009. 66
- [98] M. Komann, A. Kroller, C. Schmidt, D. Fey, and S. P. Feteke. Emergent algorithms for centroid and orientation detection in high-performance embedded cameras. *Computing Frontiers*, 14(1):221–230, 2008. 66

References

- [99] A. Vyas, M. B. Roopashree, and B. R. Prasad. Centroid detection by gaussian pattern matching in adaptive optics. *International Journal of Computer Applications*, 1(25):30–35, 2010. 66
- [100] Q. C. Vuong and M. Tarr. Rotation direction affects object recognition. *Vision Research*, 44:1717–1730, 2004. 55
- [101] T. Fawcett. An introduction to roc analysis. *Pattern Recogn. Lett.*, 27(8):861–874, June 2006.
- [102] S. Rueda and M. Alcaniz. An approach for the automatic cephalometric landmark detection using mathematical morphology and active appearance models. In *Proceedings of MICCAI, Springer LNCS*, 2006. 97
- [103] K. Domijan and S. Wilson. A bayesian method for automatic landmark detection in segmented images. In *Proceedings of the 22nd International Conference on Machine Learning*, Bonn, Germany, 2005. 97
- [104] R. Kafieh, S. Sadri, A. Mehri, and H. Raji. Discrimination of bony structures in cephalograms for automatic landmark detection. In *Advances in Computer Science and Engineering*, pages 609–620. Springer-Verlag, 2009. 97
- [105] B. Roeschies and S. Winter. Feature processing for automatic anatomical landmark detection using reservoir networks. In H. P. Meinzer, T. M. Deserno, H. Handels, and T. Tolxdorff, editors, *Bildverarbeitung fr die Medizin 2009*, Informatik aktuell, pages 277–281. Springer Berlin Heidelberg, 2009. 97
- [106] M. A. Martn-Fernndez, R. Crdenes, E. Muoz-Moreno, R. Luis-Garca, M. Martn-Fernndez, and C. Alberola-Lpez. Automatic articulated registration of hand radiographs. *Image and Vision Computing*, 27:1207–1222, 2009. 97
- [107] D. Liu, K. S. Zhou, D. Bernhardt, and D. Comaniciu. Search strategies for multiple landmark detection by submodular maximization. *Computer Vision and Pattern Recognition (CVPR)*, pages 2831–2838, 2010. 97
- [108] J. Tan, D. Chen, V. Chaudhary, and I. Sethi. A template based technique for automatic detection of fiducial markers in 3d brain images. In *Proceedings 20th International Congress on Computer Assisted Radiology and Surgery (CARS), Osaka, Japan*, 2006. 97

References

- [109] D. Chen, J. Tan, V. Chaudhary, and I. K. Sethi. Automatic fiducial localization in brain images. *International Journal of Computer Assisted Radiology and Surgery*, 1:45–46, 2006. 97
- [110] H. G. Hanumantharaju and H. K. Shivanand. Static analysis of bi-polar femur bone implant using fea. *International Journal of Recent Trends in Engineering*, 1(5):19–24, 2009. 99
- [111] Coccyx. wikipedia. <http://en.wikipedia.org/wiki/Coccyx>. Accessed: 28/06/2012. 99
- [112] A. K. Bhandutia, J. A. Gruskay, M. D. Helgeson, N. K. Yadlapalli, A. L. Gowda, B. W. Su, J. K. Ratliff, D. G. Anderson, and A. R. Vaccaro. Treatments and outcomes for lower lumbar (l3l5) burst fractures: A systematic review. *Contemporary Spine Surgery*, 12(4):1–7, 2011. 99
- [113] Carina of trachea, medical definition. <http://www.medilexicon.com/medicaldictionary.php?t=14580>. Accessed: 28/06/2012. 99
- [114] C. B. Rosdahl and M. T. Kowalski. *Textbook of basic nursing*. Lippincott, Williams Wilkins, Philadelphia, 9th edition, 2008. 99
- [115] N. James, K. Todorov, and C. Hudelot. Ontology matching for the semantic annotation of images. In *IEEE International Conference on Fuzzy Systems*, pages 1–8, 2010. 110
- [116] A. W. Joshi. *Elements of Group Theory for Physicists*. New Age International (P) Ltd., Daryaganj, New Delhi, 1997. 124
- [117] C. Yang, E. Zeng, T. Li, and G. Narasimhan. Clustering genes using gene expression and text literature data. *Proceedings of the 2005 IEEE Computational Systems Bioinformatics Conference*, 14(1):329–340, 2005. 150
- [118] M. A. Hearst. Untangling text data mining. In *Proceedings of the 37th annual meeting of the Association for Computational Linguistics on Computational Linguistics*, ACL '99, pages 3–10, Stroudsburg, PA, USA, 1999. Association for Computational Linguistics. 150
- [119] K. B. Cohen and L. Hunter. Getting started in text mining. *PLoS Comput Biol*, 4, 2008. 150

References

- [120] N. Pasquier, C. Pasquier, L. Brisson, and M. Collard. Mining gene expression data using domain knowledge. *International Journal of Software and Informatics*, 2(2):215–231, 2008. 150
- [121] J. Hemert and R. Baldock. Mining spatial gene expression data for association rules. In S. Hochreiter and R. Wagner, editors, *Bioinformatics Research and Development*, volume 4414 of *Lecture Notes in Computer Science*, pages 66–76. Berlin, Heidelberg, Springer, 2007. 150
- [122] G. Schaefer and T. Nakashima. Data mining of gene expression data by fuzzy and hybrid fuzzy methods. *IEEE Information Technology in Biomedicine*, 14(1):23–29, 2010. 150
- [123] M. Gerner, G. Nenadic, and C. M. Bergman. An exploration of mining gene expression mentions and their anatomical locations from biomedical text. In *Proceedings of the 2010 Workshop on Biomedical Natural Language Processing*, BioNLP '10, pages 72–80, Stroudsburg, PA, USA, 2010. Association for Computational Linguistics. 150
- [124] Knowledge based system for data mining. http://www.theecommercesolution.com/usefull_links/KBS_Data_Mining.php. Accessed: 28/06/2012. 150
- [125] F. W. Leberl, K. Maurice, J. K. Thomas, and M. Millot. Automated radar image matching experiment. *{ISPRS} Journal of Photogrammetry and Remote Sensing*, 49(3):19 – 33, 1994. 151
- [126] A. Shrivastava, T. Malisiewicz, A. Gupta, and A. A. Efros. Data-driven visual similarity for cross-domain image matching. *ACM Trans. Graph.*, 30(6):154:1–154:10, December 2011. 151
- [127] Y. Yamamoto, J. H. Jeong, and M. Takagi. *Technical Report: Establishing Spatial Database for Slope Failure with GPS Digital Camera*. Infrastructure Systems Engineering, Kochi University of Technology, 2007. 151
- [128] Embryo imaging. <http://embryoimaging.org>.